

DISCLAIMER

This report was prepared as an account of work sponsored by an agency of the United States Government. Neither the United States Government nor any agency thereof, nor any of their employees, makes any warranty, express or implied, or assumes any legal liability or responsibility for the accuracy, completeness, or usefulness of any information, apparatus, product, or process disclosed, or represents that its use would not infringe privately owned rights. Reference herein to any specific commercial product, process, or service by trade name, trademark, manufacturer, or otherwise, does not necessarily constitute or imply its endorsement, recommendation, or favoring by the United States Government or any agency thereof. The views and opinions of authors expressed herein do not necessarily state or reflect those of the United States Government or any agency thereof.

Printed in the United States of America. Available from:
National Technical Information Service
U.S. Department of Commerce
5285 Port Royal Road
Springfield, VA 22161

NTIS price codes

Paper copy: **A08**

Microfiche copy: **A01**

**A STUDY OF HEAT TRANSFER DURING STEAM INJECTION AND
EFFECT OF SURFACTANTS ON STEAM MOBILITY REDUCTION**

SUPRI TR-55

**By
Fred P. Wang
W.E. Brigham**

October 1986

Work Performed Under Contract No. AC03-81SF11564

**Prepared for
U.S. Department of Energy
Assistant Secretary for Fossil Energy**

**H. J. Lechtenberg, Technical Project Officer
San Francisco Operations Office
1333 Broadway
Oakland, California 94612**

**Prepared by
Stanford University Petroleum Research Institute
Stanford, California 94305-4042**

TABLE OF CONTENTS

	<u>Page</u>
LIST OF TABLES	iii
LIST OF FIGURES	iv
ACKNOWLEDGMENT	vi
ABSTRACT	vii
1. INTRODUCTION	1
1.1 Mechanisms of Oil Recovery by Steam Injection	1
1.2 Gravity Override and Channeling	1
1.3 Performance Prediction	1
1.4 Additives for Steam Injection	2
1.5 Scope of Study	2
2. LITERATURE SURVEY	3
2.1 Heat Transfer Models for Steam Drive	3
2.2 Steam Injection with Additives	8
3. STATEMENT OF PROBLEM	11
4. MATHEMATICAL MODEL OF STEAM DISPLACEMENT IN A CYLINDRICAL CORE WITH A COMPOSITE INSULATION	12
4.1 Mathematical Model	12
4.2 Steady-State Solution	15
4.3 Sensitivity Study	16
5. APPARATUS AND EXPERIMENTAL PROCEDURE	29
5.1 Description of Apparatus	29
5.2 Materials and Their Properties	31
5.3 Experimental Procedures	37
6. RESULTS AND DISCUSSION OF STEAM DISPLACEMENT EXPERIMENTS	41
6.1 Repeatability of Runs	41
6.2 Pressure Effect on Heat-Zone Development	41
6.3 Overall Heat Transfer Coefficient	64
6.4 Effect of Initial Oil Saturation on Oil Recovery	64
7. EXTENSION OF MARX AND LANGENHEIM EQUATION FOR STEAM SWEEPED VOLUME	65
7.1 Critical Time	65
7.2 Method for Predicting Steam Swept Volume	68
8. STEAM MOBILITY REDUCTION BY SUNTECH IV SOLUTIONS	85
8.1 Comparison of Pressure and Temperature Data	85
8.2 Approximate Calculation of Steam Mobility	85
8.3 Results and Discussion	88
9. CONCLUSIONS	125
NOMENCLATURE	127
REFERENCES	132
APPENDIX A: EVALUATION OF HEAT LOSS RATE FROM THE STEAM ZONE	138
APPENDIX B: SOLUTION IN LAPLACE SPACE FOR HEAT CONDUCTION IN A COMPOSITE FINITE RADIAL SYSTEM	146
APPENDIX C: STEADY-STATE SOLUTION OF HEAT FRONT IN A THREE LAYER MODEL	150
APPENDIX D: EQUATIONS FOR PROPERTIES OF MATERIALS	152

LIST OF TABLES

	<u>page</u>
4.1 Physical Properties of Sandpack and Insulation.....	22
5.1 Size Distribution of Ottawa Sand F-150.....	34
6.1 Data for Steam Displacements at Constant Pressure.....	43
6.2 Measured and Calculated Heat Frontal Position (Run #19).....	45
6.3 Measured and Calculated Heat Frontal Position (Run #21).....	46
6.4 Measured and Calculated Heat Frontal Position (Run #23).....	47
6.5 Measured and Calculated Heat Frontal Position (Run #27).....	48
6.6 Measured and Calculated Heat Frontal Position (Run #25).....	49
6.7 Measured and Calculated Heat Frontal Position (Run #38).....	50
6.8 Data for Steam Displacements at Variable Pressure.....	52
6.9 Measured and Calculated Heat Frontal Position (Run #10).....	54
6.10 Measured and Calculated Heat Frontal Position (Run #11).....	56
6.11 Measured and Calculated Heat Frontal Position (Run #12).....	58
6.12 Measured and Calculated Heat Frontal Position (Run #16).....	60
6.13 Measured and Calculated Heat Frontal Position (Run #17).....	62
7.1 Values of $(t_{cd})_{mv}$, n_1 , n_2 and β as a Function of f_{hv} for $f_{ic} = 2.5$	66
7.2 Values of G_1 Function for Steam Swept Volume for $f_{ic} = 2.5$ from this Study.....	74
7.3 Values of G_1 Function for Steam Swept Volume from Hearn Method (1969).....	77
7.4 Values of G_1 Function for Steam Swept Volume from Myhill and Stegemeier Equation.....	80
7.5 Values of G_1 Function for Steam Swept Volume from Yortsos and Galvalas Equation.....	81
8.1 Operating Conditions of Steam Drive with Suntech IV Slugs.....	89

LIST OF FIGURES

	<u>page</u>
4.1 Schematic Diagram of a Linear/Tubular Model.....	13
4.2 Idealized Temperature Profile for Steam Displacement.....	13
4.3 Effect of Particle Size on Wall/Bed Heat Transfer Coefficient.....	18
4.4 Effect of Biot Number at Inner Boundary on Heat Frontal Movement.....	21
4.5 Effect of Biot Number at Outer Boundary on Heat Frontal Movement.....	21
4.6 Effect of Conductivity Ratio on Heat Frontal Movement.....	23
4.7 Effect of Thermal Diffusivity Ratio on Heat Frontal Movement.....	23
4.8 Effect of Thickness of Inner Layer on Heat Frontal Movement.....	25
4.9 Effect of Radius of Outer Layer on Heat Frontal Movement.....	25
4.10 Effect of Volumetric Heat Capacity Ratio on Heat Frontal Movement.....	26
4.11 Comparison of Heat Frontal Movements Among One-Layer, Two-Layer One-Lumped-Layer I and One-Lumped-Layer II Models.....	27
4.12 Single-Layer Approximation For the Two-Layer Models.....	27
5.1 Schematic Diagram of Steam Displacement Apparatus.....	30
5.2 Stainless-Steel Sandpack Holder.....	32
5.3 Viscosities of Kaydol, Water and Steam vs Temperature.....	33
5.4 Kinematic Viscosities of Kaydol, Water and Steam vs Temperature.....	33
5.5 Viscosity Ratios of Kaydol, Water and Steam vs Temperature.....	35
5.6 Kinematic Viscosity Ratios of Kaydol, Water and Steam vs Temperature.....	35
5.7 Kinematic Viscosity of Kaydol vs Temperature.....	36
5.8 Surface Tension of Suntech IV vs Concentration.....	36
5.9 Temperature Effect on Interfacial Tension Between Suntech IV and Kaydol.....	37
5.10 Flow Chart of Experiments of Steam Displacement.....	39
6.1 Comparison of Steam Frontal Position of Two Identical Runs.....	42
6.2 Average Steam Saturation During Steam Displacements at 115 (Run #23), 166 (Run #21) and 206 psia (Run #19).....	42
6.3 Comparison Between the Calculated and Experimental Heat Fronts at 206 psia and 0.258 kg/h Mass Injection Rate.....	45
6.4 Comparison Between the Calculated and Experimental Heat Fronts at 166 psia and 0.258 kg/h Mass Injection Rate.....	46
6.5 Comparison Between the Calculated and Experimental Heat Fronts at 115 psia and 0.258 kg/h Mass Injection Rate.....	47
6.6 Comparison Between the Calculated and Experimental Heat Fronts at 85 psia and 0.258 kg/h Mass Injection Rate.....	48
6.7 Comparison Between the Calculated and Experimental Heat Fronts at 65 psia and 0.258 kg/h Mass Injection Rate.....	49
6.8 Comparison Between the Calculated and Experimental Heat Fronts at 16 psia and 0.103 kg/h Mass Injection Rate.....	50
6.9 Apparent Thermal Conductivity of Insulation (Fiberfrax, Tubings and Thermocouples) vs Temperature.....	51
6.10 Temperature Profiles of Steam Displacement (Run #10).....	53
6.11 Comparison Between the Calculated and Experimental Heat Fronts of Run #10.....	53
6.12 Temperature Profiles of Steam Displacement (Run #11).....	55
6.13 Comparison Between the Calculated and Experimental Heat Fronts of Run #11.....	55
6.14 Temperature Profiles of Steam Displacement (Run #12).....	57
6.15 Comparison Between the Calculated and Experimental Heat Fronts of Run #12.....	57
6.16 Temperature Profiles of Steam Displacement (Run #16).....	59
6.17 Comparison Between the Calculated and Experimental Heat Fronts of Run #16.....	59
6.18 Temperature Profiles of (Run #17).....	61
6.19 Comparison Between the Calculated and Experimental Heat Fronts of Run #17.....	61

6.20	Temperature Profiles of Steam Displacement (Run #40)	63
6.21	Oil Recovery from Steam Displacements at Different Initial Oil Saturation	63
7.1	Mandl and Volek Dimensionless Time vs f_{hv}	67
7.2	Graphic Representation of the Method of Approximating Steam Swept Volume by Shifting the Time Scale.....	67
7.3	Values of n_1 and n_2 vs f_{hv}	71
7.4	Values of β vs f_{hv}	71
7.5	Values of G_1 for Steam Swept Volume vs t_D from 0 to 10 for $f_{ic} = 2.5$	73
7.6	Values of G_1 for Steam Swept Volume vs t_D from 0 to 100 for $f_{ic} = 2.5$	73
7.7	Thermal Efficiency of Steam Swept Zone for $f_{ic} = 2.5$	75
7.8	Thermal Efficiency of Steam Swept Zone for $f_{ic} = 5$	75
7.9	Comparison of Values of G_1 for Steam Swept Zone Between Methods from this Study and by Myhill and Stegemeier.....	78
7.10	Comparison of Values of Thermal Efficiency for Steam Swept Zone Between Methods from this Study and by Myhill and Stegemeier.....	78
7.11	Comparison of Values of G_1 for Steam Swept Zone Between Methods from this Study and by Yortsos and Gavalas.....	79
7.12	Comparison of Values of Thermal Efficiency for Steam Swept Zone Between Methods from this Study and by Yortsos and Gavalas.....	79
7.13	Comparison of Heat Loss Rates from Steam Swept Zone Among Methods by Hearn, Yortsos and Gavalas, and this Study.....	82
7.14	Mandl and Volek Dimensionless Time, $(t_{cD})_{MV}$, vs f_{hv} for Steam Displacement in a Cylindrical Model	83
7.15	Comparisons Between Calculated and Experimental Heat and Steam Fronts of Run #38	83
8.1	Comparisons Between Calculated and Measured Steam Saturation Pressure	86
8.2	Pressure Gradients vs Time for Run #18.....	90
8.3	Relative Steam Mobility vs Time for Run #18.....	90
8.4	Apparent Relative Steam Permeability vs Time for Run #18.....	91
8.5	Average Steam Saturation vs Time for Run #18	91
8.6	Pressure Gradients vs Time for Run #20.....	93
8.7	Relative Steam Mobility vs Time for Run #20.....	93
8.8	Apparent Relative Steam Permeability vs Time for Run #20.....	94
8.9	Average Steam Saturation vs Time for Run #20	94
8.10	Pressure Gradients vs Time for Run #22	95
8.11	Relative Steam Mobility vs Time for Run #22	95
8.12	Apparent Relative Steam Permeability vs Time for Run #22	96
8.13	Average Steam Saturation vs Time for Run #22.....	96
8.14	Dimensionless Concentration of Suntech IV in Produced Fluid for Run #22.....	97
8.15	Pressure Gradients vs Time for Run #26	98
8.16	Relative Steam Mobility vs Time for Run #26.....	98
8.17	Apparent Relative Steam Permeability vs Time for Run #26	99
8.18	Average Steam Saturation vs Time for Run #26.....	99
8.19	Pressure Gradients vs Time for Run #37	101
8.20	Relative Steam Mobility vs Time for Run #37.....	101
8.21	Apparent Relative Steam Permeability vs Time for Run #37	102
8.22	Dimensionless Concentration of Suntech IV in Produced Fluid for Run #37.....	102
8.23	Pressure Gradients vs Time for Run #41	103
8.24	Relative Steam Mobility vs Time for Run #41	103
8.25	Apparent Relative Steam Permeability vs Time for Run #41	104
8.26	Dimensionless Concentration of Suntech IV in produced Fluid for Run #41.....	104
8.27	Steam Mobility Reduction Factor vs Concentration of Suntech IV for Run Set II at 0.101 MPa	105
8.28	Pressure Gradients vs Time for Run #54	107

8.29	Relative Steam Mobility vs Time for Run #54	107
8.30	Apparent Relative Steam Permeability vs Time for Run #54	108
8.31	Pressure Gradients vs Time for Run #28	109
8.32	Relative Steam Mobility vs Time for Run #28	109
8.33	Apparent Relative Steam Permeability vs Time for Run #28	110
8.34	Dimensionless Concentration of Suntech IV in Produced Fluid for Run #28.....	110
8.35	Pressure Gradients vs Time for Run #47	111
8.36	Relative Steam Mobility vs Time for Run #47	111
8.37	Apparent Relative Steam Permeability vs Time for Run #47	112
8.38	Pressure Gradients vs Time for Run #34	113
8.39	Relative Steam Mobility vs Time for Run #34	113
8.40	Apparent Relative Steam Permeability vs Time for Run #34	114
8.41	Dimensionless Concentration of Suntech IV in Produced Fluid for Run #34.....	114
8.42	Steam Mobility Reduction Factor vs Concentration of Suntech IV for Runs at 0.584 MPa	115
8.43	Pressure Gradients vs Time for Run #55	117
8.44	Pressure Gradients vs Time for Run #50	117
8.45	Relative Steam Mobility vs Time for Run #50	118
8.46	Apparent Relative Steam Permeability vs Time for Run #50	118
8.47	Pressure Gradients vs Time for Run #51	119
8.48	Relative Steam Mobility vs Time for Run #51	119
8.49	Apparent Relative Steam Permeability vs Time for Run #51	120
8.50	Pressure Gradients vs Time for Run #52	121
8.51	Relative Steam Mobility vs Time for Run #52	121
8.52	Apparent Relative Steam Permeability vs Time for Run #52	122
8.53	Steam Mobility Reduction Factor for the First Section vs Nitrogen Concentration in Steam for Runs at 0.584 MPa	123
8.54	Steam Mobility Reduction Factor for the Second Section vs Nitrogen Concentration in Steam for Runs at 0.584 MPa	123
8.55	Steam Mobility Reduction Factor for the Entire Sandpack vs Nitrogen Concentration in Steam for Buns at 0.584 MPa	124
A.1	Effect of β on Rate of Heat Loss from Steam Zone for $f_{hv} = 0.1$	141
A.2	Effect of β on Rate of Heat Loss from Steam Zone for $f_{hv} = 0.2$	141
A.3	Effect of β on Rate of Heat Loss from Steam Zone for $f_{hv} = 0.3$	142
A.4	Effect of β on Rate of Heat Loss from Steam Zone for $f_{hv} = 0.4$	142
A.5	Effect of β on Rate of Heat Loss from Steam Zone for $f_{hv} = 0.5$	143
A.6	Effect of β on Rate of Heat Loss from Steam Zone for $f_{hv} = 0.6$	143
A.7	Effect of β on Rate of Heat Loss from Steam Zone for $f_{hv} = 0.7$	144
A.8	Effect of β on Rate of Heat Loss from Steam Zone for $f_{hv} = 0$	144

ACKNOWLEDGMENT

I acknowledge the financial support provided by Stanford University Petroleum Research Institute through DOE contract no. DE-AC03-81SF11564.

Special thanks are due Mr. Theodore Sumida and Dr. Louis M. Castanier, for their assistance.

ABSTRACT

A system of differential equations describing the temperature distribution in the insulation and the heat frontal movement in a cylindrical core during steam injection is derived and solved in Laplace space. The real-time solution is obtained by using the Stehfest algorithm. The solution shows that movement of the heat front is strongly dependent on the heat transfer coefficients at the inner and outer boundaries.

Experimental results of steam injection are shown at pressures varying from 0.11 to 1.42 MPa (16 to 206 psia). The apparent thermal conductivity of the insulation as a function of temperature was obtained by comparing experimental data with an analytic solution. When the pressure of the steam zone changed during a run, it was found that changes of volumetric heat content in the heated core and the insulation may be treated as though they were changes in heat injection rate. The method of succession of steady states can also be used to approximate the heat frontal movement for cases of variable pressure. For displacements using Kaydol as the in-place oil, the initial oil saturation had little effect on irreducible oil saturation.

A method for approximating the steam swept volume is presented using an adjustment to the Marx and Langenheim equation and a new definition of the critical time. This method is to change the time scale using f_{hv}^n as a factor to adjust the time scale after the critical time, where f_{hv} is the fraction of total heat which is latent heat, and where n is determined empirically. The f_{hv} varies from 0.1 to 0.9 and n varies from 0.4 to 1.9. This method improves the approximation of the steam swept volume.

The steam mobility can be reduced by alternate injection of steam and surfactant slugs. The steam mobility decreased with an increase of surfactant concentration and with an increase in the slug sizes of the surfactant solutions. The number of surfactant slugs required to obtain the maximum mobility reduction was found to be a function of surfactant concentration and backpressure. The addition of nitrogen in the injected steam further reduced the steam mobility, with very little effect seen at concentrations of nitrogen above about one mole percent.

1. INTRODUCTION

According to a recent report (Leonard 1986), the crude oil produced by steam injection accounted for 77.5% of the oil produced in the United States by enhanced oil recovery methods. The rate of oil produced by steam injection was about 470,000 BOPD at that time.

Steam injection includes both cyclic steam stimulation and steam drive. For heavy oil reservoirs, as a general rule, a steam injection project is started with cyclic steam injection and followed by a steam drive to maximize oil recovery. After the steam drive has reached the mature stage, the injection can be converted to a low-quality steam injection or a hot-water injection (Afoeju 1974, Ault *et al.* 1985, Hong 1985, Oglesby *et al.* 1982).

1.1. MECHANISMS OF OIL RECOVERY BY STEAM INJECTION

The pioneering study of steam injection by Willman *et al.* (1961) illustrated that the mechanisms of oil recovery by steam drive are viscosity reduction, distillation, solvent extraction, thermal swelling and gas drive. The oil recovery from steam drive is superior to that from hot-water drive. Prats (1982) attributes this superiority to the presence and effects of condensing vapor. He explains:

"The presence of gas phase causes light components in the crude to be distilled and carried along as hydrocarbon components in the gas phase. Where the steam condenses the condensable hydrocarbon components do likewise, thus reducing the viscosity of the crude at the condensation front. Moreover, the condensing steam makes the displacement process more efficient and improves the sweep efficiency. Thus, the net effect is that recovery from steam drives is significantly higher than that from hot water drives."

The condensation phenomenon not only makes the process more stable (Miller 1975) but also significantly suppresses the degree of gravity override and improves the vertical sweep efficiency. The condensing steam carries heat from the steam/water interface downwards to the oil zone. Therefore, heat transfer during steam injection is complicated by gravity override and hot-water underrun.

1.2. GRAVITY OVERRIDE AND CHANNELING

Gravity override affects steam drive in two ways: it provides a communicating path that avoids operational difficulties early in the injection period, and it reduces the vertical sweep efficiency and oil recovery. In order to reduce gravity override and heat loss, steam injection should be operated at high injection rates (Ramey 1964) before steam breaks through. In addition to gravity override, channeling due to the reservoir heterogeneity further complicates the process. Both gravity override and channeling lead to the early breakthrough of steam at the production wells and reduces oil recovery.

1.3. PERFORMANCE PREDICTION

Because of the complexities of steam injection, a detailed description of the heat and the fluid flow requires a numerical simulation study. However, analytical techniques based on simplified heat transfer and fluid flow models are tools easy to use and provide reliable results if the reservoir is properly described. The prediction of oil recovery due to steam injection is based on sizes and shapes of the steam swept zone and the hot liquid zone.

1.4. ADDITIVES FOR STEAM INJECTION

Two effective ways which may enhance oil recovery from steam injection are mobility control and improving oil displacement mechanisms. Steam mobility control can increase the pressure drop across the reservoir and improve the vertical sweep efficiency. Additives such as surfactants, polymers and noncondensable gases have been studied to determine their ability to reduce steam mobility. Additives such as surfactants and metasilicates have been tested to improve oil recovery through lowering interfacial tension between oil and hot water. Surfactants can produce both effects.

1.5. SCOPE OF STUDY

This study includes two main subjects: (1) improvement on the theory of the development of the heated and the steam zones in various geometries from the aspect of heat transfer, and (2) the effect of Suntech IV solutions on steam mobility reduction. A review of the previous work on these two subjects is given in Section 2 and the problems to be studied are stated in Section 3. Section 4 covers the mathematical treatment of the movement of a heat front during steam injection in a cylindrical core, the system studied experimentally herein. Section 5 describes the apparatus, properties of materials and experimental procedures. Section 6 discusses the pressure effect on the movement of a heat front during steam injection in cylindrical cores and the temperature effect on thermal conductivity of the insulation. Section 7 discusses the theory of the development of the steam swept volume and also presents a method for approximating steam swept volume using appropriate extension of the Marx and Langenheim equation. Section 8 discusses the effect of Suntech IV solutions on steam mobility reduction. The conclusions reached in this study are given in Section 9.

2. LITERATURE SURVEY

This section is a review of the literature on heat transfer and fluid mechanics of steam drive, and surfactant effects on steam mobility reduction.

2.1. HEAT TRANSFER MODELS FOR STEAM DRIVE

The large specific volume and the large amount of latent heat that are given up upon condensation are distinct features of steam injection compared to hot-water injection. The large specific volume of steam makes steam injection a more efficient process for oil recovery. The latent heat of steam creates a large steam zone with a small temperature gradient so that the oil viscosity can be reduced to the same degree over all the steam zone. Moreover, the condensation of steam makes the process of steam injection more stable due to the change of volume in the steam zone.

In 1959, Marx and Langenheim applied the Carter (1957) mathematical model for calculating fracture length to the problem of reservoir heating by injecting hot fluids. Their model is a lumped-parameter model which is a heat balance on the rate of heat injection, the rate of heat loss, and the rate of heat stored in the reservoir (see Eq. A.1 shown in Appendix A). This model is for reservoirs with infinitely thick adjacent formations. The following assumptions are inherent in this model:

- (1) local equilibrium of temperatures between fluids and solids,
- (2) no vertical temperature variation within the reservoir,
- (3) infinitely large heat transfer coefficient at the interfaces between the reservoir and the adjacent formations,
- (4) an idealized step function temperature profile between the heated and unheated zones,
- (5) constant thermal conductivity of the adjacent formations, and
- (6) negligible heat conduction along the flow direction in the adjacent formations.

The solution of this model (Eq. A.3) for the radial system is shown in Appendix A.

Ramey (1959) pointed out that the Marx and Langenheim model was not restricted to specific geometries, and could be applied better to steam injection than to hot-water injection because of the assumption that the heated region would remain at a constant elevated temperature. He also showed that superposition can be applied to the Marx and Langenheim equation for cases of variable injection rates.

Ramey (1964) showed that, for constant heat injection rate, the fraction of injected heat lost to the adjacent formation given by the Marx and Langenheim model is the same as that given by the Lauwerier (1955) hot-water injection model while the Rubinshtein (1959) model yields slightly less heat loss. Rubinshtein considered the vertical temperature variation within the reservoir while Marx and Langenheim, and Lauwerier did not. Temperatures of the reservoir adjacent to the overburden and the underburden are less than those near the center of the reservoir in the Rubinshtein model. As a result of this, the heat loss in the Rubinshtein model is less than that in the other two models.

The main difference between the Marx and Langenheim model and the Lauwerier model is the temperature distribution in the reservoir. The Marx and Langenheim model uses the step-function temperature profile while the Lauwerier model assumes that heating is only by sensible heat and allows the temperature to vary along the path of fluid flow. The same total heat in adjacent formations for both models means that the thermal efficiency is independent of the temperature distribution in the reservoir.

Ramey (1964) also observed that the distribution of heat between the reservoir and the adjacent formations is independent of the heat injection rate and is a function only of the dimensionless time for a constant heat injection rate.

Prats (1969) showed that Eq. A.6 (in Appendix A) is good for representing the thermal efficiency of heat transfer models considering horizontal heat conduction in both the reservoir and the adjacent formations. He stated that the heat efficiency (the fraction of injected heat remaining in the reservoir) calculated by Eq. A.6 is also valid for cases of variable steam temperature and variable mass injection rate as long as the net heat injection rate is constant. In steam injection (or *in-situ* combustion), the volumetric heat capacity of the steam swept zone (or burned zone) may be significantly smaller than that of the hot-liquid zone (or steam plateau zone). For these two-zone cases, he showed the heat efficiency may be higher than that calculated by Eq. A.6 for single-zone cases.

The Marx and Langenheim equation is good for calculating the heated volume (V_h) and the steam swept volume (V_s) with high heat injection rates. Willman *et al.* in 1961 proposed an equation for approximating the steam swept volume for radial systems. In this equation, the rate of latent heat injection was used.

Hearn in 1969 discussed the effect of the latent heat injection on the steam swept volume. He explained:

"Since the steam zone around an injection well is at steam temperature, vertical heat lost to the cap and base rock from this zone must be supplied entirely by latent heat. Initially, the rate of vertical heat loss will be less than the latent heat injection rate. This means that some latent heat will be available at the condensation front to heat additional reservoir. In this case, the entire heated zone will contain steam and the Marx and Langenheim equation is adequate to calculate the swept area. At later times, however, the total rate of vertical heat loss will become greater than the latent heat injection rate. All latent heat content of injected steam will be used up to supply the heat that is lost from the steam zone."

He applied the above theory to calculate the steam swept area numerically using

$$\dot{H}_{fg} = \int_0^{A_s} \frac{2k_s \Delta T}{\sqrt{\pi \alpha_s (t - t_A)}} dA \quad (2.1)$$

where

\dot{H}_{fg} = latent heat injection rate,

A = area,

A_s = steam swept area,

k_s = thermal conductivity of the adjacent formations,

α_s = thermal diffusivity of the adjacent formations,

ΔT = temperature difference between steam and initial reservoir,

t = elapsed time,

t_A = time when the differential element is first contacted by the heat front.

The calculated steam swept volume could therefore be considered to be the upper bound of the true swept volume because at later times, the latent heat used to heat additional reservoir to steam temperature has been neglected in the calculation. It is noted that, in Hearn's calculations, the time at which the steam swept volume started to deviate from the heated volume was the same as the critical time defined by Mandl and Volek (1969).

Mandl and Volek attempted to separate the steam swept volume from the total heated volume by extending the Marx and Langenheim model. Mandl and Volek considered the heated volume calculated by Eq. A.3 using total heat injection rate as the upper bound of the steam swept volume and derived an approximate solution as the lower bound of the steam swept volume using the latent heat injection rate. They then defined a critical time (t_{cMV}) as the time when the heat flow of hot liquids ahead of the steam zone becomes significant. When the time is less than the critical time, the steam swept volume was the same as the upper bound solution. When the time is greater than t_{cMV} , the steam swept volume was approximated by taking the arithmetic average of the upper and lower bounds of the steam swept volume. They also conducted steam injection experiments with a 0.91 m \times 0.10 m \times 0.10 m (36 in. \times 4 in. \times 4 in.) sandpack surrounded by 0.10 to 0.15 m (4 to 6 in.) thick insulation. The Marx and Langenheim equation matched their experimental results when both the quality and the rate of injected steam were high. Their derived solution for the steam swept volume did not match experimental results very well when both the quality and the rate of the injected steam were low. The observed time when the steam swept volume started to deviate from the Marx and Langenheim solution was smaller than the critical time defined by them. The drawback of this model was that it did not produce a zero steam volume for the case of hot-water injection.

In 1978, Myhill and Stegemeier reported an approximate solution for the steam-zone heat efficiency. This solution was obtained by revising the Mandl and Volek model. A new weighting factor (the sensible heat fraction) for averaging the upper and lower bounds of the steam swept volume was used to replace the factor of one half used by Mandl and Volek. The use of this new weighting factor eliminates one drawback of the Mandl and Volek model. Myhill and Stegemeier mentioned that this weighting factor is arbitrarily determined but it gives reasonable steam-zone thermal efficiencies for steam qualities greater than 0.2.

In 1982, Yortsos and Gavalas presented another approximate solution for calculating the steam swept volume. This solution was also derived from the Marx and Langenheim model and the concept of the critical time defined by Mandl and Volek. Before the critical time, the steam swept volume is calculated by the Marx and Langenheim equation. After the critical time, the rate of the steam-zone development is approximated by

$$v_{sD} = a \sqrt{\frac{\pi}{t_D}} \quad (2.2)$$

where

- v_{sD} = dimensionless rate of steam-zone development,
- a = constant determined by the dimensionless critical time,
- t_D = dimensionless time defined in Appendix A.

It is assumed that the rate of steam-zone development given by Eq. 2.2 equals the rate of the heated-zone development at the critical time. The constant a can then be obtained by solving the Marx and Langenheim equation at the Mandl and Volek critical time and setting it equal to Eq. 2.2 as follows:

$$e^{t_{cDMV}} \operatorname{erfc}(\sqrt{t_{cDMV}}) = 1 - f_{hv} = a \sqrt{\frac{\pi}{t_{cDMV}}} \quad (2.3)$$

where f_{hv} is the fraction of latent to total heat injected.

All the models mentioned heretofore are the so-called frontal advance models. Most of them are based on the Marx and Langenheim model. The merit of the Marx and Langenheim model is that it applies to all geometries as long as the ratio between heated volume and heat transfer surface is constant. For cases of constant vertical sweep efficiency, this ratio can be used to define the dimensionless variables as shown by de Haan and Schenk (1969), van Lookeren (1983), and Yortsos and Gavalas (1982). In other words, simple factors may be used to account for gravity override. Gravity override resulting from the density difference between steam and oil (or water) is common in both field operations (de Haan and Schenk, 1969; Blevins *et al.*, 1969; Pollock and Buxton, 1969; Volek and Pryor, 1972) and laboratory models (Baker 1973, van Lookeren 1983).

J. van Lookeren (1983) analyzed the degree of gravity override in linear and radial systems using segregated flow theory. A balance between the viscous and the gravity forces at the front defines the slope of the interface. He obtained the vertical sweep efficiency in terms of the gravity number by assuming that the mass rate of flowing steam at a certain vertical distance at the front is proportional to the steam swept volume. The calculated vertical sweep efficiency agreed satisfactorily with the experimental results. He then calculated an average thickness as the ratio of the swept volume to the heated upper surface area for cases in which steam does not reach the base rock. He used an arithmetic average for thermal properties of the caprock and the rock underlying the steam zone. The formula is given as:

$$2(k\rho C)_S = (k\rho C)_{\text{cap rock}} + (k\rho C)_{\text{underlying rock}} \quad (2.4)$$

where

k = thermal conductivity,

ρC = volumetric heat capacity.

The dimensionless time and heat injection rate can be defined with this average thickness and the steam swept volume can be calculated explicitly.

Baker (1969 and 1973) studied rate and pressure effects on steam zone development in a radial model. The model used was a 0.076 m (3 in.) thick reservoir with 0.91 m (36 in.) O.D.. A water-filled sand was used to simulate the overburden and the underburden. Experiments were carried out at pressures from 0.11 to 0.71 MPa (1 to 103 psig), and at rates from 0.01 to 0.1 kg/s·m (24 to 240 lb_m/hr·ft). The vertical sweep efficiency was measured with lines of thermocouples at different locations at three radial distances. It was observed that the heat efficiency of steam flooding decreased with the decrease of mass injection rate and that pressure had a relatively small effect on heat efficiency. Vertical sweep efficiency decreased with a decrease in the mass injection rate but did not vary significantly with time. Steam saturations in the steam zone were greater at higher mass injection rates and lower pressures. Another important observation was that the process was stable when steam displaced either water or moderately viscous oils.

Crichlow (1972) investigated the rate effect on hot-water and steam injections using a linear/tubular model. This model was a 0.025 m I.D. × 0.91 m (1 in. I.D. × 3 ft) sandpack surrounded with 0.071 m (2.8 in.) of Santocel-A insulation. The mass injection rate of steam varied from 1.1×10^{-3} to 2.0×10^{-3} kg/s·m² (0.8 to 1.5 lb_m/hr·ft²). These rates were low enough that the system reached the stagnation point beyond which the steam front did not advance. The stagnation point is the time and location where the rate of heat loss through insulation equals the rate of latent heat injected. Using this stagnation point, Crichlow calculated the overall heat transfer coefficient of the system by:

$$U = \frac{\dot{m}h_{fg}}{2\pi r_1(T_s - T_\infty)x_s} \quad (2.5)$$

where

- U = overall heat transfer coefficient, Btu/hr·ft²·°F,
- \dot{m} = mass injection rate of steam, lb_m/hr·ft²,
- h_{fg} = latent heat of injected steam, Btu/lb_m,
- T_s = steam injection temperature, °F,
- r_1 = radius of the core, ft
- T_∞ = ambient temperature, °F,
- x_s = distance to stagnation point, ft.

The overall heat transfer coefficients for Crichlow's system were 2.0 and 2.4 W/m²·°K (0.36 and 0.42 Btu/hr·ft²·°F) for 1.1×10⁻³ and 2.0×10⁻³ kg/s·m².

Arihara (1975) studied the rate effect on the overall heat transfer coefficient (U) of consolidated sandstones. The mass injection rate of steam varied from 1.64×10⁻³ to 2.30×10⁻³ kg/s·m² (1.21 to 1.69 lb_m/hr·ft²). Because the pressure gradient of his experiment could not be neglected, he included the resulting temperature gradient in the equation for calculating U :

$$U = \frac{\dot{m}h_{fg}}{\pi r_1 \left[\frac{dT}{dx} x_s^2 + 2(T_s - T_\infty) x_s \right]} \quad (2.6)$$

where dT/dx is the temperature gradient in the steam zone. For Berea sandstone, the overall heat transfer coefficient was 9.3 W/m²·°K (1.64 Btu/hr·ft²·°F) for injection rate of 1.64×10⁻³ kg/s·m² (1.21 lb_m/hr·ft²) and 7.8 W/m²·°K (1.38 Btu/hr·ft²·°F) for injection rate of 2.30×10⁻³ kg/s·m².

The preceding review was on studies on steam displacement assuming that steam is the only component in the gas phase. In practice, hydrocarbon gases and noncondensable gases are always present in the steam zone. A study of the steam plateau phenomena in *in-situ* combustion was given by Satman, Brigham and Ramey (1979). They used Raoult's law, Dalton's law and Clausius-Clapeyron equation in the partial differential equation to account for the mass change of steam as a result of condensation. Then, the first-order nonlinear partial differential equation was solved by the method of characteristics. In their model, the heat loss was handled by using the steady-state convective equation with an overall heat transfer coefficient.

Using the convective heat transfer equation to represent the heat loss can simplify the heat transfer problems related with porous media. However, the steady-state overall heat transfer equation often does not fully describe the transient effect of heat loss. Zolotukhin (1979) assumed that the overall heat-transfer coefficient is time-dependent and used it in a heat-transfer model considering horizontal heat conduction, convection and heat loss. He assumed that the fraction of heat loss from his model was the same as the exact value of heat loss obtained by Rubinshtein (1961) and obtained an analytic equation for the time-dependent overall heat transfer coefficient for radial slab reservoirs. He further simplified this equation to:

$$U(t) = \sqrt{\frac{2(k\rho C)_S}{\pi t}} \quad (2.7)$$

where

- $U(t)$ = time-dependent overall heat-transfer coefficient,
- $(k\rho C)_S$ = thermal constant of the surroundings.

Equation 2.7 indicates that the heat loss rate at the heat transfer surface is inversely proportional to the square root of time. Strictly speaking, Eq. 2.7 is only valid for infinite systems with constant boundary temperature. The use of Eq. 2.7 in a differential equation, in fact, results in slightly less heat loss than the exact solution because the actual boundary temperature varies with time. Using Eq. 2.7, he obtained an analytical solution for temperature distribution within the reservoir in a simple exponential form. The simplicity of this method and the closeness of the temperature profiles given by this solution compared to the exact solution offset the slight inaccuracy in heat loss.

Satman, Zolotukhin and Soliman (1980) applied this time-dependent overall heat transfer coefficient to a linear core and the steam plateau model developed by Satman *et al.* (1979) by including the horizontal heat conduction. The solution for temperature distribution in a linear core accurately matched the experimental results given by Ersoy (1969).

2.2. STEAM INJECTION WITH ADDITIVES

Foam is a gas dispersed in a liquid. The liquid is always the continuous phase and the gas is always the discontinuous phase. The apparent high viscosity of foam results mainly from the drag of the thin liquid film, formation and breaking of films and the resulting complex flow mechanisms. Foams are often considered as either pseudoplastic or Bingham plastic fluids. Foams are unstable because the liquid films drain continuously through gravity force until they break.

Schwartz, Perry and Berch (1958) reviewed the work on foam prepared with surfactants before 1958. Their reviews are summarized below:

- (1) Foam properties vary with the nature of the gas phase. Carbon dioxide foams behave differently from air foams.
- (2) Foaming power increases with the surfactant concentration and reaches a maximum at the critical micelle concentration (CMC).
- (3) The minimum concentration required to produce foam is relatively independent of temperature and decreases as the carbon chain length increases.
- (4) Foam stability can be related to the surface viscosity. Films with high surface viscosity are usually slow-draining films. Solutions with high surface viscosity tend to form voluminous stable foams.
- (5) Pure surfactant solutions usually form fast-draining films. Electrolytes, gums and organic liquids increase the foam stability. For example, pure lauryl sulfate forms fast-draining films, while lauryl sulfates plus some free lauryl alcohol form slow-draining films.
- (6) Slow-draining films possess surface layers of a condensed (closely packed) type and are less permeable than fast-draining films. Slow-draining films change to fast-draining films when the temperature is increased.

In petroleum engineering, foams have been applied to operations such as drilling, fracturing, blocking of highly permeable formations, sealing leaks in gas storage reservoirs, and mobility control. Hirasaki and Lawson (1983) presented a comprehensive analysis of foam flow through capillary tubes by both analytical and experimental techniques. Mahmood (1986) gave a review of the rheology of gas/foam flow through capillary tubes and porous media. The effectiveness of foam on mobility reduction is a function of type of surfactant, surfactant concentration, foam quality, flow rate and absolute permeability.

The efficiency of steam drive is severely reduced by gravity override and channelling. Additives such as surfactants, polymers, solvents and gases have been proposed as materials to be injected with

or prior to steam in order to improve the volumetric sweep efficiency and to enhance oil recovery. Surfactants have been employed alone or with other additives to reduce steam mobility by generating foam with steam and to reduce the interfacial tension between oil and water.

The simultaneous injection of steam and surfactant solution can generate foam in-situ which will, in turn, reduce the steam mobility in the steam channels and divert steam toward the unswept part of the reservoir. Consequently, both vertical conformance and oil recovery are improved. Also, the surfactant in the condensed water flows into the liquid zone and can reduce the interfacial tension between oleic and aqueous phases. Laboratory studies and field tests have been conducted to enhance oil recovery by using surfactant additives to improve the vertical sweep efficiency or recovery mechanisms.

Marsden *et al.* (1977) reviewed papers and patents pertaining to foam flow through porous media and the use of foam in steam injection before 1977. Their review indicated that the advantages of using foam in steam displacement are to reduce gravity override, to overcome channeling through highly permeable zones including gas caps and bottom water, and to reduce emulsification between crude oils and steam. This review was brought up to date in 1986 by Marsden.

Clampitt in 1976 and 1981 claimed two patents on applying surfactants and polymers to plug highly permeable strata. Polymers, which prevent surfactant from foaming, were used to plug the steam channels in the early stage. Later on, the polymers degraded and the steam started to generate foam with the surfactant solution, and the plugging process continued. At 325°F (163°C), carboxymethyl cellulose (CMC) degraded after about 5 hours of heating, and polyacrylamide solution remained stable for about 12 days.

Gopalakrishnan *et al.* (1978) studied both the interfacial phenomenon of a surfactant and refined oil system and oil recovery by steam displacement with surfactant. A sodium petroleum sulfonate of molecular weight of 500 and a 30°API oil were used. They used alternating injections of steam and slugs of surfactant solutions. Their results showed that four 0.05 pore volume slugs of surfactant solution yielded higher oil recovery than a single 0.2 pore volume slug.

Isaacs *et al.* (1982) investigated the effect of the surfactant, TRS 10-80, on bitumen recovery using cylindrical testing cells. They injected 0.01 kg/kg TRS 10-80 and 0.01 kg/kg NaCl solution into the steam stream and the bitumen recovery increased from 27% without using the surfactant solution to 52% as a result of improved displacement efficiency. The recovery was higher when TRS 10-80 injection started at the same time as steam injection. They also measured the interfacial tensions between surfactant solutions and the crude oil. However, oil recovery was not clearly related to the interfacial tension.

Dilgren *et al.* (1978) claimed that noncondensable gases such as nitrogen could highly improve the performance of a steam/foam process. In laboratory tests, a high pressure gradient was obtained by injecting small amounts of nitrogen with steam. Several other parameters such as surfactant concentration, NaCl concentration and steam quality were tested. Siponate DS-10 (sodium dodecylbenzene sulfonate) was superior to both sodium lignin and ammonium lignin sulfonates. Addition of sodium chloride in the surfactant solution further increased the effectiveness of the steam/gas foam. They observed that the steam mobility decreased dramatically with the increase of surfactant concentration when the concentration was low and leveled off to a certain value.

In 1982, Dilgren *et al.* published more of their test results. Siponate A-168 and Bioterge A-30 were found to be the best foaming agents among eight surfactants tested. Both of them were C₁₆-C₁₈ alpha olefin sodium sulfonates. For 0.005 kg/kg of Siponate A-168 solution, 0.01 kg/kg NaCl could reduce the steam mobility to the same degree as 0.05 kg/kg NaCl. For 0.005 kg/kg Witco Exp.

4498-43B, the steam mobility was reduced with increasing NaCl concentration. The optimal surfactant concentrations were 0.0005 kg/kg for Saponate A-168 and 0.0025 kg/kg for Witco Exp. 4498-43B.

Doscher and Hammershaimb (1982) tested the foamability of ten surfactants using static and dynamic methods. The results indicated that Thermophoam BW-D, Lakeway 301-10 and Bioterge AS-40 were better than other surfactants. In dynamic tests, the pressure gradient was about 15 psi/ft (0.34 MPa/m) when 0.01 kg/kg Thermophoam solution was injected with steam. However, the pressure gradient increased four times when four mole percent of nitrogen was injected with the surfactant solution and steam. They also observed that the pressure gradient was higher in that half of the sandpack closer to the inlet.

The economical efficiency of a steam/foam process depends on the amount of surfactant used to produce a barrel of additional crude oil. In addition to thermal degradation, partitioning of surfactants into the oleic phase, adsorption of surfactants on the reservoir rock and reaction with salt may cause the loss of surfactant and increase the surfactant consumption. Al-Khafaji *et al.* (1983) investigated these factors at steam injection conditions [204°C (400°F) and 2.75 MPa (400 psig)]. Suntech IV was thermally more stable than CORCO 180A and Petrostep 420. Partitioning of Suntech IV into Kern River crude was of the Langmuir type. Partitioning increased rapidly with the increase of surfactant concentration at low concentrations and reached a plateau of about 0.0025 kg/kg at the concentration of Suntech IV in water of 0.04 kg/kg. Adsorption of Suntech IV on a sand clay mixture (Ottawa sand containing 0.05 kg/kg kaolinite) was about two micromoles per gram of absorbent mix at the critical micelle concentration (CMC). The adsorption isotherm appeared to be of a Langmuir type. The effect of NaCl, NaHCO₃, KCl and CaCl₂ on Suntech IV solutions was examined at room temperature as well as at 204°C (400°F). Salts containing monovalent cations such as NaCl, KCl and NaHCO₃, had little effect when the concentration of the salt was lower than one percent by weight. For CaCl₂, the salt tolerance of Suntech IV solutions was below a half percent by weight.

Duerksen (1984) tested 35 commercial surfactants and 15 CRC (Chevron Research Company) sulfonates at steam injection conditions. The concentration of surfactants used was 0.005 kg/kg. Results indicated that Stepanflo 30, Suntech IV and most of the CRC sulfonates were thermally stable and able to generate voluminous foams at temperature up to 218°C (425°F). The pressure drop across the foam generator decreased linearly with temperature. All tested surfactants showed a dependence on the nitrogen concentration in the gaseous phase. Resistance factors decreased with the decrease of nitrogen concentration. The dependence of resistance factors on nitrogen concentration varied with the surfactant used. CRC sulfonates #8 and #13 showed the least dependence on nitrogen concentration. CaCl₂ was detrimental to foam generation. The oil used was a Kern River crude oil. The residual oil saturation was reduced when foaming agents such as Thermophoam BW-D, Stepanflo 30 and CRC sulfonates were used. When CRC sulfonates were used, he observed higher pressure gradients at lower residual oil saturations.

Mahmood (1986) extensively studied gas/surfactant foam flow using a homogeneous two-dimensional (x-z) sandpack. His results showed that one of the main mechanisms of foam flood is to increase the pressure gradient in the reservoir to increase the oil production. In most of his displacements, he observed the significant override and underrun. He applied a segregated flow theory to model gravity underride and fractional flow theory to gravity override, and combined the two theories to obtain analytical solutions for predicting both oil recovery and pressure performance.

3. STATEMENT OF PROBLEM

In field operations, both the total heat injection rate and the steam quality vary with time because of the heat transmission in the wellbore and normal operating variables. The pressure in the steam swept zone also changes with time as a result of the formation and production of an oil bank ahead of the steam zone. The development of the heated and the steam zones are complicated by these changes.

Only a few analytical solutions of heat-transfer models can be applied to laboratory steam injection. Therefore, the first goal of this study was to develop an analytical solution for studying the heat frontal movement and to investigate the pressure effect on the development of the heated zone using both analytical and experimental methods. In order to minimize the gravity effect, a long cylindrical laboratory model was used.

For engineering purposes, it is desirable to analyze steam injection with analytical methods and to perform experiments where reservoir nonuniformity is minimized. One way for estimating oil recovery of a steam drive is based on the calculation of the steam swept volume. All previous studies on the development of the volume swept by steam displacement used the critical time defined by Mandl and Volek (1969). This is the time when the heat loss rate from the heated zone equals the latent heat injection rate. The drawback of these models is that the predicted rate of heat loss from the steam zone is either constant or decreasing when time is greater than the critical time, while the actual heat loss rate increases with time since the size of steam zone is increasing. The second goal of this study was to examine the heat transfer mechanisms of the development of the steam swept zone from the point of view of fluid dynamics and heat loss, and to devise a better method for approximating the steam swept volume.

Gravity override and channeling are severe problems in steam injection. The performance of a steam displacement can be improved by the sufficient control of steam mobility. Injecting foaming agents with steam to reduce steam mobility has been tested both in laboratories and fields under various conditions. The technique of alternate injection of foaming agents and steam slugs to reduce the steam mobility has not been extensively tested before. Therefore, the third goal of this study was to attempt to study various factors of surfactant solutions and reservoir conditions affecting the steam mobility using laboratory sandpacks and the slug injection technique, and to attempt to optimize the use of foaming agents using surfactant slug injection.

4. MATHEMATICAL MODEL OF STEAM DISPLACEMENT IN A CYLINDRICAL CORE WITH A COMPOSITE INSULATION

In laboratory studies of steam injection, layers of insulating materials of finite thickness are usually used. The Marx and Langenheim model (1959), which is good for slabs with an infinitely thick insulation, is only applicable to laboratory models in limited cases. A mathematical model and its solutions for calculating the steam-displacement heat front in cylindrical cores with a finite and composite insulation are presented in this section.

4.1. MATHEMATICAL MODEL

The main component of a laboratory model shown in Fig. 4.1 is a cylindrical core surrounded by a stainless steel tube and an insulation. Steam is injected into the core to create a heated zone and heat is lost from the heated zone radially through the insulation. As shown in Fig. 4.2, the heated zone is a larger than actual steam zone. A step function temperature profile is shown between the heated and unheated zones, which approximates the actual temperature profile. The heat content of this step function zone is the same as the actual heat content. The temperature remains constant throughout the heated zone and the thermal conductivity of the insulation is assumed to be constant. Heat conduction in the insulation along the direction of steam flow direction is neglected. Accordingly, for a constant heat injection rate, the movement of the heat front can be described by an equation similar to that of Marx and Langenheim:

$$\dot{H} = \int_0^t \left\{ -k_1 \left[\frac{\partial T(t - \tau)}{\partial r} \right]_{r=r_1} 2\pi r_1 \left[\frac{dX}{d\tau} \right] \right\} dt + (\rho C)_R \Delta T \pi r_1^2 \frac{dX}{dt} \quad (4.1)$$

where

- \dot{H} = rate of heat injected,
- T = temperature in the insulation,
- ΔT = difference between steam and initial reservoir temperature,
- k_1 = thermal conductivity of layer 1,
- $(\rho C)_R$ = volumetric heat capacity of the sandpack,
- $\frac{dX}{dt}$ = heat frontal velocity,
- r_1 = radius of the sandpack.

The integral term on the right-hand side of Eq. 4.1 is the rate of heat loss from the heated zone. The equation simply states that the rate of heat stored in the sandpack equals the rate of heat injected minus the rate of heat loss. The rate of heat loss per unit area at the sandpack boundary $[(\partial T/\partial r)_{r=r_1}]$ is obtained by solving the following linear partial differential equations with the appropriate initial and boundary conditions:

Governing differential equations

$$\frac{\partial^2 T_1}{\partial r^2} + \frac{1}{r} \left[\frac{\partial T_1}{\partial r} \right] = \frac{1}{\alpha_1} \left[\frac{\partial T_1}{\partial t} \right] \quad (4.2)$$

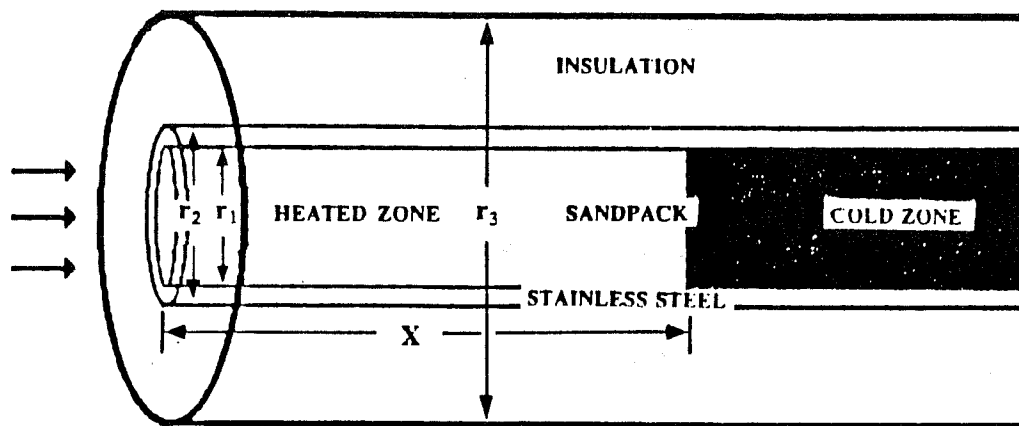


Fig. 4.1 Schematic Diagram of a Linear/Tubular Model.

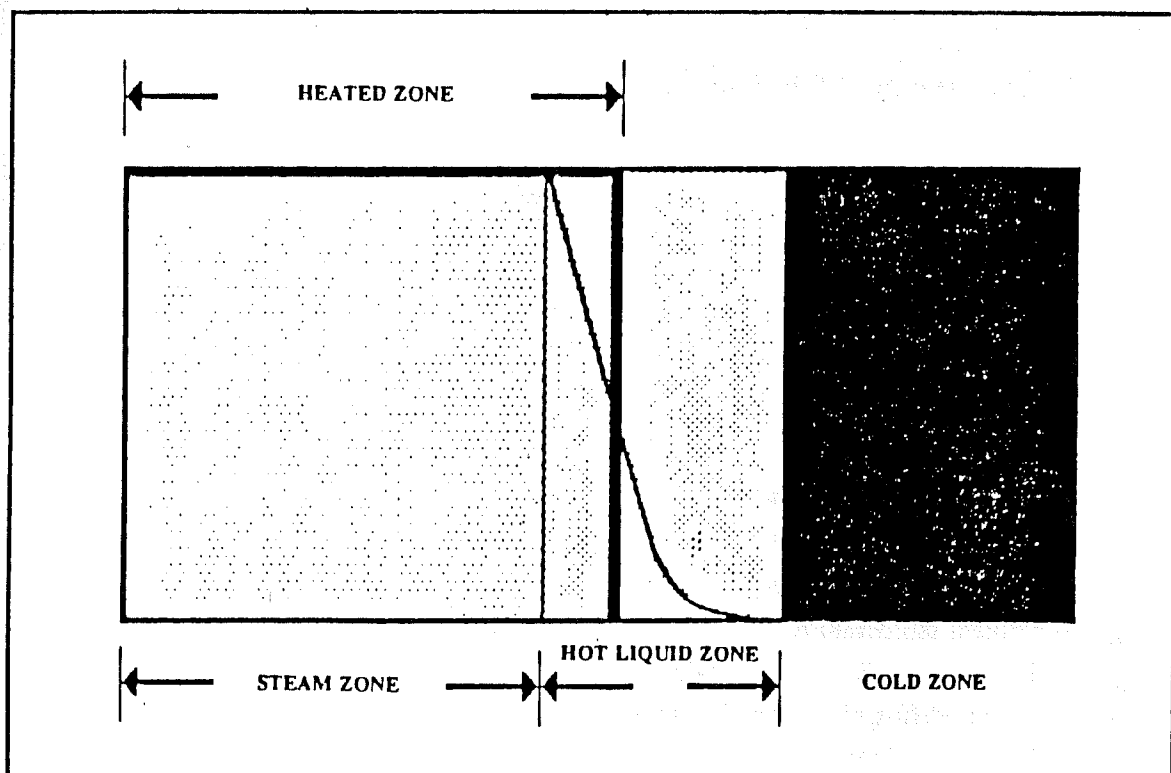


Fig. 4.2 Idealized Temperature Profile for Steam Displacement.

for the stainless steel tube and

$$\frac{\partial^2 T_2}{\partial r^2} + \frac{1}{r} \left[\frac{\partial T_2}{\partial r} \right] = \frac{1}{\alpha_2} \left[\frac{\partial T_2}{\partial t} \right] \quad (4.3)$$

for the insulation;

Boundary conditions

at $r = r_1$, the inner boundary of the stainless steel tube:

$$h_{f1}(T_s - T_1) = -k_1 \left[\frac{\partial T_1}{\partial r} \right] \quad (4.4)$$

at $r = r_2$, the boundary between the stainless steel tube and the insulation:

$$T_1 = T_2 \quad (4.5)$$

$$-k_1 \left[\frac{\partial T_1}{\partial r} \right] = -k_2 \left[\frac{\partial T_2}{\partial r} \right] \quad (4.6)$$

at $r = r_3$, the outer boundary of the insulation:

$$-k_2 \left[\frac{\partial T_2}{\partial r} \right] = h_{f2}(T_2 - T_\infty) \quad (4.7)$$

Initial Condition

$$T_1(r, 0) = T_2(r, 0) = T_\infty \quad (4.8)$$

where

- T_1 = temperature in the stainless steel tube,
- T_2 = temperature in the insulation,
- T_s = temperature in the steam zone,
- T_∞ = ambient temperature,
- α_1 = thermal diffusivity of the stainless steel tube,
- α_2 = thermal diffusivity of the insulation.
- k_1 = thermal conductivity of the stainless steel tube,
- k_2 = thermal conductivity of the insulation,
- h_{f1} = heat transfer coefficient at inner boundary (r_1),
- h_{f2} = heat transfer coefficient at outer boundary (r_3).

The solution of the flow rate at the inner boundary in Laplace space is given in Appendix B and this solution is coupled with Eq. 4.1 in Laplace space to calculate the heat frontal position. By employing the following dimensionless terms,

$$\begin{aligned}
 t_D &= \frac{\alpha_2 t}{r_1^2}, & r_D &= \frac{r}{r_1}, \\
 Bi_1 &= \frac{h_{f1} r_1}{k_1}, & Bi_2 &= \frac{h_{f2} r_1}{k_2}, \\
 \alpha_D &= \frac{\alpha_1}{\alpha_2}, & \lambda_D &= \frac{k_1}{k_2}, \\
 \sigma &= \frac{(\rho C)_2}{(\rho C)_R}, & \dot{H}_D &= \frac{H}{\pi L \alpha_2 (\rho C)_R \Delta T}, \\
 T_D &= \frac{T - T_\infty}{T_s - T_\infty} \quad \text{and} \quad X_D = \frac{X}{H_D L}
 \end{aligned}$$

where

$(\rho C)_2$ = volumetric heat capacity of the insulation,

L = length of the sandpack,

the solution of Eq. 4.1 in Laplace space is obtained in dimensionless form as:

$$\bar{X}_D = \frac{1}{s^2 \left\{ -2\sigma \left[\frac{\partial \bar{T}_{1D}}{\partial r_D} \right]_{r_D=1} + 1 \right\}} \quad (4.9)$$

Equation 4.9 can be inverted into the real time solution numerically by the Stehfest algorithm (1970). For constant heat injection rate, the heat efficiency is given by:

$$E_t = \frac{H_R}{H_{inj}} = \frac{X_D}{t_D} \quad (4.10)$$

where H_R is the heat stored in the heated zone and H_{inj} is the cumulative injected heat.

4.2. STEADY-STATE SOLUTION

Because the thickness of the insulation of this model is finite and the inner and outer boundary temperatures can be considered as constant at large times, the heat front will approach a steady-state position after a period of injection. The steady-state solution for this model simplified from Eq. C.13 in Appendix C is given by:

$$2\sigma X_D = \ln r_{3D} - \ln r_{2D} + \frac{\ln r_{2D}}{\lambda_D} + \frac{1}{Bi_1 \lambda_D} + \frac{1}{Bi_2 r_{3D}} \quad (4.11)$$

where

$$r_{2D} = \frac{r_2}{r_1}$$

$$r_{3D} = \frac{r_3}{r_1}$$

It is noted that the variable, $2\sigma X_D$ is independent of σ . This is expected because the heat capacity only affects the transient behavior. Therefore, $2\sigma X_D$ instead of X_D is used in the following discussion. $2\sigma X_D$ is a function of λ_D , Bi_1 , Bi_2 , r_{2D} and r_{3D} . The steady-state solution can be used as a value for checking the numerical solution of this model. In practice, this steady-state solution of heat frontal position is called the "stagnation point". The stagnation point determined from experiments can be used to calculate the overall heat transfer coefficient of the physical model and the heat transfer coefficient at the inner tube wall.

4.3. SENSITIVITY STUDY

In this model, it is assumed that the temperatures of the sand and the fluid are the same, and the pressure drop across the steam zone is negligible. For steam injection, the heat transfer coefficient (h_f) between the fluid and the sand is large. If the size of the sand grains is small, one can assume that the temperature of the fluid and of its adjacent grains are the same (Jenkins and Aronofsky, 1954). Factors which may affect the steam zone development are the heat transfer coefficients at the inner and the outer boundaries, radii of various layers, the volumetric heat capacity ratio, and the thermal conductivities and diffusivities the layers. Lastly, comparisons between a single-layer model, a two-layer model and a lumped single-layer model are shown.

4.3.1. Heat Transfer Coefficients at Inner and Outer Boundaries

The convective heat transfer from a flowing phase to a stationary phase is quantified by the heat transfer coefficient and the temperature difference between the two phases, and can be expressed as:

$$q_c = h_f A \Delta T \quad (4.12)$$

where

- q_c = rate of heat transfer by convection,
- h_f = heat transfer coefficient,
- A = area of heat transfer surface,
- ΔT = temperature difference between surface and fluid.

In the stationary phase, the heat is transferred by conduction.

4.3.1.1. Estimation of Heat Transfer Coefficient

Numerous studies on both the theory and the measurement of the heat transfer coefficient at the tube wall for packed and fluidized beds can be found in the literature. Colburn (1931), Leva (1947) and Leva *et al.* (1948) showed that the heat transfer coefficient at a tube wall decreases with the decrease of particle sizes when D_p / D_t is smaller than 0.15. Leva *et al.* studied the heat transfer

coefficient for cooling of gases through packed tubes and proposed the following equation for estimating the heat transfer coefficient:

$$h_f = 3.5 \frac{k_l}{D_t} e^{-4.6 \frac{D_p}{D_t}} \left[\frac{D_p \dot{m}}{\mu} \right]^{0.7} \quad (4.13)$$

where

- h_f = heat transfer coefficient, Btu/hr·°F·ft²,
- \dot{m} = mass injection rate, lb_m/hr·ft²,
- k_l = thermal conductivity of the flowing liquid, Btu/hr·°F·ft,
- μ = viscosity of the flowing liquid, lb_m/hr·ft,
- D_p = particle diameter, ft,
- D_t = tube diameter, ft.

Figure 4.3 shows their data on the effects of rate and particle size on the heat transfer coefficient.

The study of reservoir heating by hot-fluid injection using cylindrical cores is analogous to the Leva *et al.* study. However, the ratio of D_p/D_t for sandpacks is on the order of 10^{-3} or less. Under this condition, the value of $e^{-4.6D_p/D_t}$ is very close to one and so Eq. 4.13 reduces to:

$$h_f = 3.5 \frac{k_l}{D_t} \left[\frac{D_p \dot{m}}{\mu} \right]^{0.7} \quad (4.14)$$

It is noticed that for a constant tube diameter, h_f is a function of a modified Reynolds number. For sandpacks h_f estimated by Eq. 4.14 is fairly close to h_f for empty tubes.

Ersoy (1969) studied the effect of mass injection rate on the heat transfer of hot-water displacement in unconsolidated sandpacks. He observed that the heat efficiency of hot-water displacement decreased with mass injection rate. Crichlow (1972) also observed the same rate effect on hot-water displacement. He considered this effect to be the result of the increase of the heat transfer coefficient at the tube wall with the mass injection rate. He calculated this coefficient from his experimental results and gave the following correlation:

$$h_f = 2.6 \dot{m}^{1.87} \quad (4.15)$$

Arihara (1975) investigated the rate effect on hot-water displacement in synthetic and Berea sandstones. His data showed that the overall heat transfer coefficient (U) of the insulation increased with the mass injection rate. Atkinson (1977) analyzed Arihara's data and calculated the heat transfer coefficients. He concluded that the heat transfer coefficients calculated by using Arihara's results were consistent with those reported by Crichlow and that there was no significant effect of particle size on the heat transfer coefficient when synthetic and Berea cores were used. There is insufficient data available to find a proper correlation for the heat transfer coefficient for cores normally used in thermal recovery experiments. Equation 4.15 suggests that the heat transfer coefficients for cores are different from those predicted by Eq. 4.14. In general, empirical correlations should not be used in the range where no experimental data are available.

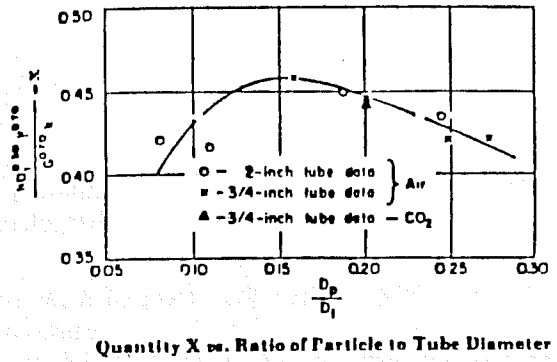
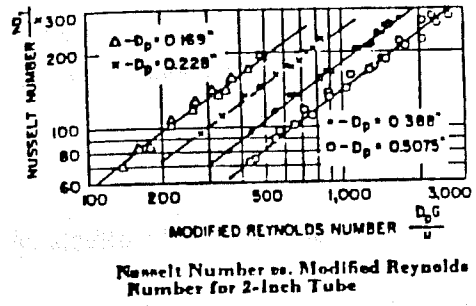
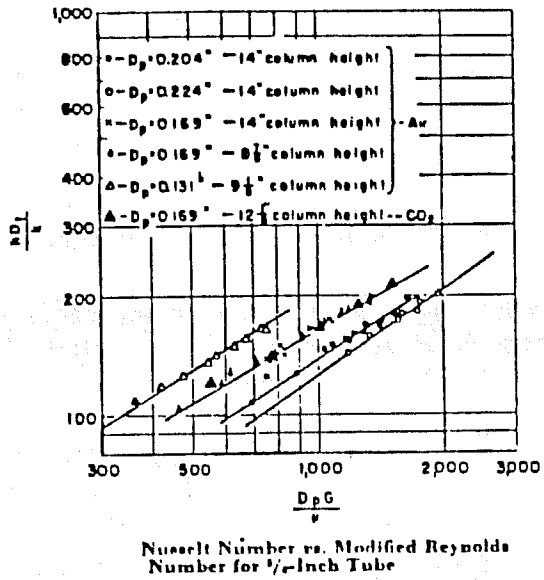


Fig. 4.3 Effect of Particle Size on Wall/Bed Heat Transfer Coefficient.

The heat transfer coefficient for convection with phase change is significantly higher than that without phase change. Data on heat transfer coefficients of condensing steam in packed beds are scarce. Crichlow (1972) and Arihara (1975) reported overall heat transfer coefficients of their model during steam injection. The heat transfer coefficients of condensing steam at the tube wall can be evaluated from the overall heat transfer coefficient. Due to the limited data and errors in this type of experiment, the h_f was not evaluated, but it was likely very large. Nevertheless, data on h_f of condensing steam inside empty tubes can provide information about the magnitude of h_f to be expected when steam is flowing in a sandpack. Akers, Deans and Crosser (1959) gave the following correlation for evaluating h_f of condensing steam inside empty horizontal tubes:

$$N_u = 5.03R_e^{\frac{1}{3}}P_r^{\frac{1}{3}} \quad R_e < 5 \times 10^4 \quad (4.16)$$

where

$$\begin{aligned} N_u &= h_f D_t / k_t, \\ R_e &= D_t \dot{m}_E / k_t, \\ P_r &= C_p \mu / k_t, \\ \dot{m}_E &= \dot{m}_l + \dot{m}_g \left[\rho_l / \rho_g \right]^{0.5}. \end{aligned}$$

All fluid properties are evaluated at the average film temperature. One can notice that the Nusselt number is proportional to the Reynolds number and is independent of temperature difference. The following example gives the lower limiting value of the Biot modulus encountered in steam flow.

Example: Saturated steam of 355°F (179°C) flows through a 2 in. (0.051 m) I.D.

horizontal tube at 26 lb_m/hr·ft² (0.035 kg/s·m²). The average film temperature is 350°F (177°C) and the average quality of flowing steam is 0.5. The density of steam is 0.3 lb_m/ft³ (4.8 kg/m³). Various properties of water are given as:

T (°F)	μ (lb _m /hr · ft)	k (Btu/hr · ft · °F)	ρ (lb _m /ft ³)	P_r
350	0.378	0.391	55.6	1.02

$$\dot{m}_E = 13.0 + 13.0 \left[\frac{55.6}{0.30} \right]^{0.5} = 190.0 \text{ lb}_m/\text{hr} \cdot \text{ft}^2 \quad (0.26 \text{ kg/s} \cdot \text{m}^2)$$

$$R_e = \frac{(2/12)(190.0)}{0.38} = 83.8$$

$$N_u = (5.03)(83.8 \times 1.02)^{1/3} = 22.2$$

$$h_f = \frac{22.2 \times 0.39}{(2/12)} = 52.0 \text{ Btu/ft} \cdot \text{hr} \cdot \text{°F} \quad (295 \text{ W/ m}^2 \cdot \text{°K})$$

If the tube is surrounded by an insulation material with thermal conductivity of 0.036 Btu/ft·hr·°F (0.062 W/m²·°K), the Biot modulus is 241. The presence of noncondensable gases in steam can reduce this heat transfer coefficient.

4.3.1.2. Modified Biot Modulus

When the boundary conditions used for the heat loss are convection-conduction types as indicated in Eqs. 4.4 and 4.7, the Biot modulus is the number which measures the relative importance of convection and conduction at each boundary. A modified Biot modulus is defined as:

$$B_j = h_{ff} r_{i+1} / k_S \quad (4.17)$$

where

- i = layer number,
- j = boundary number,
- h_{ff} = heat transfer coefficient at the inner ($j = 1$) or outer ($j = 2$) boundary,
- r_{i+1} = radius of the inner ($i = 0$) or outer boundary,
- k_S = thermal conductivity of the reference layer.

This modified Biot modulus is directly proportional to the heat transfer coefficient and radius of the boundary, and is inversely proportional to the thermal conductivity. Equation 4.17 is a convenient definition of Biot modulus for composite systems. For systems with a common reference layer, this Biot modulus does not vary with the thermal conductivity of the inner or outer layer. By using this definition, Eq. (4.11) can be rewritten as:

$$2\sigma X_D = \ln r_{3D} - \ln r_{2D} + \frac{\ln r_{2D}}{\lambda_D} + \frac{1}{B_1} + \frac{1}{B_2} \quad (4.18)$$

In the following section, various parameters which affect the movement of heat front are to be discussed. The values of these parameters for the base case are listed in Table 4.1, which are for the bench model used in this study. For each case, only one parameter is varied while other parameters remain the same as those for the base case.

4.3.1.3. Effect of Variation in Biot Modulus

Figure 4.4 shows the effect of Biot modulus at the inner boundary (B_1) on the heat frontal movement. Except for the Biot modulus, values of other dimensionless parameters are as listed in Table 4.1. The heat front moves faster when the Biot number is small because the rate of heat loss is small. The effect of the Biot modulus may be neglected when the Biot number is greater than 100. In other words, the inner boundary condition can be treated as a constant-temperature one and the effect of mass injection rate on the heat frontal movement is negligible if B_1 is greater than 100. Both the Marx and Langenheim equation, and the Lauwerier solution are independent of mass rate because the models use the constant-temperature boundary condition. As discussed before for steam injection, the Biot modulus is greater than 100 and no effect of mass rate is expected. However, for single-phase non-isothermal fluid flow through porous media, the process is dependent on rate because the Biot modulus is normally much less than 100.

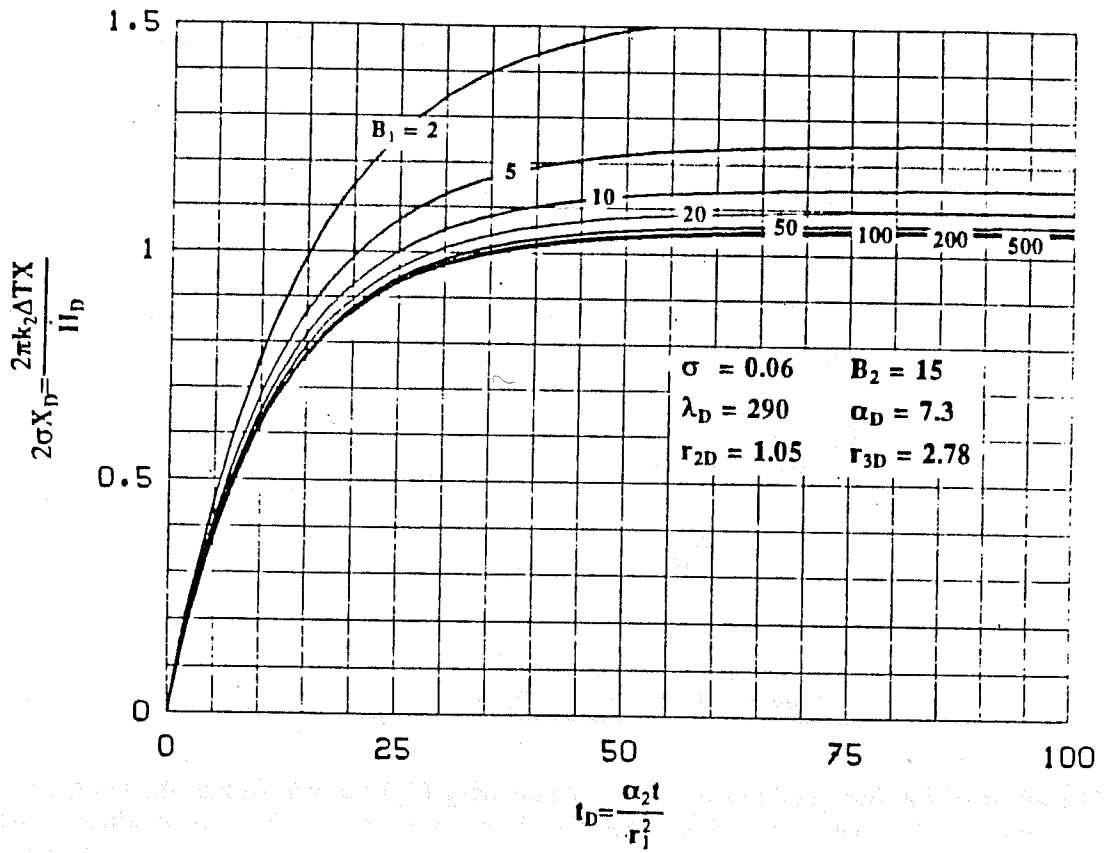


Fig. 4.4 Effect of Biot Number at Inner Boundary on Heat Frontal Movement.

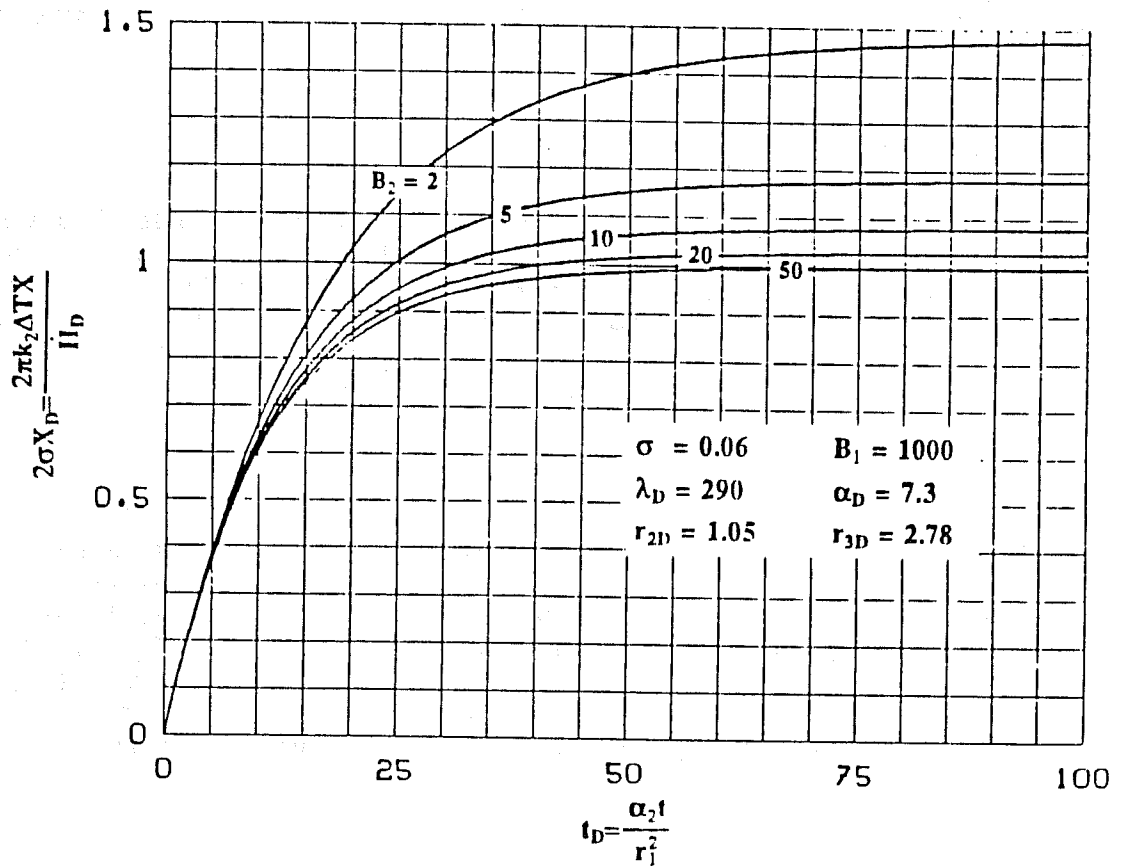


Fig. 4.5 Effect of Biot Number at Inner Boundary on Heat Frontal Movement.

TABLE 4.1 PHYSICAL PROPERTIES OF SANDPACK AND INSULATION

Sandpack	
Diameter (m)	0.0546
Length (m)	1.83
Porosity	0.35
Permeability (Darcy)	5.0
Stainless Steel (#321) Tube	
Thickness (m)	0.001245
Fiberfrax (Insulation)	
Thickness (m)	0.0508
Dimensionless Parameters	
Radius Ratio:	
Inner Layer (r_{2D})	1.05
Outer Layer (r_{3D})	2.78
Biot Modulus:	
Inner Boundary (B_1)	1000
Outer Boundary (B_2)	15
Diffusivity Ratio (α_D)	7.3
Conductivity Ratio (λ_D)	290.0
Volumetric Heat Capacity Ratio (σ)	0.06

The effect of the Biot modulus at the outer boundary (B_2) on heat frontal movement is shown in Fig. 4.5. When t_D is smaller than 5, the solution is not affected by the Biot modulus. When t_D is greater than 5, the effect of this coefficient becomes apparent. The heat front develops faster at smaller B_2 . When this number is less than 20, the effect of B_2 is significant. In the laboratory, the heat transfer coefficient varies from 1.0 to 5 Btu/ft-hr-°F depending on the operating conditions. The corresponding Biot modulus may vary from 2 to 20 and its effect on heat frontal movement is not negligible.

4.3.2. Conductivity Ratio (λ_D)

The conductivity ratio between the stainless steel and the insulation can affect both the transient and the steady-state solutions. However, its effect on the steady-state solution is small when the inner layer is thin, as was the case of the laboratory system used, and as indicated by Eq. 4.18. Its effect on the transient solution is shown in Fig. 4.6. The larger this ratio the more slowly the heat front advances. Because the highly conductive inner layer increases the temperature at the interface between the stainless steel and the insulation, the rate of heat loss increases.

4.3.3. Thermal Diffusivity Ratio

Thermal diffusivity determines how fast the temperature front moves and the thickness of the medium determines the duration of the transient behavior. The diffusivity ratio is the ratio of thermal diffusivity of the inner layer to that of the outer layer (the conductivity ratio over the volumetric heat capacity ratio). For a constant conductivity ratio, the diffusivity ratio is only dependent on the volumetric heat capacity ratio. Figure 4.7 shows the effect of the thermal diffusivity ratio (volumetric heat capacity ratio) on movement of the heat front. The steady-state solution is not affected by this ratio. This ratio is small when the volumetric heat capacity of the inner layer is large. The effect of this larger heat capacity is to make the heat front move more slowly.

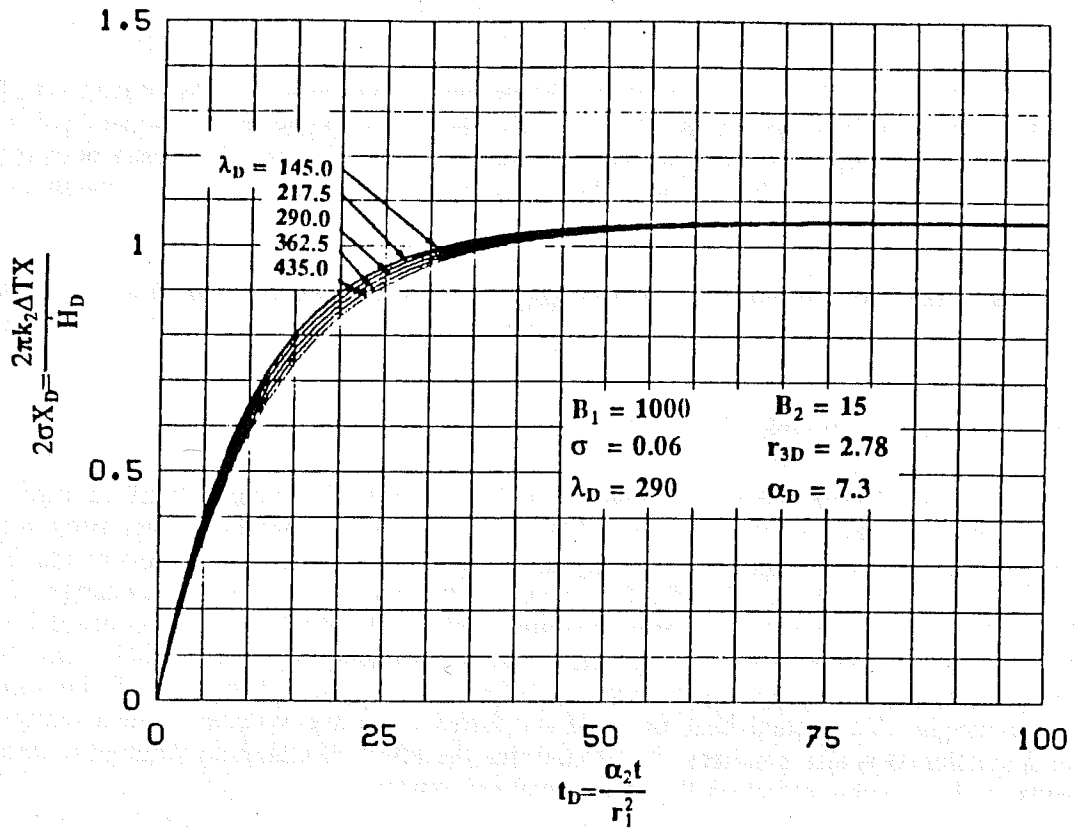


Fig. 4.6 Effect of Conductivity Ratio on Heat Frontal Movement.

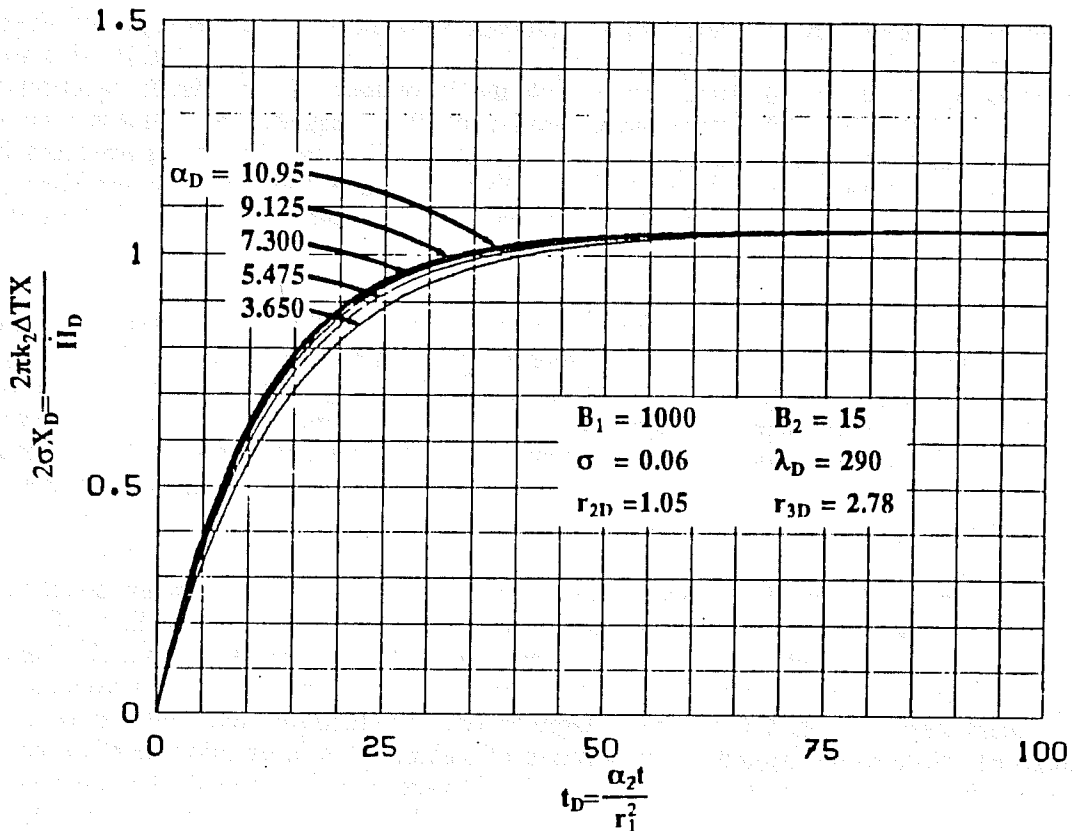


Fig. 4.7 Effect of Thermal Diffusivity Ratio on Heat Frontal Movement.

4.3.4. Thicknesses of Inner and Outer Layers (r_{2D} and r_{3D})

Figure 4.8 shows the effect of the thickness of the inner layer (r_{2D}) on the movement of the heat front. In this case, both the thermal conductivity and the heat capacity of the inner layer are larger than those of the outer layer. Increasing the thickness of the inner layer increases both the thermal conductivity and the heat capacity of the system and hence slows down the movement of the heat front.

In Fig. 4.9, the effect of the outer radius (r_{3D}) is shown while the dimensionless outer radius varies from 2 to 50. Increasing the outer radius increases the length of time for transient behavior.

4.3.5. Volumetric Heat Capacity Ratio (σ)

Volumetric heat capacity ratio (σ) is defined as the volumetric heat capacity of the insulation over the volumetric heat capacity of the reservoir. This ratio changes the transient heat front solution but not the steady-state solution. Figure 4.10 shows the effect of σ on heat frontal movements for σ varying from 0.045 to 0.075. The smaller the σ , the slower the heat front moves. A change of σ can be caused by a change of the volumetric heat capacity of either the sandpack or the insulation. Figure 4.10 directly represents the case of varying volumetric heat capacity of the sandpack. For the case of varying the volumetric heat capacity of the insulation, the thermal diffusivity of the insulation is changed accordingly. The actual heat front moves faster when the volumetric heat capacity of the insulation is smaller (σ is also smaller). It is found that the effect of changing volumetric heat capacity of the insulation has a small effect on the heat frontal movement.

4.3.6. Single Layer Approximations

In the 1970's, when the multidimensional thermal simulators for steam injection first became available, researchers (Coats *et al.* 1974, Shutler 1970 and Weinstein *et al.* 1977) tried to validate their simulators by matching simulated results with the laboratory data of steam injection given by Willman *et al.* (1961). The laboratory model used could be considered as a linear core with two layers of insulation: a steel plus lead layer and an insulation. The calculations of heat loss in insulations were handled differently by some researchers. Shutler lumped the steel plus lead layer with the insulation layer; Coats *et al.* lumped the steel plus lead layer into the core; and Weinstein *et al.* considered this layer separately.

In Fig. 4.11, four curves represent solutions of heat front for the model used in this study handled in four different ways. Curve 1 is the solution for a single-layer model which neglects the stainless-steel layer; Curve 2 is the solution for a lumped single-layer model in which the volumetric heat capacity of the stainless steel is lumped into the insulation (lumped-one-layer I); Curve 3 is the solution for a two-layer model given by Eq. 4.9 ; and Curve 4 is the solution for a lumped single-layer model in which the volumetric heat capacity of the stainless steel is lumped into the sandpack (lumped-one-layer II).

The heat front for the one-layer model moves faster than that for the two-layer model because the stainless-steel layer increases both the transient and the steady-state rates of heat loss. The heat front of the lumped-one-layer I model moves a little more slowly than the one-layer model. This indicates that the heat capacity of the insulation has only a small effect the heat frontal movement. Provided that the stainless steel layer is thin and has a large thermal conductivity, the temperature of this layer quickly becomes close to the saturation temperature of steam. This layer may therefore be treated as part of the sandpack and the system becomes the lumped-one-layer II model. The heat front of this lumped one-layer II model moves a little more slowly than the front of the two-layer model during the

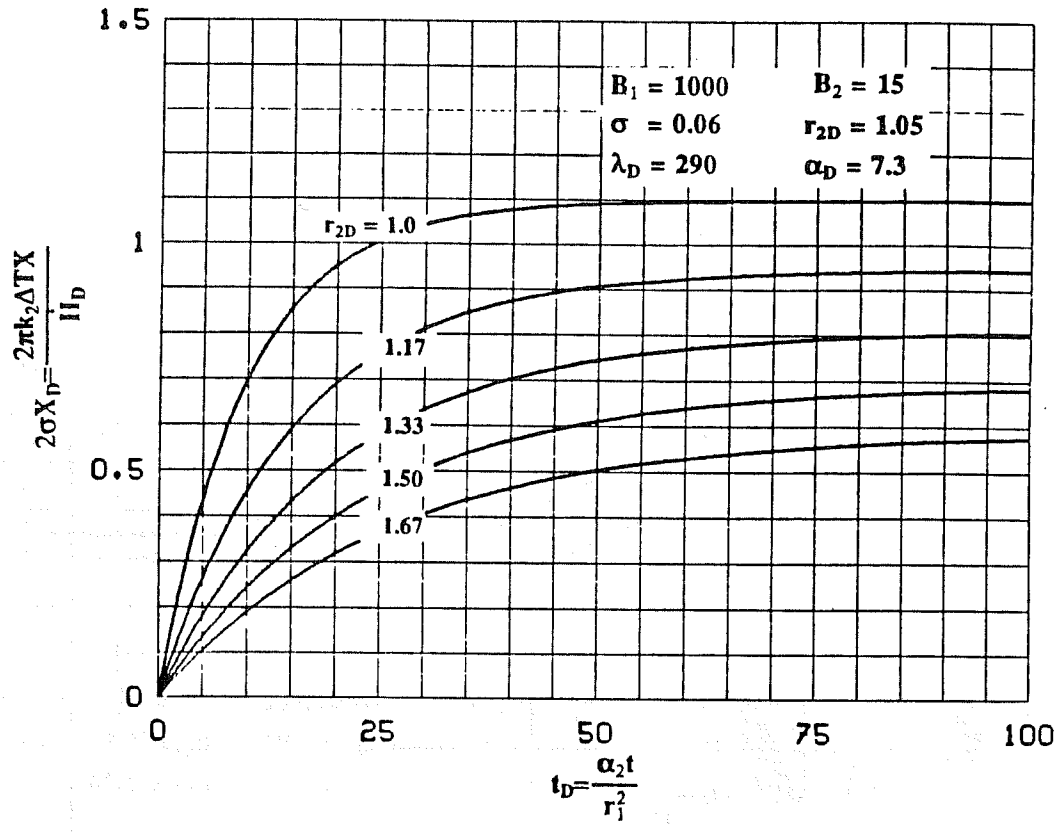


Fig. 4.8 Effect of Thickness of Inner Layer on Heat Frontal Movement.

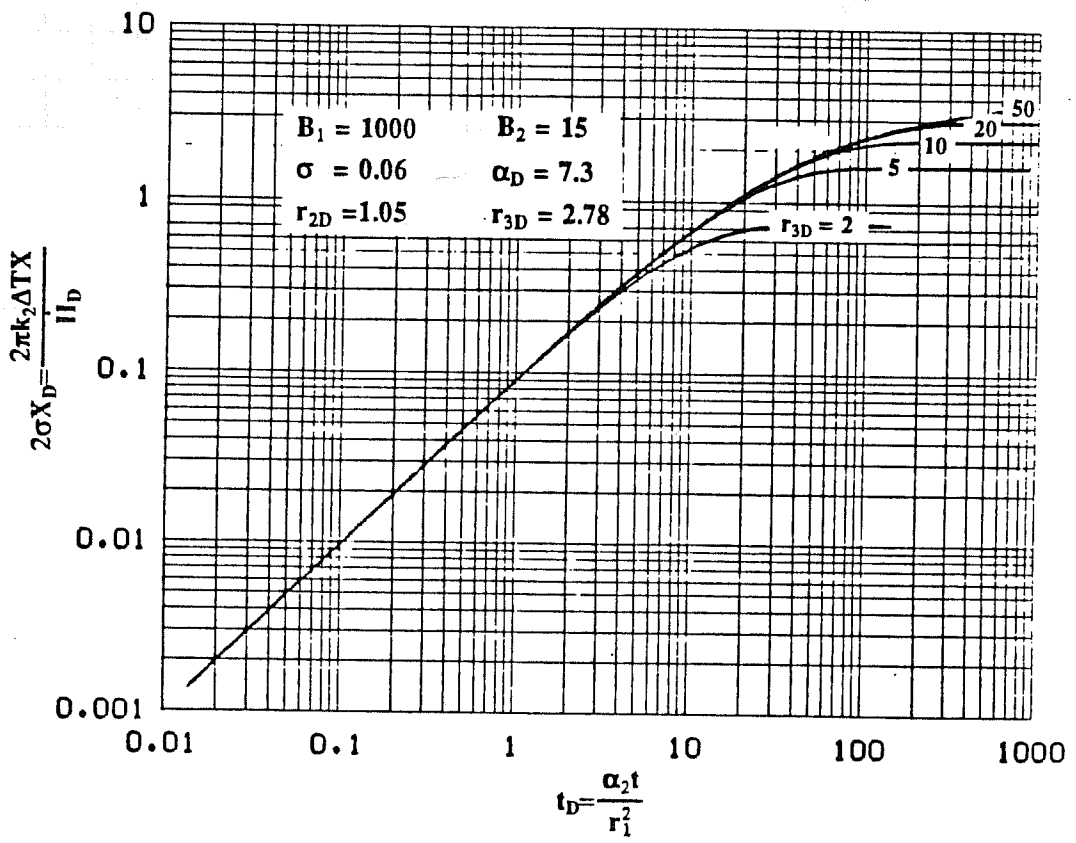


Fig. 4.9 Effect of Radius of Outer Layer on Heat Frontal Movement.

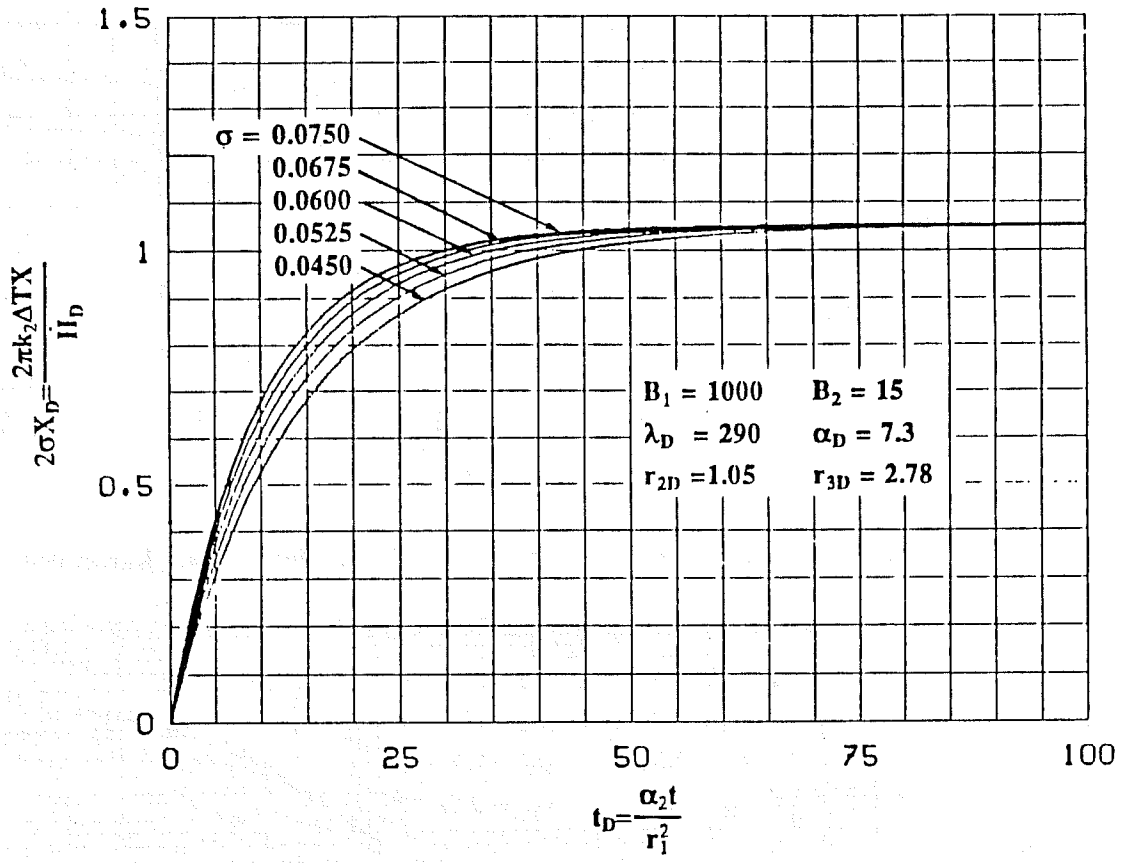


Fig. 4.10 Effect of Volumetric Heat Capacity Ratio on Heat Frontal Movement.

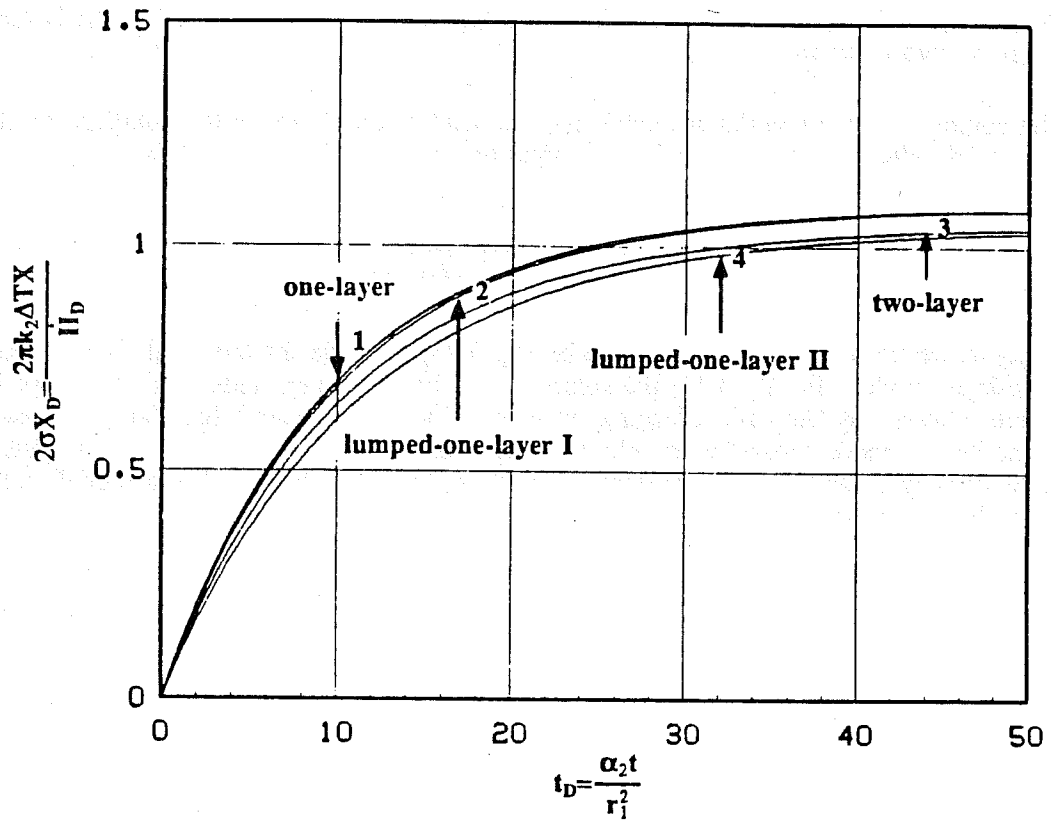


Fig. 4.11 Comparison of Heat Frontal Movements Among One-Layer, Two-Layer One-Lumped-Layer I and One-Lumped-Layer II Models.

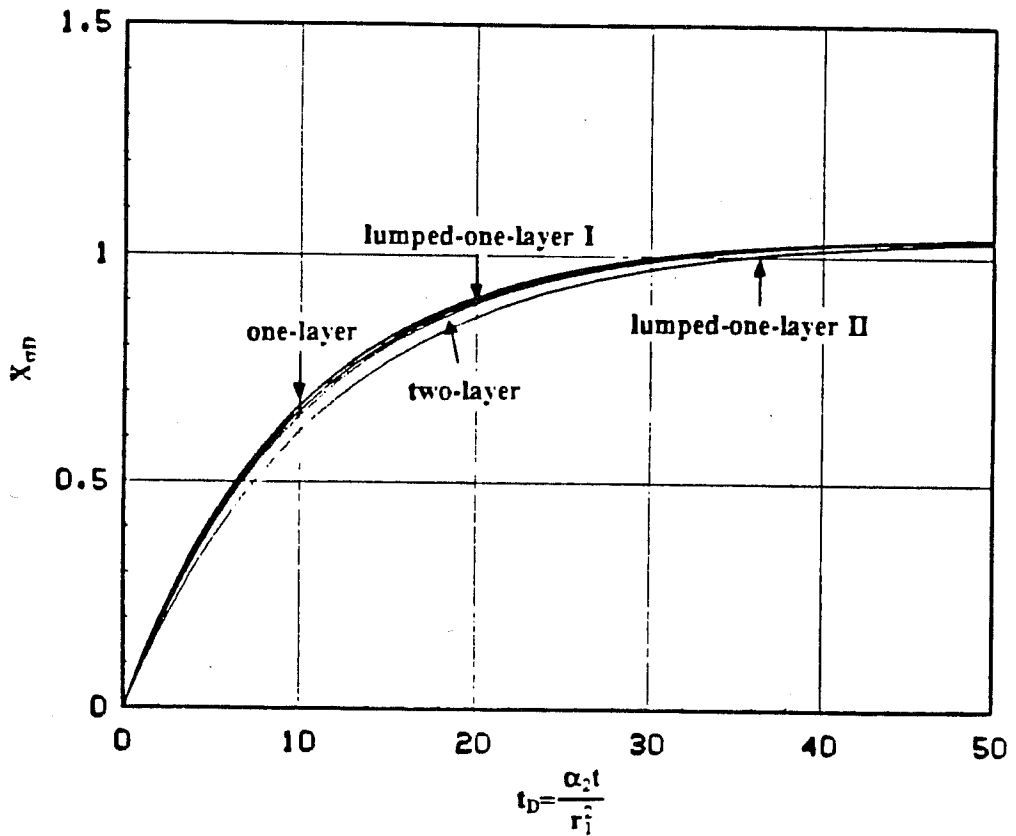


Fig. 4.12 Single-Layer Approximation For the Two-Layer Models.

transient flow period because the volumetric heat capacity of the sandpack for the lumped model is larger than the two-layer one.

The solution for a single-layer model may be used to approximate the solution for the two-layer model by multiplying the ratio of steady-state solutions between the two models:

$$X_{\sigma D} = (2\sigma X_D)_1 \frac{(2\sigma X_{DSS})_2}{(2\sigma X_{DSS})_1} \quad (4.19)$$

where X_{DSS} is the steady-state solution given by Eq. 4.18, 1 stands for the single-layer model and 2 for the double-layer model. In Fig. 4.12, the solutions for the one-layer model and the lumped-one-layer I model were adjusted by the ratio of steady-state solutions. It is clear that, for the present case, the lumped-one-layer I model provides the closest approximation to the actual two-layer system and even the simple one-layer model can approximate the heat front of the two-layer model better than the lumped-one-layer II model.

5. APPARATUS AND EXPERIMENTAL PROCEDURE

This section is a description of the apparatus, the materials and their properties, and the experimental procedures.

5.1. DESCRIPTION OF APPARATUS

The cylindrical model was designed to conduct steam injection with and without surfactants. It consisted of a fluid injection system, a linear sandpack, a data monitoring system and a fluid production system (see Fig. 5.1).

5.1.1. Fluid Injection System

Two Constametric Model III pumps were used to pump fluids into the sandpack. Each pump had two displacement pistons with a 180 degree phase difference between them. Thus, the pulses were reduced to the minimum. Their rates were constant within the range of 0-41.25 MPa (0-6000 psig). The original 10^{-5} m (10 micron) stainless steel filter at the suction end was replaced by a 8×10^{-6} m (8 micron) in-line paper filter that could be changed after each experiment.

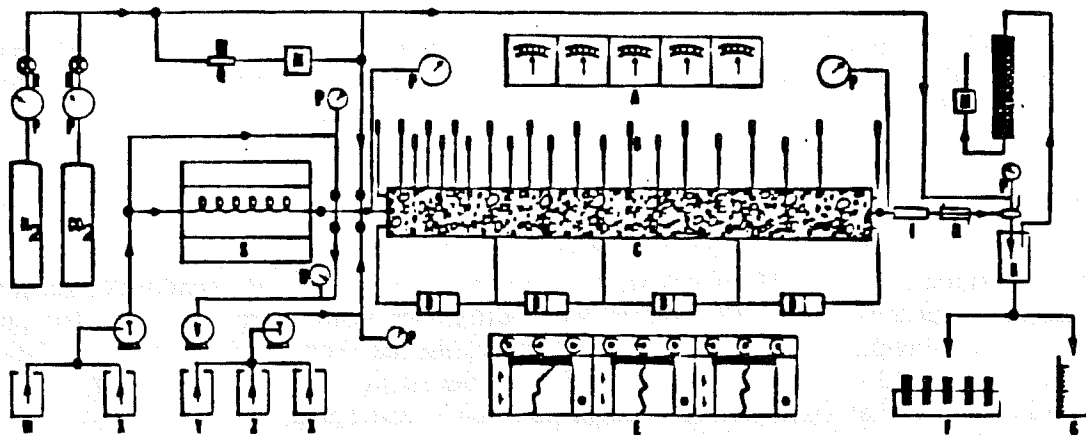
For steam-displacement experiments, steam was generated by a tubular furnace (Marshall Model #1056) containing a coiled tube 3.35 m (11 ft) long and 0.00635 m (1/4 in.) O.D.. A steam bypass line was used during the time when the furnace was being heated before steam was injected into the sandpack, or during the interim when cold surfactant slugs were injected. Heating tape was normally used to compensate for the heat loss along the injection line. The dead volume of the injection line was about $7.5 \times 10^{-6} \text{ m}^3$ (7.5 cm^3).

Either nitrogen or carbon dioxide could be injected through the gas injection line either singly or with steam or surfactant solutions. Carbon dioxide could also be used for cleaning purposes. The whole system could be evacuated through the vacuum line when necessary. In general, vacuum was only needed with a newly packed dry sandpack.

5.1.2. Linear Sandpack

The linear model includes a horizontal, cylindrical sandpack and layers of insulation. A stainless steel tube [SS #321, 1.83 m (6 ft) long and 0.057 m (2.25 in.) O.D. with 1.25×10^{-3} m (0.049 in.) wall thickness] was packed with commercially-graded Ottawa sand. The tube was horizontally placed on a frame. Layers of the insulating material (a fibrous aluminum-silica mixture from Fiberfrax) were wrapped around the tube. As shown in Fig. 5.2, 21 thermocouples [$1.6 \text{ mm} + 1 \times 10^{-3}$ m (1/16 in.) O.D., from Conax] were mounted on the tube to measure the temperatures along the sandpack. For most experiments, thermocouples were located in the center of the tube; for the remaining experiments thermocouples were located alternately at the center and at 0.013 m (0.5 in.) from the top of the core as Fig. 5.2 indicates. Five pressure taps were located along the tube at 0.41, 0.82, 1.32 and 1.83 m (16, 32, 52 and 72 in.) distances starting from the inlet.

Two flanges were used at the ends of the tube. Each flange was made of two pieces of 0.089 m \times 0.0143 m (3.5 in. \times 9/16 in.) stainless steel bar. One was welded on the stainless tube and the other was bolted to it and sealed with a brass O-ring. The three lines attached to the flange were the fluid intake, the thermocouple and the pressure tap.



- | | |
|--------------------------------------|---|
| A: temperature controllers | N: nitrogen cylinder |
| B: thermocouples | O: carbon dioxide cylinder |
| C: sandpack | P: pressure gauge |
| D: pressure transducers | Q: gas flow controller |
| E: recorders | R: gas flow regulator |
| F: fraction collector | S: steam generator |
| G: graduated cylinder | T: pump |
| H: heat exchanger (condenser) | U: vacuum gauge |
| I: sight glass | V: vacuum pump |
| J: backpressure regulator | W: water container |
| K: gas/liquid separator | X: cleaning fluid |
| L: moisture drier | Y: oil container |
| M: gas flow meter | Z: surfactant solution container |

Fig. 5.1 Schematic Diagram of Steam Displacement Apparatus.

5.1.3. Fluid Production System

The main components of the fluid production system were a sight glass, a condenser, a backpressure regulator and a fraction collector. The sight glass was used to observe the emulsion and the steam/foam coming from the sandpack. The backpressure was controlled by a diaphragm type backpressure regulator (Grove Valve and Regulation Co., Model 591W).

The fluids produced were collected by a fraction collector (Buchler, Model Fractomette Alpha 200). A volume control unit, operating on the siphon principle, was used to give a fairly constant volume of production for each tube. A brine-containing cell with two metal wires was used to provide signals when the unit siphons the fluid to the collecting tube.

5.1.4. Data Monitoring System

The data monitoring system was composed of strip chart recorders and a computer monitored recording system. Temperatures along the sandpack were measured by thermocouples and recorded by a 24 channel strip chart recorder (Leeds and Northrop, Speedomax). Pressure data were measured by transducers (Celesco, Model #KP-15). Signals from transducers were transformed into 0-10 volt DC outputs through carrier demodulators (Celesco, CD10B). The voltage outputs were recorded by two three-pen strip chart records (Soltec, Model #1253). Recorders were also connected with the fraction collector to synchronize the production and pressure data utilizing an event marker. When the collector switched the tubes, a pulse of 1.5 volts from a battery was given to each pen through a relay.

The above system of recorders served as a supplemental system to a computerized recording system. Both temperature and pressure output were connected with a data logger. The data logger converted the analog data into digital form and transmitted them to a Tektronics 4054 computer. After each experiment, the recorded data were transferred into a VAX 11/750 computer. For each pressure drop measurement, two sets of transducers with 5 and 100 psi (0.034 and 0.688 MPa) diaphragms were used in parallel. A switch was linked to give controlling signals of zero or 1.5 volts indicating whether the 5 or 100 psi diaphragm was in use.

5.2. MATERIALS AND THEIR PROPERTIES

Materials used in this study were distilled water, steam, white mineral oil (Kaydol), Suntech IV, Ottawa sand, and Fiberfrax insulation. Density and viscosity of Kaydol, as well as the surface tension of Suntech IV were measured. Properties of saturated water and steam were obtained from the literature (Keenan and Keyes, 1967; Hilsenrath and Touloukian, 1954). All equations used to calculate the physical properties such as density, viscosity, heat capacity, enthalpy and thermal conductivity are listed in Appendix D.

5.2.1. Water and Steam

In most experiments, distilled water was used and steam was generated from distilled water. The viscosities and kinematic viscosities of water and steam versus temperature are presented in Figs. 5.3 and 5.4. The ratios of viscosities and kinematic viscosities between oil and steam, oil and water, and water and steam versus temperature are shown in Figs. 5.5 and 5.6. Water and steam in these figures represent saturated water and saturated steam. The solid lines were calculated by the equations in Appendix D. The difference between the viscosity and the kinematic viscosity of steam is tremendous. When the temperature was less than 204°C (400°F), the kinematic viscosity of steam was greater than

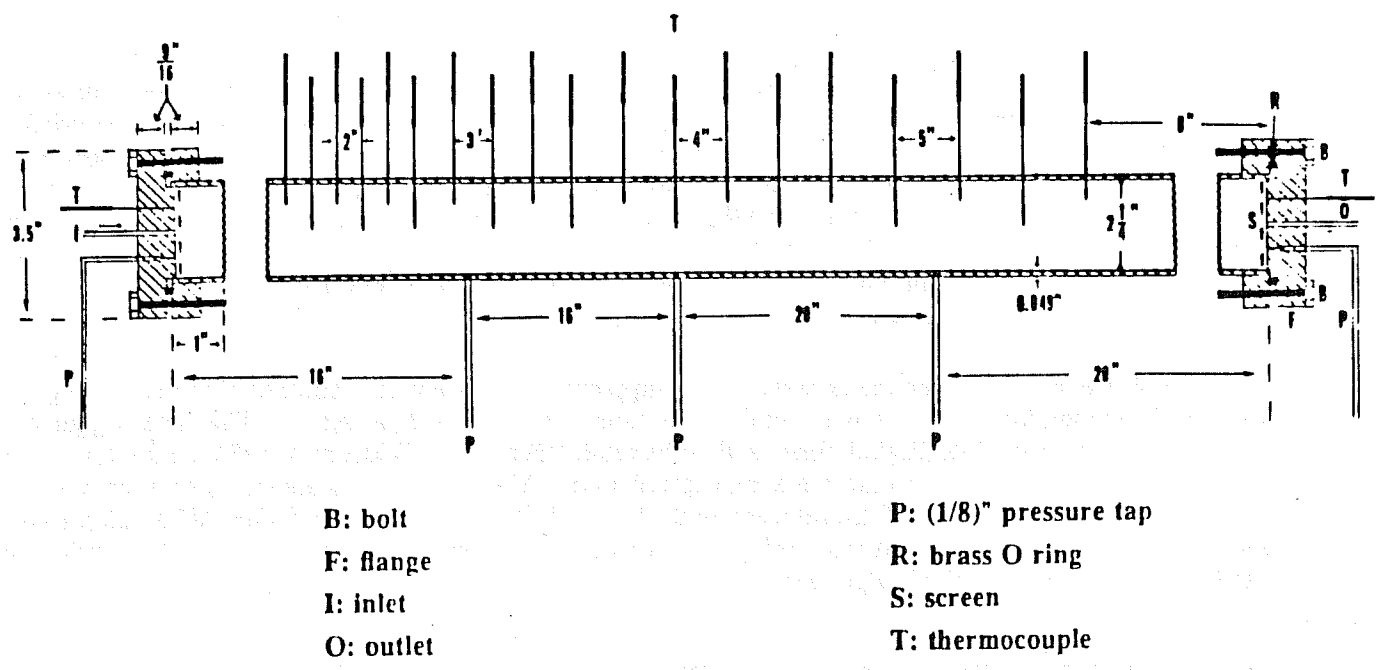


Fig. 5.2 Stainless-Steel Sandpack Holder.

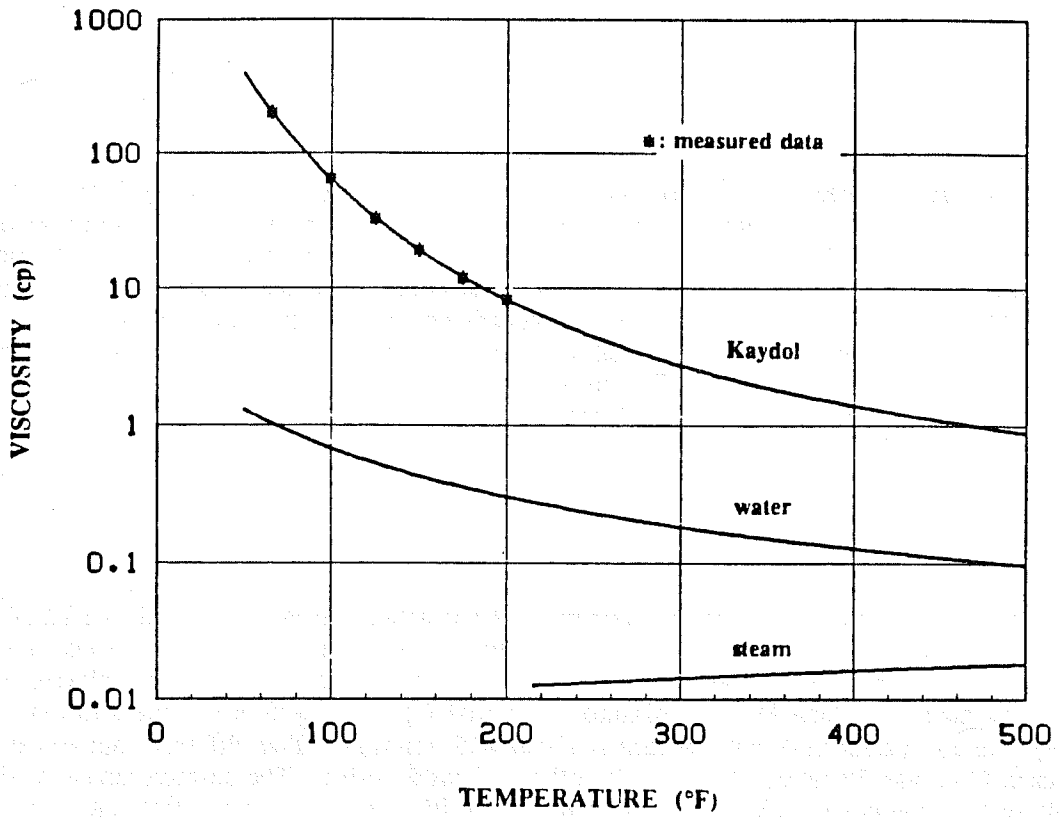


Fig. 5.3 Viscosities of Kaydol, Water and Steam vs Temperature.

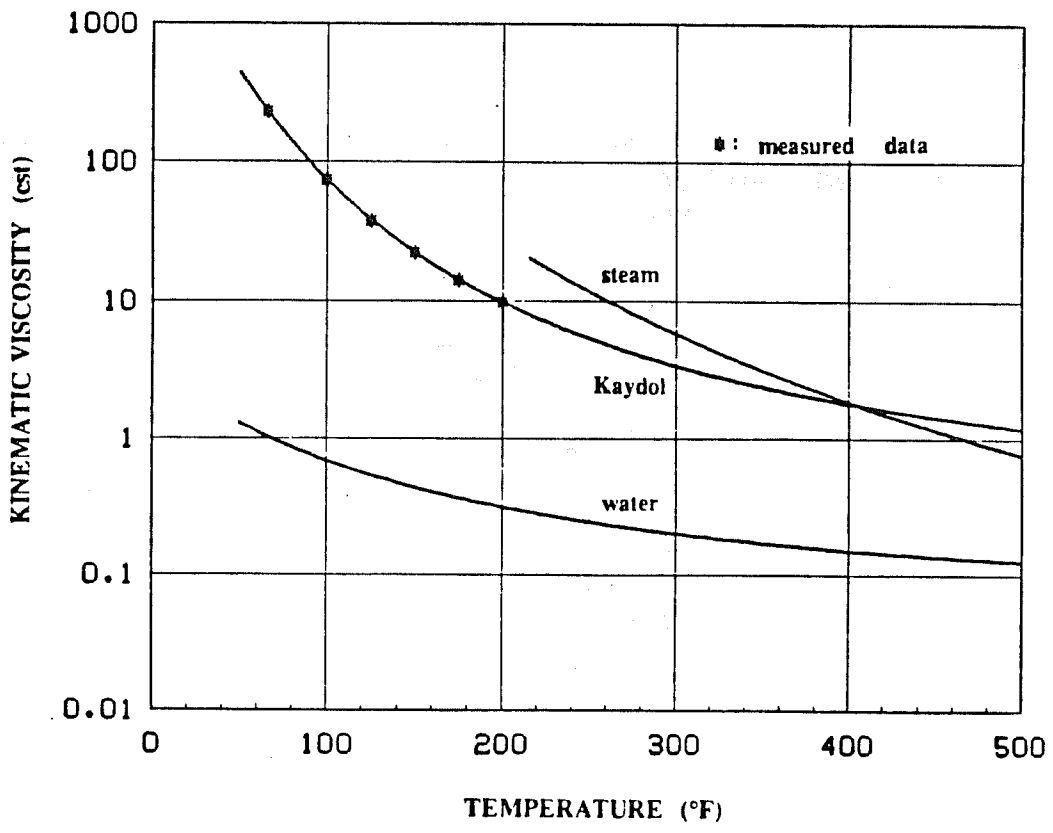


Fig. 5.4 Kinematic Viscosities of Kaydol, Water and Steam vs Temperature.

that of Kaydol. In general, in steam drive, it is the kinematic viscosity which affects the mobility (Prats, 1982).

5.2.2. Kaydol

Kaydol is a refined white mineral oil with a density of 865.5 kg/m^3 and a viscosity of $0.070 \text{ Pa}\cdot\text{s}$ (70 cp) at 37.8°C (100°F). The density and viscosity of Kaydol were measured at temperatures up to 90.5°C (195°F) at atmospheric pressure. The viscosity was measured by the Brookfield spindle viscometer with a constant-temperature thermal cell. The measured density data were fitted to Eq. D.1 in Appendix D, with a constant thermal expansion coefficient being assumed. The measured kinematic viscosity versus temperature data were fitted to a two-parameter double-log equation (Eq. D.4 in Appendix D) as shown in Fig. 5.7. The measured viscosities and kinematic viscosities are also graphed as asterisks in Figs. 5.3 and 5.4. Viscosities at temperatures greater than 90.5°C (195°F) were extrapolated using Eq. D.4.

5.2.3. Suntech IV

Suntech IV was chosen from various commercial surfactants tested at SUPRI (Al-Khafaji 1982). It is thermally stable and possesses a good foamability. Al-Khafaji reported on various properties of Suntech IV such as adsorption on sands, the partitioning between aqueous and oleic phases, and tolerance to various salts. Suntech IV is a mixture of normal C_{15} to C_{18} plus toluene sulfonates (Malmberg, 1979). Its equivalent molecular weight is about 425 gm/mole . Two different batches of Suntech IV were used: One was 25 wt% active and the other, 15 wt% active. The surface tensions of Suntech IV from these two batches are shown in Fig. 5.8. The critical micellar concentrations were estimated to be 0.3 wt%. The interfacial tensions between Suntech IV solution and Kaydol at different concentrations and temperatures, as measured by Ahmed (1984), are shown in Fig. 5.9.

5.2.4. Sand and Insulation

Two batches of sands were used in this study: one was 80-120 mesh commercially-graded silica sand from Fisher and the other was F-140 Ottawa sand. The size distribution of F-140 Ottawa sand is listed in Table 5.1. The sand was washed and

TABLE 5.1 SIZE DISTRIBUTION OF OTTAWA SAND F-140

mesh size	cum. wt%
< 60	1.11
60-80	4.26
80-100	14.76
100-120	37.12
120-140	62.56
140-170	74.74
170-200	93.31
200-230	97.11
230-270	98.82
270-325	99.46
>325	100.00

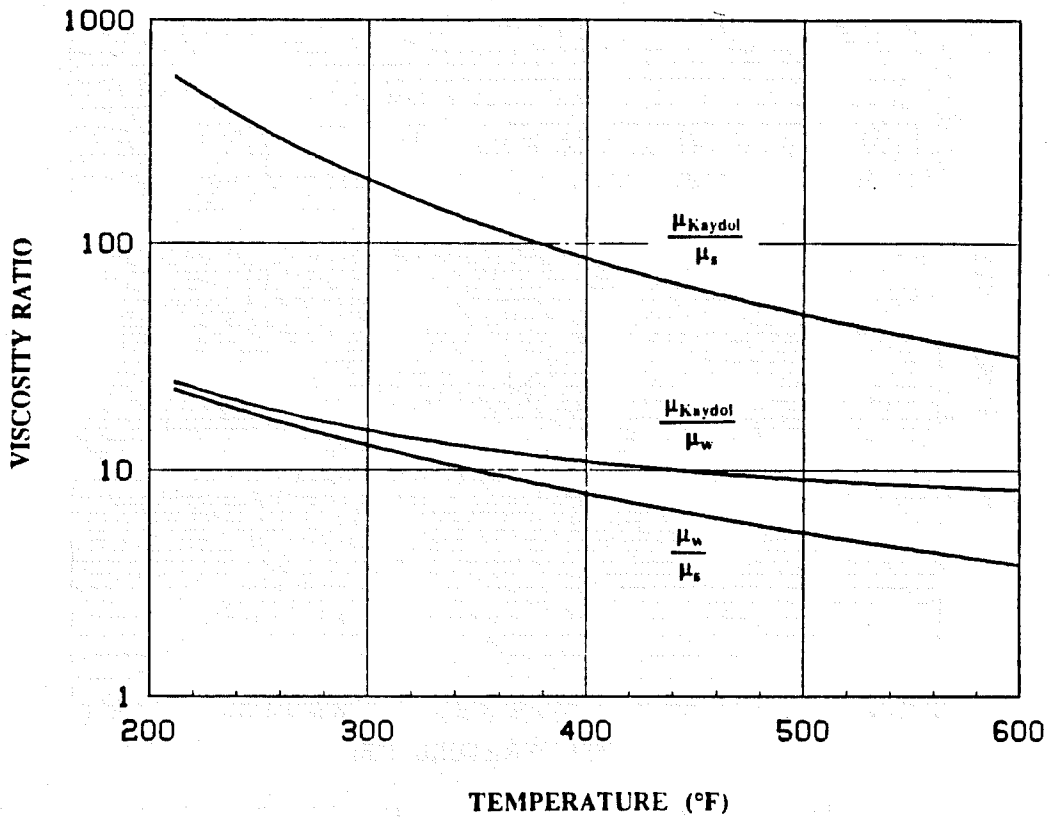


Fig. 5.5 Viscosity Ratios of Kaydol, Water and Steam vs Temperature.

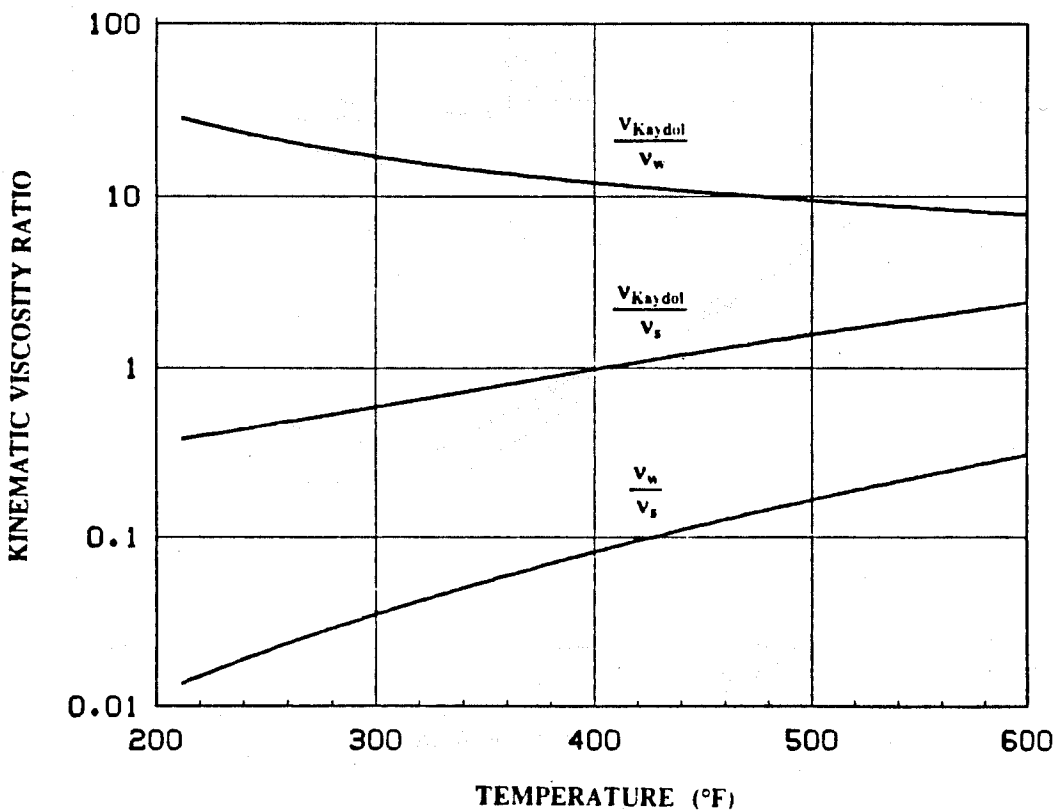


Fig. 5.6 Kinematic Viscosity Ratios of Kaydol, Water and Steam vs Temperature.

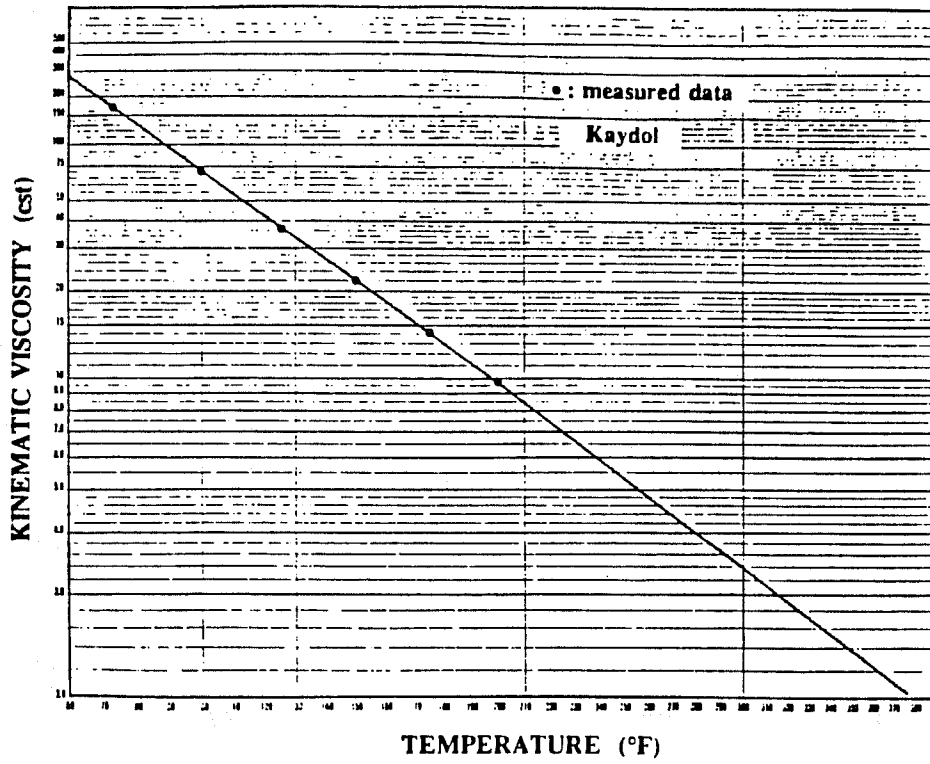


Fig. 5.7 Kinematic Viscosity of Kaydol vs Temperature.

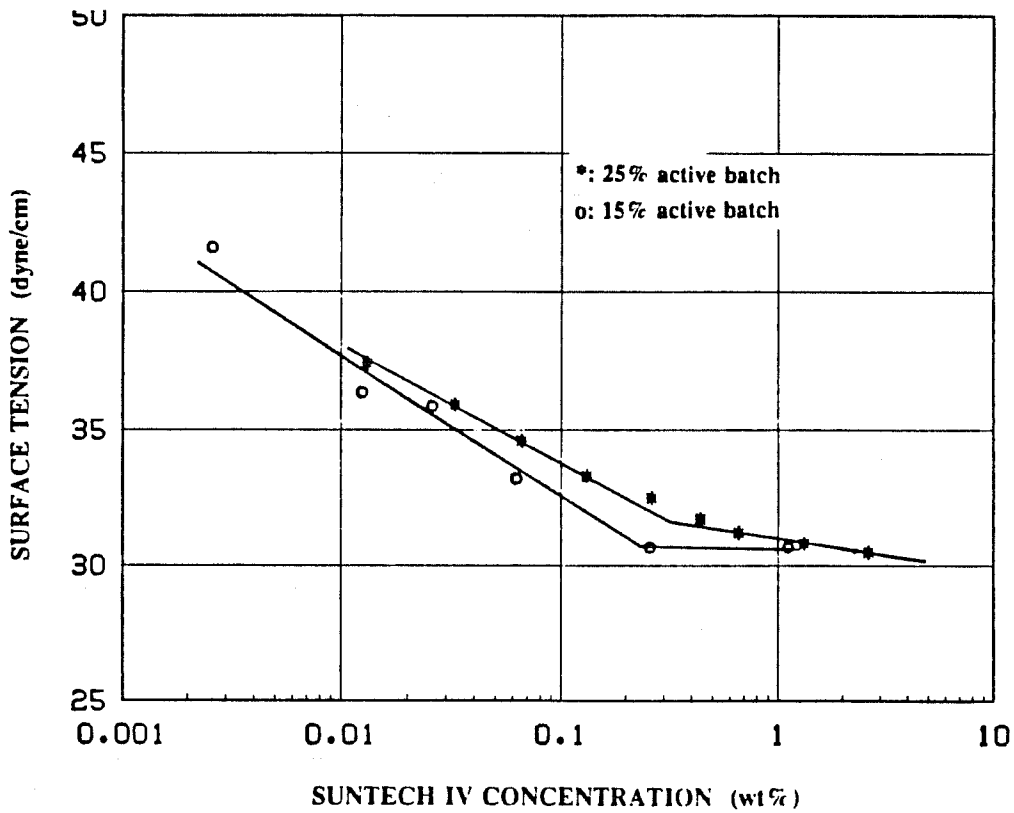


Fig. 5.8 Surface Tension of Suntech IV vs Concentration.

dried before packing. No additional sieving was attempted to narrow the size range of the sand. The porosities of sandpacks varied from 0.34 to 0.37. The water permeabilities of the sandpacks were about $5 \mu\text{m}^2$ (about 5 Darcy) for F-140 Ottawa sand and $16 \mu\text{m}^2$ (about 16 Darcy) for the 80-120 mesh sand from Fisher. The heat capacity of the sand was estimated by Eq. D.15 in Appendix D. Data used for the curve fit were given by Somerton (1958).

The Fiberfrax insulating material wrapped around the sandpack is a mixture of silica and alumina with a density of 96 kg/m^3 ($6 \text{ lb}_m/\text{ft}^3$). Its apparent thermal conductivity was estimated by Eq. 6.3 in Section 6.2.1, which was derived from laboratory experiments. This equation gives a higher value of the thermal conductivity than that reported by Turner and Malloy (1981).

5.3. EXPERIMENTAL PROCEDURES

Figure 5.10 shows a flow chart of the general experimental sequence. All experiments could be categorized into steam injection or steam injection with surfactant solution slugs. Experiments in both categories were carried out under one of the following starting conditions: 100% water saturated, water saturated with oil at S_{or} , intermediate oil saturation and oil saturated with water at S_{wr} . Most experiments were conducted with an initial condition of water saturated with oil at S_{or} .

5.3.1. Core Preparation

The sand was washed and dried before packing. Two pneumatic vibrators were strapped to expedite settling of the sand. It was found that tapping the tube wall with a soft hammer could further expedite sand settling. If the packing was done with care, no settlement of sand would occur during the experiment. The weight of packed sand was carefully measured and using the sand volume and tube volume the pore volume of the sandpack was determined. Then, the sandpack was evacuated and filled with water under vacuum. The pore volume of the sandpack was also checked by the volume of water used to fill the sandpack and the permeability to water was measured. The difference in porosity determined by two methods was normally less than one percent.

In most experiments with oil, the sandpack was oil flooded to irreducible water saturation and the oil permeability was obtained at S_{wr} at ambient temperature. Two other oil saturations were used: One was at an oil saturation after the core was flooded with two pore volumes of water, and the other was evenly distributed 60% oil saturation generated by simultaneous injection of 10% oil and 90% water.

5.3.2. Steam Displacement

In all steam displacement runs, the mass injection rate of steam varied from 7.4×10^{-3} to $3.1 \times 10^{-2} \text{ kg/s} \cdot \text{m}^2$ and the backpressure varied from atmospheric pressure to 1.31 MPa (190 psig). About half an hour was required to heat up the furnace to a temperature required to generate steam. During heating, the inlet of the sandpack was closed and the steam was circulating through the bypass line. At the same time, the band heater was used to heat the inlet flange. Slightly superheated steam was used in all steam injection experiments, thus the enthalpy of the injected steam was known. When steam was injected into the sandpack, the produced fluids were collected by a fraction collector and the time was synchronized with strip chart recorders through the event marker on the collector.

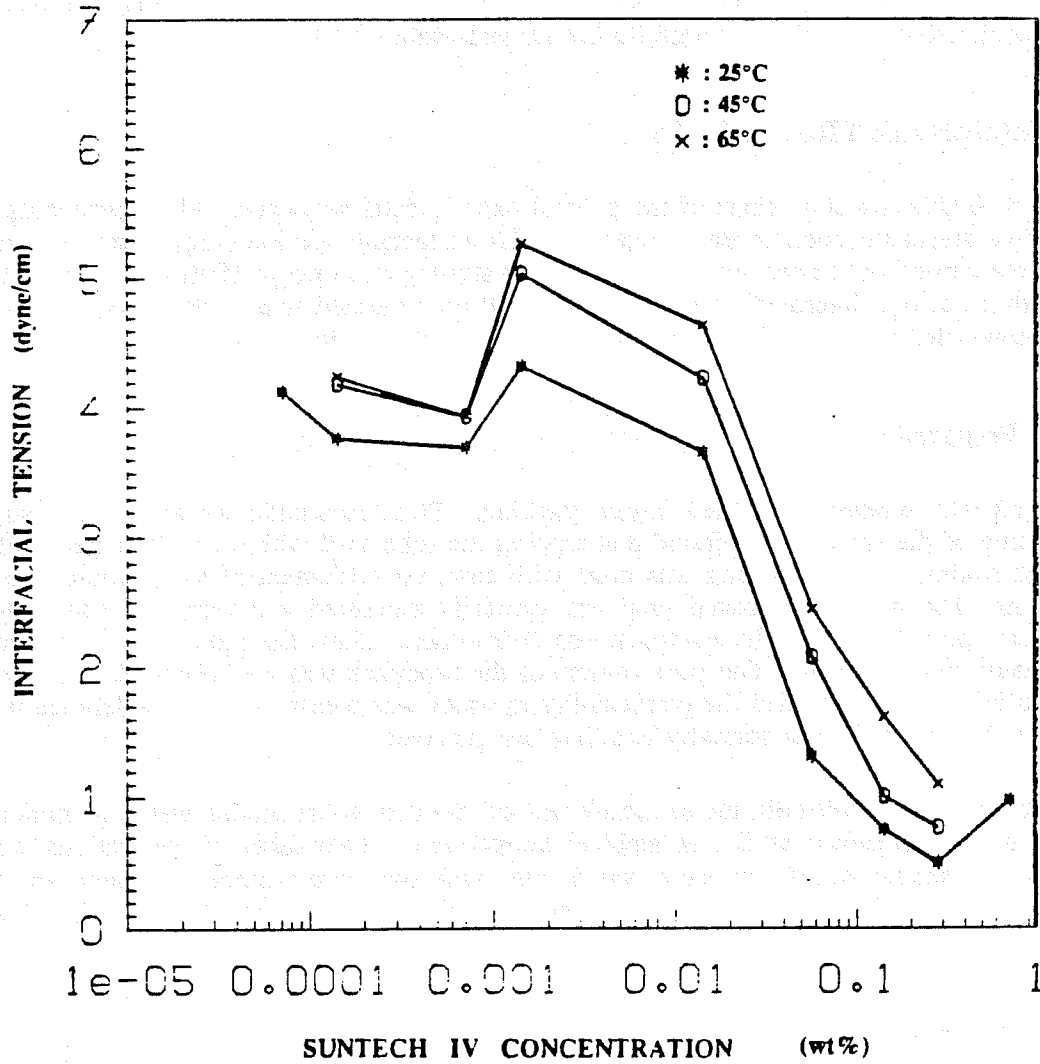


Fig. 5.9 Temperature Effect on Interfacial Tension Between Suntech IV and Kaydol.

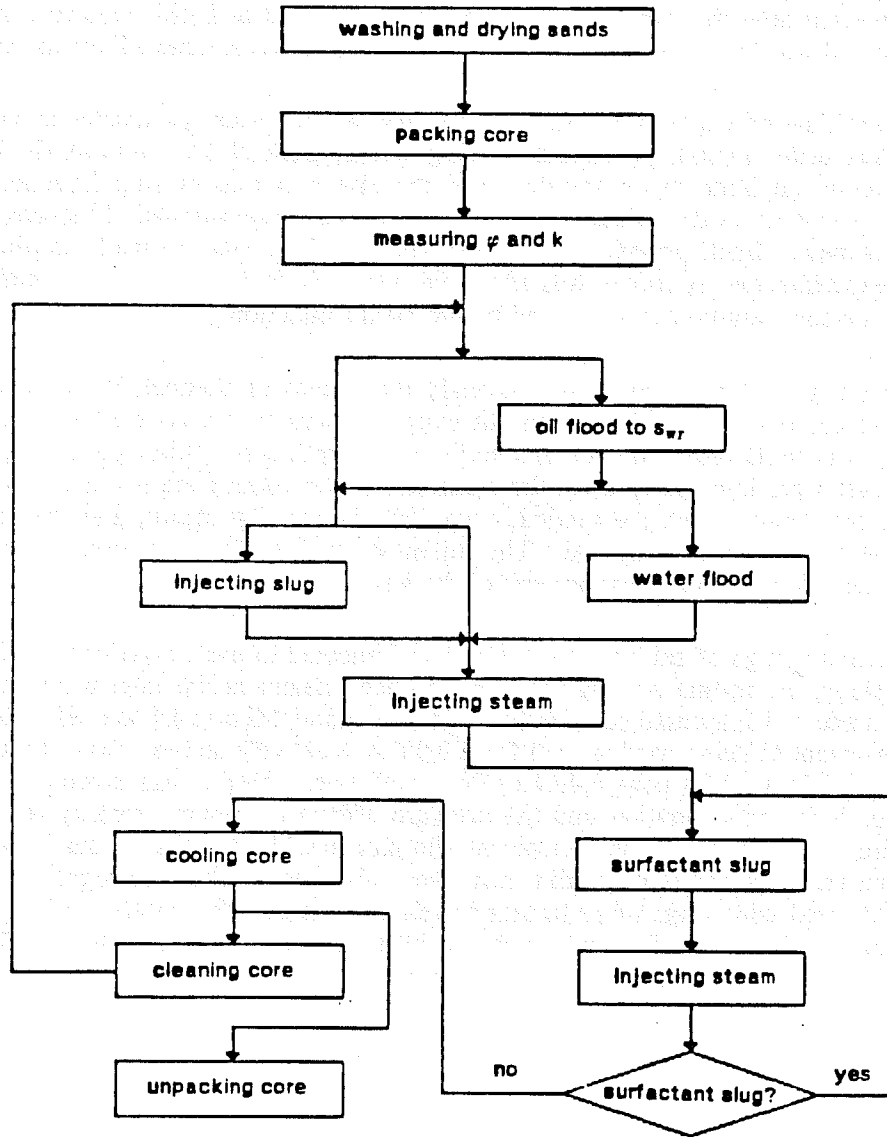


Fig. 5.10 Flow Chart of Experiments of Steam Displacement.

5.3.3. Steam Injection With Suntech IV Slugs

In this study, the slug injection technique was used to study the phenomenon of the steam/foam flow through porous media. The foaming agent was Suntech IV. Experiments were divided into two major types: in the first type, a single slug of surfactant solution was injected into an oil saturated sandpack at irreducible water saturation; in the second type, alternating slugs of surfactant solution and steam were injected after the sandpack had been steam flooded and produced to a steam-out condition where no more oil was being produced. Most experiments were conducted at this steam-out condition.

In the first type of experiment, oil recovery was an important parameter to be studied. Various other parameters were studied: concentration, slug size of Suntech IV solution, the effect of NaCl and tertiary butanol in the Suntech IV solution, and the effect of rate of slug injection. Sandpacks with permeabilities of 5 and 16 μm^2 (Darcy) were used in these experiments. The sandpack was repacked for each experiment. Back pressure of 50 psig (0.515 MPa) was normally applied in these experiments. The experimental procedure was about the same as during steam displacement to S_{or} , except that a slug of aqueous solution was injected before steam injection.

The second type of experiment was to study the effects of Suntech IV on steam mobility reduction at a steam-out condition. The steam-out condition was to simulate steam channels in the field. The sandpack was used repeatedly in this series of experiments. After each run, two to three pore volumes of water were injected to wash the sandpack and to reduce the residue of surfactant left in the sandpack. In each experiment, the sandpack was first flooded by steam, and then alternating slugs of surfactant solution and steam followed. The initial steam injection was used to study pressure, temperature and rate effects on the development of the steam zone.

Three or more slugs of surfactant solution were injected in each experiment. During the injection of surfactant slugs, the in-line heating tape and the band heater at the inlet were shut off. Two series of runs were made at backpressures of either 0.101 or 0.584 MPa (14.7 and 85 psia). The concentration of the surfactant solution used ranged from 0.08 to 1.12 wt% active. Slug sizes of surfactant solution varied from 0.05 to 0.30 pore volume. One-tenth pore volume was taken as a standard slug size for studying both the concentration and the pressure effects on steam mobility reduction. A run was also made with water slugs with no surfactant alternating with steam as a base case to compare with these surfactant runs. A series of similar runs were also made where nitrogen was injected with the steam as it alternated with slugs of surfactant solutions. Nitrogen has been shown (Dilgren *et al.* 1978 and Doscher *et al.* 1982) to further reduce the mobility in surfactant/steam flow. The concentration of nitrogen varied from 0 to 2.1 mole percent of the steam injected.

6. RESULTS AND DISCUSSION OF STEAM-DISPLACEMENT EXPERIMENTS

In this section, the results of steam-displacement experiments at various operating conditions are presented as well as comparisons between the experimental and the calculated heat fronts. Two main objectives of this section are to study the effects of pressure on the heat-frontal movements, and the effect of initial oil saturation on oil recovery.

6.1. REPEATABILITY OF RUNS

In every steam-displacement run, slightly superheated steam was injected so that the injected enthalpy was known accurately. Runs #27 and #29 were conducted at irreducible oil saturation under identical conditions to verify the repeatability of this experiment. The mass rate of steam was $3.05 \times 10^{-2} \text{ kg/s} \cdot \text{m}^2$ and the backpressure was 0.584 MPa (85 psia). There was a difference of about 0.56°C (1°F) in the ambient temperature. Figure 6.1 shows the movements of the steam fronts from the two experiments. A comparison of the data confirms the repeatability of this test and the data measuring system.

6.2. PRESSURE EFFECT ON HEAT-ZONE DEVELOPMENT

The study of pressure effect on heat-zone development includes:

- (1) Experiments at different pressure levels with a constant pressure during each experiment.
- (2) Experiments with variable pressure during each experiment.

The objectives of this section are to study the temperature effect on the thermal conductivity of the insulation and effects of pressure and heat injection rate on the heat-frontal movement.

6.2.1. Constant Pressure Cases

The Marx and Langenheim model for calculating the heat front is appropriate for cases of constant temperature in the steam zone, constant volumetric heat capacity ratio, and constant thermal diffusivity of the insulation. However, in experiments, a small temperature gradient is always present in the steam zone to overcome the flow resistance and the thermal conductivity of the insulation is temperature-dependent. A nonlinear physical problem may be modeled by using the analytical or semi-analytical solutions for linear or nonlinear equations when proper average values are used for the nonlinear coefficients. Comparisons between the calculated and the experimental results give direct support to the utility of these solutions.

The average temperature of the heated zone increases with the operating pressure. An increase in the steam zone temperature increases the rate of heat loss from the heated zone and consequently slows down the movement of the heat front. For most insulations, both the thermal conductivity and the thermal diffusivity are functions of temperature. Seven runs at residual oil saturation were conducted at 0.11, 0.448, 0.586, 0.793, 1.145 and 1.42 MPa (17, 65, 85, 115, 166 and 206 psia) backpressure to find these functions. The mass rates of steam injection were $3.05 \times 10^{-2} \text{ kg/s} \cdot \text{m}^2$ ($22.6 \text{ lb}_m/\text{h} \cdot \text{ft}^2$) for Runs #19 to #27, $1.22 \times 10^{-2} \text{ kg/s} \cdot \text{m}^2$ ($9.0 \text{ lb}_m/\text{h} \cdot \text{ft}^2$) for Run #38 and $7.4 \times 10^{-3} \text{ kg/s} \cdot \text{m}^2$ ($5.48 \text{ lb}_m/\text{h} \cdot \text{ft}^2$) for Run #40. Other operating conditions are listed in Table 6.1. From material balances made during the runs the average steam saturations in the steam zones of Runs #19, #21 and #23 were calculated and are graphed in Fig. 6.2. All the saturation profiles indicate that the average steam saturation decreased slightly with time from about 75% to 68% with time. Data at times less than 40 minutes were not accurate because the inherent errors in material balance calculations are more pronounced when the steam zone is small.

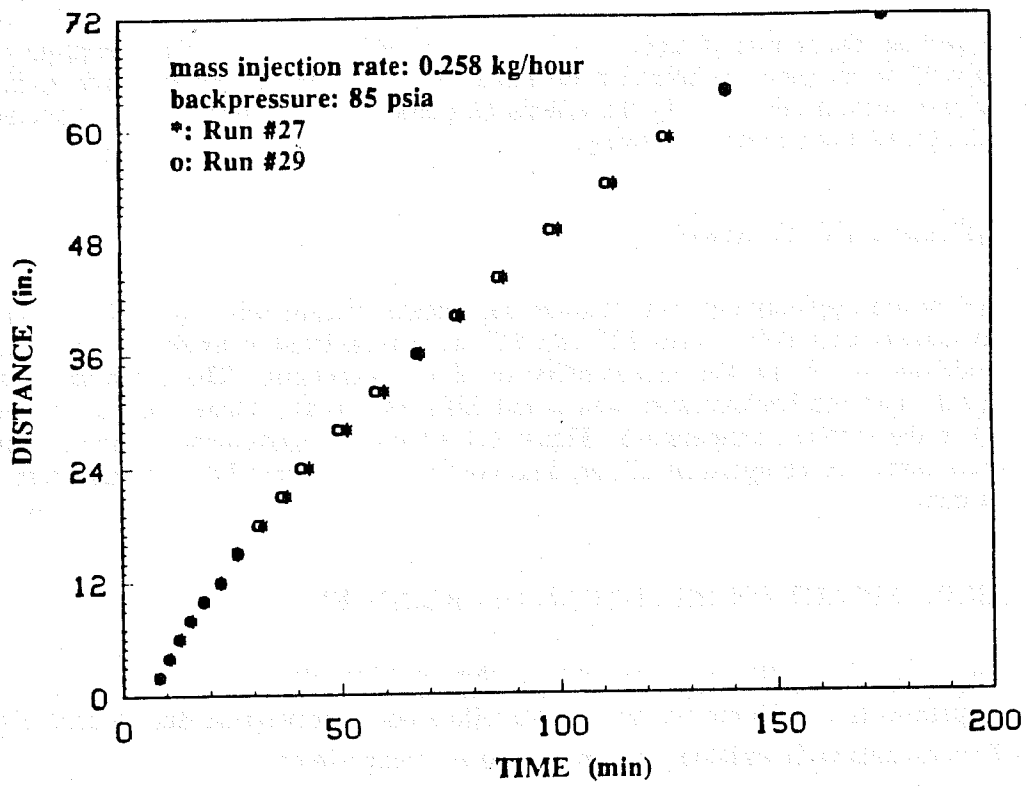


Fig. 6.1 Comparison of Steam Frontal Position of Two Identical Runs.

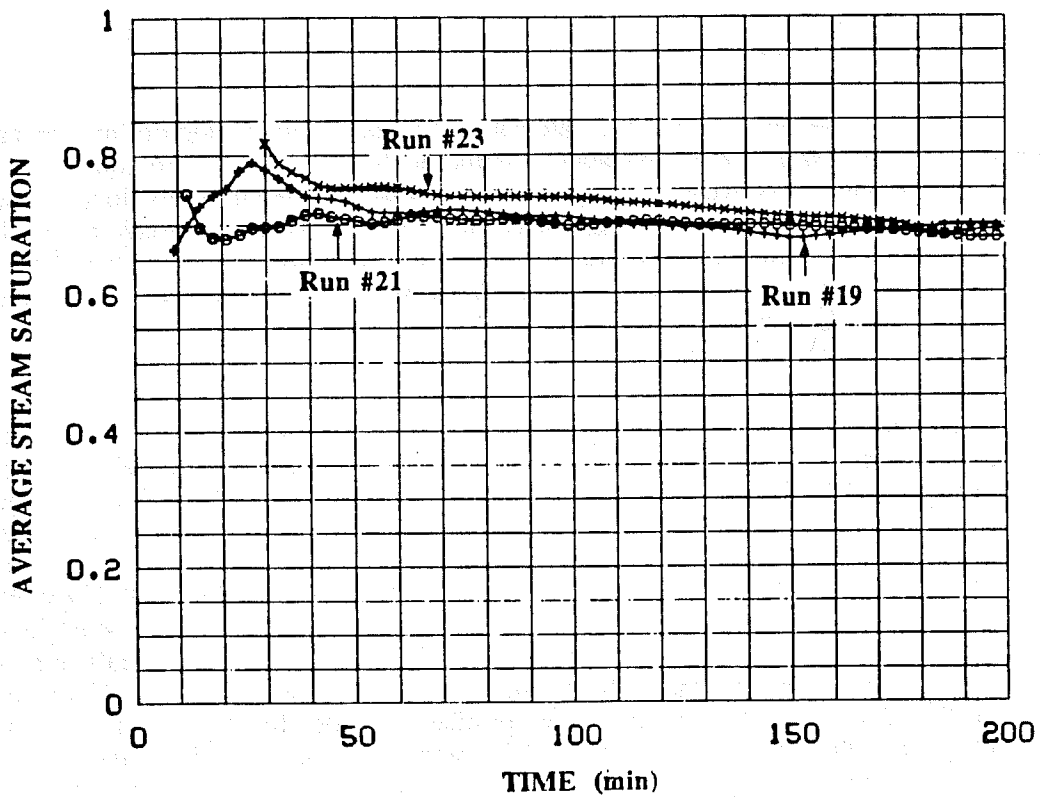


Fig. 6.2 Average Steam Saturation During Steam Displacements at 115 (Run #23), 166 (Run #21) and 206 psia (Run #19).

TABLE 6.1 DATA FOR STEAM DISPLACEMENTS AT CONSTANT PRESSURE

run no.	19	21	23	25	27	38	40
mass injection rate (kg/s·m ²)	0.0305	0.0305	0.0305	0.0305	0.0305	0.012	0.0074
backpressure (MPa)	1.42	1.145	0.793	0.448	0.586	0.11	0.11
injection pressure (MPa)	1.51	1.22	0.875	0.53	0.71	0.207	0.155
injection temperature (°C)	204	197	199	197	197	143	138
saturated steam temperature (°C)	199	188	173	154	162	115.6	112
ambient temperature (°C)	24	21	23	21.7	21	22.8	25
fraction of latent heat (f_{hv})	0.71	0.74	0.764	0.795	0.78	0.814	0.815
α_s (mm ² /s)	0.56	0.594	0.542	0.516	0.516	0.465	0.465
M_R (MJ/ m ³)	0.993	0.988	0.955	0.953	0.985	0.966	0.89
saturation (S_s)	0.70	0.70	0.74	0.74	0.72	0.75	0.75
residual oil saturation (S_{or})	0.16	0.16	0.16	0.16	0.16	0.16	0.16

In order to examine the validity of the solution of Eq. 4.9 to the experimental heat fronts, proper physical properties of the core and the insulation must be specified. The volumetric heat capacity of the core can be evaluated by

$$(\rho C)_R = (\hat{h}_r^2 - \hat{h}_r^1)/(T_h - T_{ini}) \quad (6.1)$$

where

T_{ini} = initial temperature of the core,

T_h = temperature of the heated zone,

and subscript 1 stands for initial condition and 2 for the heated condition, and \hat{h} is given by

$$\hat{h}_r^i = \left\{ (1-\phi)(\rho h)_m + \phi[S_o(\rho h)_o + S_w(\rho h)_w + S_s(\rho h)_s] \right\}_i \quad (6.2)$$

where

ϕ = porosity,

S_o = oil saturation,

S_w = water saturation,

S_s = steam saturation,

$(\rho h)_m$ = volumetric enthalpy of matrix (sand),

$(\rho h)_o$ = volumetric enthalpy of oil,

$(\rho h)_w$ = volumetric enthalpy of water,

$(\rho h)_s$ = volumetric enthalpy of steam.

Equations in Appendix D were used with Eqs. 6.1 and 6.2 to calculate various properties of each phase. The volumetric enthalpy of the sand amounts to more than 80% of the total volumetric enthalpy of the sandpack. The variation of steam saturation during a run as shown in Fig. 6.2 results in less than a 3% difference in the calculated volumetric enthalpy when the steam saturation varies from 68% to 75%. Thus, the volumetric enthalpy of the steam zone can be treated as a constant during an experiment.

Because these runs were performed at residual oil saturations, the pressure gradients in the steam zone were not negligible. The pressure gradients in the steam zone varied from 0.04 to 0.083 MPa/m (1.8 to 3.7 psi/ft). However, the average temperatures of the steam zone remained fairly constant (see Tables 6.2 to 6.7). The mass injection rate of Run #40 was very small and the experimental error caused by the excessive heating by the band heater was large. Therefore, heat frontal data of Run #40 were not used for history matching. Comparisons of heat frontal positions calculated by the solution of Eq. 4.9 and those obtained from the other six experiments are shown in Figs. 6.3 to 6.8. Except for the small-time data, good matches were obtained by using appropriate values for the thermal conductivity of the insulation. The discrepancies between the experimental and calculated heat fronts during the early injection periods were mostly due to the excessive heating of the end flange by the injecting steam. For Run #38, the heat injection rate was low and the preheating of the flange by a band heater resulted in the experimental heat front moving faster than the calculated heat fronts. The apparent thermal conductivities of the insulation obtained from these matches are graphed in Fig. 6.9 against the steam temperature. These data can be fitted to a quadratic equation:

$$k_2 = 0.0225 + 1.47 \times 10^{-5}T + 7.16 \times 10^{-8}T^2 \quad (6.3)$$

where T is in °F. Values of the apparent thermal conductivity were higher by two fold than those reported in the literature (Turner and Malloy, 1981). This was probably caused partly by the additional heat conduction through fittings, tubing and thermocouples.

6.2.2. Variable Pressure Cases

When steam-displacement experiments are conducted in a sandpack with movable oil, both the pressure and the temperature of the steam zone vary with time during an experiment. The movement of the heat front is complicated by the pressure change. An examination of this problem reveals that the change of the steam-zone temperature changes three variables: the heat injection rate, the volumetric heat content in the heated zone and the heat loss rate to the insulation. Superposition can only handle the change of the heat injection rate. Both the changes in the volumetric heat content and the heat loss may be treated as heat sources or sinks. However, the additional amount of increased (or decreased) heat loss can not be readily calculated.

Prats (1969 and 1982) proposed a method for handling cases of variable injection temperature. He stated that the heat efficiency for the Marx and Langenheim (1959) model applies even if the injection temperature or mass rate varies, as long as the net rate of heat input is constant. This method is, in fact, to apply the method of succession of pseudosteady states to nonlinear transient problems. A change in the injection temperature results from a change in injection pressure. If the transient heat flow resulting from a pressure change is not fast enough to reach equilibrium, this approach tends to give a larger than correct steam swept volume when the steam temperature decreases with time and to give a lower than correct steam swept volume when the steam temperature increases with time.

The method of succession of pseudosteady states is simple and efficient. The heat front at a certain time can be approximated by using the solution for the Marx and Langenheim model at the instantaneous values for the steam-zone temperature, and instantaneous values of the properties of the reservoir and the adjacent formations. When all properties of the reservoir and adjacent formations are independent of temperature, the heat frontal position is inversely related to the steam-zone temperature. Superposition can be applied to the method of succession of steady states to handle cases of variable heat injection rate.

For a cylindrical model, the heat efficiency is given by Eq. 4.10 for constant heat injection rate. In cases of variable heat injection rate, X_D is more convenient to use with superposition than E_h . The

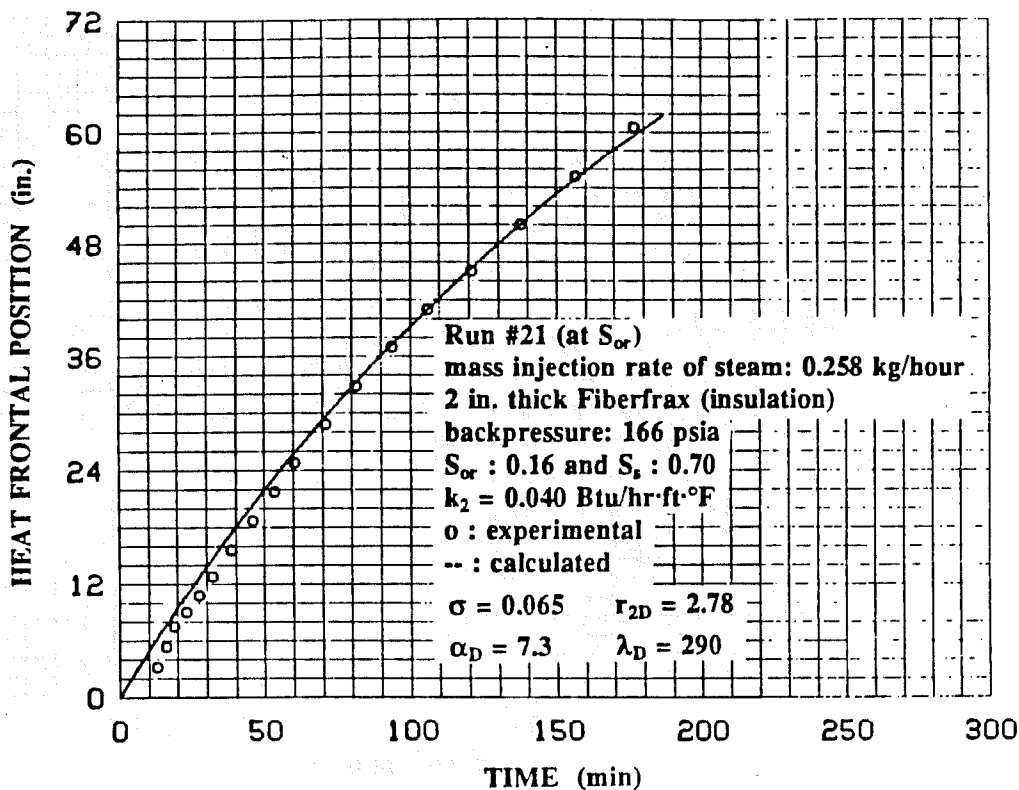


Fig. 6.4 Comparison Between the Calculated and Experimental Heat Fronts at 166 psia and 0.258 kg/h Mass Injection Rate.

TABLE 6.3
EXPERIMENTAL AND CALCULATED HEAT FRONTAL POSITION (RUN #21)

heat capacity ratio=	0.0646	diffusivity ratio =	7.300
conductivity ratio=	290.00	radius ratio =	2.778
oil saturation=	0.16	mass injection rate=	4.300 gm/min
water saturation=	0.140	initial temperature=	70.000 °F
steam saturation=	0.70	back pressure =	166.000 psia
porosity=	0.34	Insulation conductivity=	0.04003Btu/hr-ft-F

time min	T_{in} °F	T_{ave}	t_D	H_D	f_{av}	x_t (in.)	
						measured	calculated
13.00	372.00	372.00	0.6290	0.18612	0.73508	3.200	6.886
16.00	373.00	373.00	0.7752	0.18197	0.73446	5.300	8.328
19.00	375.00	374.00	0.9217	0.18123	0.73476	7.500	9.864
23.00	375.00	374.00	1.1158	0.18464	0.73476	9.000	11.721
27.50	375.00	374.00	1.3341	0.18464	0.73476	10.800	13.647
32.00	375.00	374.00	1.5524	0.18464	0.73476	12.800	15.946
38.50	375.00	373.50	1.8665	0.18672	0.73554	15.600	18.817
46.00	376.00	374.00	2.2316	0.18299	0.73569	18.700	21.744
53.50	376.50	374.00	2.6954	0.18480	0.73576	21.700	24.505
60.50	377.00	374.50	2.9369	0.18249	0.73584	24.800	27.684
71.00	377.00	374.50	3.4466	0.18441	0.73584	28.800	31.373
81.50	379.00	374.50	3.9563	0.18462	0.73614	32.800	35.226
94.00	383.00	375.00	4.5661	0.18266	0.73673	36.900	39.076
106.00	384.00	375.00	5.1490	0.18469	0.73688	40.900	43.134
121.00	386.00	375.00	5.8777	0.18489	0.73717	45.000	47.615
137.80	387.00	373.00	6.6760	0.19390	0.73887	50.000	52.595
156.80	387.00	373.00	7.5965	0.18680	0.73887	55.200	57.328
176.80	387.00	373.00	8.5655	0.18680	0.73887	60.500	61.798

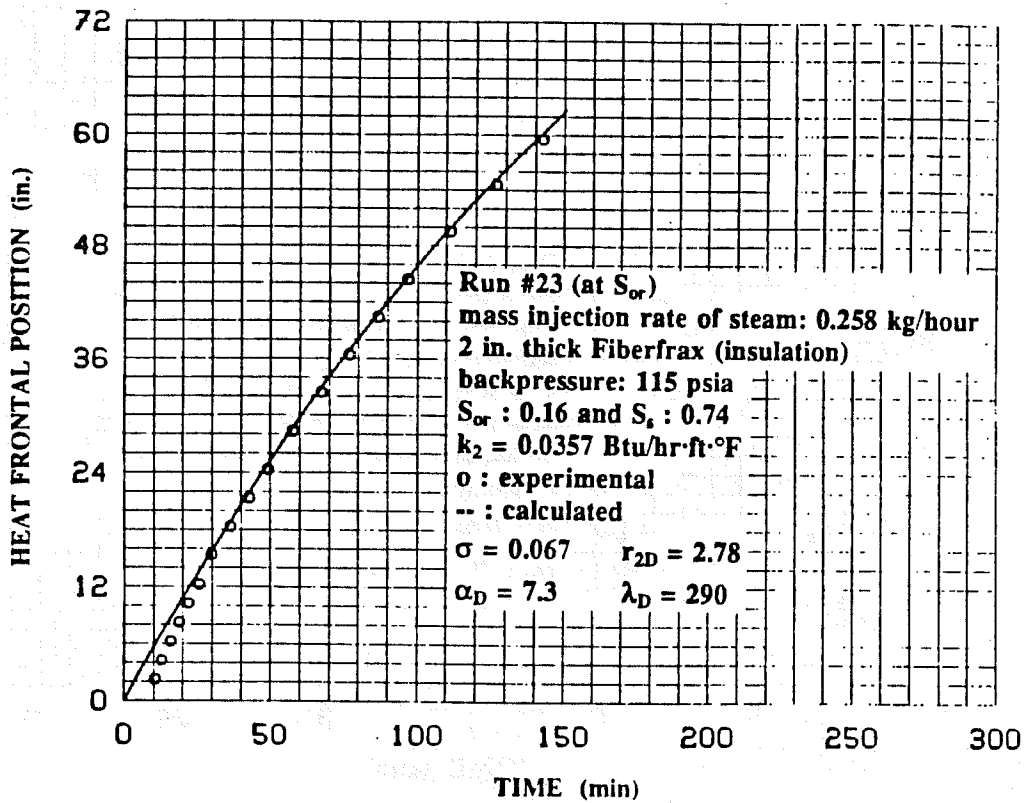


Fig. 6.5 Comparison Between the Calculated and Experimental Heat Fronts at 115 psia and 0.258 kg/h Mass Injection Rate.

TABLE 6.4
 EXPERIMENTAL AND CALCULATED HEAT FRONTAL POSITION (RUN #23)

heat capacity ratio=	0.0668	diffusivity ratio =	7.300
conductivity ratio=	290.00	radius ratio =	2.778
oil saturation=	0.16	mass injection rate=	4.300 gm/min
water saturation=	0.100	initial temperature=	74.000 °F
steam saturation=	0.74	back pressure =	115.000 psia
porosity=	0.34	insulation conductivity=	0.03573Btu/hr-ft-F

time min	T_{wv} °F	T_{ave}	t_D	H_D	f_{hv}	x_t (in.)	
						measured	calculated
10.50	347.00	347.00	0.4537	0.23671	0.76035	2.200	6.465
13.00	348.00	348.00	0.5625	0.23114	0.75935	4.200	7.881
16.00	351.00	348.00	0.6923	0.23586	0.75974	6.200	9.427
19.00	355.00	347.00	0.8209	0.24327	0.76138	8.200	10.989
22.00	357.00	347.00	0.9505	0.23799	0.76164	10.200	12.629
25.50	361.00	347.00	1.1018	0.23847	0.76206	12.200	14.619
30.00	366.00	347.00	1.2862	0.23912	0.76350	15.300	17.308
36.50	372.00	347.00	1.5770	0.23986	0.76423	18.300	20.418
43.00	377.00	347.00	1.8579	0.24048	0.76483	21.300	23.455
49.50	380.00	347.00	2.1387	0.24084	0.76592	24.300	26.864
68.00	382.00	346.00	2.5025	0.24749	0.76680	28.300	30.920
67.50	384.00	346.00	2.8124	0.24257	0.76769	32.400	34.955
77.00	386.00	347.00	3.3269	0.23559	0.76792	36.400	38.846
87.00	387.00	347.00	3.7589	0.24164	0.76797	40.400	42.771
97.00	387.00	347.00	4.1910	0.24160	0.76818	44.400	47.362
111.50	387.00	347.50	4.8208	0.23833	0.76847	49.500	52.597
127.00	387.00	347.50	5.4910	0.24092	0.76840	54.500	57.746
142.50	387.00	347.50	6.1611	0.24090	0.76833	59.500	62.728

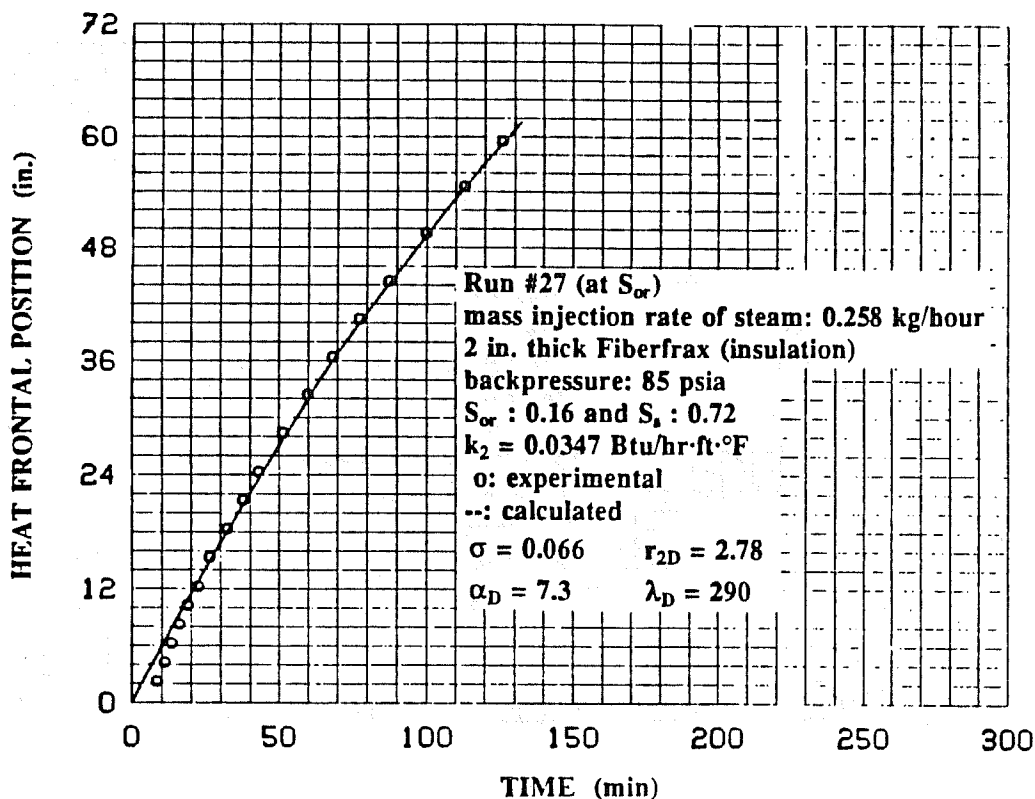


Fig. 6.6 Comparison Between the Calculated and Experimental Heat Fronts at 85 psia and 0.258 kg/h Mass Injection Rate.

TABLE 6.5
 EXPERIMENTAL AND CALCULATED HEAT FRONTAL POSITION (RUN #27)

heat capacity ratio=	0.0662	diffusivity ratio =	7.300
conductivity ratio=	290.00	radius ratio =	2.778
oil saturation=	0.16	mass injection rate=	4.310 gm/min
water saturation=	0.120	initial temperature=	70.000 °F
steam saturation=	0.72	back pressure =	85.000 psia
porosity=	0.34	insulation conductivity=	0.03470Btu/ hr-ft-F

time min	T_{wD} °F	T_{ave} °F	t_D	H_D	f_{hv}	x_f (in.)	
						measured	calculated
8.50	330.00	330.00	0.3588	0.25263	0.77256	2.200	6.652
11.00	328.00	328.00	0.4631	0.26429	0.77373	4.200	7.090
13.50	331.00	326.00	0.5668	0.26919	0.77649	6.200	8.568
16.10	335.00	326.00	0.6760	0.25889	0.77596	8.200	10.019
18.80	338.00	325.00	0.7883	0.26667	0.77700	10.200	11.802
22.50	345.00	325.00	0.9435	0.26167	0.77781	12.200	13.882
26.50	352.00	325.00	1.1112	0.26260	0.77860	15.300	16.492
32.30	362.00	325.00	1.3544	0.26391	0.78106	18.300	19.453
37.80	368.00	325.00	1.5851	0.26469	0.78171	21.300	22.204
43.00	372.00	325.00	1.8031	0.26520	0.78281	24.300	25.649
51.50	376.00	325.00	2.1595	0.26571	0.78323	28.400	29.804
60.00	380.00	324.00	2.5126	0.27405	0.78431	32.400	33.943
68.50	382.00	324.00	2.8686	0.26795	0.78519	36.400	37.971
77.50	384.00	325.00	3.2498	0.25972	0.78472	40.400	42.062
87.50	385.00	326.00	3.6740	0.25884	0.78549	44.400	46.697
100.00	386.00	326.00	4.1989	0.26552	0.78560	49.500	51.850
113.00	387.00	326.00	4.7447	0.26564	0.78570	54.500	56.843
126.00	387.00	326.00	5.2906	0.26564	0.78570	59.600	61.666

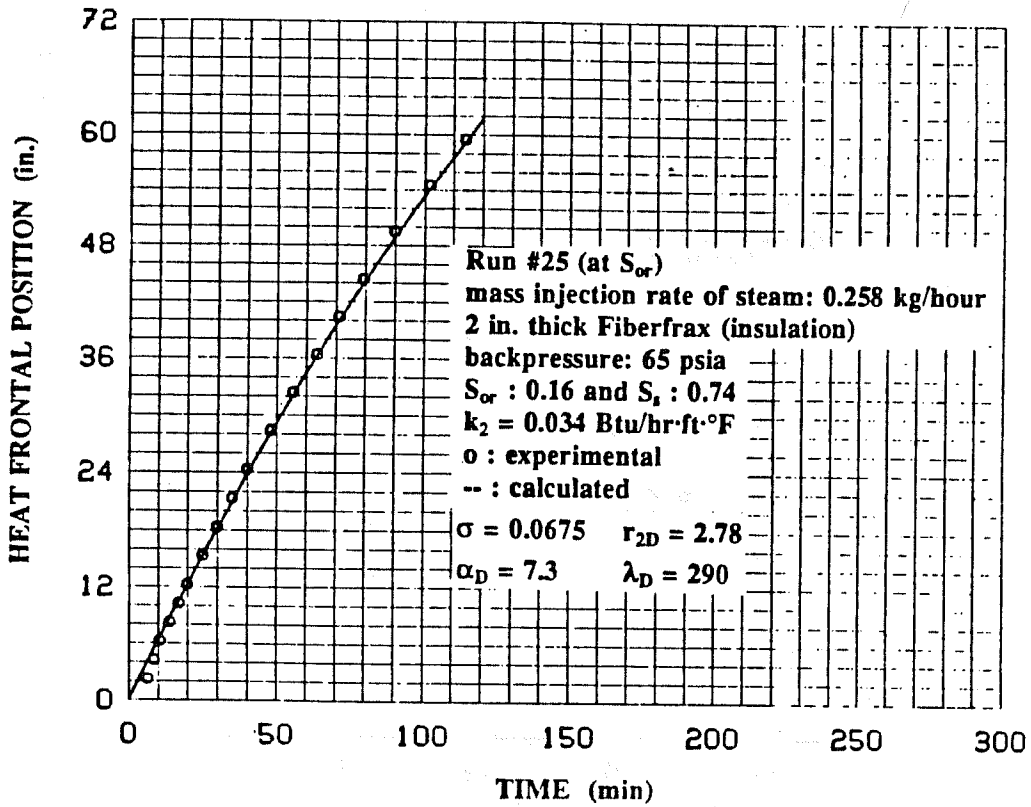


Fig. 6.7 Comparison Between the Calculated and Experimental Heat Fronts at 65 psia and 0.258 kg/h Mass Injection Rate.

TABLE 6.6
 EXPERIMENTAL AND CALCULATED HEAT FRONTAL POSITION (RUN #25)

heat capacity ratio=	0.0675	diffusivity ratio =	7.300
conductivity ratio=	290.00	radius ratio =	2.778
oil saturation=	0.16	mass injection rate=	4.310 gm/min
water saturation=	0.100	initial temperature=	71.000 °F
steam saturation=	0.74	back pressure =	65.000 psia
porosity=	0.34	Insulation conductivity=	0.03404Btu/ hr-ft-F

time min	T_{hw} °F	T_{ave} °F	t_D	H_D	f_{hw}	xt (in.)	
						measured	calculated
6.50	314.00	314.00	0.2686	0.27891	0.78680	2.200	4.738
8.50	315.00	315.00	0.3517	0.27316	0.78699	4.200	5.932
10.50	317.00	312.00	0.4328	0.28851	0.78909	6.200	7.674
14.00	325.00	310.50	0.6759	0.29528	0.79153	8.200	9.682
17.00	333.00	311.50	0.7003	0.28013	0.79145	10.200	11.430
20.00	340.00	311.00	0.8233	0.29189	0.79283	12.200	13.806
25.00	350.00	311.00	1.0291	0.29006	0.79384	15.300	16.706
30.00	358.00	311.00	1.2349	0.29112	0.79505	18.300	19.658
35.00	365.00	311.00	1.4408	0.29203	0.79615	21.300	22.362
40.00	370.00	311.00	1.6466	0.29265	0.79694	24.300	25.932
48.00	375.00	311.50	1.9772	0.28908	0.79720	28.400	30.025
55.50	377.00	311.00	2.2847	0.29737	0.79803	32.400	34.105
63.50	380.00	311.00	2.6140	0.29389	0.79863	36.400	38.016
71.00	382.00	311.00	2.9227	0.29416	0.79881	40.400	41.936
79.50	383.00	311.00	3.2726	0.29426	0.79934	44.400	46.435
90.00	384.00	311.50	3.7073	0.28957	0.79923	49.500	51.462
102.00	385.00	311.00	4.1988	0.29856	0.79995	64.500	56.766
114.00	386.00	311.50	4.6959	0.28930	0.79975	69.500	61.641

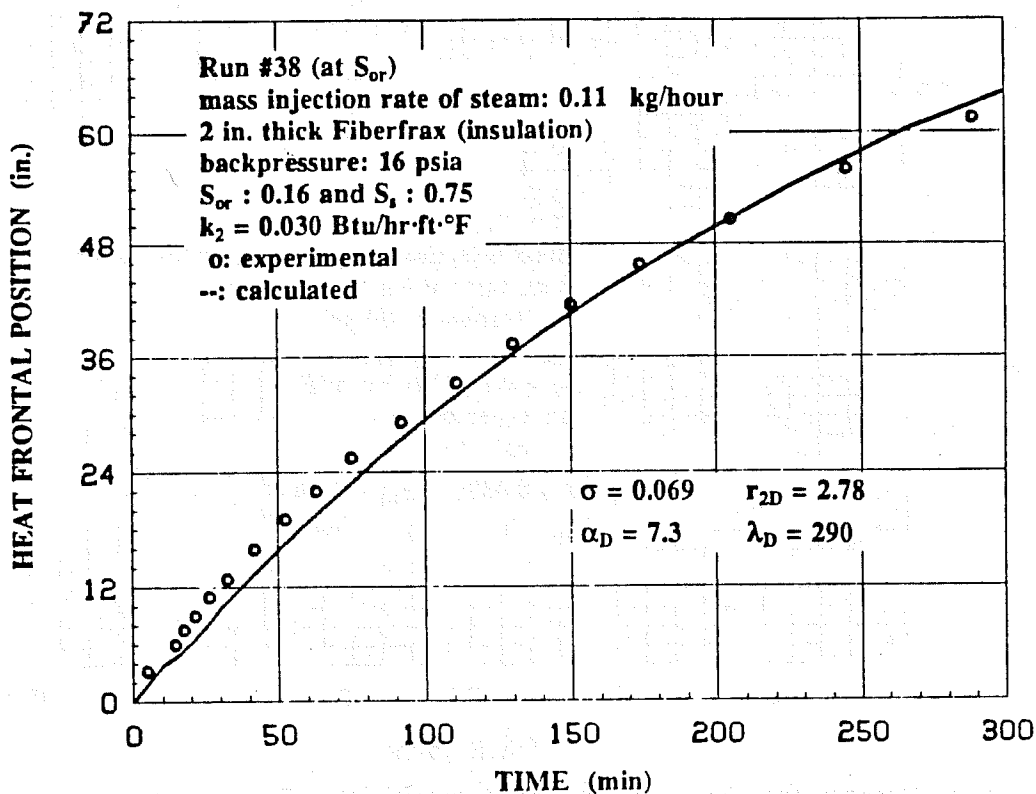


Fig. 6.8 Comparison Between the Calculated and Experimental Heat Fronts at 16 psia and 0.103 kg/h Mass Injection Rate.

TABLE 6.7
 EXPERIMENTAL AND CALCULATED HEAT FRONTAL POSITION (RUN #38)

heat capacity ratio=	0.0693	diffusivity ratio =	7.300
conductivity ratio=	290.00	radius ratio =	2.778
oil saturation=	0.16	mass injection rate=	1.717 gm/min
water saturation=	0.090	initial temperature=	72.000 $^{\circ}$ F
steam saturation=	0.75	back pressure =	15.000 psia
porosity=	0.34	insulation conductivity=	0.03009 Btu/ hr-ft- $^{\circ}$ F
		insulation diffusivity=	0.01756 ft 2 /hour

time min	T_w $^{\circ}$ F	T_{ave} $^{\circ}$ F	t_D	H_D	f_{hw}	xt (in.)	
						measured	calculated
5.00	220.00	220.00	0.1789	0.19435	0.80763	3.200	3.659
14.50	250.00	242.00	0.6315	0.10744	0.79765	6.000	4.949
17.50	257.00	243.00	0.6422	0.16092	0.79846	7.500	6.002
21.50	265.00	240.50	0.7868	0.18527	0.80249	8.900	7.614
26.50	270.00	236.50	0.9653	0.20022	0.80656	10.900	9.459
32.50	279.00	236.00	1.1832	0.18200	0.80864	12.800	11.888
42.00	288.00	235.50	1.6283	0.18391	0.81107	15.900	14.960
52.50	289.00	235.50	1.9103	0.18157	0.81166	19.000	18.026
63.00	289.00	235.00	2.2937	0.17786	0.81219	22.000	21.117
75.00	290.00	235.00	2.7276	0.18791	0.81277	25.400	25.167
92.00	291.00	236.00	3.3495	0.17568	0.81312	29.100	29.646
111.00	291.00	236.00	4.0413	0.18087	0.81354	33.200	34.043
130.00	291.00	235.50	4.7303	0.18462	0.81448	37.300	38.471
150.00	291.00	236.00	5.4612	0.17763	0.81436	41.500	42.860
174.00	291.00	236.50	6.3385	0.17716	0.81466	45.700	47.869
205.00	291.00	236.00	7.4636	0.18295	0.81559	50.500	53.962
245.00	291.00	235.50	8.9149	0.18349	0.81611	56.000	60.321
289.00	291.00	236.00	10.5218	0.17838	0.81600	61.500	66.383

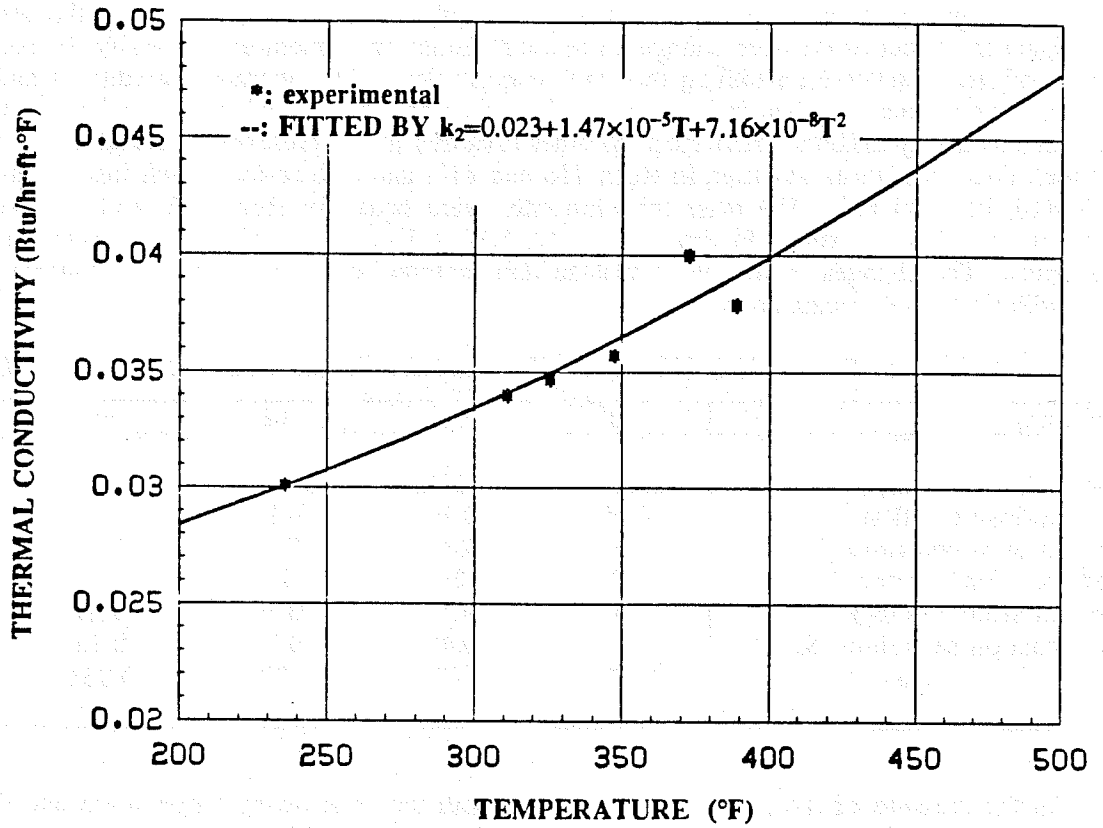


Fig. 6.9 Apparent Thermal Conductivity of Insulation (Fiberfrax, Tubings and Thermocouples) vs Temperature.

generalized solution is given by

$$X(t) = \frac{\sigma}{[\pi k_2 (\rho C)_R \Delta T]_n} \sum_{i=1}^n U(t-t_i) (\dot{H}_i - \dot{H}_{i-1}) X_D \left[(t - t_{i-1})_D \right] \quad (6.4)$$

Values of X_D may be obtained from the solution of Eq. 4.9. Based on the method of succession of steady states, only the constants of the n th time step are used in Eq. 6.4.

Five experiments were performed at different oil and steam saturations in the steam zone to investigate the effect of pressure change on the heat-frontal movement and to verify the method of succession of steady states for handling this nonlinear problem. The operating conditions and parameters of these experiments are listed in Table 6.8. The steam saturations and oil saturations of Run #11 and #12 were distinctly different from those of other runs due to the presence of surfactant in the core. A two-inch thick insulation was used in Runs #16 and #17, and a three-inch thick insulation was used in Runs #10, #11 and #12. The mass injection rates were equal for Runs #10, #11 and #12 and were higher in the other two runs. Figures 6.10, 6.12, 6.14, 6.16 and 6.18 show the temperature profiles of these runs. The changes of the steam plateau temperatures were caused by the changes in the pressures with time in the steam zone.

TABLE 6.8 DATA FOR STEAM DISPLACEMENTS AT VARIABLE PRESSURE

run no.	10	11	12	16	17
mass injection rate (kg/s·m ²)	0.0225	0.0225	0.0225	0.0246	0.0295
backpressure (MPa)	0.10	0.10	0.10	0.10	0.10
injection temperature (°C)	206	206	203	202	175
ambient temperature (°C)	22	24	21	26.7	26.7
steam saturation (S_v)	0.60	0.33	0.36	0.60	0.59
residual oil saturation (S_{or})	0.15	0.45	0.39	0.16	0.18
insulation thickness (m)	0.076	0.076	0.076	0.051	0.051

As the pressure of the steam zone increases, both the steam-zone temperature and the heat loss rate increases and the movement of the heat front slows down. The effect is just the opposite when the pressure decreases. Figures 6.11, 6.13, 6.15, 6.17 and 6.19 and Tables 6.9 to 6.13 immediately following each figure present data on heat frontal movements of these five runs. In the figures, circles indicate experimental data and the solid lines show the heat fronts calculated using Eq. 6.4. Because the apparent thermal conductivity of the insulation was found in Fig. 6.9 and Eq. 6.3 to be dependent on temperature, the dimensionless times were determined by using the instantaneous, apparent thermal conductivities from Eq. 6.3 rather than average values. The agreement between the experimental heat fronts and the heat fronts calculated by Eq. 6.4 are good for all runs. For Run #10 (Fig. 6.11), the calculated heat fronts are slightly greater than the observed heat fronts. In Runs #16 and #17 (Figs. 6.17 and 6.19), the mass injection rates of steam were not constant because of partial plugging in the pump. Although the measured mass injection rates of steam were used in the calculations in heat fronts, the rates were not very accurate and this probably accounts for the less accurate matches seen in Figs. 6.17 and 6.19.

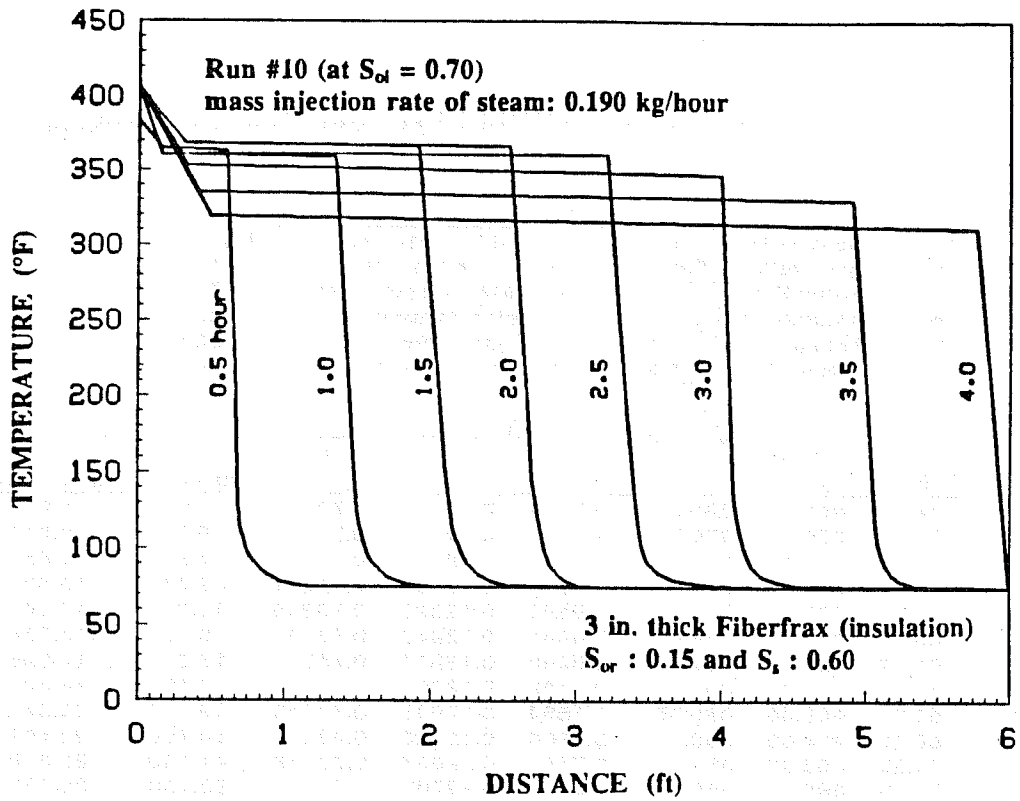


Fig. 6.10 Temperature Profiles of Steam Displacement (Run #10).

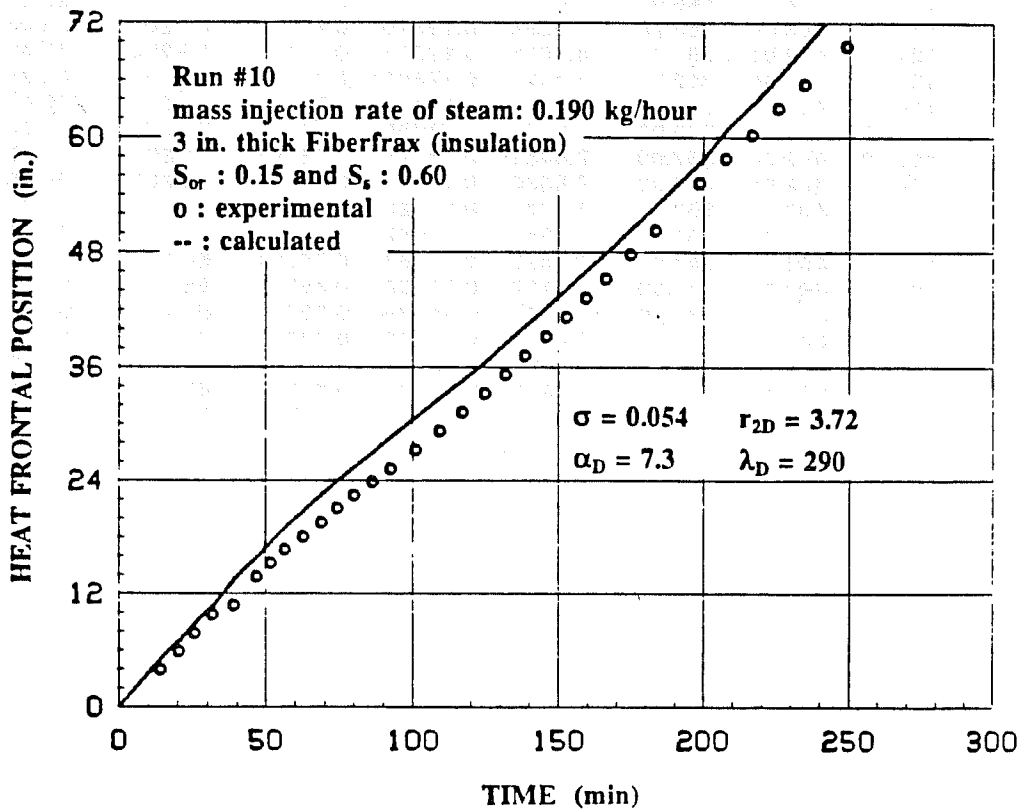


Fig. 6.11 Comparison Between the Calculated and Experimental Heat Fronts of Run #10.

TABLE 6.9
MEASURED AND CALCULATED HEAT FRONTAL POSITION (RUN#10)

heat capacity ratio=	0.0541	diffusivity ratio =	7.300
conductivity ratio=	290.00	radius ratio =	3.717
oil saturation=	0.14	mass injection rate=	3.170 gm/min
water saturation=	0.252	initial temperature=	72.000 °F
steam saturation=	0.60	back pressure =	70.000 psia
porosity=	0.37	insulation conductivity=	0.03429Btu/ hr-ft-F

time min	T _{in} °F	T _{ave}	t _D	H _D	f _{hw}	xt (in.)	
						measured	calculated
14.20	365.00	365.00	0.7185	0.12233	0.72251	3.860	4.911
20.35	370.00	370.00	1.0371	0.11970	0.71920	5.800	6.818
25.76	375.00	367.00	1.3072	0.12211	0.72312	7.750	8.652
31.90	382.00	370.00	1.6257	0.12093	0.72207	9.740	10.507
39.00	390.00	359.00	1.9568	0.12892	0.73348	10.720	13.290
46.70	395.00	359.00	2.3431	0.12942	0.73530	13.700	15.736
51.70	398.00	359.00	2.5940	0.12972	0.73590	15.200	17.298
56.70	400.00	359.00	2.8449	0.12992	0.73631	16.600	18.827
62.80	402.00	360.00	3.1554	0.12943	0.73586	18.000	20.577
69.00	404.00	360.00	3.4669	0.12963	0.73625	19.500	22.401
74.60	405.00	362.00	3.7588	0.12837	0.73476	21.000	23.819
80.20	405.00	363.00	4.0467	0.12768	0.73383	22.400	25.265
86.50	406.00	365.00	4.3770	0.12646	0.73311	23.800	26.778
92.70	406.00	365.00	4.6907	0.12646	0.73311	25.200	28.410
101.10	405.00	365.00	5.1158	0.12636	0.73291	27.200	30.549
109.40	404.00	365.00	5.5357	0.12624	0.73264	29.200	32.597
117.10	403.00	365.00	5.9254	0.12616	0.73247	31.200	34.454
124.80	402.00	364.00	6.3061	0.12671	0.73309	33.200	36.402
131.80	402.00	362.00	6.6410	0.12803	0.73479	35.200	38.344
138.70	402.00	361.00	6.9788	0.12870	0.73564	37.200	40.097
145.80	402.00	359.00	7.3154	0.13006	0.73733	39.200	42.047
152.80	402.00	357.00	7.6451	0.13144	0.73901	41.200	43.973
159.60	402.00	355.00	7.9630	0.13284	0.74068	43.200	45.853
166.30	402.00	353.00	8.2741	0.13425	0.74234	45.200	47.713
174.90	402.00	350.00	8.6658	0.13642	0.74557	47.700	50.195
183.40	402.00	347.00	9.0492	0.13863	0.74801	50.200	52.672
198.50	400.00	341.00	9.7137	0.14300	0.75321	55.200	57.202
207.60	399.00	335.00	10.0762	0.14765	0.75772	57.700	60.614
216.70	398.00	332.00	10.4752	0.15001	0.76059	60.200	63.295
225.80	397.00	328.00	10.8564	0.15329	0.76351	63.000	66.300
234.90	397.00	324.00	11.2337	0.15679	0.76657	65.500	69.414
249.20	397.00	317.00	11.8075	0.16316	0.77244	69.500	74.684

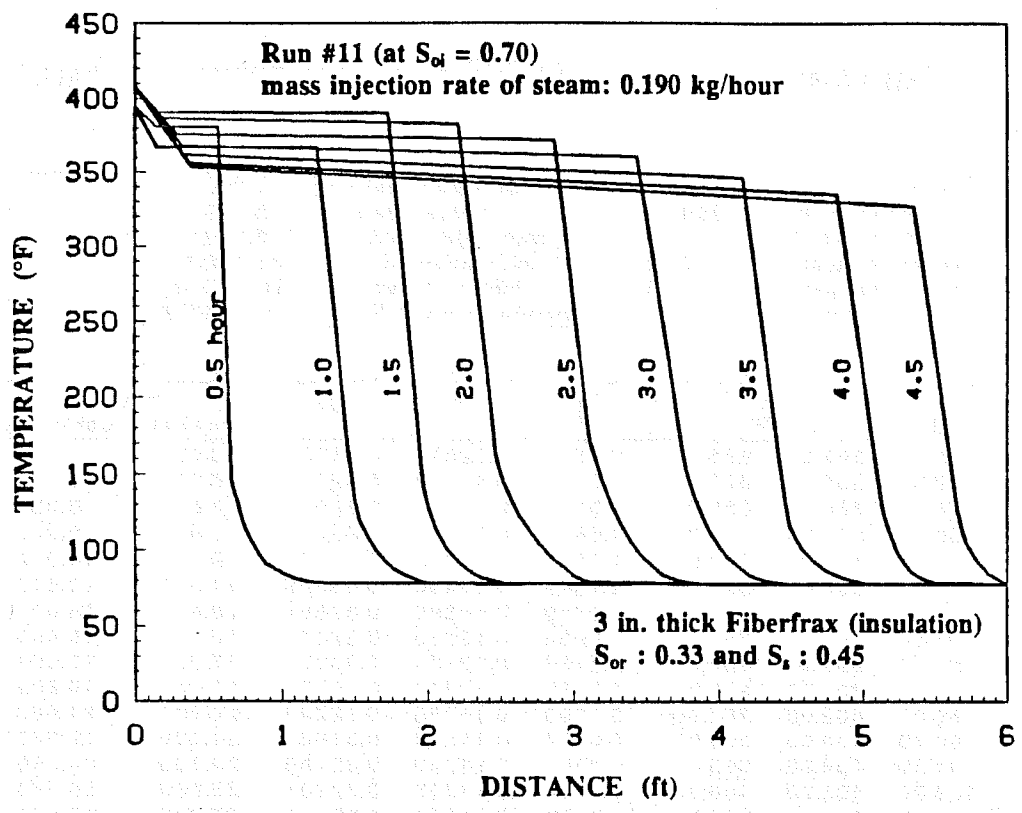


Fig. 6.12 Temperature Profiles of Steam Displacement (Run #11).

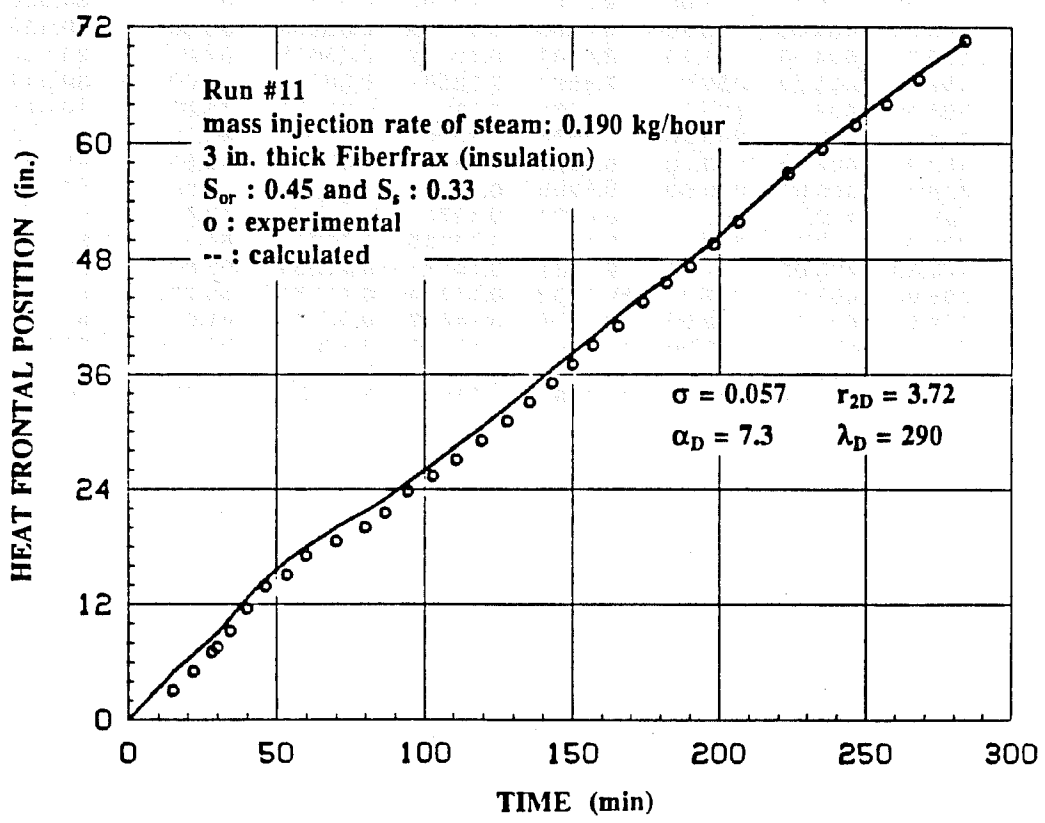


Fig. 6.13 Comparison Between the Calculated and Experimental Heat Fronts of Run #11.

TABLE 6.10
MEASURED AND CALCULATED HEAT FRONTAL POSITION (RUN#11)

heat capacity ratio=	0.0572	diffusivity ratio =	7.300
conductivity ratio=	290.00	radius ratio =	3.717
oil saturation=	0.45	mass injection rate=	3.170 gm/min
water saturation=	0.223	initial temperature=	75.000 °F
steam saturation=	0.33	back pressure =	70.000 psia
porosity=	0.38	insulation conductivity=	0.03558Btu/ hr-ft-F

time min	T _{hi} °F	T _{ave}	t _D	H _D	f _{hw}	xt (in.)	
						measured	calculated
15.00	369.00	365.00	0.6801	0.12813	0.34392	3.000	4.815
22.00	385.00	377.00	1.0191	0.12148	0.32701	5.000	6.665
28.20	390.00	380.00	1.3134	0.11997	0.32506	7.000	8.351
30.00	391.00	377.00	1.3897	0.12206	0.33211	7.500	8.947
34.40	389.00	368.00	1.5680	0.12812	0.35041	9.200	10.512
40.00	390.00	359.00	1.7942	0.13490	0.36965	11.500	12.518
46.20	392.00	357.00	2.0649	0.13666	0.37657	13.800	14.421
53.50	392.00	358.00	2.3954	0.13585	0.37250	15.000	16.440
60.00	392.00	364.00	2.7154	0.13134	0.36033	17.000	17.834
70.00	400.00	372.00	3.2136	0.12640	0.34767	18.500	19.892
80.00	402.00	382.00	3.7393	0.11985	0.32743	20.000	21.589
86.70	404.00	386.00	4.0817	0.11748	0.31984	21.500	22.832
94.50	404.00	386.00	4.4489	0.11745	0.32165	23.700	24.598
103.00	405.00	386.00	4.8490	0.11752	0.32201	25.300	26.473
111.00	405.00	384.00	5.2069	0.11877	0.32812	27.000	28.401
119.50	406.00	383.00	5.5956	0.11953	0.33096	29.000	30.314
128.00	405.00	380.00	5.9613	0.12140	0.33684	31.000	32.435
135.50	405.00	377.00	6.2767	0.12340	0.34319	33.000	34.358
143.00	404.00	373.00	6.5768	0.12599	0.35263	35.000	36.430
150.00	404.00	371.00	6.8741	0.12739	0.35678	37.000	38.137
157.00	404.00	369.00	7.1691	0.12881	0.36091	39.000	39.844
165.50	404.00	366.00	7.5168	0.13098	0.36707	41.000	42.011
174.00	402.00	363.50	7.8676	0.13261	0.37204	43.500	44.100
182.00	402.00	362.00	8.2073	0.13372	0.37592	45.500	45.912
190.00	403.00	359.50	8.5299	0.13569	0.38391	47.200	47.908
198.00	403.00	357.50	8.8574	0.13721	0.38953	49.500	49.811
206.50	403.00	353.50	9.1721	0.14035	0.39903	51.800	52.237
223.50	403.00	347.00	9.8131	0.14571	0.41239	56.800	56.871
235.00	402.00	344.00	10.2632	0.14814	0.41751	59.300	59.708
246.50	402.00	342.00	10.7274	0.14989	0.42301	61.800	62.283
257.00	402.00	340.00	11.1448	0.15160	0.42985	64.000	64.670
268.00	402.00	338.00	11.5808	0.15338	0.43508	66.500	67.134
284.00	403.00	336.00	12.2289	0.15524	0.44369	70.500	70.414

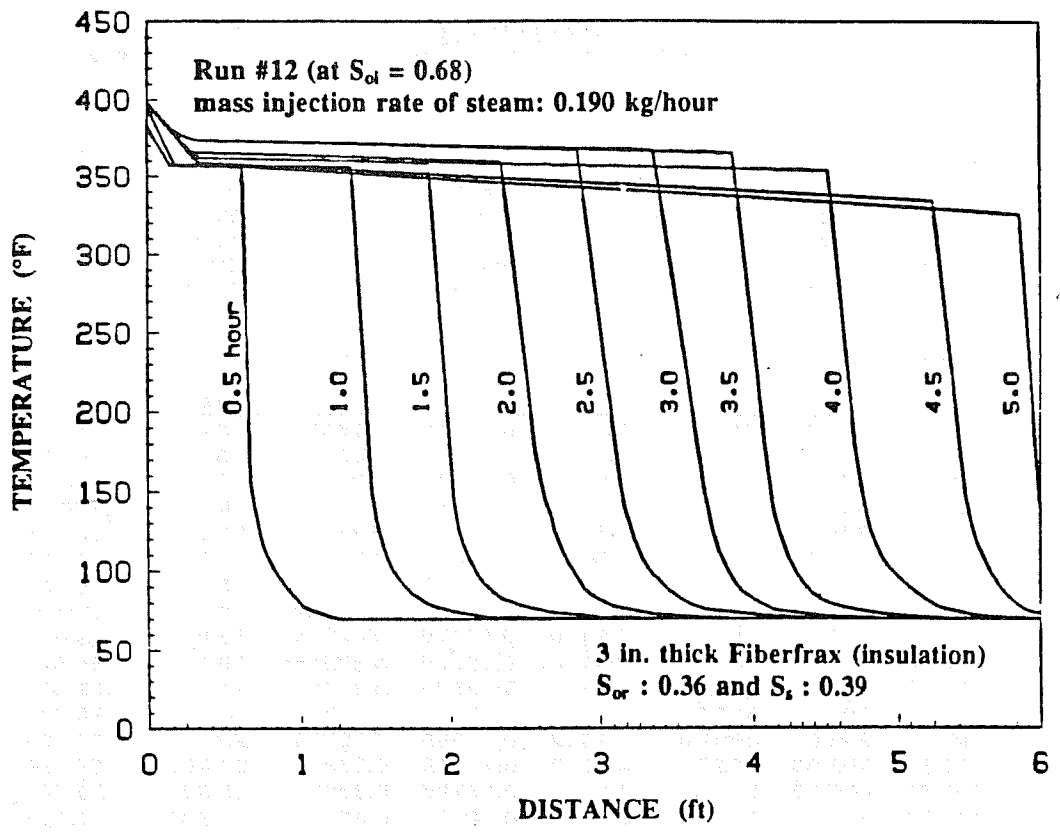


Fig. 6.14 Temperature Profiles of Steam Displacement (Run #12).

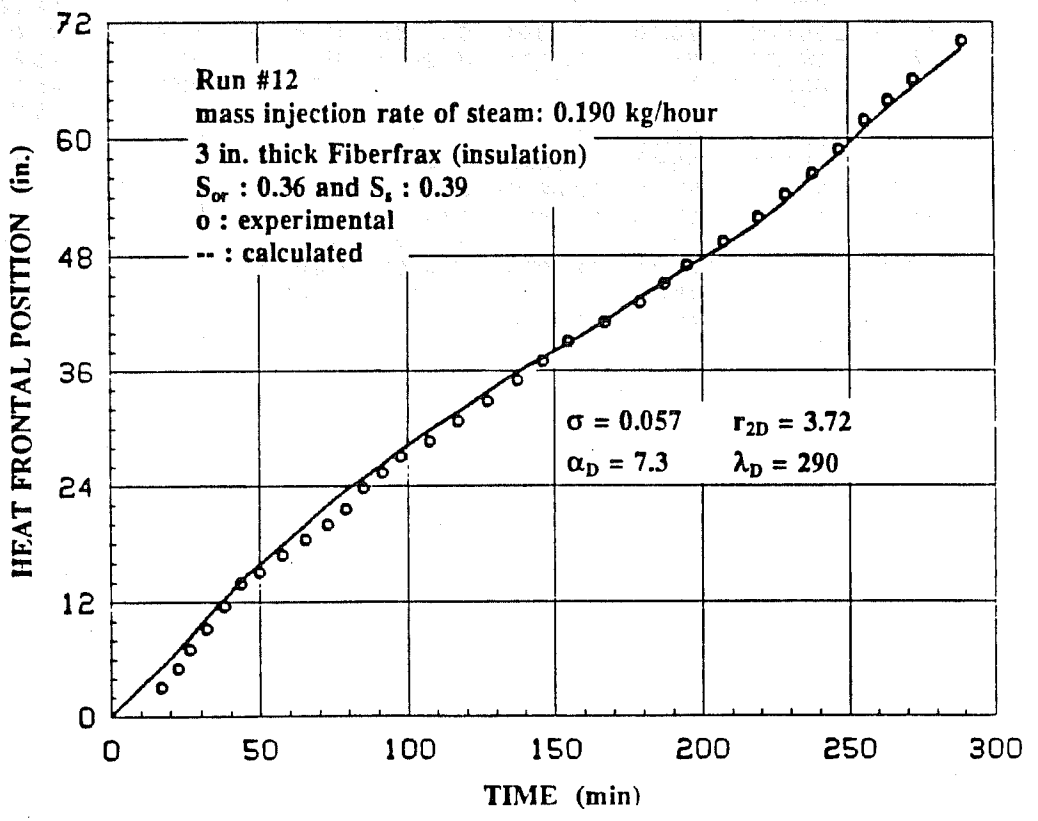


Fig. 6.15 Comparison Between the Calculated and Experimental Heat Fronts of Run #12.

TABLE 6.11
MEASURED AND CALCULATED HEAT FRONTAL POSITION (RUN#12)

heat capacity ratio=	0.0572	diffusivity ratio =	7.300
conductivity ratio=	290.00	radius ratio =	3.717
oil saturation=	0.39	mass injection rate=	3.170 gm/min
water saturation=	0.252	initial temperature=	70.000 °F
steam saturation=	0.36	back pressure =	70.000 psia
porosity=	0.38	insulation conductivity=	0.03577Btu/ hr-ft-F

time min	T _{inj} °F	T _{ave}	t _D	H _D	f _{hw}	xt (in.)	
						measured	calculated
17.00	384.00	384.00	0.7975	0.11559	0.30338	3.000	6.060
22.50	375.00	371.00	1.0311	0.12313	0.32873	6.000	6.898
28.30	375.00	361.00	1.1839	0.13018	0.35001	7.000	8.283
32.10	385.00	351.00	1.4194	0.13889	0.37574	9.200	10.381
38.00	388.00	348.00	1.6714	0.14163	0.38319	11.500	12.305
43.80	390.00	347.00	1.9231	0.14264	0.38414	13.800	14.102
49.80	392.00	349.00	2.1943	0.14122	0.38292	15.000	15.758
57.70	395.00	354.00	2.5651	0.13757	0.37437	16.800	17.691
65.50	397.00	354.00	2.9119	0.13775	0.37515	18.400	19.846
73.00	397.00	354.00	3.2453	0.13775	0.37515	19.900	21.871
79.20	397.00	355.00	3.5272	0.13695	0.37296	21.500	23.420
85.10	396.00	357.50	3.8069	0.13494	0.36846	23.700	24.708
91.50	396.00	359.00	4.1042	0.13383	0.36844	25.300	26.163
97.70	396.00	359.50	4.3862	0.13344	0.36441	27.000	27.629
107.50	396.00	361.50	4.8434	0.13195	0.36033	28.600	29.741
117.20	396.00	364.50	5.3088	0.12977	0.35418	30.700	31.608
127.20	396.00	365.50	5.7721	0.12903	0.35382	32.800	33.685
137.30	396.00	366.50	6.2418	0.12831	0.35175	34.900	35.703
146.00	396.00	368.50	6.6609	0.12691	0.34761	36.900	37.214
155.00	396.00	370.00	7.0905	0.12588	0.34363	39.000	38.786
167.00	397.00	370.00	7.6394	0.12598	0.34416	41.000	41.096
179.00	397.00	368.50	8.1664	0.12898	0.34983	43.100	43.577
187.20	397.00	368.50	8.5405	0.12698	0.34983	45.000	45.066
195.10	397.00	367.50	8.8850	0.12765	0.35360	46.900	46.649
207.30	397.00	367.00	9.4321	0.12799	0.35547	49.300	48.855
219.40	397.00	365.50	9.9559	0.12904	0.35939	51.800	51.184
228.70	398.00	362.50	10.3225	0.13131	0.36598	54.100	53.346
238.00	398.00	357.50	10.6468	0.13498	0.37930	56.300	55.981
246.90	398.00	354.00	10.9763	0.13769	0.38720	58.800	58.259
255.70	398.00	349.00	11.2668	0.14163	0.39876	61.800	60.940
264.00	398.00	346.00	11.5707	0.14409	0.40264	63.800	63.076
272.50	398.00	343.50	11.8904	0.14617	0.40810	66.000	65.131
289.50	398.00	339.00	12.5320	0.15003	0.41737	70.000	69.135

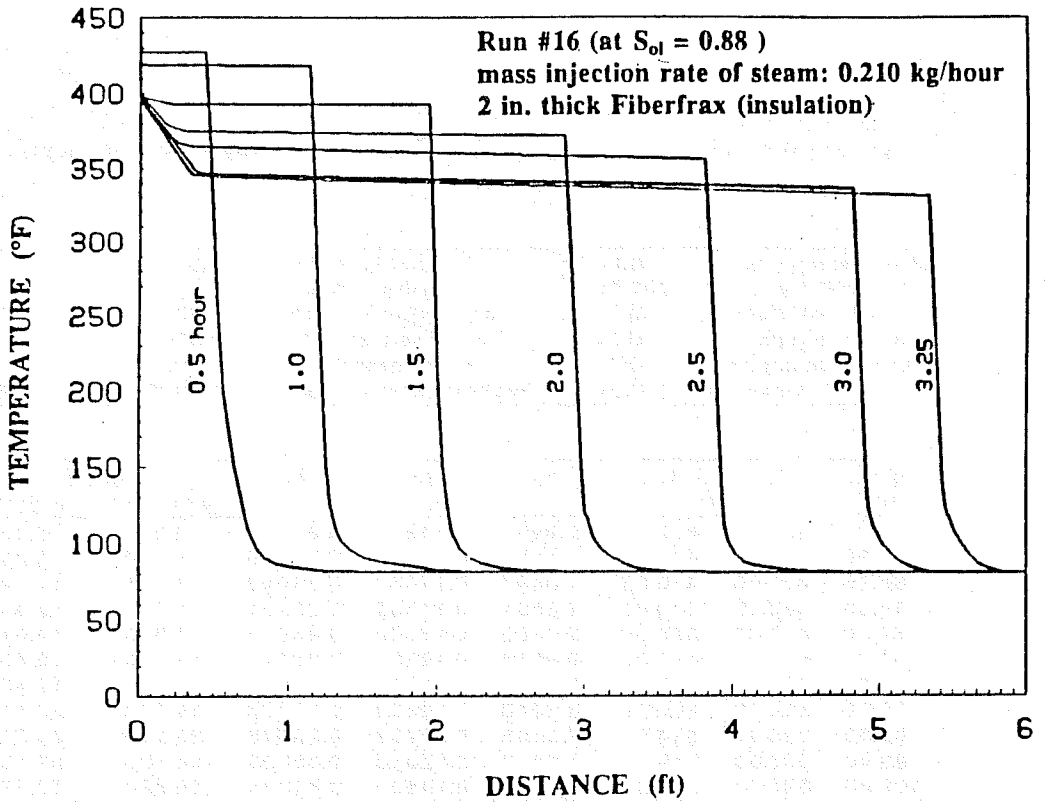


Fig. 6.16 Temperature Profiles of Steam Displacement (Run #16).

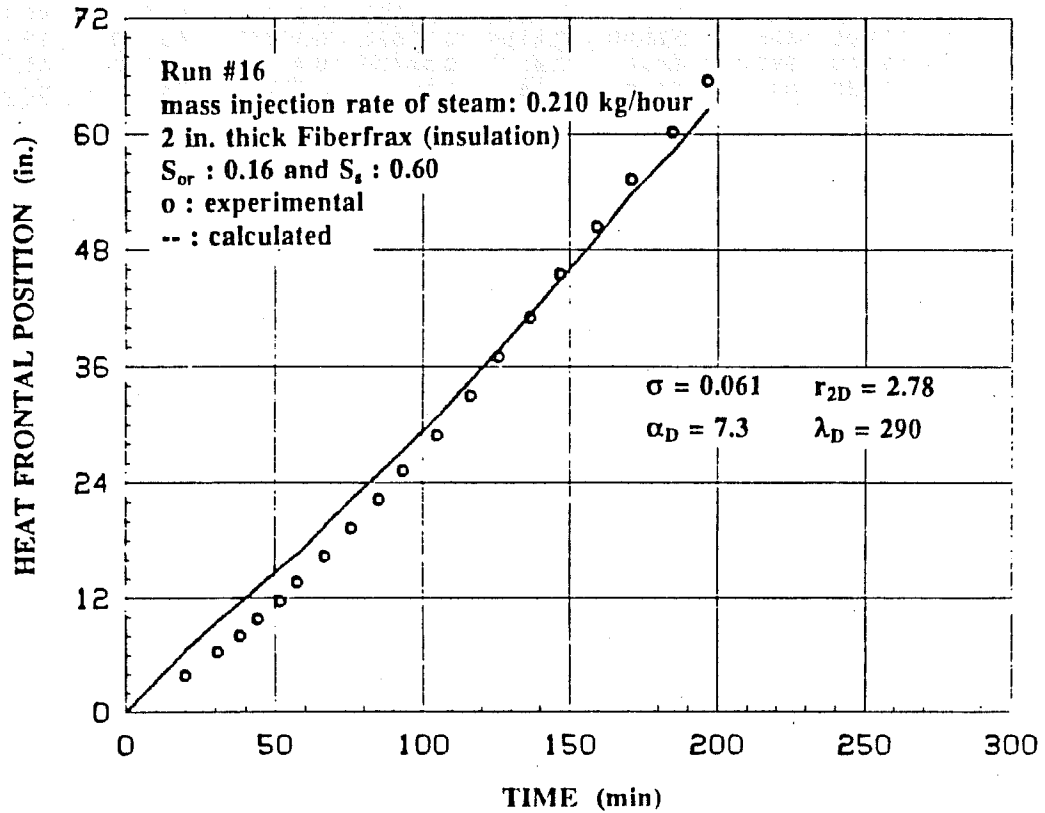


Fig. 6.17 Comparison Between the Calculated and Experimental Heat Fronts of Run #16.

TABLE 6.12
MEASURED AND CALCULATED HEAT FRONTAL POSITION (RUN#16)

heat capacity ratio=	0.0607	diffusivity ratio =	7.300
conductivity ratio=	290.00	radius ratio =	2.778
oil saturation=	0.16	mass injection rate=	3.500 gm/min
water saturation=	0.241	initial temperature=	80.000 °F
steam saturation=	0.60	back pressure =	16.000 psia
porosity=	0.34	insulation conductivity=	0.03508Btu/ hr-ft-F

time min	T _{inj} °F	T _{ave}	t _D	H _D	f _{hv}	xt (in.)	
						measured	calculated
19.90	422.00	422.00	0.9998	0.11851	0.33502	8.841	8.350
30.80	426.00	426.00	1.5586	0.11564	0.32378	8.318	9.412
38.25	430.00	430.00	1.9497	0.11337	0.31942	7.974	11.327
44.30	430.00	430.00	2.2581	0.11385	0.32231	8.700	12.936
51.80	427.00	425.00	2.6166	0.11034	0.28990	11.600	14.978
57.40	423.00	421.00	2.8785	0.10861	0.27291	13.550	16.462
66.80	409.00	407.00	3.2662	0.11646	0.29664	16.270	19.432
75.70	402.00	400.00	3.6549	0.12633	0.34775	19.220	22.111
85.10	396.00	394.00	4.0645	0.12732	0.34448	22.210	24.800
93.40	395.00	389.00	4.4209	0.12985	0.35026	25.130	27.160
105.00	395.00	383.00	4.9166	0.14500	0.41034	28.820	30.720
116.30	395.00	376.00	5.3777	0.15498	0.43945	32.890	34.496
126.00	395.00	371.00	5.7742	0.16053	0.45252	36.910	37.681
136.50	395.00	365.00	6.1886	0.16563	0.46177	40.950	41.260
147.00	395.00	357.00	6.5701	0.15841	0.42806	45.380	44.906
159.40	395.00	349.00	7.0236	0.16595	0.44089	50.250	49.132
171.00	395.00	340.00	7.4154	0.17823	0.46686	55.150	53.707
185.00	395.00	335.00	7.9519	0.18726	0.48555	60.110	58.120
196.50	395.00	328.00	8.3427	0.19246	0.48952	65.390	62.545

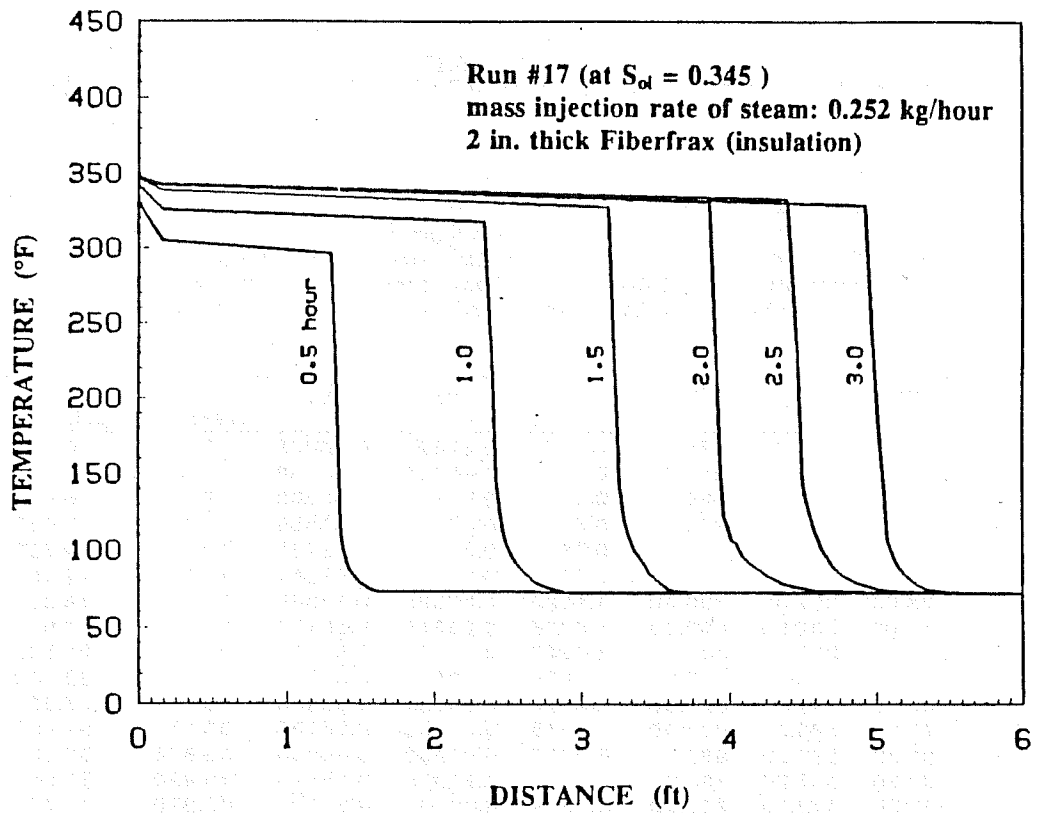


Fig. 6.18 Temperature Profiles of (Run #17).

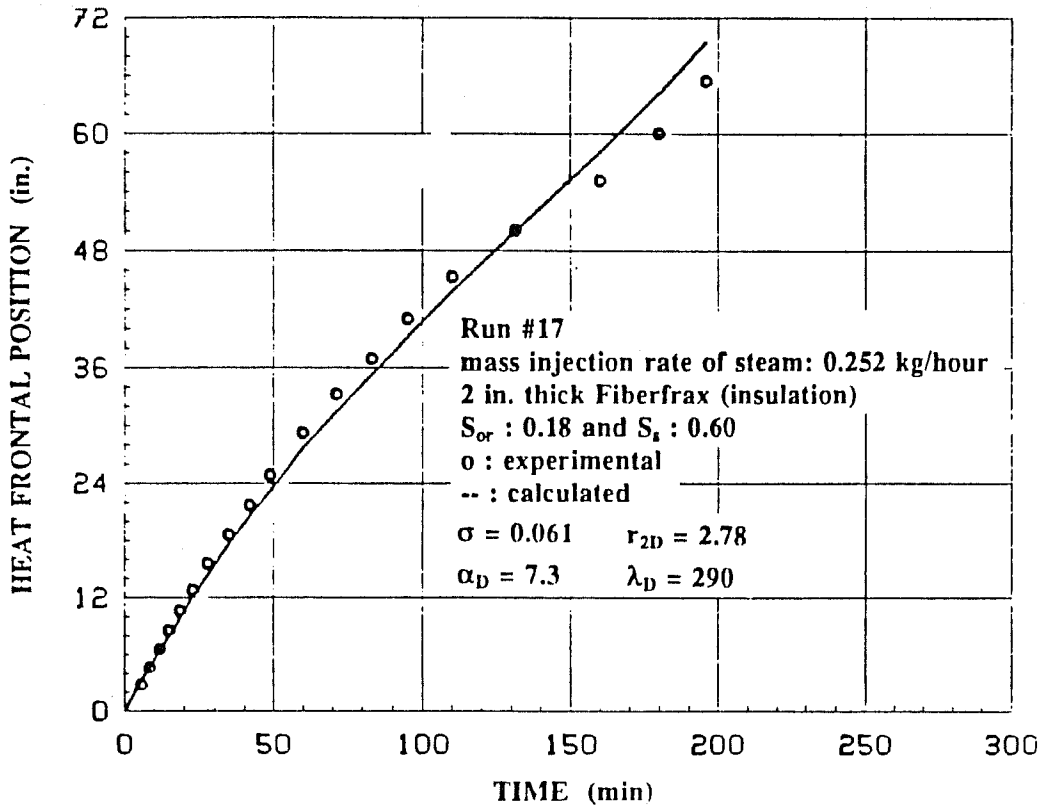


Fig. 6.19 Comparison Between the Calculated and Experimental Heat Fronts of Run #17.

TABLE 6.13
MEASURED AND CALCULATED HEAT FRONTAL POSITION (RUN#17)

heat capacity ratio=	0.0614	diffusivity ratio =	7.300
conductivity ratio=	290.00	radius ratio =	2.778
oil saturation=	0.18	mass injection rate=	4.200 gm/min
water saturation=	0.218	initial temperature=	69.000 °F
steam saturation=	0.60	back pressure =	0. psia
porosity=	0.34	insulation conductivity=	0.035158tu/hr-ft-F

time min	T _{m'} °F	T _{ave}	t _D	H _D	f _{hv}	xt (in.)	
						measured	calculated
6.62	275.00	275.00	0.2177	0.26593	0.55928	2.700	3.254
8.44	283.00	283.00	0.3315	0.26326	0.55162	4.610	4.655
11.81	295.00	285.00	0.4654	0.25263	0.55363	6.450	6.405
15.00	305.00	290.00	0.5962	0.24895	0.55859	8.460	7.917
18.50	313.00	290.00	0.7353	0.26345	0.58032	10.540	9.829
23.00	321.00	293.00	0.9188	0.26161	0.58281	12.680	12.102
28.00	327.00	300.00	1.1322	0.25624	0.58369	15.510	14.325
35.00	332.00	303.00	1.4226	0.25249	0.58152	18.500	17.663
42.00	333.00	309.00	1.7249	0.24292	0.57302	21.830	20.532
49.00	338.00	315.00	2.0335	0.23481	0.56746	24.770	23.170
60.00	341.00	321.00	2.5163	0.24031	0.58469	29.150	27.621
71.30	343.00	327.00	3.0218	0.21863	0.55125	33.160	31.405
83.30	345.00	332.00	3.5616	0.21432	0.54986	36.870	35.264
95.30	347.00	335.00	4.0963	0.21026	0.54490	40.920	39.068
110.30	348.00	337.00	4.7579	0.20764	0.54143	45.220	43.724
131.60	348.00	339.00	5.6967	0.20464	0.53742	50.000	49.872
160.00	348.00	338.00	6.9139	0.20561	0.53832	55.070	58.004
180.00	347.00	334.00	7.7234	0.20884	0.54312	60.000	64.134
196.00	345.00	329.00	8.3362	0.21430	0.55117	65.380	69.472

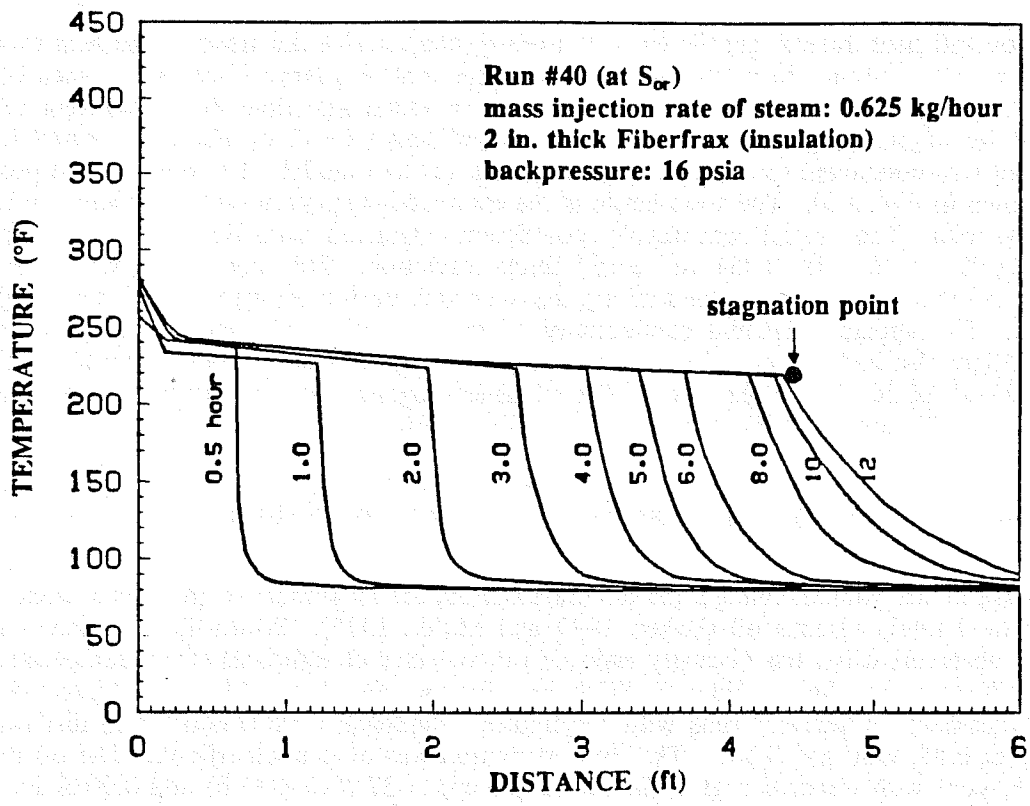


Fig. 6.20 Temperature Profiles of Steam Displacement (Run #40).

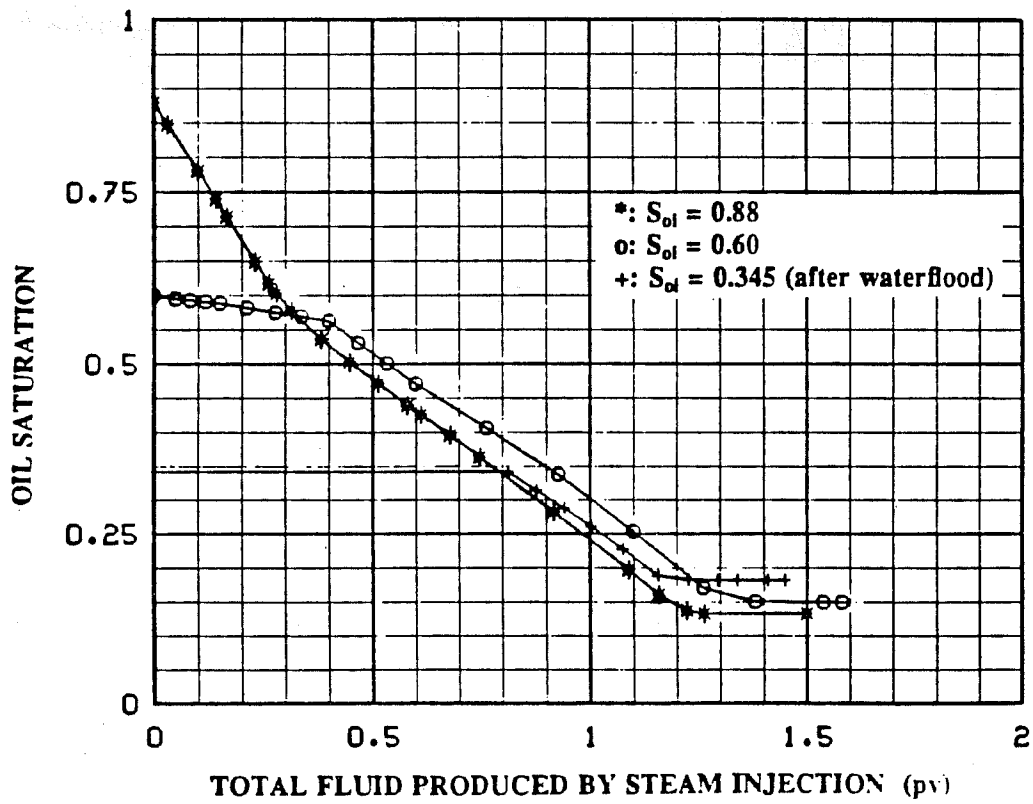


Fig. 6.21 Oil Recovery from Steam Displacements at Different Initial Oil Saturation.

6.3. OVERALL HEAT TRANSFER COEFFICIENT

The overall heat transfer coefficient was used to characterize the steady-state heat transfer rate of a finite composite system. In a laboratory study of thermal recovery, it was sometimes convenient to use this coefficient to handle heat loss calculations. In steam injection, this coefficient can be calculated from the stagnation point (steady state solution of steam front) by Eq. 2.6 referred to in Section 2. Run #40 was conducted to estimate this coefficient for this model. The temperature profiles of this run are shown in Fig. 6.20. The solid circle is the estimated stagnation point, which is at 1.35 m (4.42 ft) from the inlet. The overall heat transfer coefficient calculated from Eq. 2.6 is $1.93 \times 10^{-3} \text{ W/m}^2 \cdot \text{K}$ ($0.34 \text{ Btu/hr} \cdot \text{F} \cdot \text{ft}^2$ for the 0.051 m (2 in.) thick insulation. This coefficient would be useful for estimating the mass flow rate of steam along the sandpack during experiments of steam injection with surfactants. The apparent thermal conductivity of the insulation calculated by Eq. 6.3 is $5.1 \times 10^{-3} \text{ W/m} \cdot \text{K}$ ($0.0295 \text{ Btu/hr} \cdot \text{F} \cdot \text{ft}$) and the estimated overall heat transfer coefficient based on this value is $1.92 \times 10^{-3} \text{ W/m}^2 \cdot \text{K}$ ($0.337 \text{ Btu/hr} \cdot \text{F} \cdot \text{ft}^2$). The closeness between the observed and estimated overall heat transfer coefficients confirms that Eq. 6.3 is good for our system.

6.4. EFFECT OF INITIAL OIL SATURATION ON OIL RECOVERY

Because of the volume change due to condensation, the movement of the steam front is stable for displacing moderately viscous oil (Baker, 1973 and Miller, 1975). Piston-like displacement of oil by steam was observed when the viscosity ratio of oil to water at saturated steam temperature was less than ten (Closman and Seba, 1983; El-Saleh and Farouq Ali, 1968; Flock and Lee, 1977). Three steam displacement oil recovery runs with a cylindrical sandpack were conducted at different initial oil saturations of 0.88, 0.60 and 0.345. The third saturation was after a waterflood. The oil used in these runs was Kaydol with viscosities of $0.070 \text{ Pa} \cdot \text{s}$ (70 cp) at 37.7°C (100°F) and $0.0030 \text{ Pa} \cdot \text{s}$ (3.0 cp) at 171°C (340°F). The viscosity ratio of oil to water at 171°C (340°F) was approximately 19. The kinematic viscosity ratio between Kaydol and steam shown in Fig. 5.6 indicates that the process should be stable at temperature lower than 204°C (400°F). The oil saturation histories (Fig. 6.21) and residual oil saturations ranging from 0.14 to 0.19 are not strongly dependent of the initial oil saturation within the accuracy of the experiments. Further, the linear nature of the oil saturation versus volume produced curves indicates stable displacements as expected.

7. EXTENSION OF MARX AND LANGENHEIM EQUATION FOR STEAM SWEEP VOLUME

The theory of the development of the steam swept volume is discussed in this section. The definition of the critical time is reexamined, and based on laboratory observations and physical constraints a new method is presented for approximating the steam swept volume.

7.1. CRITICAL TIME

The development of the steam swept volume during steam displacement is mainly dominated by the transfer of injected latent heat. The injected latent heat is consumed by the lateral heat loss and the growth of the steam swept zone. The sensible heat helps accelerate the development of the steam swept zone. Therefore, both injected latent heat and sensible heat affect the development of the steam swept volume.

The critical time defined by Mandl and Volek (1969) has been used by previous investigators to indicate the time when the hot-liquid zone becomes significant. From the point of view of heat loss, this critical time is the time the calculated heat loss rate from the heated zone equals the rate of the latent heat injection. When the time is greater than the critical time, the rate of heat loss from the steam swept zone must, therefore, equal the rate of latent heat injection. This is the Hearn theory (1969). Apparently, this theory has neglected the latent heat used to heat additional reservoir to steam temperature. Although models by Myhill and Stegemeier (1978), and Yortsos and Gavalas (1982) give steam swept volumes smaller than the Hearn solution when time is greater than the critical time, in their calculations a decrease of the heat loss rate from the steam swept zone occurs during most of the time of interest. In reality, the rate of heat loss from the steam zone must continuously increase with time since the area for heat loss increases with time. It is, therefore, necessary to reexamine the concept of the critical time and the theory of the development of steam zone at times greater than the critical time.

From the point of view of fluid dynamics, Mandl and Volek (1969) defined the critical time as the time when the velocity of the heat front equals the sharp temperature front velocity of an adiabatic hot-water displacement at the same mass injection rate and injection temperature as the steam displacement. However, the critical time may be defined better as the time when the heat frontal velocity equals the injected fluid flow velocity of an adiabatic hot-water displacement at the same mass injection rate and injection temperature as the steam displacement. When the heat injection rate is constant, the steam quality must decrease with an increase of mass injection rate. A low-quality steam injection represents an equivalent adiabatic hot-water displacement with a high fluid velocity. The heat frontal velocity reaches this equivalent fluid velocity early and the low quality steam injection has a small critical time.

This critical time defined by the fluid flow velocity will give critical times smaller than those defined by Mandl and Volek by a factor which varies from 1.2 to 5 depending on the ratio of fluid velocity to the temperature velocity. This ratio depends on the volumetric heat capacities of the reservoir rock and fluids compared to the flowing water. The following equation can be used to estimate this factor:

$$f_{ic} = \frac{(\rho C)_R}{\phi(\rho C)_w}, \quad (7.1)$$

where $(\rho C)_w$ is the volumetric heat capacity of the injected hot water. The critical time defined by this fluid flow velocity criterion is thus:

$$t_{cD} = \frac{(t_{cD})_{MV}}{f_{tc}}, \quad (7.2)$$

where $(t_{cD})_{MV}$ is the Mandl and Volek critical time, which is obtained by solving the following equation from Marx and Langenheim:

$$e^{(t_{cD})_{MV}} \operatorname{erfc}(\sqrt{(t_{cD})_{MV}}) = 1 - f_{hv}, \quad (7.3)$$

where f_{hv} is the ratio of latent to total heat injection. The Newton method can be used for solving for $(t_{cD})_{MV}$ in Eq. 7.3 with f_{hv} ranging from 0.1 to 0.85. Figure 7.1 graphs $(t_{cD})_{MV}$ as a function of f_{hv} . Notice in this figure that $\log((t_{cD})_{MV})$ is nearly a linear function of f_{hv} in the range from 0.3 to 0.7. The following equation can be used to find $(t_{cD})_{MV}$ with relative error less than 4% for $0.3 \leq f_{hv} \leq 0.7$:

$$(t_{cD})_{MV} = 0.01332e^{7.5681 f_{hv}}. \quad (7.4)$$

Values of $(t_{cD})_{MV}$ are also listed in Table 7.1.

TABLE 7.1 VALUES FOR $(t_{cD})_{MV}$, n_1 , n_2 AND β AS A FUNCTION OF f_{hv} FOR $f_{tc} = 2.5$

f_{hv}	$(t_{cD})_{MV}$	n_1	n_2	β
0.1	0.00927	1.066	0.411	2.10
0.2	0.04465	1.118	0.540	1.25
0.3	0.12415	1.1742	0.674	0.80
0.4	0.28225	1.2380	0.812	0.50
0.5	0.59148	1.3145	0.955	0.25
0.6	1.22570	1.4092	1.102	0.12
0.7	2.69150	1.5307	1.254	
0.8	7.04230	1.6897	1.411	
0.9	31.42900	1.8864	1.57	

The critical time defined by Eq. 7.2 is not the true critical time. The true critical time is believed to be smaller than the critical time given by Eq. 7.2 because the water saturation in both the steam zone and the hot-liquid zone are less than one.

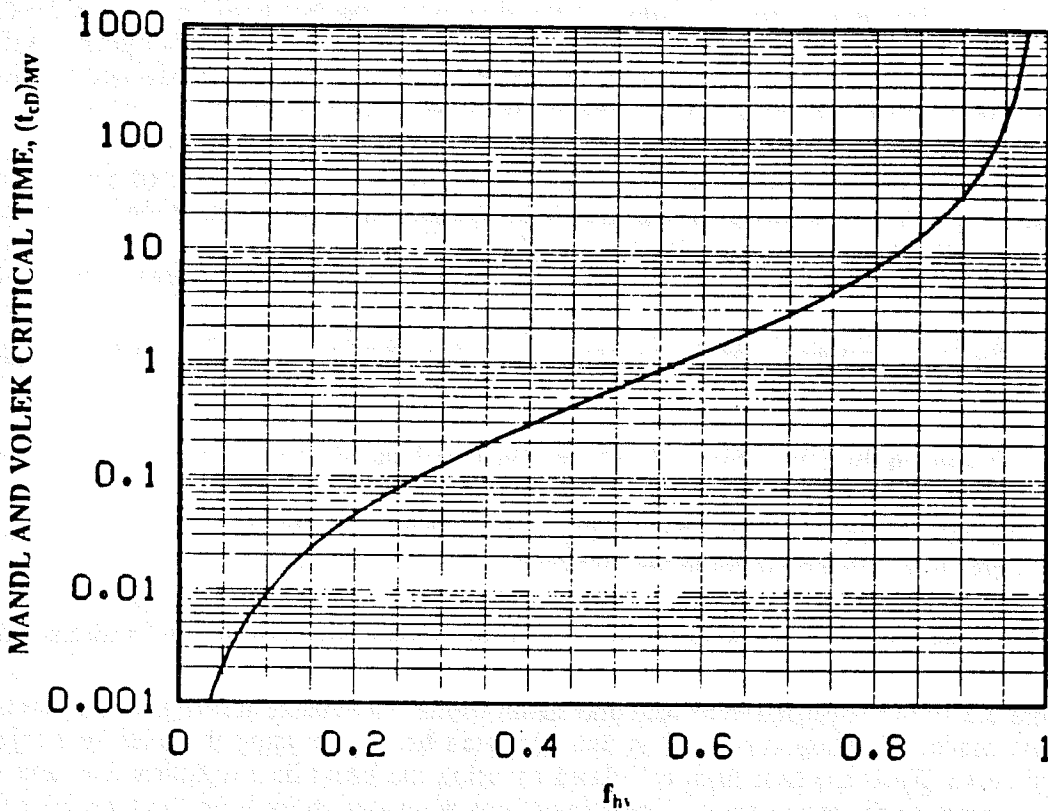


Fig. 7.1 Mandl and Volek Dimensionless Time vs f_{hv} .

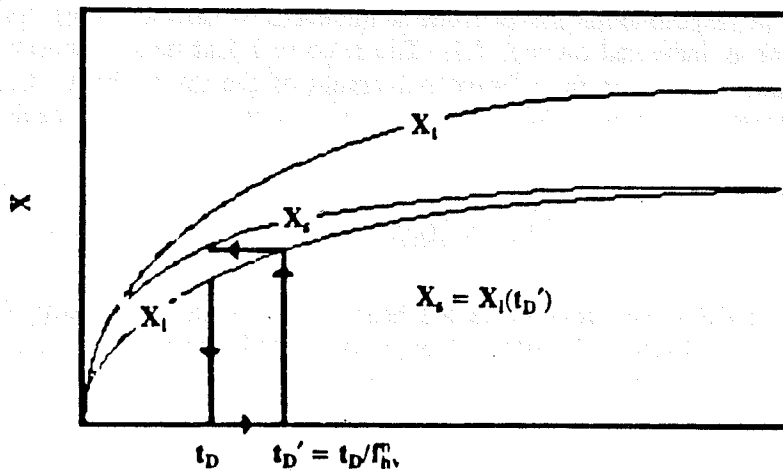


Fig. 7.2 Graphic Representation of the Method of Approximating Steam Volume by Shifting the Time Scale.

7.2. METHOD FOR PREDICTING STEAM SWEPT VOLUME

The critical time is only an indication of the time when the hot-liquid zone ahead of the steam swept zone becomes significant. It does not tell us anything about how the sensible heat will flow into the hot-liquid zone. If the heat flowing into the hot-liquid zone can be properly approximated, it has been found that the exact values of critical time do not have to be known very accurately.

The development of the steam swept volume is complicated by the injected sensible heat. Neither a heat balance equation based on the total heat injection rate nor an equation based on the latent heat injection rate can satisfactorily describe the development of the steam swept volume. Methods applying some physical constraints may lead to a better approximation of the steam swept volume.

Two physical constraints can be recognized for the development of the steam swept volume. They are:

1. the rate of heat loss from the steam swept volume cannot exceed the rate of latent heat injection and
2. the rate of heat flow into the hot-liquid zone increases with time from zero to a maximum equal to the rate of sensible heat injection.

A method for approximating the steam swept volume using these two constraints is discussed.

Figure 7.2 shows an example of heat and steam frontal movement during a steam displacement in a laboratory model. The top curve (X_t) is the calculated heat front using the total heat injection rate; the bottom curve (X_l) is the heat front calculated by using the latent heat injection rate; and the middle curve (X_s) represents the steam front. The steam front gradually shifts from the total heat front curve to the latent heat front curve. Neither of the two curves can satisfactorily describe the experimental steam frontal behavior.

Because the thickness of the insulation of laboratory models is finite, the steam front can reach the steady-state position (stagnation point) after a period of injection. It is clear that the effect of the injected sensible heat is to expedite the steam front movement but not to vary the steady-state position. One way to match the experimental steam front is therefore to shift the time scale of the latent heat front curve to the left as indicated on Fig. 7.2. The ratio of latent heat to total heat injected (f_{hv}) is a parameter which should determine the relative movement of the steam front. Using this concept, the heat injection ratio raised to a power (f_{hv}^n) could be used to change the time scale and the steam front could be given by:

$$X_s(t) = X_l(t/f_{hv}^n) = X_l(t'), \quad (7.5)$$

where X_s is the calculated steam front, X_l is the heat front calculated by using the rate of latent heat injection and n is a power index to be determined empirically by evaluating the heat loss rate from the steam swept zone. The other way to calculate X_s using superposition might be stated as:

$$X_s = X(t_c) + [X_l(t') - X_l(t'_c)], \quad (7.6)$$

where

$$\begin{aligned} t' &= t/f_{hv}^n \\ t_c' &= t_c/f_{hv}^n \end{aligned}$$

The concept introduced in Eq. 7.6 may be extended to systems with infinitely thick adjacent formations by using the Marx and Langenheim equation. Using this equation, the steam swept volume in the dimensionless form is given by:

$$G_1(t_D) = G(t_{cD}) + f_{hv}[G(t_D') - G(t_{cD}')] , \quad (7.7)$$

where

$$\begin{aligned} G_1 &= \text{dimensionless heated volume, } V_s/\dot{H}_D h^3, \\ \dot{H}_D &= \text{dimensionless heat injection rate, } \dot{H}/4\sigma K_S h \Delta T, \\ t_D &= \text{dimensionless time, } 4\sigma^2 \alpha_s t/h^2, \\ t_D' &= \text{shifted dimensionless time, } t_D/f_{hv}^n, \\ \sigma &= (\rho C)_S/(\rho C)_R, \\ f_{hv}^n &= \text{weighting factor.} \end{aligned}$$

The function $G(t_D)$ is given by the Marx and Langenheim solution:

$$G(t_D) = 2\sqrt{\frac{t_D}{\pi}} - 1 + e^{t_D} \text{erfc}(\sqrt{t_D}). \quad (7.8)$$

In general, the index (n) is expected to be a function of time, critical time (t_c), fraction of latent heat (f_{hv}) and the geometry of the steam swept zone. Except for the the effect of the geometry of the steam swept zone, the value of n as a function of f_{hv} and time could be expected to be capable of being estimated empirically by the critical time and the two physical constraints mentioned earlier.

7.2.1. Time Range of Validity of Eq. 7.7

Before the critical time, it is assumed that no heat is flowing into the liquid zone. After the critical time, the rate of heat flowing into the hot-liquid zone increases with time and gradually reaches the rate of sensible heat injected. This concept can be used quantitatively. From differentiating Eq. 7.7, the rate of the growth of the steam swept volume is given by:

$$\frac{dG_1}{dt_D} = f_{hv}^{1-n} G'(t_D') \quad (7.9)$$

and the rate of heat loss from the steam swept volume is given by:

$$\dot{H}_{lsD} = \int_0^{t_D} \frac{1}{\sqrt{\pi(t_D - \tau_D)}} \frac{dA_D}{d\tau_D} d\tau_D, \quad (7.10)$$

where A_D is the steam swept area, defined as $A_s/h^2\dot{H}_D$, t_D is the present time and t_{sD} is the time that the heat front arrived at the present steam front. The heat loss rate can be evaluated numerically by using the trapezoidal rule. The detailed procedure for evaluating this rate is given in Appendix A.2.

From a heat balance, the dimensionless rate of heat flowing into the hot-liquid zone (\dot{H}_{wD}) is given by:

$$\dot{H}_{wD} = 1 - \frac{dG_1}{dt_D} - \dot{H}_{lsD} \quad (7.11)$$

The first term on the right hand side (1) represents the dimensionless total heat injection rate, the second is the dimensionless rate of heat stored in the steam zone and the third is the dimensionless rate of heat loss from the steam zone. The rate calculated from this equation is not a continuously increasing function with respect to time for all times and all values of f_{hv} . To be consistent with known physical constraints, Eq. 7.7 can only be used in the time range where Eq. 7.11 is increasing with time. From calculations, it was found that as f_{hv} becomes larger, this time range becomes smaller. At f_{hv} of 0.9, it was found that a dimensionless time of 80 was the point where Eq. 7.11 reached a maximum heat flow rate into the hot-liquid zone. All lower values of f_{hv} produced larger times. The dimensionless time of 80 is longer than the durations of most of steam injection projects in the field. Thus, this equation appears to be valid for most conditions.

7.2.2. Determination of n

The power n for f_{hv} could be used to adjust the characteristic curves of the heat loss rate from the steam zone based on the physical constraints and engineering judgement. From trial calculations, it was found that n varies from a maximum value at the critical time to a minimum value at large times.

Because it is assumed that the actual steam swept volume starts to deviate from the calculated heated volume at a critical time, a value of n for each f_{hv} at that time, which will be called n_1 , may be determined by:

$$G'(t_{cD}) = f_{hv}^{1-n_1} G'(t_{cD}/f_{hv}^{n_1}), \quad (7.12)$$

where t_{cD} is given by Eq. 7.2. Equation 7.12 states that the growth rate of the steam swept volume calculated by Eq. 7.7 equals the growth rate of the heated volume given by the Marx and Langenheim equation at the dimensionless critical time. Using this equation, a number of values of n_1 were determined and shown as diamonds for f_{ic} of 2.5, and circles for f_{ic} of 5 in Fig. 7.3. The values of n_1 for f_{ic} of 2.5 are also listed in Table 7.1, and were least squares fit to the following equation:

$$n_1 = 1.075 + 0.011 f_{hv} + 0.956 f_{hv}^2 \quad (7.13)$$

Further study revealed that if n_1 is used for large times, the calculated rate of heat loss from the steam zone will exceed the latent heat injection rate. Thus, the power index (n) should be a function of time. According to the physical constraints, the calculated rate of heat loss from the steam swept zone must be smaller than the latent heat injection rate and the estimated rate of heat flowing into the hot-liquid zone must be smaller than the rate of sensible heat injection at the large times. The power indexes (n) determined by these large-time physical constraints are called n_2 . Because of the empirical nature of this method, the value of n_2 is not unique for each f_{hv} . Figure 7.3 shows the values of n_2

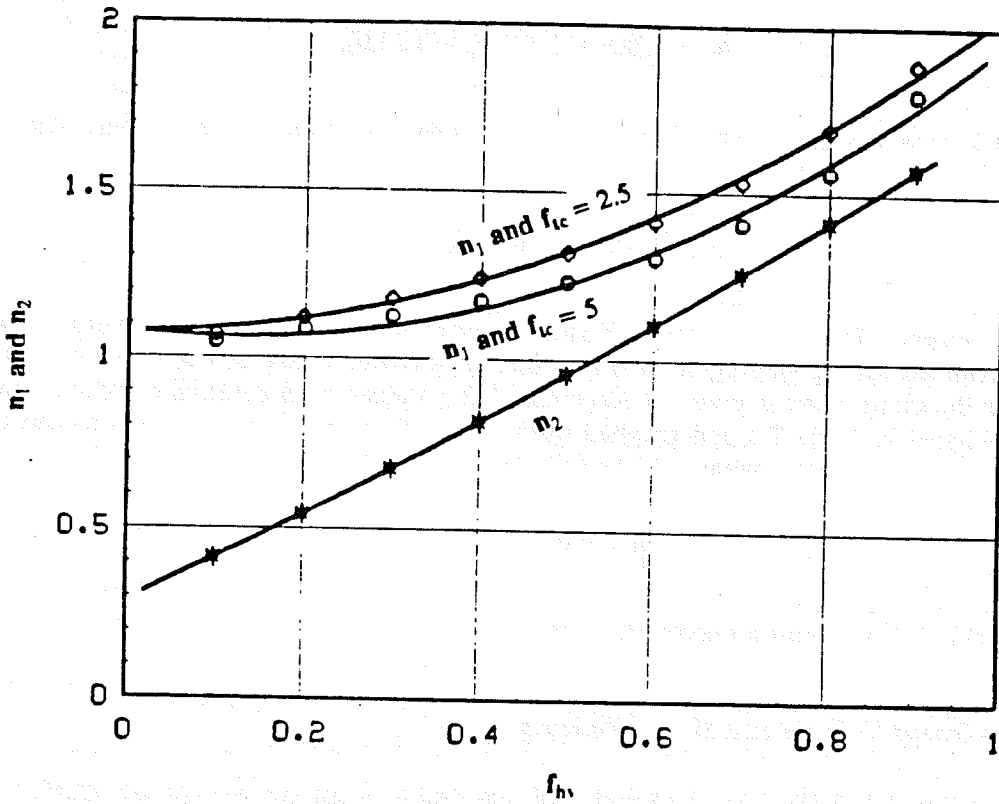


Fig. 7.3 Values of n_1 and n_2 vs f_{hv} .

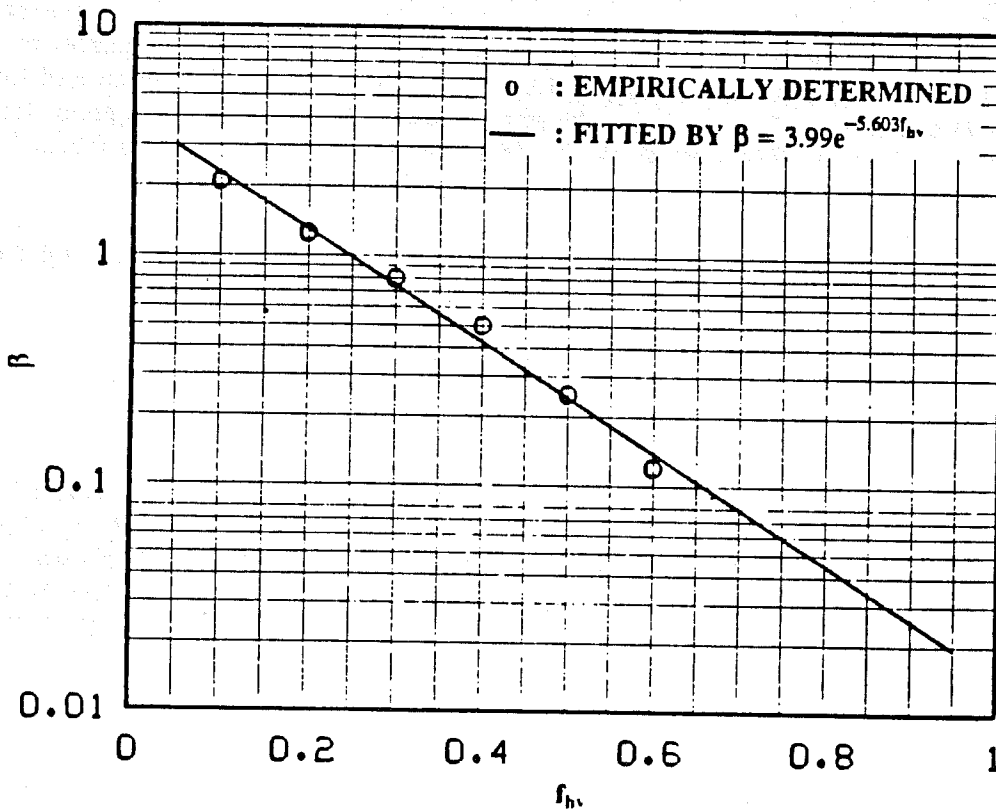


Fig. 7.4 Values of β vs f_{hv} .

determined from this study. Equation 7.14 is a fitted equation which matches the determined n_2 :

$$n_2 = 0.286 + 1.227f_{hv} + 0.223f_{hv}^2 \quad (7.14)$$

It is not known how the n varies from n_1 at the critical time to n_2 at large times. An exponential decay form was tried in this study:

$$n(t_D, f_{hv}) = n_2 + (n_1 - n_2)e^{-\beta\sqrt{t_D - t_{cD}}}, \quad (7.15)$$

where β is a constant. By using the form of square root of time for the exponent, constant values of β could be determined for f_{hv} varying from 0.1 to 0.6. A detailed study of the effect of β on the heat loss rate from the steam zone is given in Appendix A.2. Values of β determined for f_{hv} ranging from 0.1 to 0.6 are listed in Table 7.1 and graphed in Fig. 7.4. From the graph, it can be seen that β may be estimated by using an exponential form as follows:

$$\beta = 3.9934e^{-5.6027f_{hv}} \quad (7.16)$$

The curve in Fig. 7.4 is calculated using Eq. 7.16.

7.2.3. Steam Swept Volume and Heat Efficiency

By using Eqs 7.7, 7.13, 7.14, 7.15 and 7.16, the steam swept volume can be approximated when both total heat and latent heat injection rates are constant. The G_1 function is independent of the heat injection rates. Values of G_1 for f_{hv} varying from 0.1 to 1 were calculated, and are graphed in Fig. 7.5 for t_D varying from 0 to 10 and in Fig. 7.6 for t_D varying from 0 to 100. These values, which are also listed in Table 7.2, are for $f_{ic} = 2.5$ which is near the laboratory value. The curve of $f_{hv} = 1$ is for the Marx and Langenheim solution based on the total heat injection rate. The curves for f_{hv} of 0.8 and 0.9 almost overlap with the curve for f_{hv} of 1.0. As shown in Fig. 7.5, the Marx and Langenheim solution ($f_{hv} = 1$) can be used for calculating the steam swept volume when f_{hv} is greater than 0.8 and t_D is less than ten. In most field operations, f_{hv} falls within the range of 0.2 to 0.8 and the steam swept volume is significantly smaller than the total heated volume.

The steam-zone heat efficiency E_s for cases of constant total heat and latent heat injection rates is expressed as:

$$E_s(t_D) = \frac{H_s}{H_{inj}} = \frac{G_1}{t_D}, \quad (7.17)$$

where H_s is the heat stored in the steam zone. E_s is plotted as a function of dimensionless time and f_{hv} in Fig. 7.7 for f_{ic} of 2.5 and in Fig. 7.8 for f_{ic} of 5. It is noted that the differing values of f_{ic} vary the small time behavior slightly but have virtually no effect at dimensionless times greater than one. When f_{hv} is less than 0.2, the curves are not smooth at times just after the dimensionless critical times. This is because the calculated rates of heat loss from the steam zone at these times are slightly smaller than the rates at the critical times.

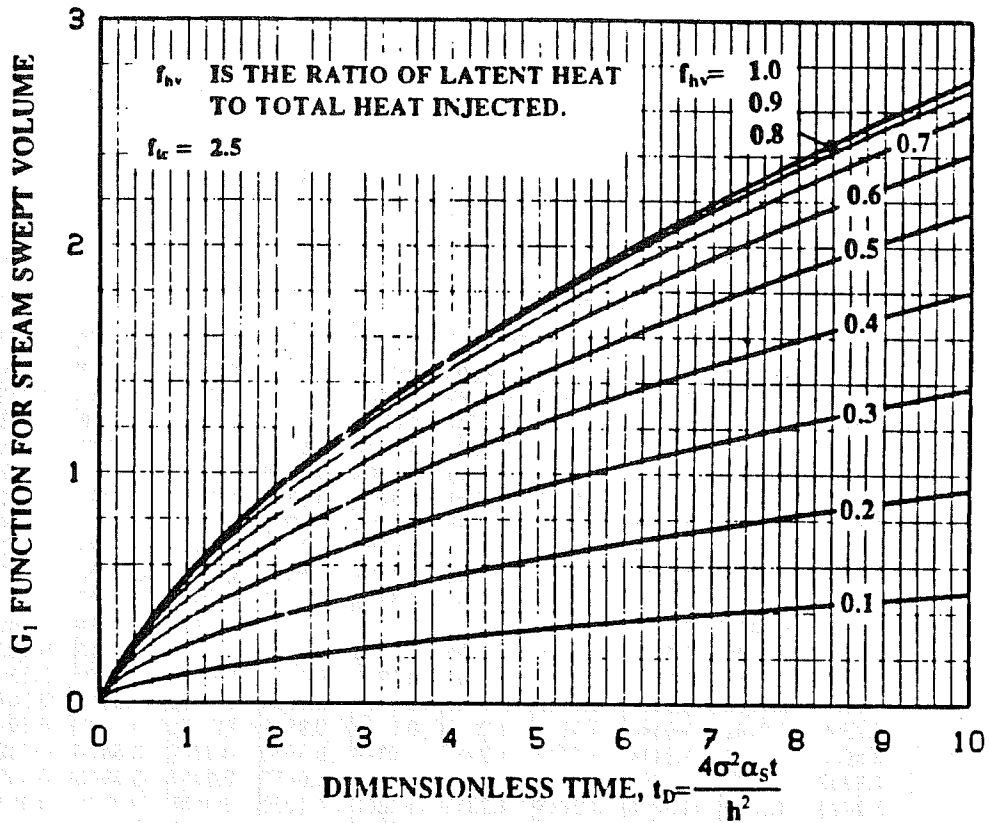


Fig. 7.5 Values of G_1 for Steam Swept Volume vs t_D from 0 to 10 for $f_{i_c} = 2.5$.

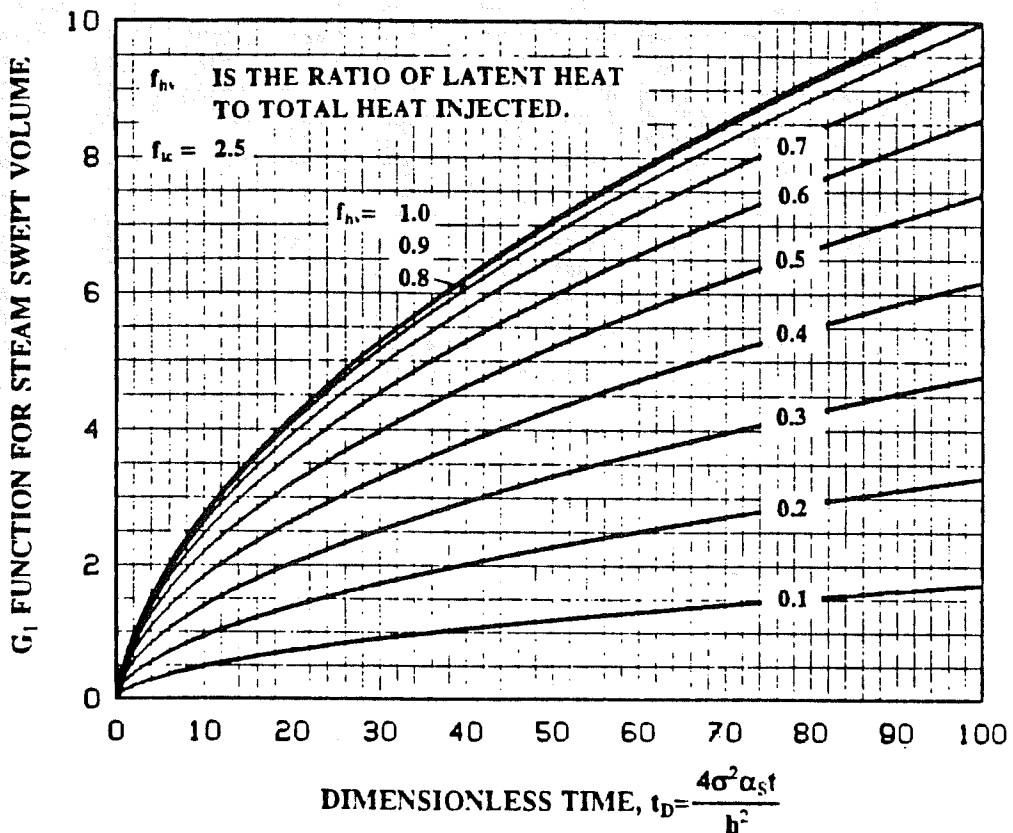


Fig. 7.6 Values of G_1 for Steam Swept Volume vs t_D from 0 to 100 for $f_{i_c} = 2.5$.

TABLE 7.2 VALUES OF G_1 FUNCTION FOR STEAM
SWEEPED VOLUME FOR $f_{lc}=2.5$ FROM THIS STUDY

t_D	f_{hv}									
	1.0	0.9	0.8	0.7	0.6	0.5	0.4	0.3	0.2	0.1
0.0100	0.0093	0.0093	0.0093	0.0093	0.0093	0.0093	0.0093	0.0093	0.0093	0.0073
0.0400	0.0347	0.0347	0.0347	0.0347	0.0347	0.0347	0.0347	0.0347	0.0293	0.0195
0.0900	0.0731	0.0731	0.0731	0.0731	0.0731	0.0731	0.0731	0.0670	0.0537	0.0324
0.1600	0.1221	0.1221	0.1221	0.1221	0.1221	0.1221	0.1180	0.1047	0.0804	0.0451
0.2500	0.1799	0.1799	0.1799	0.1799	0.1799	0.1788	0.1682	0.1456	0.1081	0.0578
0.3600	0.2448	0.2448	0.2448	0.2448	0.2448	0.2397	0.2222	0.1886	0.1363	0.0706
0.4900	0.3158	0.3158	0.3158	0.3158	0.3158	0.3048	0.2789	0.2328	0.1648	0.0835
0.6400	0.3918	0.3918	0.3918	0.3918	0.3889	0.3728	0.3374	0.2778	0.1936	0.0968
0.8100	0.4721	0.4721	0.4721	0.4721	0.4659	0.4430	0.3972	0.3234	0.2225	0.1104
1.0000	0.5560	0.5560	0.5560	0.5560	0.5453	0.5150	0.4580	0.3692	0.2515	0.1244
1.2100	0.6429	0.6429	0.6429	0.6416	0.6266	0.5882	0.5196	0.4154	0.2808	0.1387
1.4400	0.7326	0.7326	0.7326	0.7296	0.7095	0.6626	0.5816	0.4616	0.3102	0.1535
1.6900	0.8245	0.8245	0.8245	0.8194	0.7936	0.7377	0.6441	0.5080	0.3399	0.1685
1.9600	0.9185	0.9185	0.9185	0.9105	0.8787	0.8136	0.7068	0.5544	0.3698	0.1839
2.2500	1.0142	1.0142	1.0142	1.0029	0.9647	0.8899	0.7696	0.6009	0.3999	0.1996
2.5600	1.1114	1.1114	1.1114	1.0962	1.0514	0.9666	0.8326	0.6474	0.4303	0.2156
2.8900	1.2099	1.2099	1.2093	1.1904	1.1388	1.0437	0.8957	0.6940	0.4609	0.2317
3.2400	1.3096	1.3096	1.3079	1.2852	1.2266	1.1210	0.9588	0.7406	0.4917	0.2482
3.6100	1.4104	1.4104	1.4075	1.3808	1.3148	1.1985	1.0220	0.7873	0.5228	0.2648
4.0000	1.5122	1.5122	1.5079	1.4768	1.4034	1.2762	1.0851	0.8340	0.5541	0.2815
6.2500	2.0318	2.0318	2.0182	1.9630	1.8501	1.6656	1.4005	1.0688	0.7139	0.3672
9.0000	2.5643	2.5643	2.5375	2.4555	2.3000	2.0552	1.7154	1.3059	0.8780	0.4549
12.2500	3.1049	3.1049	3.0619	2.9514	2.7510	2.4441	2.0298	1.5454	1.0453	0.5436
16.0000	3.6509	3.6468	3.5897	3.4490	3.2020	2.8319	2.3443	1.7873	1.2148	0.6329
20.2500	4.2007	4.1929	4.1195	3.9475	3.6526	3.2188	2.6592	2.0315	1.3857	0.7225
25.0000	4.7533	4.7413	4.6506	4.4462	4.1025	3.6047	2.9747	2.2775	1.5575	0.8123
30.2500	5.3080	5.2912	5.1825	4.9450	4.5516	3.9900	3.2910	2.5251	1.7300	0.9022
36.0000	5.8642	5.8423	5.7150	5.4436	4.9999	4.3749	3.6082	2.7740	1.9029	0.9923
42.2500	6.4216	6.3943	6.2479	5.9418	5.4474	4.7594	3.9263	3.0239	2.0761	1.0824
49.0000	6.9800	6.9468	6.7808	6.4396	5.8941	5.1437	4.2453	3.2746	2.2495	1.1726
56.2500	7.5391	7.4999	7.3138	6.9370	6.3402	5.5280	4.5652	3.5260	2.4230	1.2628
64.0000	8.0989	8.0533	7.8468	7.4339	6.7857	5.9124	4.8860	3.7779	2.5966	1.3531
72.2500	8.6592	8.6069	8.3797	7.9303	7.2307	6.2969	5.2075	4.0302	2.7704	1.4433
81.0000	9.2199	9.1608	8.9125	8.4262	7.6752	6.6816	5.5298	4.2827	2.9441	1.5337
90.2500	9.7810	9.7148	9.4450	8.9217	8.1193	7.0666	5.8526	4.5355	3.1179	1.6240
100.0000	10.3424	10.2690	9.9774	9.4167	8.5631	7.4519	6.1761	4.7885	3.2918	1.7144

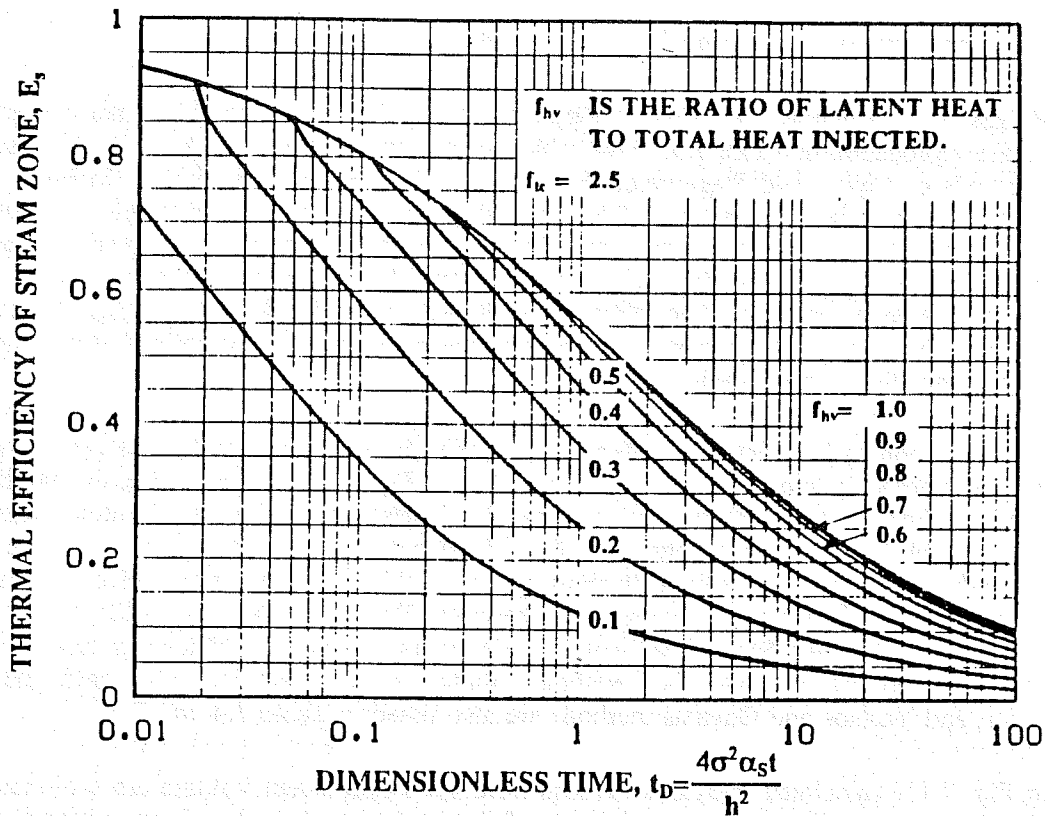


Fig. 7.7 Thermal Efficiency of Steam Swept Zone for $f_{lc} = 2.5$.

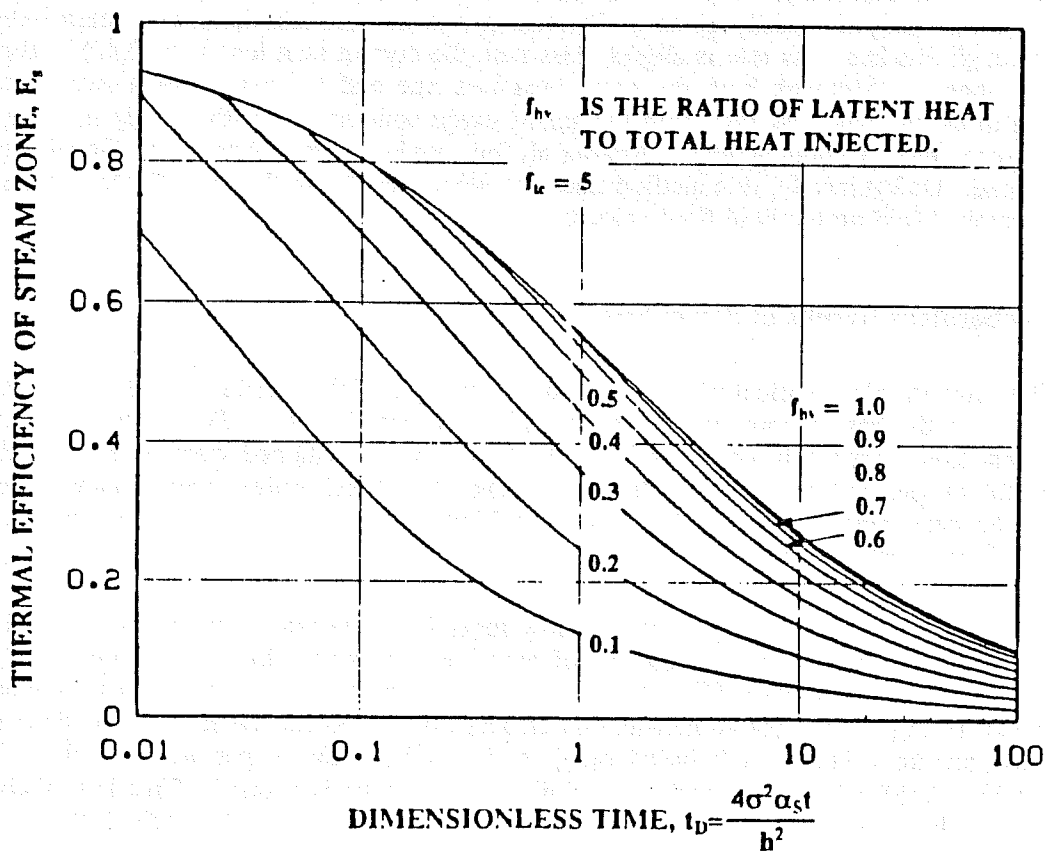


Fig. 7.8 Thermal Efficiency of Steam Swept Zone for $f_{lc} = 5$.

7.2.4. Comparisons of G_1 Among Various Models

Values of G_1 calculated by Hearn (1969), which are the upper bound of the actual steam swept volume, are reproduced in Table 7.3. This table can be used to examine the valid ranges of f_{hv} and t_D using methods of Myhill and Stegemeier, Yortsos and Gavalas, and this study. In Figs. 7.9 and 7.10, the values of G_1 calculated by methods from this study, and Myhill and Stegemeier are compared. The thick curves denote G_1 from this study and the thin curves denote G_1 calculated by the Myhill and Stegemeier method. It is clear that values of G_1 given by this study are smaller than those by the Myhill and Stegemeier method. The differences increase with the decrease of f_{hv} . Figure 7.10 is the comparison of heat efficiency curves. It amplifies the differences in calculated steam swept volumes between two models at small times.

Similarly, comparison between values of G_1 given by this study and those given by the Yortsos and Gavalas method is shown in Figs. 7.11 and 7.12. Figure 7.11 shows that the method from this study gives values of G_1 slightly smaller than the Yortsos and Gavalas method. The differences become negligible when f_{hv} is greater than 0.5. In general, values of G_1 given by the Yortsos and Gavalas method agree more closely with those given by this study than those given by the Myhill and Stegemeier method. However, a comparison between Fig. 7.10 and Fig. 7.12 at t_D less than two reveals that the Myhill and Stegemeier method gives values of thermal efficiency closer to our method than does the Yortsos and Gavalas method. Values of G_1 calculated by both the Myhill and Stegemeier, and Yortsos and Gavalas methods are also listed in Table 7.4 and 7.5.

In Fig. 7.13, calculated rates of heat loss from the steam swept volume are presented using three methods. The straight line represents the rate of the heat loss given by Hearn method; the diamonds represent the heat loss rate given by the Yortsos and Gavalas method; and the curve represents the rate given by the present study. The discrepancies in the Hearn, and Yortsos and Gavalas models are clearly shown. Only this study gives an increasing rate of heat loss from the steam swept zone with time, although this heat loss rate is slightly less than the correct heat loss rate (0.47) at the critical time at t_D less than 1. Although both the exact heat loss rate and the exact steam swept volume remain unknown to us, the heat loss rate from the steam swept zone given by this study is more rational in a physical sense than previous studies. Among all four methods, the Yortsos and Gavalas method is the simplest one. Unfortunately, this method does not work well using the new dimensionless critical time defined herein based on the fluid flow velocity.

7.2.5. Laboratory Results of Steam Swept Volume

The dimensionless critical time defined by Mandl and Volek (1969) is the time when the rate of heat loss from the heated zone equals the rate of latent heat injected. For a linear/tubular model, the rate of heat loss from the heated zone ($1 - dG_D/dt_D$), can be obtained from an analytical solution for the heat frontal position presented in Section 4. The Mandl and Volek dimensionless critical time can therefore be determined. Figure 7.14 shows the Mandl and Volek dimensionless critical time calculated as a function of f_{hv} and σ .

Run #38 was a steam displacement at low mass injection rate. The purpose of this run was to study the critical time, and the movements of both heat and steam fronts. For this run, σ was 0.675 and f_{hv} was 0.82. The corresponding Mandl and Volek dimensionless time is 14.0 as indicated by the solid square in Fig. 7.14. The dimensionless critical time corrected by the ratio of fluid flow velocity to the temperature velocity is 9 based on f_{ic} equal to 1.5. The experimental data of Run #38 (as shown in Fig. 7.15) indicate that the dimensionless critical time is about 7. This is probably due to the fact that S_w is less than 1.0 and the apparent f_{ic} is higher than 1.5 (approximately 2.0).

TABLE 7.3 VALUES OF G_v FUNCTION FOR STEAM SWEEP VOLUME FROM HEARN'S METHOD (1969)

t_D	f_{hv}							
	1.0	0.8	0.7	0.6	0.5	0.4	0.3	0.2
0.0400	0.0347	0.0347	0.0347	0.0347	0.0347	0.0347	0.0347	0.0347
0.1600	0.1221	0.1221	0.1221	0.1221	0.1221	0.1221	0.121	0.103
0.3600	0.2448	0.2448	0.2448	0.2448	0.2448	0.243	0.221	0.171
0.6400	0.3918	0.3918	0.3918	0.3918	0.3918	0.372	0.321	0.240
1.0000	0.5560	0.5560	0.5560	0.5560	0.546	0.502	0.422	0.309
1.4400	0.7326	0.7326	0.7326	0.732	0.702	0.632	0.523	0.378
1.9600	0.9185	0.9185	0.9185	0.910	0.858	0.762	0.624	0.448
2.5600	1.1114	1.1114	1.1114	1.089	1.016	0.894	0.726	0.517
3.2400	1.3096	1.3096	1.308	1.268	1.173	1.025	0.827	0.586
4.0000	1.5122	1.5122	1.506	1.448	1.330	1.156	0.929	0.656
6.2500	2.0318	2.0318	2.002	1.899	1.726	1.485	1.184	0.829
9.0000	2.5643	2.563	2.501	2.352	2.122	1.814	1.439	1.003
12.2500	3.1049	3.094	2.999	2.806	2.518	2.144	1.694	1.177
16.0000	3.6509	3.628	3.499	3.260	2.915	2.475	1.949	1.351
20.2500	4.2007	4.162	3.999	3.714	3.313	2.805	2.204	1.525
25.0000	4.7533	4.696	4.500	4.169	3.710	3.316	2.460	1.699
36.0000	5.8642	5.766	5.503	5.079	4.506	3.798	2.971	2.047
49.0000	6.9800	6.837	6.506	5.990	5.303	4.460	3.483	2.396
64.0000	8.0989	7.908	7.510	6.902	6.099	5.122	3.995	2.744
81.0000	9.2199	8.980	8.514	7.814	6.896	5.785	4.506	3.092
100.0000	10.3424	10.052	9.518	8.726	7.693	6.447	5.018	3.441

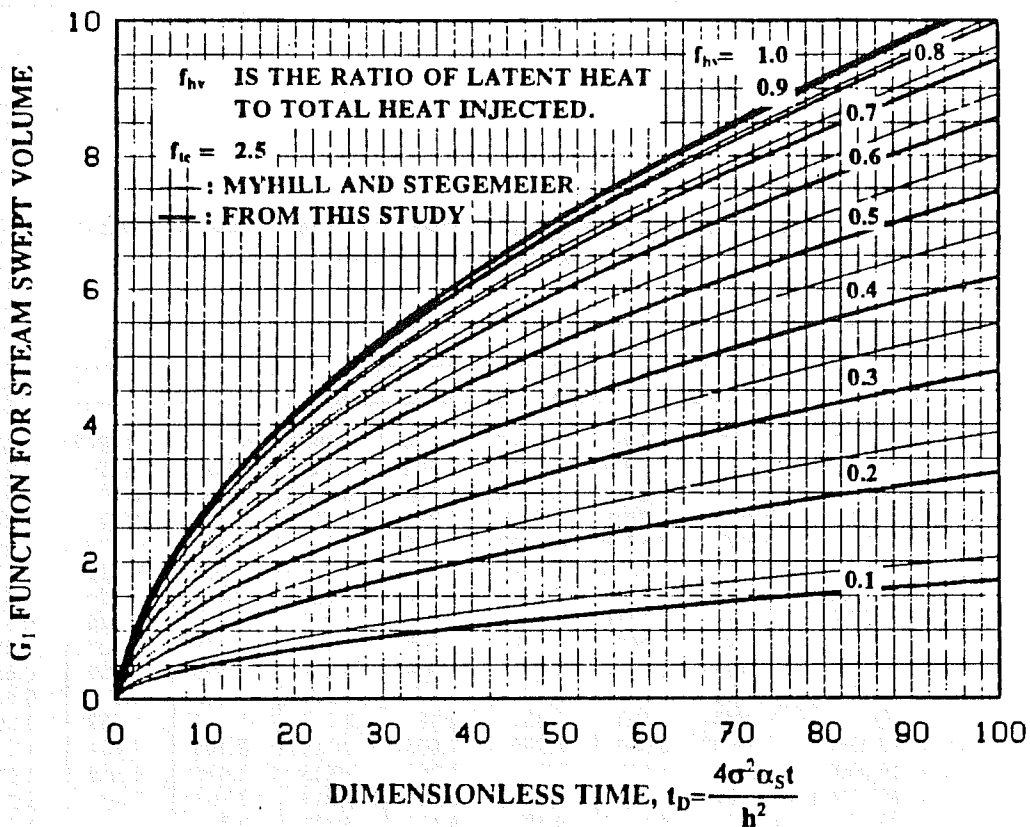


Fig. 7.9 Comparison of Values of G_1 for Steam Swept Zone Between Methods from this Study and by Myhill and Stegemeier.

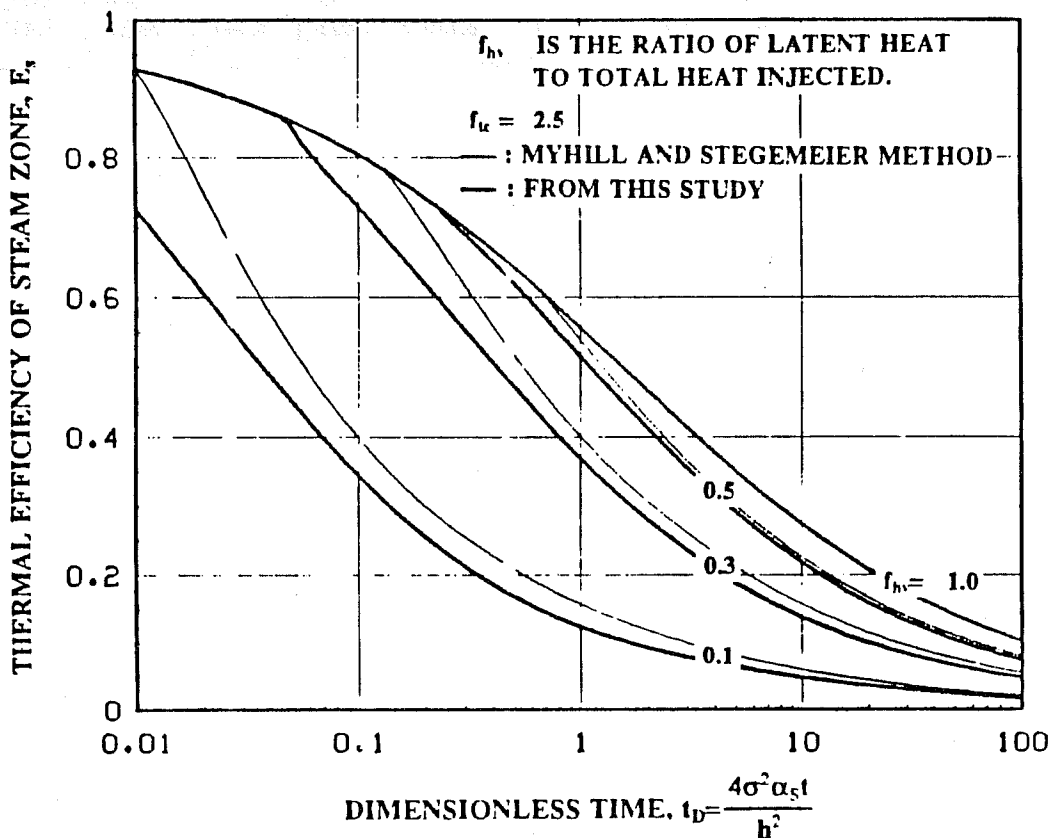


Fig. 7.10 Comparison of Values of Thermal Efficiency for Steam Swept Zone Between Methods from this Study and by Myhill and Stegemeier.

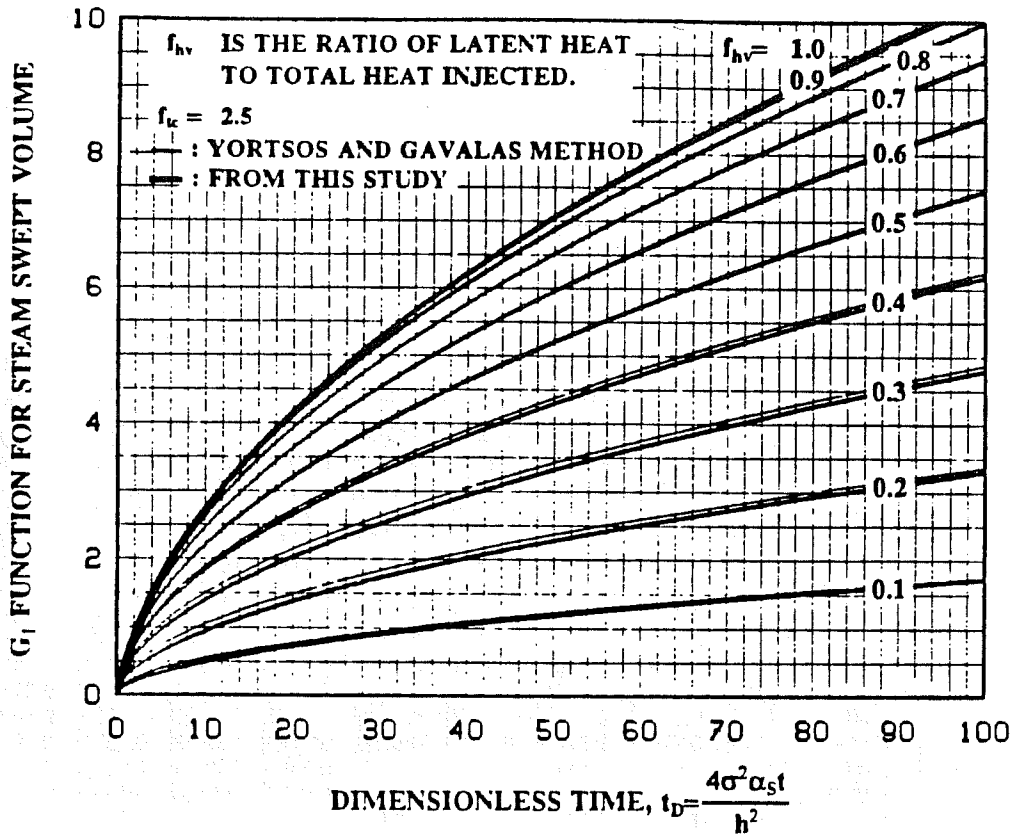


Fig. 7.11 Comparison of Values of G_1 for Steam Swept Zone Between Methods from this Study and by Yortsos and Gavalas.

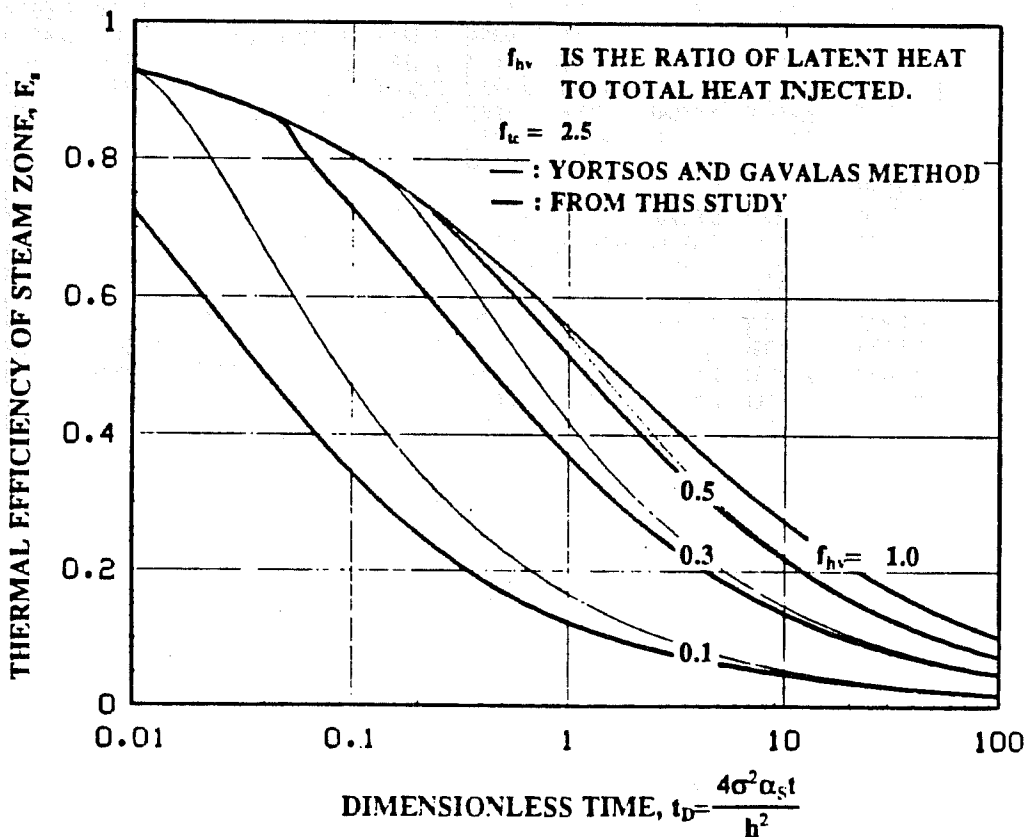


Fig. 7.12 Comparison of Values of Thermal Efficiency for Steam Swept Zone Between Methods from this Study and by Yortsos and Gavalas.

TABLE 7.4 VALUES OF G, FUNCTION FOR STEAM SWEEP VOLUME FROM MYHILL AND STEGEMEIER EQUATION

t_D	f_{Av}									
	1.0	0.9	0.8	0.7	0.6	0.5	0.4	0.3	0.2	0.1
0.0100	0.0093	0.0093	0.0093	0.0093	0.0093	0.0093	0.0093	0.0093	0.0093	0.0093
0.0400	0.0347	0.0347	0.0347	0.0347	0.0347	0.0347	0.0347	0.0347	0.0347	0.0230
0.0900	0.0731	0.0731	0.0731	0.0731	0.0731	0.0731	0.0731	0.0731	0.0731	0.0644
0.1600	0.1221	0.1221	0.1221	0.1221	0.1221	0.1221	0.1221	0.1192	0.0935	0.0525
0.2500	0.1799	0.1799	0.1799	0.1799	0.1799	0.1799	0.1799	0.1799	0.1633	0.0685
0.3600	0.2448	0.2448	0.2448	0.2448	0.2448	0.2448	0.2448	0.2408	0.2082	0.0852
0.4900	0.3158	0.3158	0.3158	0.3158	0.3158	0.3158	0.3158	0.2999	0.2544	0.1025
0.6400	0.3918	0.3918	0.3918	0.3918	0.3918	0.3918	0.3910	0.3597	0.3017	0.1202
0.8100	0.4721	0.4721	0.4721	0.4721	0.4721	0.4643	0.4206	0.3501	0.2555	0.1384
1.0000	0.5560	0.5560	0.5560	0.5560	0.5560	0.5377	0.4826	0.3995	0.2905	0.1570
1.2100	0.6429	0.6429	0.6429	0.6429	0.6429	0.6118	0.5455	0.4497	0.3261	0.1759
1.4400	0.7326	0.7326	0.7326	0.7326	0.7296	0.6868	0.6093	0.5006	0.3621	0.1950
1.6900	0.8245	0.8245	0.8245	0.8245	0.8156	0.7625	0.6738	0.5521	0.3987	0.2144
1.9600	0.9185	0.9185	0.9185	0.9185	0.9019	0.8390	0.7391	0.6043	0.4356	0.2339
2.2500	1.0142	1.0142	1.0142	1.0142	0.9887	0.9162	0.8050	0.6569	0.4728	0.2536
2.5600	1.1114	1.1114	1.1114	1.1114	1.0760	0.9939	0.8714	0.7099	0.5104	0.2735
2.8900	1.2099	1.2099	1.2099	1.2092	1.1639	1.0722	0.9383	0.7633	0.5482	0.2935
3.2400	1.3096	1.3096	1.3096	1.3060	1.2522	1.1510	1.0056	0.8171	0.5862	0.3137
3.6100	1.4104	1.4104	1.4104	1.4030	1.3410	1.2303	1.0733	0.8711	0.6245	0.3339
4.0000	1.5122	1.5122	1.5122	1.5001	1.4302	1.3099	1.1413	0.9255	0.6629	0.3542
6.2500	2.0318	2.0318	2.0318	1.9899	1.8814	1.7129	1.4856	1.2003	0.8572	0.4570
9.0000	2.5643	2.5643	2.5597	2.4857	2.3388	2.1216	1.8347	1.4788	1.0541	0.5610
12.2500	3.1049	3.1049	3.0883	2.9857	2.8004	2.5339	2.1869	1.7596	1.2525	0.6659
16.0000	3.6509	3.6509	3.6194	3.4886	3.2647	2.9487	2.5411	2.0421	1.4520	0.7713
20.2500	4.2007	4.2007	4.1524	3.9937	3.7311	3.3653	2.8967	2.3256	1.6523	0.8770
25.0000	4.7533	4.7533	4.6870	4.5004	4.1988	3.7831	3.2534	2.6100	1.8531	0.9831
30.2500	5.3080	5.3080	5.2228	5.0082	4.6677	4.2018	3.6108	2.8949	2.0543	1.0893
36.0000	5.8642	5.8626	5.7595	5.5169	5.1374	4.6213	3.9688	3.1803	2.2559	1.1957
42.2500	6.4216	6.4176	6.2969	6.0263	5.6077	5.0413	4.3273	3.4661	2.4576	1.3022
49.0000	6.9800	6.9728	6.8349	6.5363	6.0785	5.4618	4.6862	3.7521	2.6596	1.4089
56.2500	7.5391	7.5284	7.3734	7.0468	6.5498	5.8826	5.0454	4.0384	2.8617	1.5155
64.0000	8.0989	8.0843	7.9122	7.5576	7.0213	6.3037	5.4048	4.3248	3.0640	1.6223
72.2500	8.6592	8.6405	8.4514	8.0687	7.4932	6.7250	5.7644	4.6114	3.2663	1.7291
81.0000	9.2199	9.1969	8.9909	8.5801	7.9653	7.1466	6.1241	4.8981	3.4687	1.8360
90.2500	9.7810	9.7535	9.5305	9.0917	8.4375	7.5683	6.4840	5.1850	3.6712	1.9428
100.0000	10.3424	10.3103	10.0704	9.6034	8.9100	7.9901	6.8441	5.4719	3.8738	2.0498

TABLE 7.5 VALUES OF G_1 FUNCTION FOR STEAM SWEEP VOLUME FROM YORTSOS AND GAVALAS EQUATION

t_D	f_{nv}									
	1.0	0.9	0.8	0.7	0.6	0.5	0.4	0.3	0.2	0.1
0.0100	0.0093	0.0093	0.0093	0.0093	0.0093	0.0093	0.0093	0.0093	0.0093	0.0093
0.0400	0.0347	0.0347	0.0347	0.0347	0.0347	0.0347	0.0347	0.0347	0.0347	0.0266
0.0900	0.0731	0.0731	0.0731	0.0731	0.0731	0.0731	0.0731	0.0731	0.0684	0.0439
0.1600	0.1221	0.1221	0.1221	0.1221	0.1221	0.1221	0.1221	0.1211	0.1022	0.0613
0.2500	0.1799	0.1799	0.1799	0.1799	0.1799	0.1799	0.1799	0.1704	0.1360	0.0786
0.3600	0.2448	0.2448	0.2448	0.2448	0.2448	0.2448	0.2433	0.2197	0.1699	0.0959
0.4900	0.3158	0.3158	0.3158	0.3158	0.3158	0.3158	0.3070	0.2691	0.2037	0.1133
0.6400	0.3918	0.3918	0.3918	0.3918	0.3918	0.3918	0.3708	0.3184	0.2375	0.1306
0.8100	0.4721	0.4721	0.4721	0.4721	0.4721	0.4685	0.4346	0.3677	0.2713	0.1479
1.0000	0.5560	0.5560	0.5560	0.5560	0.5560	0.5454	0.4983	0.4171	0.3051	0.1653
1.2100	0.6429	0.6429	0.6429	0.6429	0.6429	0.6223	0.5621	0.4664	0.3389	0.1826
1.4400	0.7326	0.7326	0.7326	0.7326	0.7315	0.6992	0.6258	0.5157	0.3727	0.1999
1.6900	0.8245	0.8245	0.8245	0.8245	0.8201	0.7761	0.6896	0.5651	0.4065	0.2172
1.9600	0.9185	0.9185	0.9185	0.9185	0.9086	0.8530	0.7533	0.6144	0.4403	0.2346
2.2500	1.0142	1.0142	1.0142	1.0142	0.9972	0.9300	0.8171	0.6637	0.4741	0.2519
2.5600	1.1114	1.1114	1.1114	1.1114	1.0858	1.0069	0.8808	0.7130	0.5079	0.2692
2.8900	1.2099	1.2099	1.2099	1.2097	1.1744	1.0838	0.9446	0.7624	0.5418	0.2866
3.2400	1.3096	1.3096	1.3096	1.3081	1.2629	1.1607	1.0083	0.8117	0.5756	0.3039
3.6100	1.4104	1.4104	1.4104	1.4066	1.3515	1.2376	1.0721	0.8610	0.6094	0.3212
4.0000	1.5122	1.5122	1.5122	1.5050	1.4401	1.3145	1.1358	0.9104	0.6432	0.3386
6.2500	2.0318	2.0318	2.0318	1.9972	1.8829	1.6990	1.4546	1.1570	0.8122	0.4252
9.0000	2.5643	2.5643	2.5620	2.4893	2.3257	2.0836	1.7734	1.4037	0.9813	0.5119
12.2500	3.1049	3.1049	3.0927	2.9815	2.7686	2.4681	2.0921	1.6503	1.1503	0.5985
16.0000	3.6509	3.6509	3.6235	3.4737	3.2114	2.8527	2.4109	1.8969	1.3194	0.6852
20.2500	4.2007	4.2007	4.1542	3.9659	3.6543	3.2372	2.7297	2.1436	1.4884	0.7718
25.0000	4.7533	4.7533	4.6850	4.4580	4.0971	3.6217	3.0484	2.3902	1.6575	0.8585
30.2500	5.3080	5.3080	5.2157	4.9502	4.5399	4.0063	3.3672	2.6369	1.8265	0.9451
36.0000	5.8642	5.8679	5.7465	5.4424	4.9828	4.3908	3.6860	2.8835	1.9956	1.0318
42.2500	6.4216	6.4291	6.2772	5.9346	5.4256	4.7754	4.0047	3.1302	2.1646	1.1184
49.0000	6.9800	6.9903	6.8080	6.4268	5.8685	5.1599	4.3235	3.3768	2.3337	1.2051
56.2500	7.5391	7.5515	7.3387	6.9189	6.3113	5.5444	4.6423	3.6235	2.5027	1.2917
64.0000	8.0989	8.1126	7.8695	7.4111	6.7541	5.9290	4.9610	3.8701	2.6718	1.3784
72.2500	8.6592	8.6738	8.4002	7.9033	7.1970	6.3135	5.2798	4.1168	2.8408	1.4650
81.0000	9.2199	9.2350	8.9310	8.3955	7.6398	6.6981	5.5986	4.3634	3.0099	1.5517
90.2500	9.7810	9.7962	9.4617	8.8876	8.0827	7.0826	5.9173	4.6101	3.1789	1.6383
100.0000	10.3424	10.3573	9.9924	9.3798	8.5255	7.4671	6.2361	4.8567	3.3480	1.7250

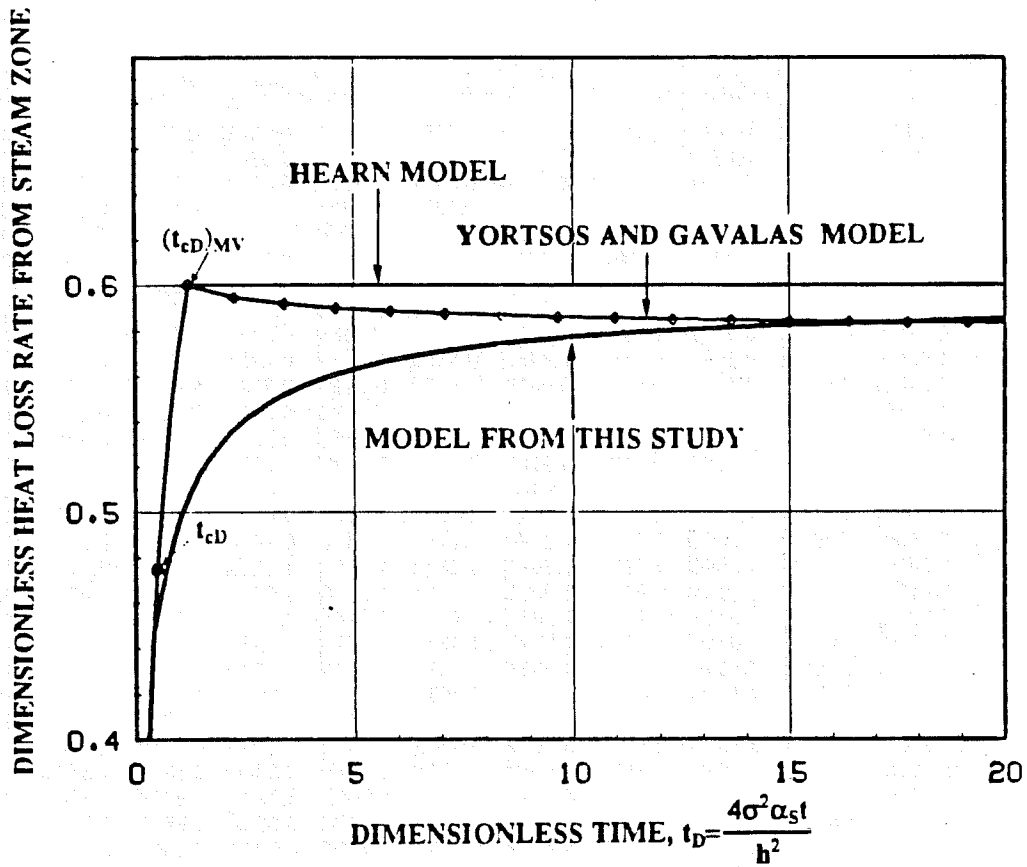


Fig. 7.13 Comparison of Heat Loss Rates from Steam Swept Zone Among Methods by Hearn, Yortsos and Gavalas, and this Study.

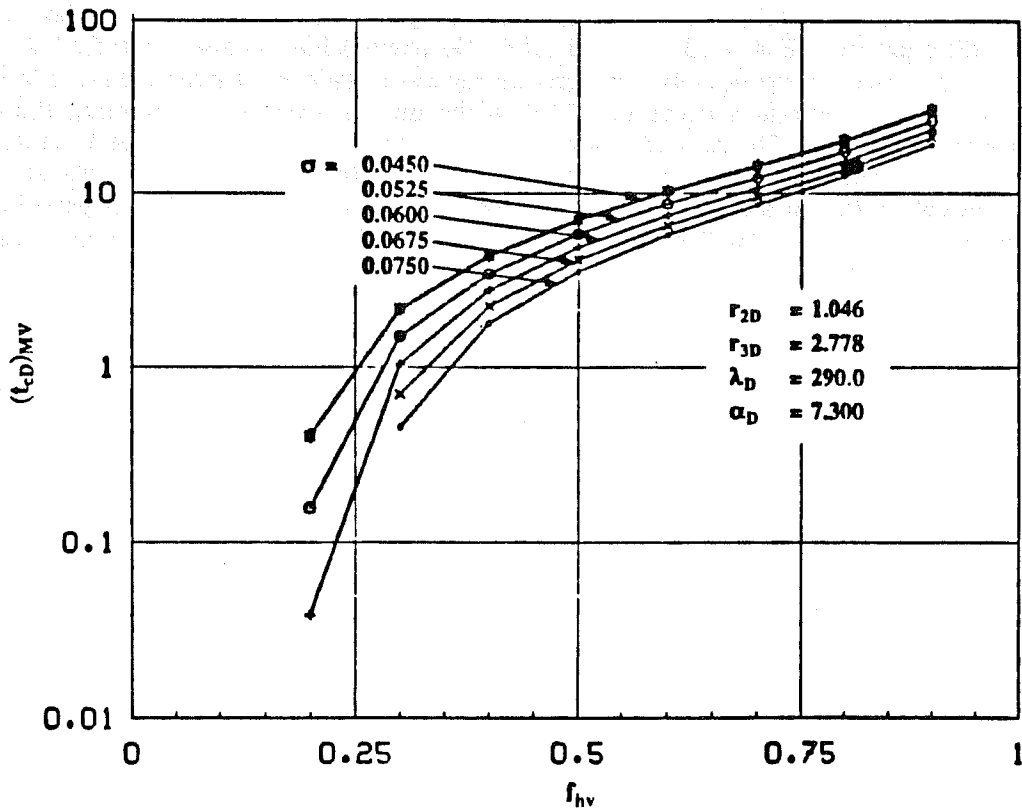


Fig. 7.14 Mandl and Volek Dimensionless Time, $(t_{cD})_{MV}$, vs f_{hv} for Steam Displacement in a Cylindrical Model.

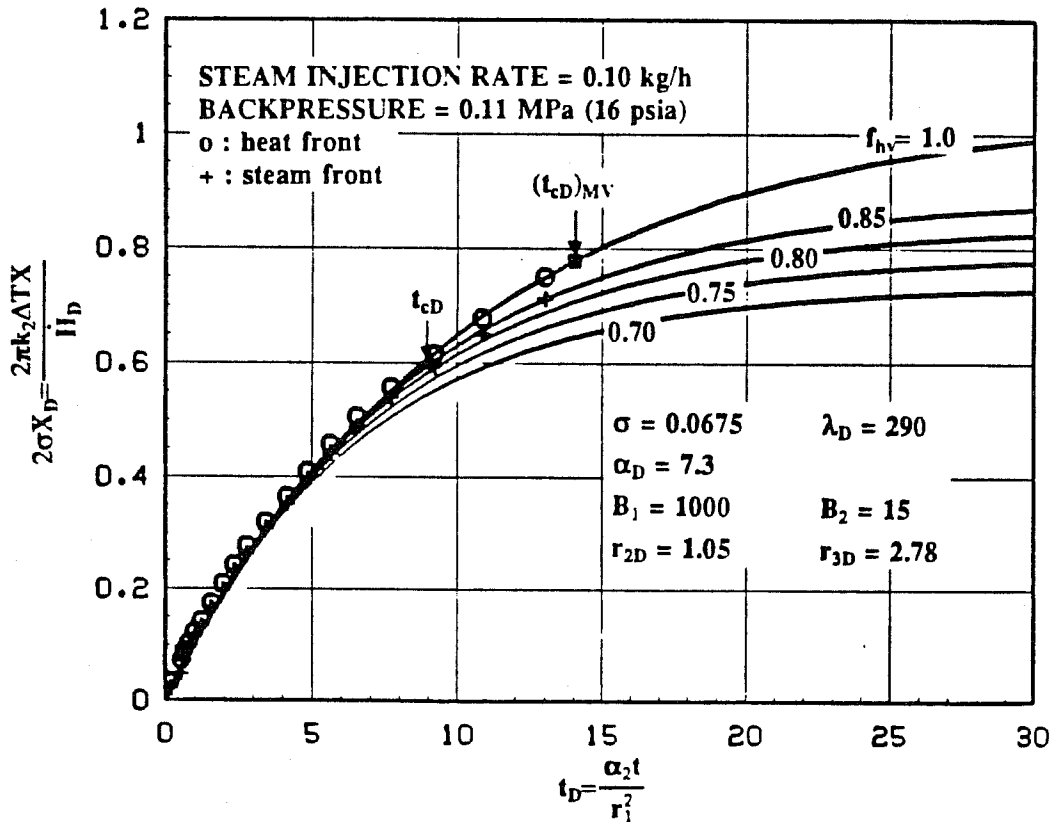


Fig. 7.15 Comparisons Between Calculated and Experimental Heat and Steam Fronts of Run #38.

The method for calculating the steam swept volume discussed in Section 7.2 is applicable to a system with finite thickness insulation. The equations stating the relationship between the power index (n) and f_{hv} are different from Eqs. 7.13 7.14 and 7.16. No attempt has been made to find the equations for this finite system because the equations depend on too many factors. Nevertheless, it is interesting to apply Eq. 7.5 with a constant n using Eq. 7.14 on the finite system and comparing the calculated results to experimental data. Figure 7.15 shows both the calculated and the experimental heat and steam fronts. Circles stand for experimental heat fronts and crosses for experimental steam fronts. The curves were calculated for steam fronts with f_{hv} varying from 0.7 to 1.0. The experimental steam fronts lie between curves for f_{hv} of 0.80 and 0.85. The f_{hv} of this run was 0.82. The calculated and experimental heat and steam fronts show good agreement.

8. STEAM MOBILITY REDUCTION BY SUNTECH IV SOLUTIONS

In this section, results are presented of a study on effects of surfactant (Suntech IV) on steam mobility reduction. Factors studied are concentration of surfactant solution, size and number of slugs of surfactant solution, backpressure and nitrogen fraction. The objective of this part of the study was to determine whether the data can be used to optimize the use of surfactant with steam drive.

8.1. COMPARISON OF PRESSURE AND TEMPERATURE DATA

In steam-displacement experiments, most of the sandpack was at steam saturation temperature. Therefore, the measured temperature could be used to calculate the steam saturation pressure. In the laboratory model, a thermocouple and a pressure tap were both located at a position 0.813 m (32 in.) from the inlet. Figure 8.1 shows a comparison of the measured pressure and the saturation pressure calculated from the measured temperature at this position. All measured pressures are slightly lower than the calculated pressures. At approximately 0.48 MPa (70 psia), there is a difference of about 0.021 MPa (3 psi) between the two pressures. When the measured pressures are below 0.275 MPa (40 psia), the differences are less than 0.0069 MPa (1 psi). However, such differences might have stemmed from experimental errors.

8.2. APPROXIMATE CALCULATION OF STEAM MOBILITY

Foams are compressible viscous fluids. When foams flow through porous media, several mechanisms such as bubble flow, membrane breaking and reforming, and channel blocking can occur simultaneously (Owete, 1982). Apparent viscosity, permeability reduction and mobility reduction have been used to quantify the effectiveness of foam flow through porous media. Marsden and Khan (1966) used the relative permeability to viscosity ratio instead of mobility. This ratio will be referred as the relative mobility. In this section, formulas for calculating relative steam mobility and steam permeability are given.

Because the sandpack was 1.83 m (6 ft) long, the heat loss from the heated sandpack significantly reduced the mass flow rate of steam along the sandpack. If the mass injection rate of steam is used to calculate the steam mobility near the downstream end, the introduced error would be significant. The mass flow rate of steam along the core can be estimated by heat balance. Because the sandpack had been flooded by steam to a steady-state condition before the surfactant solution was injected, the heat loss rate from the steam zone from inlet to position x (\dot{H}_{lx}) can be described by the steady-state convection equation:

$$\dot{H}_{lx} = 2\pi r_1 U \int_0^x (T_s(x') - T_\infty) dx' \quad (8.1)$$

where U is the overall heat transfer coefficient and T_s is the saturation temperature of steam. This temperature is a function of position, x' . Using a heat balance, the quality of flowing steam (f_{st}) at position x can then be calculated:

$$f_{st}(x) = 1 - \frac{2\pi r_1 U \int_0^x (T_s(x') - T_\infty) dx'}{Am_i h_v} \quad (8.2)$$

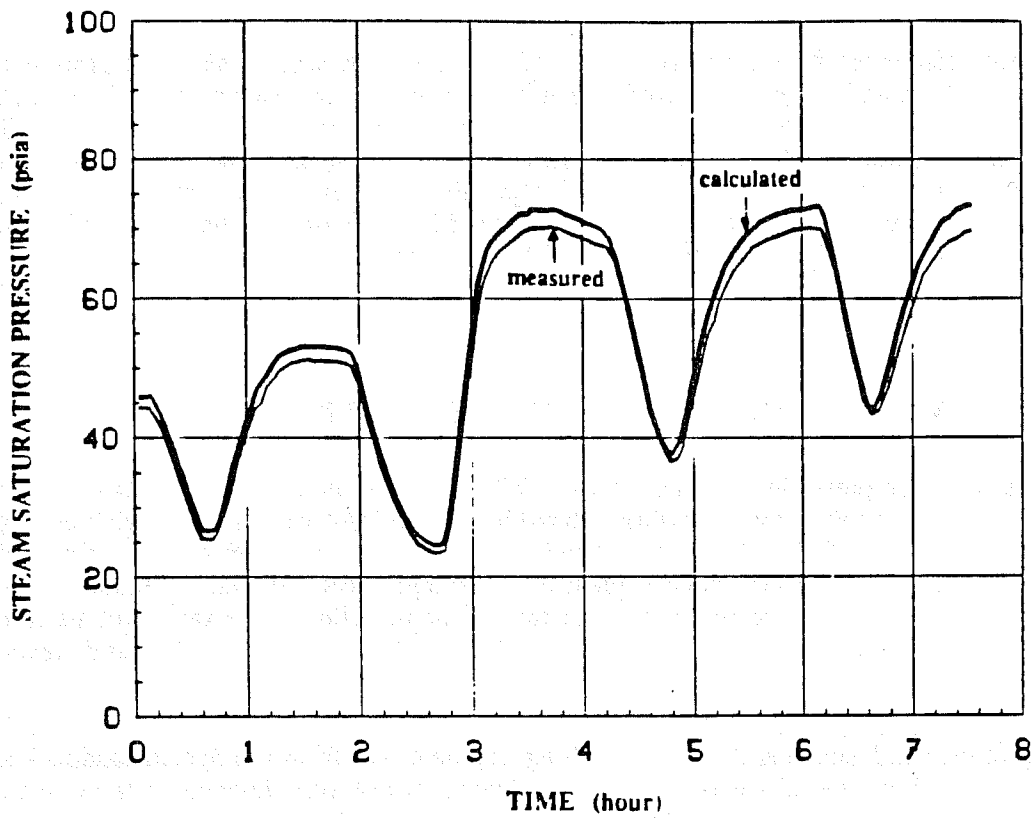


Fig. 8.1 Comparisons Between Calculated and Measured Steam Saturation Pressure.

where h_v is the enthalpy of the superheated steam being injected. The volumetric flow rate of steam per unit area at position x is $\dot{m}_i f_{st} / \rho_s$ and Darcy's law can be written as:

$$\frac{\dot{m}_i f_{st}}{\rho_s} = -k_a \left[\frac{k_r}{\mu} \right]_s \frac{dp}{dx}, \quad (8.3)$$

where

- \dot{m}_i = mass injection rate of steam per unit area,
- f_{st} = steam quality given by Eq. 8.2,
- k_a = absolute permeability,
- $\left[\frac{k_r}{\mu} \right]_s$ = relative steam mobility,
- p = pressure,
- x = distance.

The density of saturation steam is a function of saturation pressure. When pressures are less than 2.75 MPa (400 psia), Equation 8.4 can be used:

$$\rho_s = \beta_1 p_s^{\gamma_1}, \quad (8.4)$$

where β_1 is 0.00004528 and γ_1 is 0.95365. When the steam flow rate and the measured pressures are known, the relative steam mobility can be calculated:

$$\left[\frac{k_r}{\mu} \right]_s = \frac{(1+\gamma_1) \dot{m}_i \int_{x_1}^{x_2} f_{st} dx}{k_a \beta_1 (p_1^{1+\gamma_1} - p_2^{1+\gamma_1})}, \quad (8.5)$$

where p_1 is the upstream pressure, p_2 is the downstream pressure and f_{st} is given by Eq. 8.2.

Sometimes, the steam permeability instead of the steam mobility has been used to indicate the effectiveness of additives on steam flow through porous media. A formula similar to Eq. 8.4 can be used to relate the kinematic viscosity to the saturation pressure of steam:

$$\frac{\rho_s}{\mu_s} = \beta_2 p_s^{\gamma_2}, \quad (8.6)$$

where β_2 is 0.004466 and γ_2 is 0.8704. The relative permeability of steam can then be expressed as:

$$k_{rs} = \frac{(1+\gamma_2) \dot{m}_i \int_{x_1}^{x_2} f_{st} dx}{k_a \beta_2 (p_1^{1+\gamma_2} - p_2^{1+\gamma_2})}. \quad (8.7)$$

When steam permeability is calculated, the steam viscosity is assumed to be the same as the viscosity of pure steam. For steam/foam flow, this permeability is a function of absolute permeability, foam quality, surfactant concentration, steam saturation and flow rate. Although this permeability has been used in the literature, it is merely an indication of flow behavior rather than a true definition. The steam mobility reduction factor (SMRF) is defined as the ratio of steam mobility in presence of surfactant (s_2) to that in absence of surfactant (s_1):

$$SMRF = \frac{\left[\frac{k}{\mu} \right]_{s_2}}{\left[\frac{k}{\mu} \right]_{s_1}} = \frac{k_{rs2}}{k_{rs1}} \quad (8.8)$$

8.3. RESULTS AND DISCUSSIONS

Three injection techniques are commonly used to inject surfactants and gases for mobility control: preformed foam, simultaneous injection of gas and surfactant solution, and alternating slug injection of surfactant solution and gas. In steam injection, concurrent injection of surfactant solution, steam and nitrogen have been used in many laboratory and field experiments. Concurrent injection can be further divided into two types: simultaneous injection and slug injection of surfactants and noncondensable gases. The presumed advantage of the slug injection technique is to reduce the surfactant consumption. The alternate slug injection technique has been tested by Lawson and Reisberg (1980) for mobility control during chemical flooding, Chiang (1980), Mahmood (1983), and Ali *et al.* (1984) for low temperature gas/foam flood, Doscher *et al.* (1982) for steam/foam flood, and by Gopalakrishnan *et al.* (1978) for oil recovery improvement during steam displacement. In this study, the technique of alternating slugs of surfactant and steam was adopted to study the effectiveness of steam mobility reduction. From an economic point of view, the process should be optimized to obtain the maximum steam mobility reduction by using a minimum amount of surfactant.

In order to simulate steam channels with a linear sandpack, steam injection without surfactant was performed to reach irreducible oil saturation. Experiments were conducted at atmospheric pressure (0.101 MPa) and 0.584 MPa (85 psia) at the outlet end. Factors studied were backpressure, nitrogen fraction, and concentration, size and number of surfactant solution slugs. The duration of the experiments and the magnitude of steam mobility reduction were not scaled to any specific reservoir condition, therefore, the results of these experiments can only be used for surfactant screening and preliminary process design purposes.

8.3.1. Runs at Atmospheric Pressure (0.101 MPa) at Outlet End

The runs at atmospheric pressure tend to form two sets of data with differing results for each groups. The reasons are not clear; possibly it was due to wettability change. However, the data within each set appear to be consistent. The first set (Run Set I) includes Runs #18, #20, #22 and #26. The second set (Run Set II) includes Runs #37, #39, and #41. The operating conditions of these sets of runs are listed in Table 8.1. In these runs, only steam was injected during the cycles of steam injection.

TABLE 8.1 OPERATING CONDITIONS OF STEAM DRIVE WITH SUNTECH IV SLUGS

run no.	backpressure psia	concentration		slug size (pore volume)				
		Suntech IV wt%	nitrogen mole%	1	2	3	4	5
018	14.7	0.26	0.0	0.10	0.15	0.10		
020	14.7	0.26	0.0	0.14	0.14	0.13		
022	14.7	0.10	0.0	0.05	0.08	0.08	0.08	0.10
026	14.7	0.026	0.0	0.05	0.08	0.10	0.15	
037	14.7	0.10	0.0	0.10	0.10	0.10	0.10	
039	14.7	0.25	0.0	0.10	0.10	0.10		
041	14.7	1.00	0.0	0.10	0.10	0.10		
028	85.0	0.05	0.0	0.10	0.10	0.10		
030	85.0	0.09	0.0	0.10	0.10	0.10		
032	85.0	0.30	0.0	0.10	0.10	0.10	0.10	0.10
034	85.0	1.12	0.0	0.10	0.10	0.10	0.10	
047	85.0	0.22	0.0	0.10	0.10	0.10		
054	85.0	0.0	0.0	0.10	0.10	0.10		
050	85.0	0.22	0.75	0.10	0.10	0.10		
051	85.0	0.22	1.1	0.10	0.10	0.10		
052	85.0	0.22	2.1	0.10	0.10	0.10		
054	85.0	0.0	0.0	0.10	0.10	0.10		
055	85.0	0.0	1.1	0.10	0.10	0.10		

8.3.1.1. Run Set I

Run #18 was an injection of three alternate surfactant and steam slugs. The surfactant concentration used was 0.26 wt%. The sizes of surfactant slugs were 0.10, 0.15 and 0.10 pore volumes. Figure 8.2 shows the pressure gradient data from Run #18. The five curves represent the pressure gradients of four continuous sections along the sandpack (1.33, 1.33, 1.67 and 1.67 m apart from the inlet as shown in Fig. 5.2) as well as the average pressure gradient. The mass injection rate of steam was 6.9×10^{-5} kg/s. This amounts to about forty pore volumes of steam per hour. The pressure gradients decreased during the injection of each surfactant slug as a result of cooling, and increased to peak values shortly after steam had reached each section and decreased gradually during the remaining period of steam injection following each slug. However, the pressure gradient over the entire sandpack remained fairly constant during steam injection following each surfactant slug. This indicated that the injection pressures were fairly constant. The pressure gradients in the second section increased dramatically after the second surfactant slug had been injected.

Figure 8.3 shows data on the relative steam mobility calculated using Eq. 8.5 and Fig. 8.4 shows data on relative steam permeability calculated using Eq. 8.7. During surfactant injection, the sandpack was cooled by the surfactant solution, and both the relative mobility and the apparent relative steam permeability were assumed to be zero. The steam mobility reduction was more pronounced in the inlet half of the sandpack than the outlet half. The apparent relative steam permeability in absence of surfactant ranged from 0.18 to 0.26 with an average value of 0.21. The apparent relative steam permeability was reduced by the first surfactant slug to about 0.05 in the first section; about 0.09 in the second section; and about 0.17 in the outlet half of sandpack. The second surfactant slug of 0.15 pore volume further reduced steam mobilities in all sections by a factor of two while the third surfactant slug maintained the level of reduction. The calculated average steam saturation in the sandpack is graphed in Fig. 8.5 and the surfactant concentration in the produced fluid was not measured.

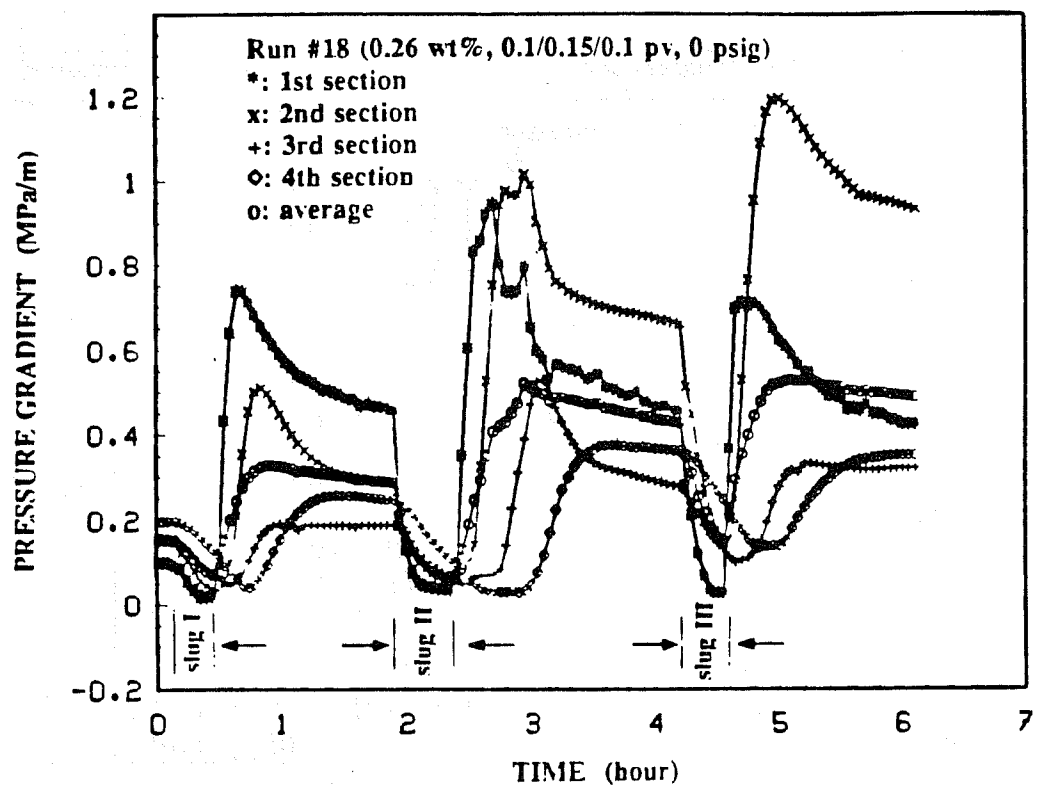


Fig. 8.2 Pressure Gradients vs Time for Run #18.

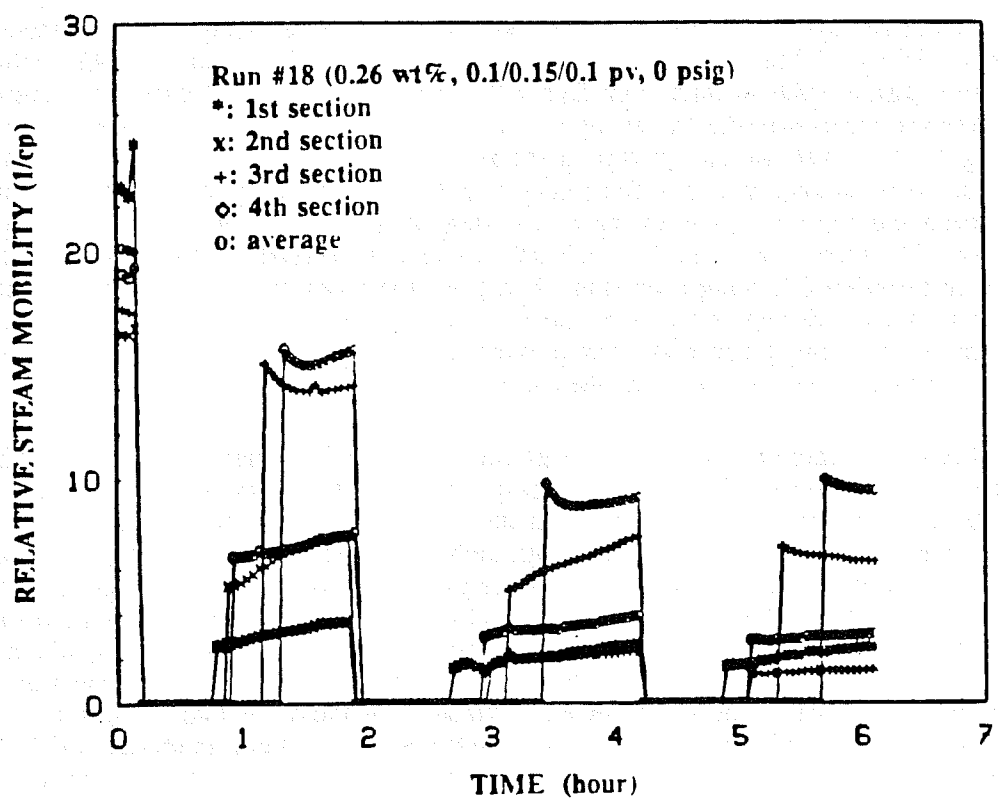


Fig. 8.3 Relative Steam Mobility vs Time for Run #18.

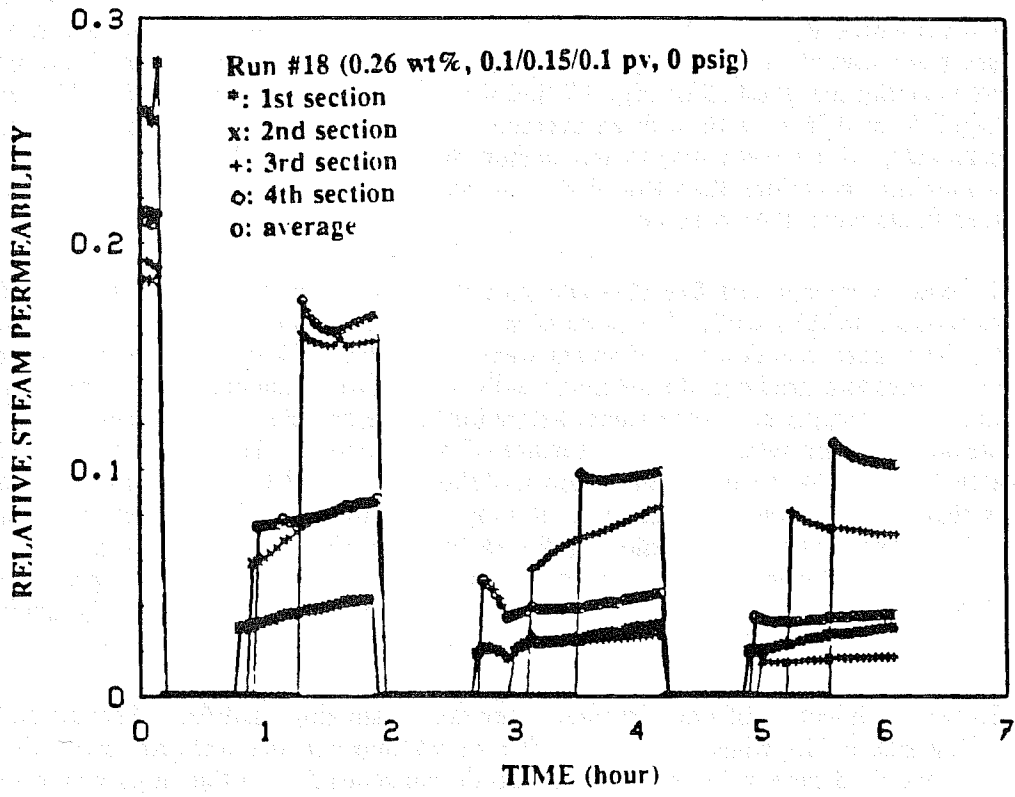


Fig. 8.4 Apparent Relative Steam Permeability vs Time for Run #18.

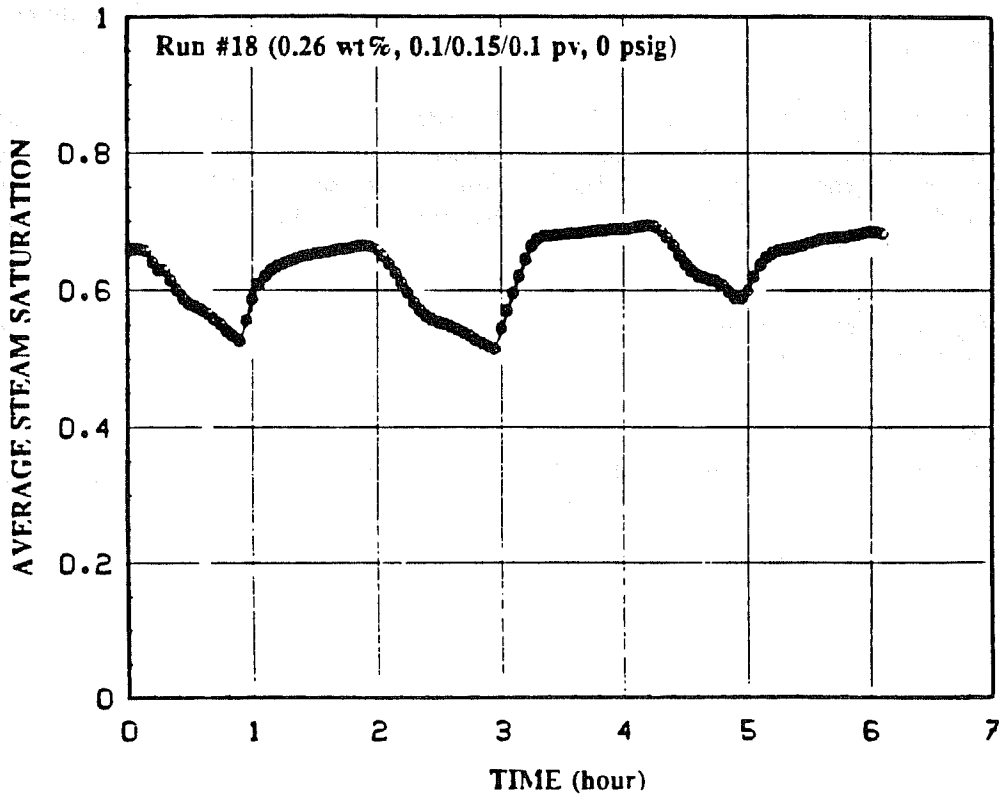


Fig. 8.5 Average Steam Saturation vs Time for Run #18.

Run #20 was the same as Run #18 except that the sizes of surfactant slugs were larger, being 0.14, 0.14 and 0.13 pore volumes. Figure 8.6 shows the pressure gradient data of this run. The pressure responses were similar to those in Run #18. Data on the relative mobility and the apparent relative steam permeability are graphed in Fig. 8.7 and 8.8. The relative steam permeability in absence of surfactant ranged from 0.38 to 0.46 with an average of 0.41 as Fig. 8.8 indicates. The higher relative steam permeabilities, which were due to the higher steam saturation shown in Fig. 8.9, resulted in higher steam mobility reductions than Run #18 by a factor of about two. The surfactant concentration in the produced fluids were not measured.

Run #22 was an injection of five alternate surfactant and steam slugs. The surfactant concentration used was reduced to 0.10 wt%. The sizes of surfactant slugs were 0.05, 0.08, 0.08, 0.08 and 0.10 pore volumes. The mass injection rate of steam was again 6.9×10^{-5} kg/s. Figures 8.10, 8.11 and 8.12 show data on the pressure gradient, the relative steam mobility and apparent relative steam permeability of this run. The calculated average steam saturation in the sandpack is graphed in Fig. 8.13. The high initial steam saturation resulted from a release of backpressure. The first surfactant slug of 0.05 pore volume had essentially no effect on steam mobility. In Fig. 8.13, the average steam saturation profile shows that this slug was not produced. It simply resulted in an increase of water saturation in the sandpack. The producing concentration profile in Fig 8.14 also shows that no surfactant was produced from this slug. After the second surfactant slug of 0.08 pore volume was injected, a reduction of steam mobility was observed (see Figs. 8.11 and 8.12). The third, fourth and fifth surfactant slugs further reduced steam mobility slightly in the inlet half of the sandpack.

Run #26 was an injection of one alternate water and steam slug, and four alternate surfactant and steam slugs. The size of the water slug was 0.10 pore volume and the sizes of surfactant slugs were 0.05, 0.08, 0.10 and 0.15 pore volumes. The surfactant concentration in the slugs was a low value of 0.026 wt%. The mass injection rate of steam was again 6.9×10^{-5} kg/s. Figures 8.15, 8.16 and 8.17 show data on the pressure gradient, the relative steam mobility and apparent relative steam permeability. Because the surfactant concentration was one tenth of the critical micellar concentration, the effect of surfactant on steam mobility reduction was low. This was expected. The final 0.15 pore volume slug reduced steam mobilities more than other smaller slugs. Figure 8.18 shows data on the average steam saturation.

The purposes of Run Set I were to observe the effects of surfactant concentration, slug size and the number of Suntech IV slugs on steam mobility reduction. In these runs, slug size and surfactant concentration were changed at the same time and this caused some difficulties in comparing various effects. Nevertheless, several points can be observed from these data regarding effectiveness of Suntech IV on steam mobility reduction. These are as follows:

- (1) Significant reduction of steam mobility was achieved when concentration of Suntech IV was greater than 0.1 wt%.
- (2) A minimum slug size of 0.08 pore volume was required to achieve significant reduction of steam mobility.
- (3) The effect of the number of slugs is a function of concentration and slug size. For example, the second and third slugs were not very effective for the concentration of 0.1 wt% using 0.08 pv slugs.

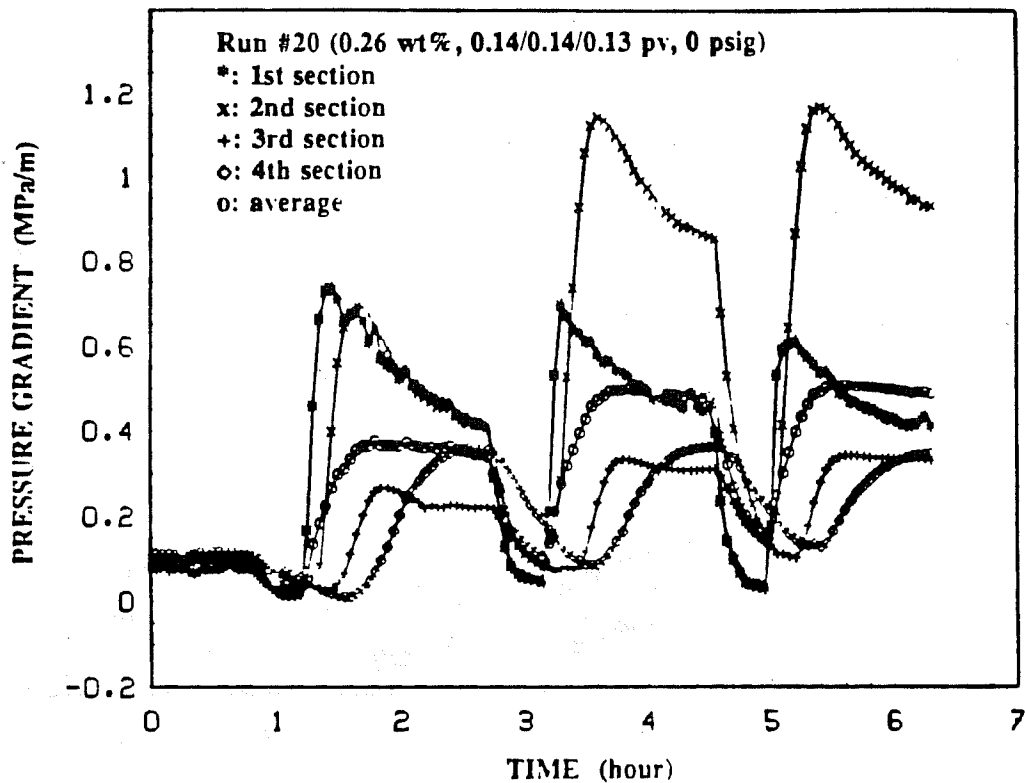


Fig. 8.6 Pressure Gradients vs Time for Run #20.

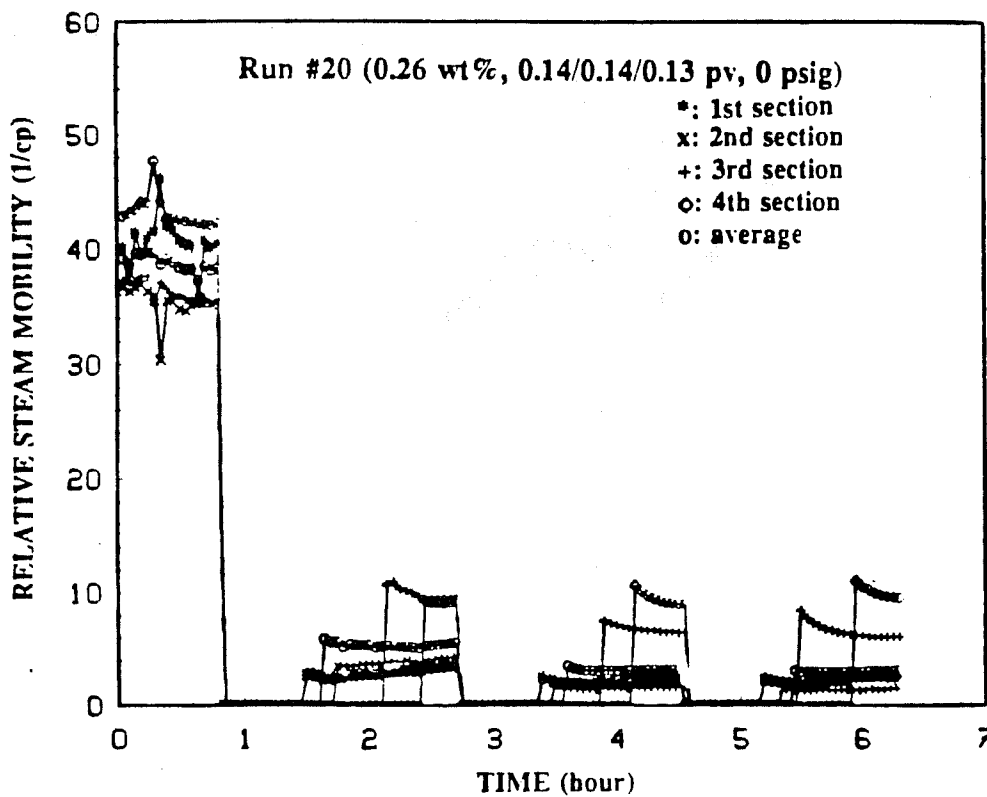


Fig. 8.7 Relative Steam Mobility vs Time for Run #20.

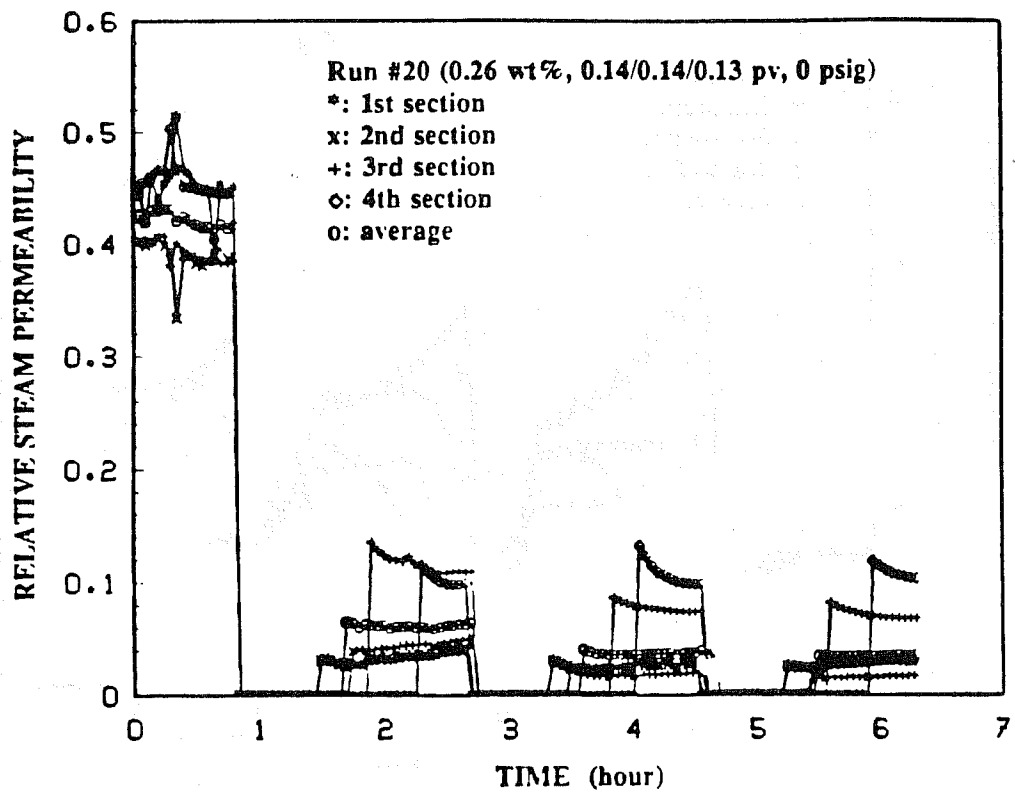


Fig. 8.8 Apparent Relative Steam Permeability vs Time for Run #20.

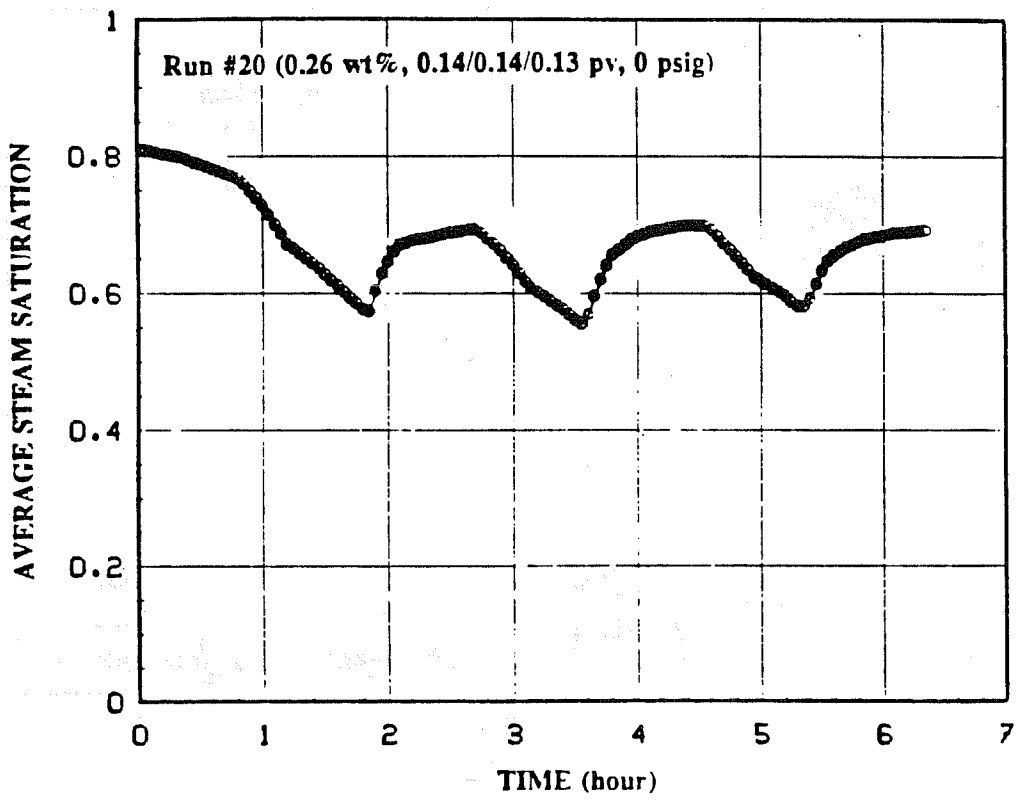


Fig. 8.9 Average Steam Saturation vs Time for Run #20.

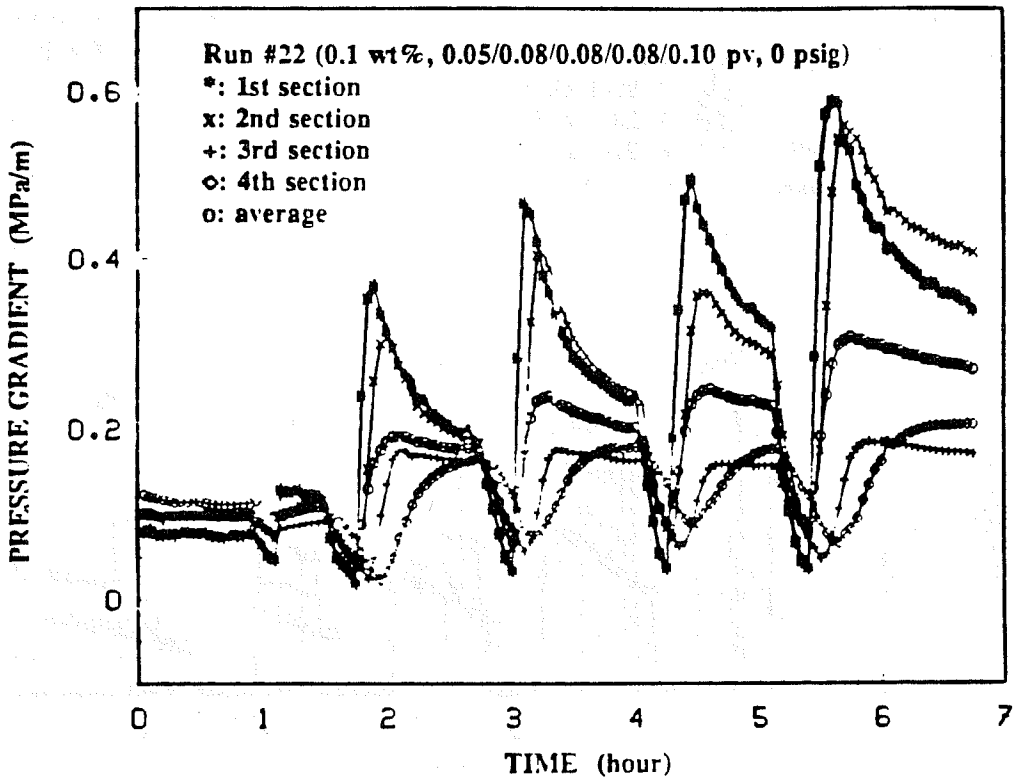


Fig. 8.10 Pressure Gradients vs Time for Run #22.

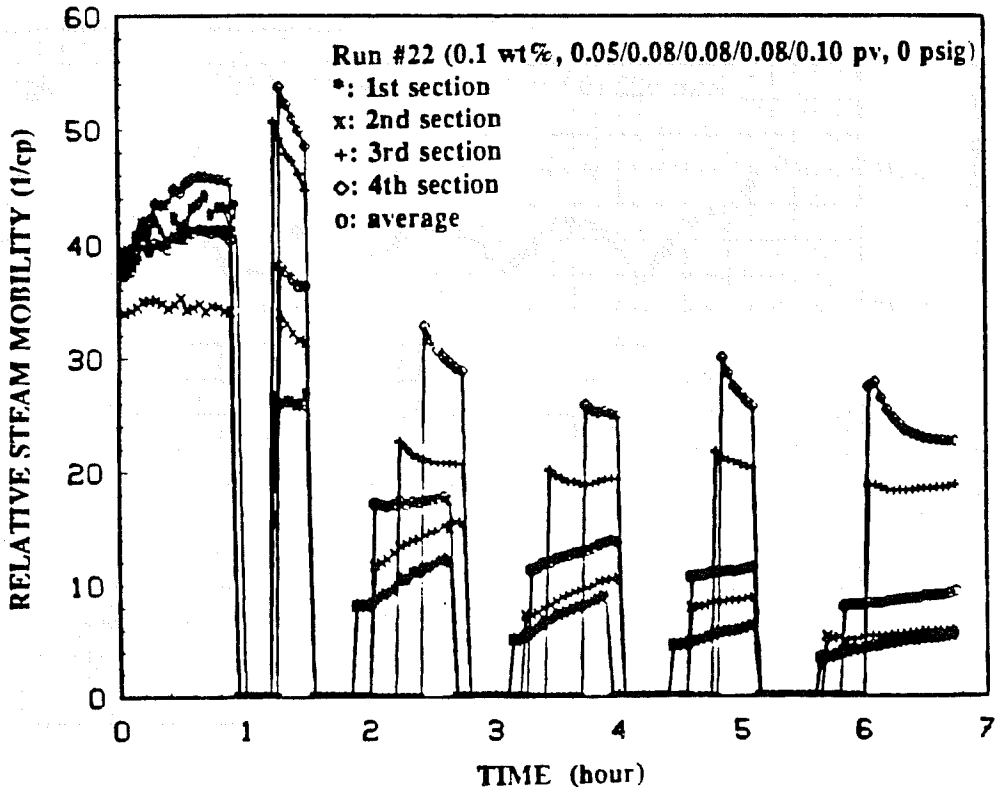


Fig. 8.11 Relative Steam Mobility vs Time for Run #22.

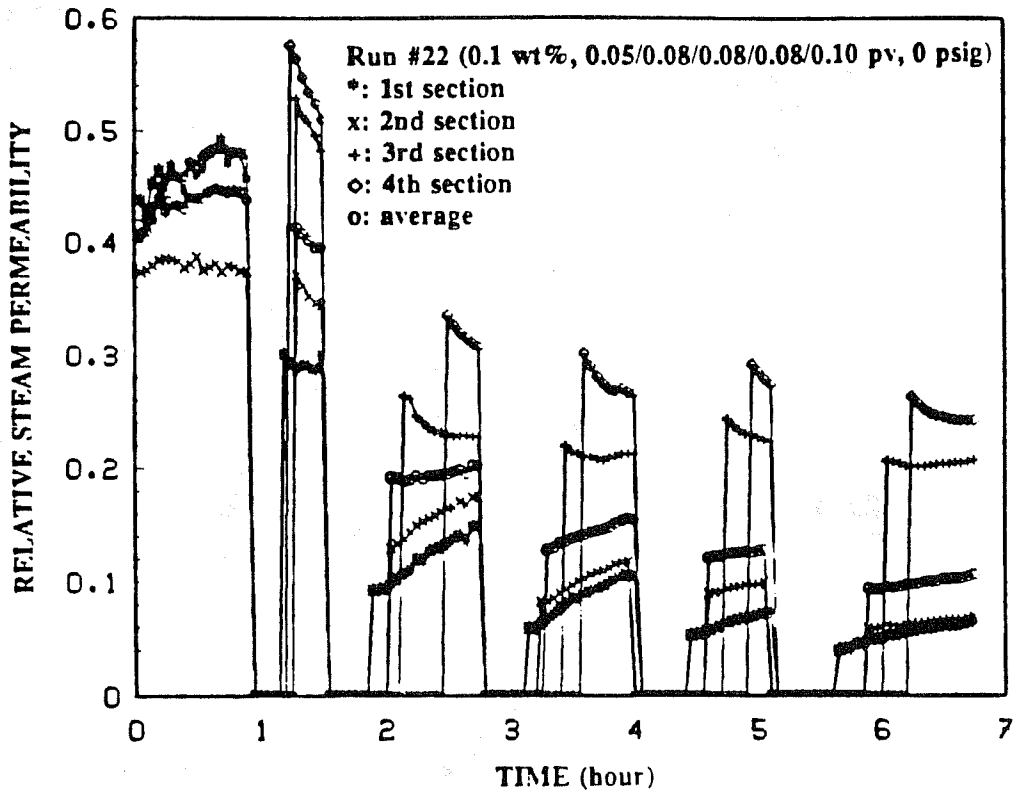


Fig. 8.12 Apparent Relative Steam Permeability vs Time for Run #22.

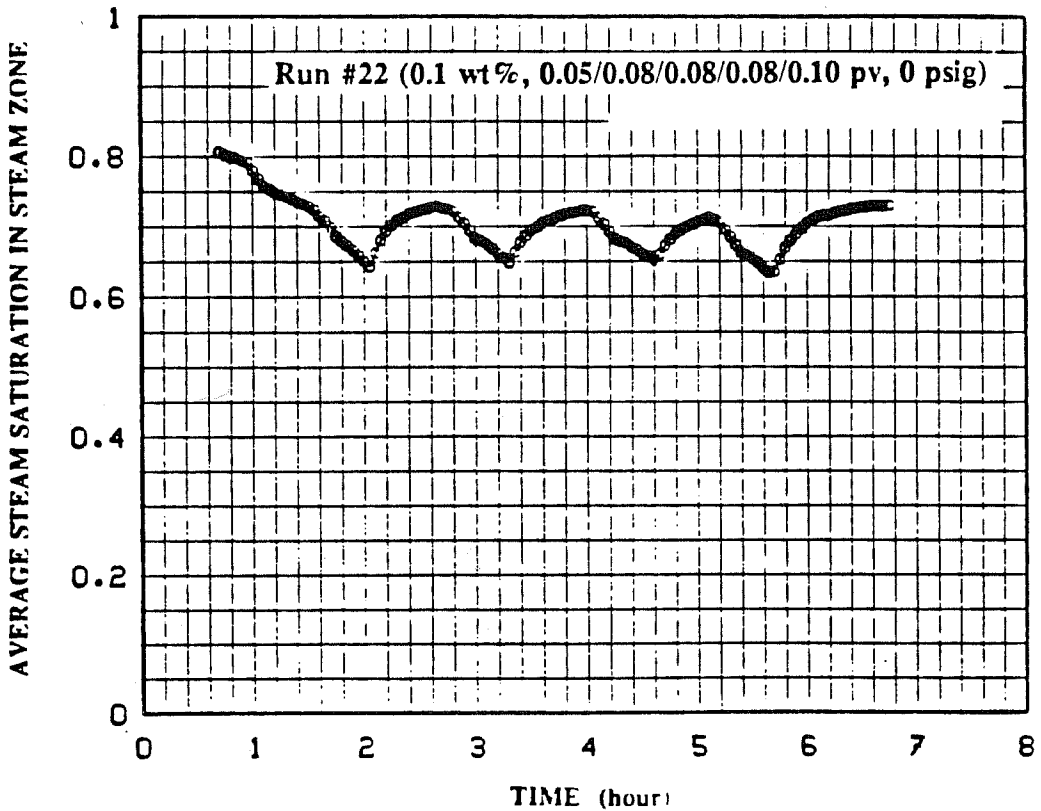


Fig. 8.13 Average Steam Saturation vs Time for Run #22.

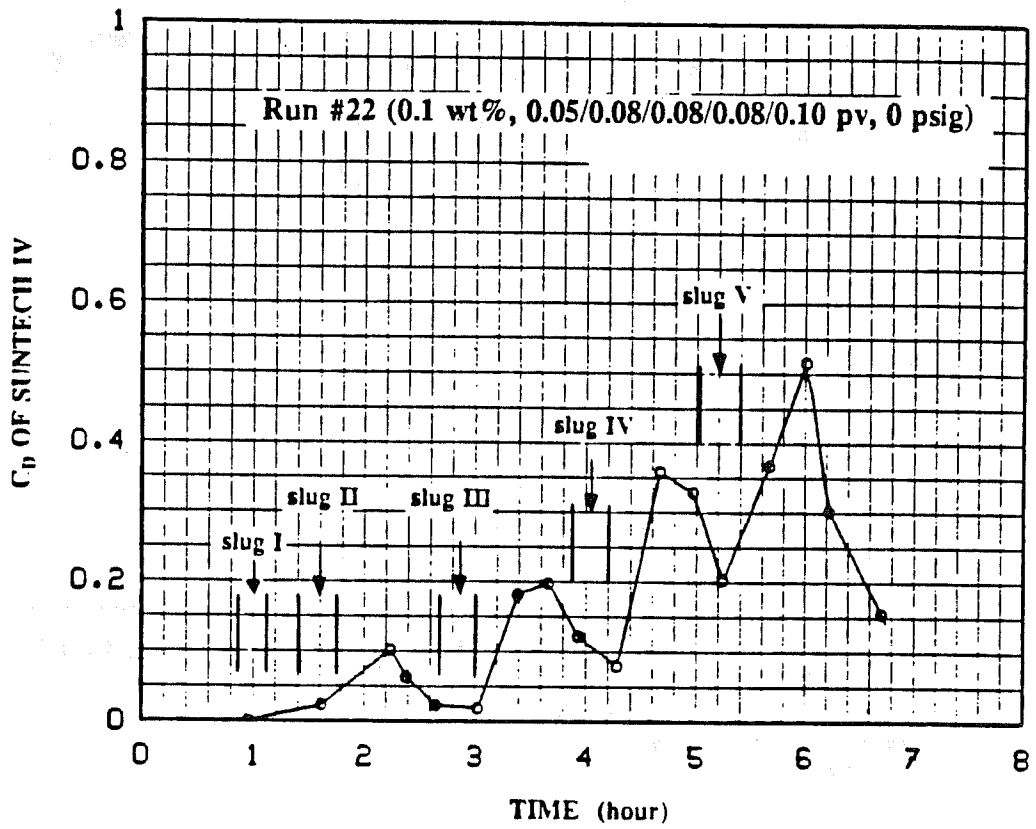


Fig. 8.14 Dimensionless Concentration of Suntech IV in Produced Fluid for Run #24.

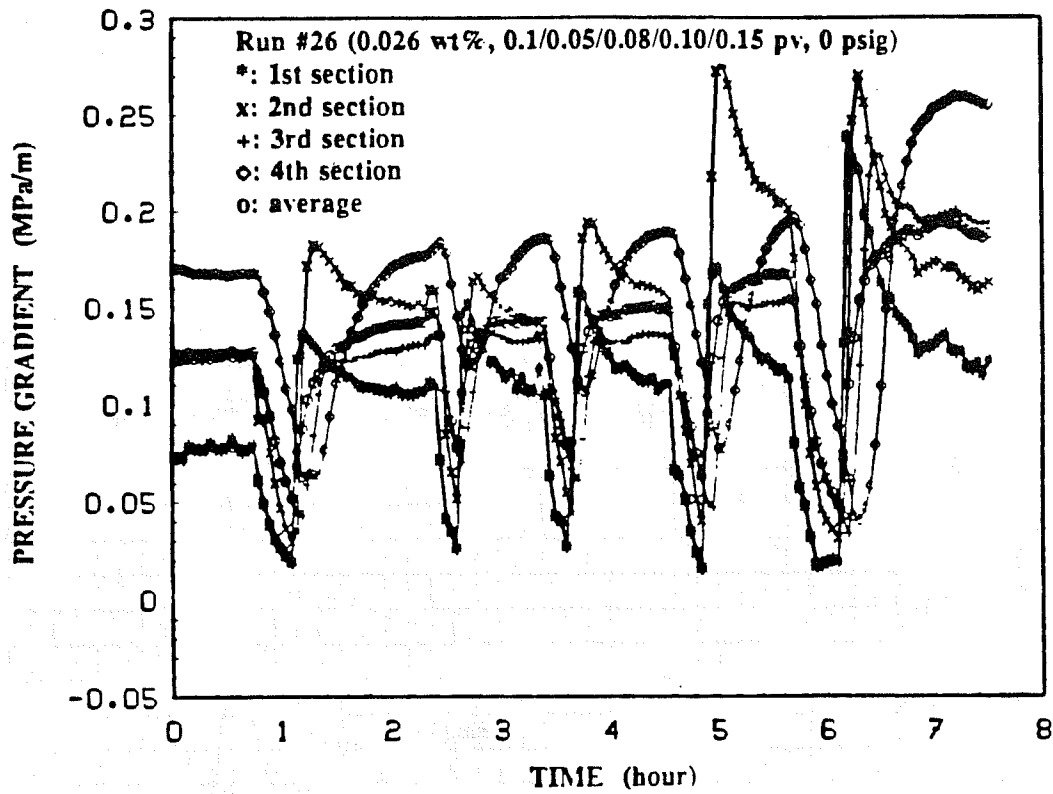


Fig. 8.15 Pressure Gradients vs Time for Run #26.

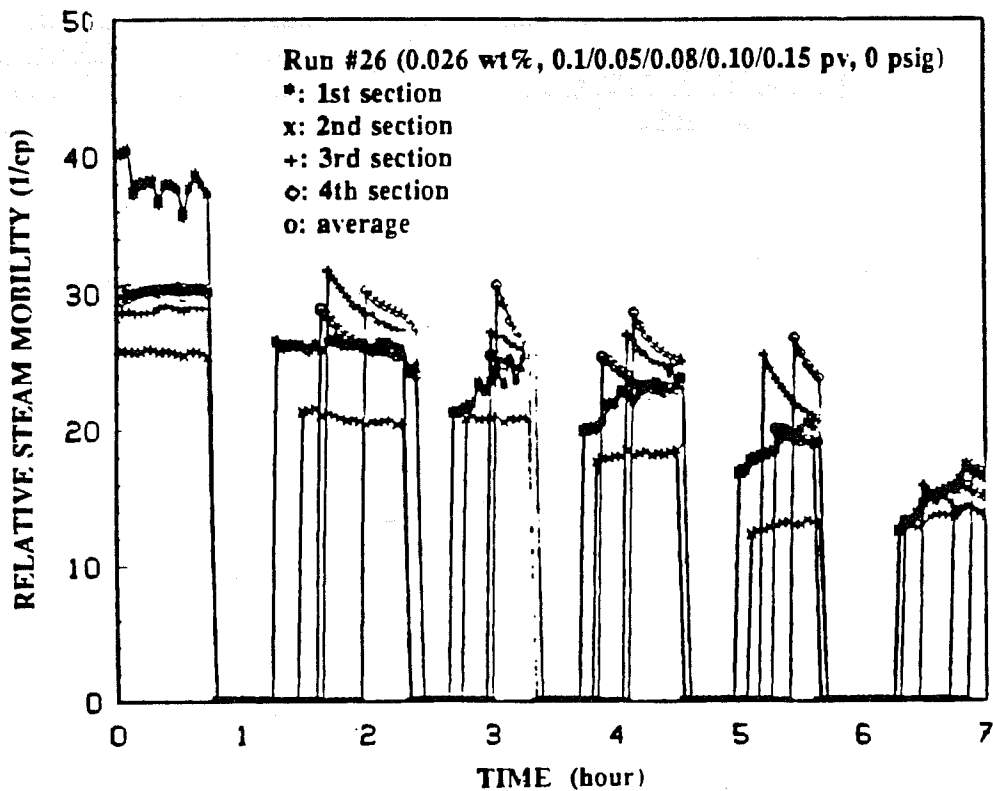


Fig. 8.16 Relative Steam Mobility vs Time for Run #26.

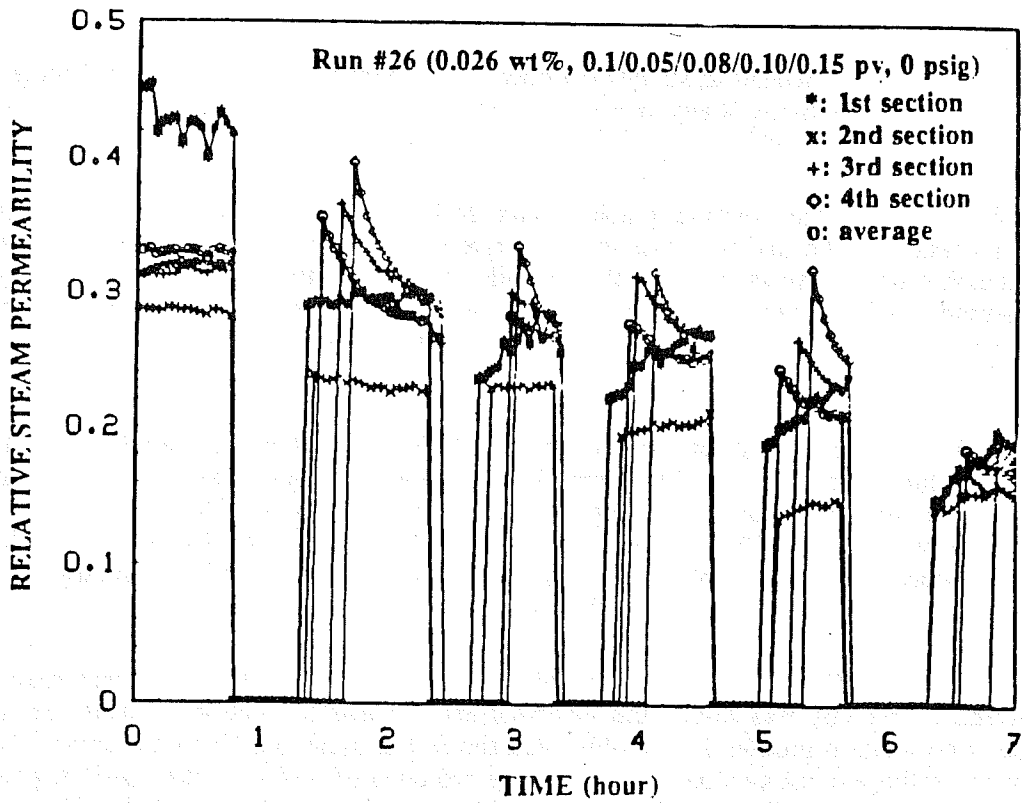


Fig. 8.17 Apparent Relative Steam Permeability vs Time for Run #26.

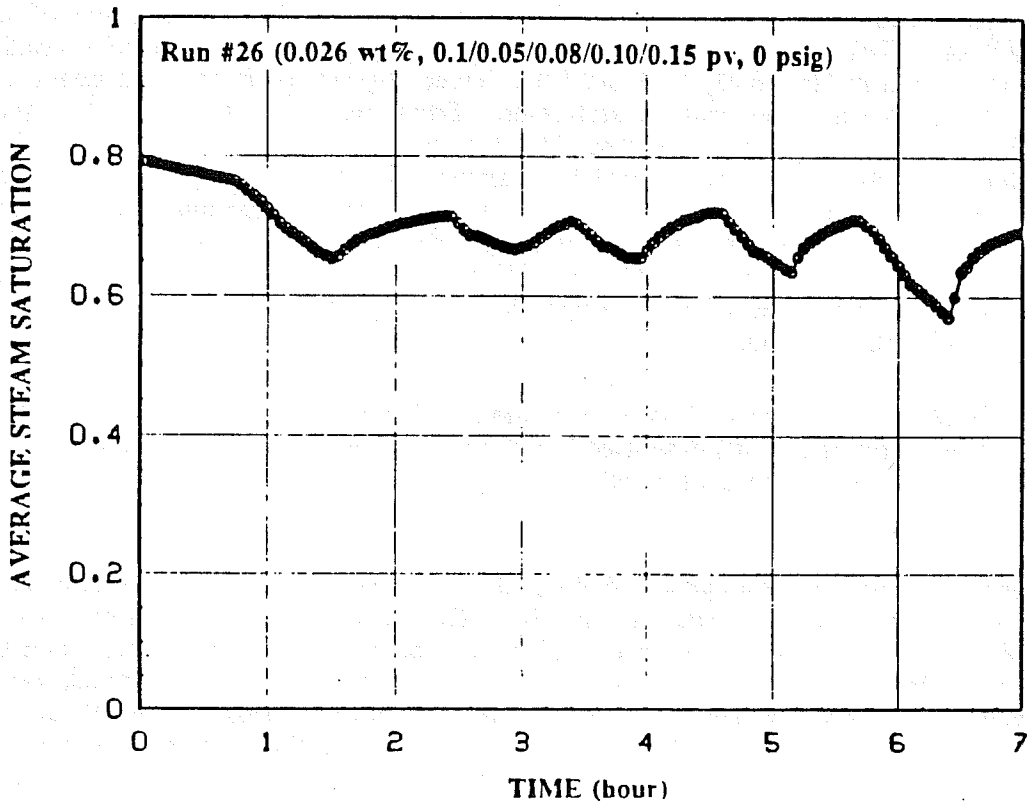


Fig. 8.18 Average Steam Saturation vs Time for Run #26.

8.3.1.2. Run Set II

This set of runs was intended to study the effects of concentration and number of slugs. The slug sizes used were 0.1 pore volume. Only two out of three runs in this set will be discussed in the following.

Figure 8.19 presents the pressure gradient data during Run #37. The surfactant concentration used in this run was 0.1 wt% and the mass injection rate of steam was 7.2×10^{-5} kg/s. The run started with steam injection without surfactant, which was followed by injecting a series of four 0.1 pv surfactant slugs alternating with steam slugs. The first slug affected only the pressure gradients of the first and second sections. The three consecutive surfactant slugs further increased the pressure gradients, especially in the second section.

Figure 8.20 shows relative steam mobility data and Fig. 8.21 shows the apparent relative steam permeability data during this run. During steam flow in absence of surfactant, the relative steam permeability decreased along the sandpack as Fig. 8.21 indicates. In general, the surfactant slug reduced steam mobility more in the inlet half of the sandpack than the outlet half. As Fig. 8.20 indicates, the steam mobility reduced about four fold in the first and second sections while essentially no reduction was observed in the fourth section even after the fourth surfactant slug.

Figure 8.22 graphs dimensionless concentrations of Suntech IV in the produced fluids. Almost all the surfactant in first slug was lost to the sandpack and the loss became less severe for later slugs. The produced concentration profiles for the third and the fourth slugs are about the same. The shapes of concentration profile are not symmetrical due to the presence of residual water and oil phases. The dispersion model presented by Salter and Mohanty (1982) may be modified to model this type of concentration profile, however, detailed modelling on concentration profiles is beyond the scope of this study.

The surfactant concentration used in Run #41 was 1.0 wt% and the mass injection of steam was again 7.2×10^{-5} kg/s. Data on pressure gradient, relative steam mobility and apparent relative steam permeability are shown in Figs. 8.23, 8.24 and 8.25. Three alternate surfactant and steam slugs were injected after first injecting steam without surfactant. From Figs. 8.24 and 8.25, both the relative steam mobility and the relative steam permeability decreased with time during the period of steam injection without surfactant. This was caused by a change of steam injection rate from 2.2×10^{-5} to 7.2×10^{-5} kg/s during the run. However, most of the sandpack except for the fourth section had reached steady state before the first surfactant slug was injected. The reductions in steam mobility in this run were not as pronounced as seen in Run #18 and #20 where the surfactant concentrations used were 0.26 wt%. The second and third surfactant slugs did not show further reductions on steam mobility beyond that seen after the first slug.

Figure 8.26 shows the dimensionless concentration of Suntech IV in the produced fluid. Because a surfactant concentration of 1.0 wt% was used in this run, there was a significant amount of surfactant produced from the first slug. The concentration profiles for the second and the third slugs are similar to each other and reached a peak value of around 0.6.

The steam mobility reduction factor is defined by Eq. 8.8 as the ratio of steam mobility with surfactant to steam mobility without surfactant. In Fig. 8.27, the reciprocal of steam mobility reduction factor from Run Set II is graphed as a function of the surfactant concentration. This graph shows the increased pressure drop. The average relative steam mobilities over the entire sandpack were used in these calculations. By comparing steam mobility results from Run Set I to Run Set II, the magnitude of steam mobility reduction shown in Fig. 8.27 is not the same as the magnitude of steam mobility reduction seen in Run Set I, therefore, no further explanation is given on the results in Fig. 8.27.

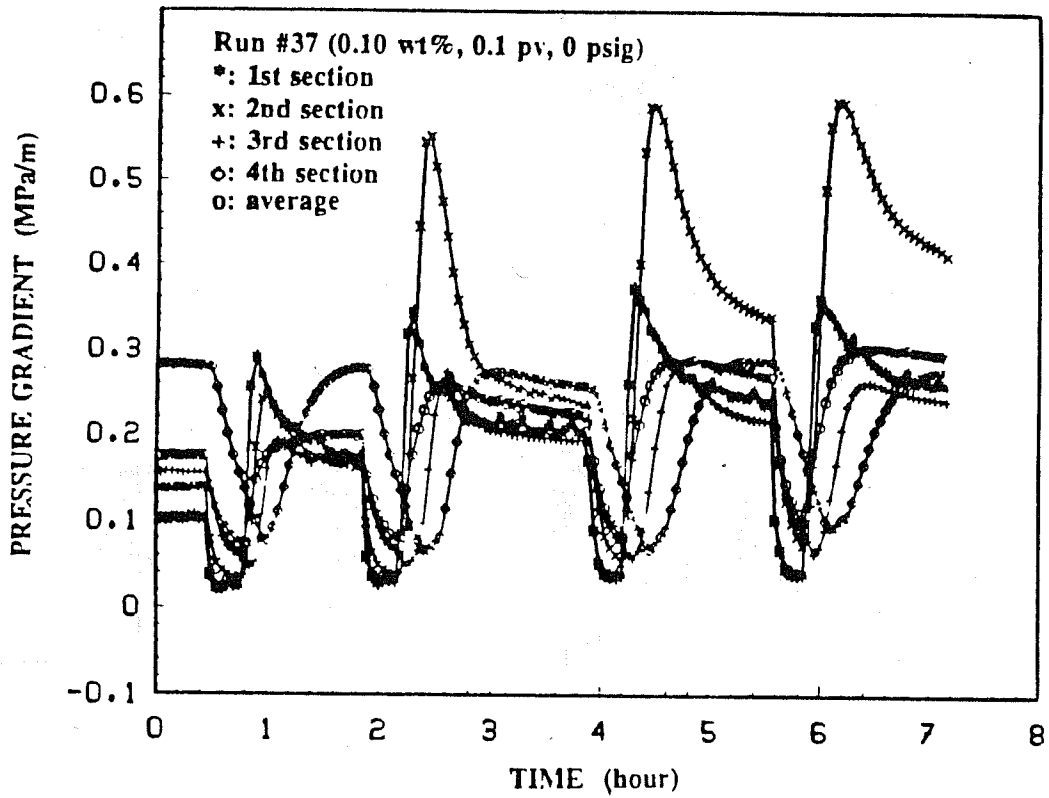


Fig. 8.19 Pressure Gradients vs Time for Run #37.

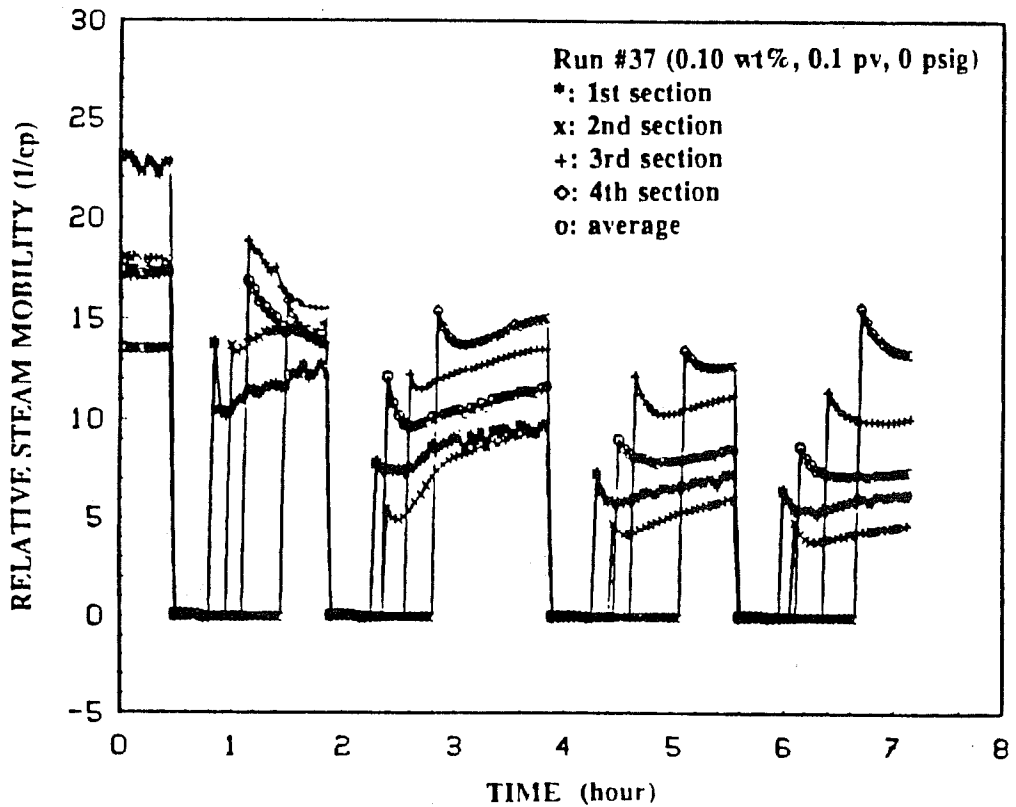


Fig. 8.20 Relative Steam Mobility vs Time for Run #37.

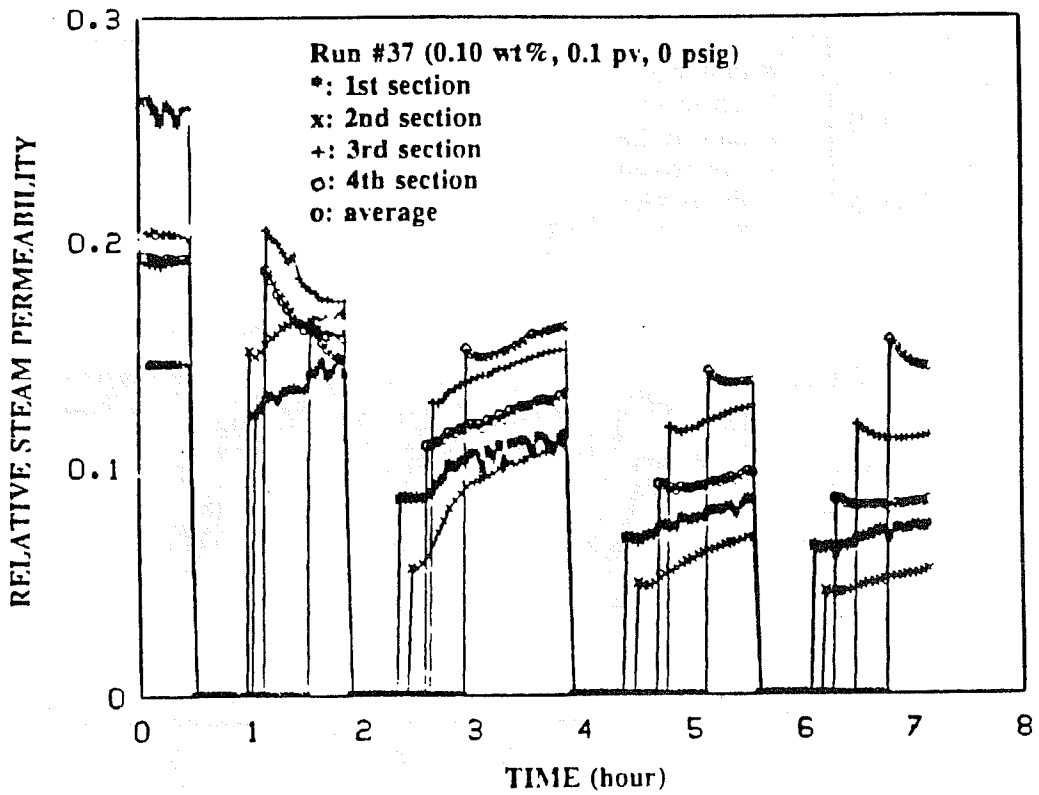


Fig. 8.21 Apparent Relative Steam Permeability vs Time for Run #37.

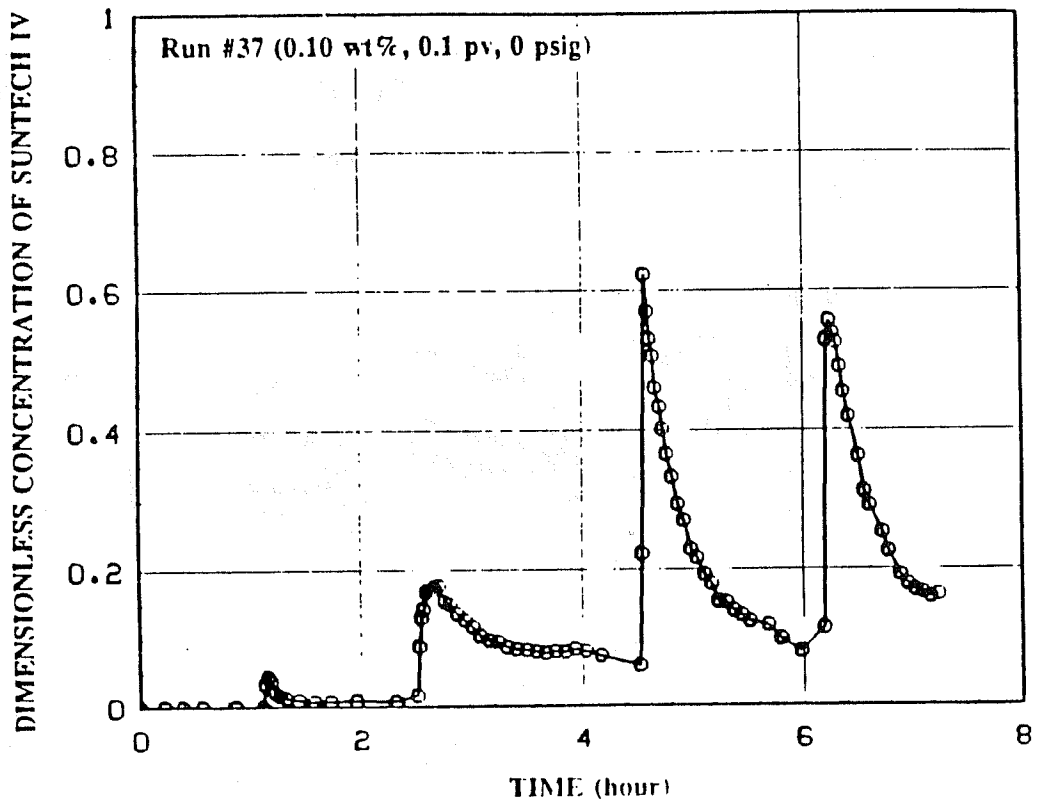


Fig. 8.22 Dimensionless Concentration of Suntech IV in Produced Fluid for Run #37.

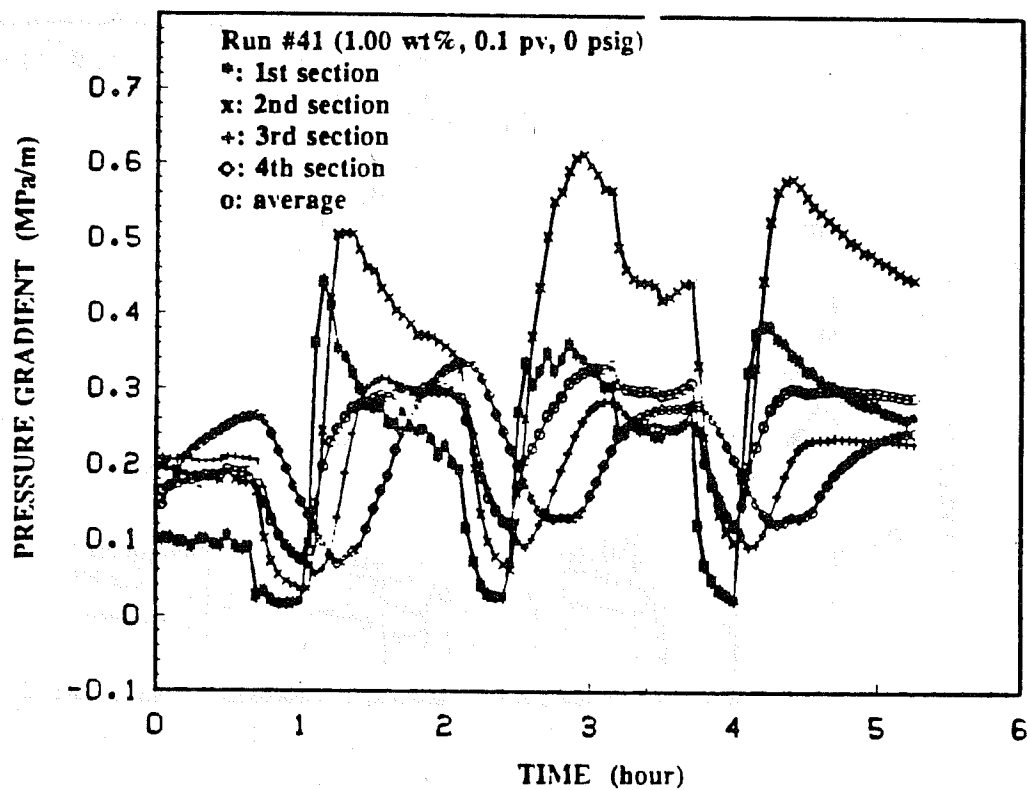


Fig. 8.23 Pressure Gradients vs Time for Run #41.

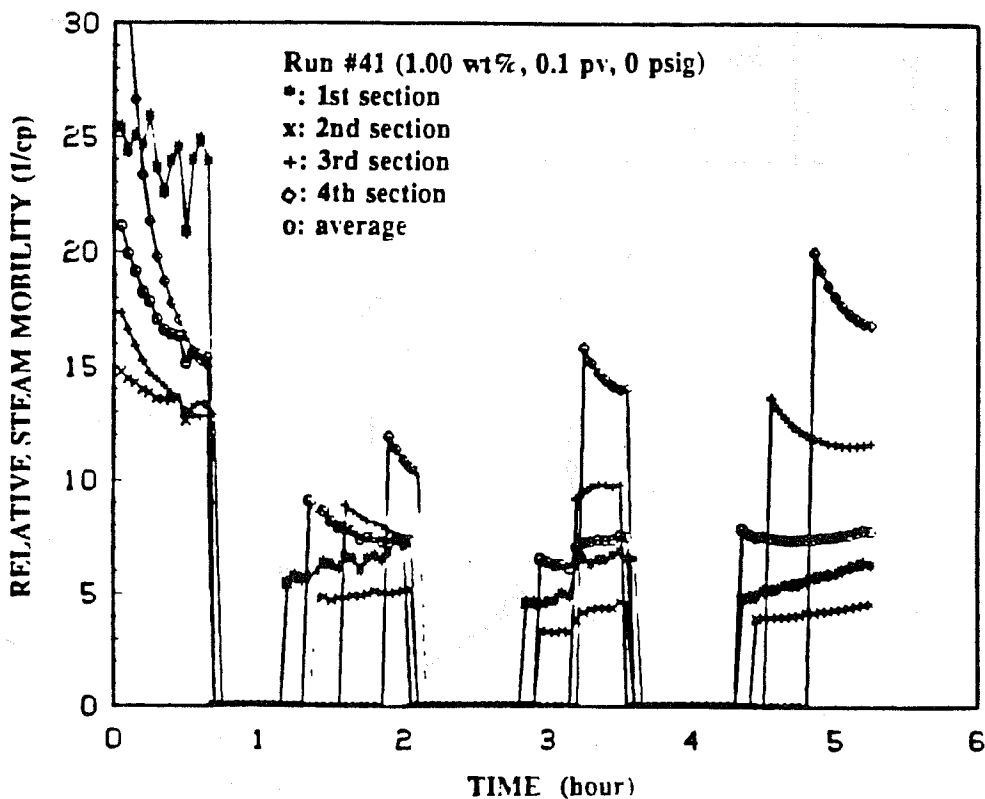


Fig. 8.24 Relative Steam Mobility vs Time for Run #41.

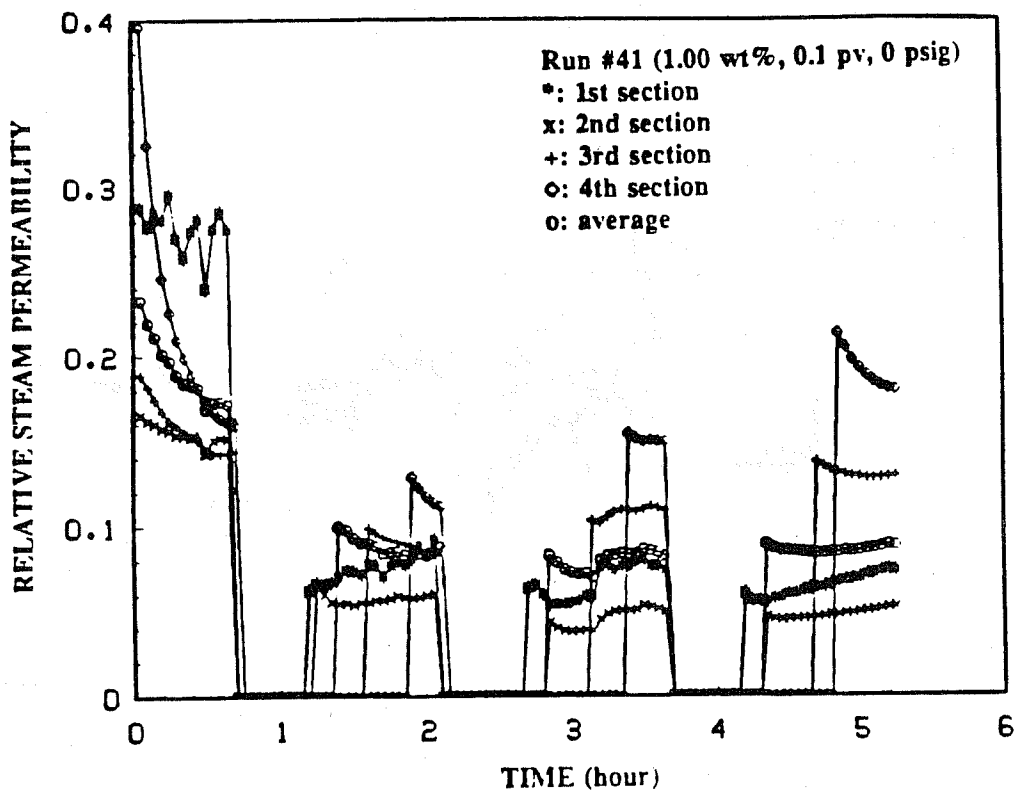


Fig. 8.25 Apparent Relative Steam Permeability vs Time for Run #41.

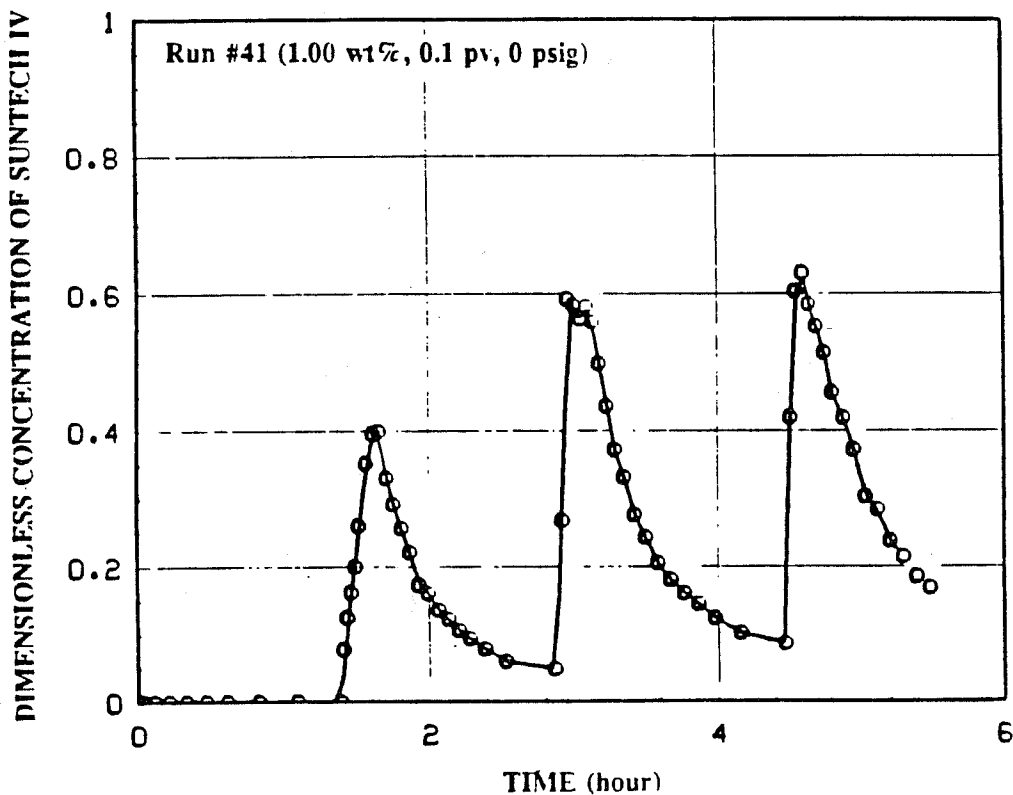


Fig. 8.26 Dimensionless Concentration of Suntech IV in produced Fluid for Run #41.

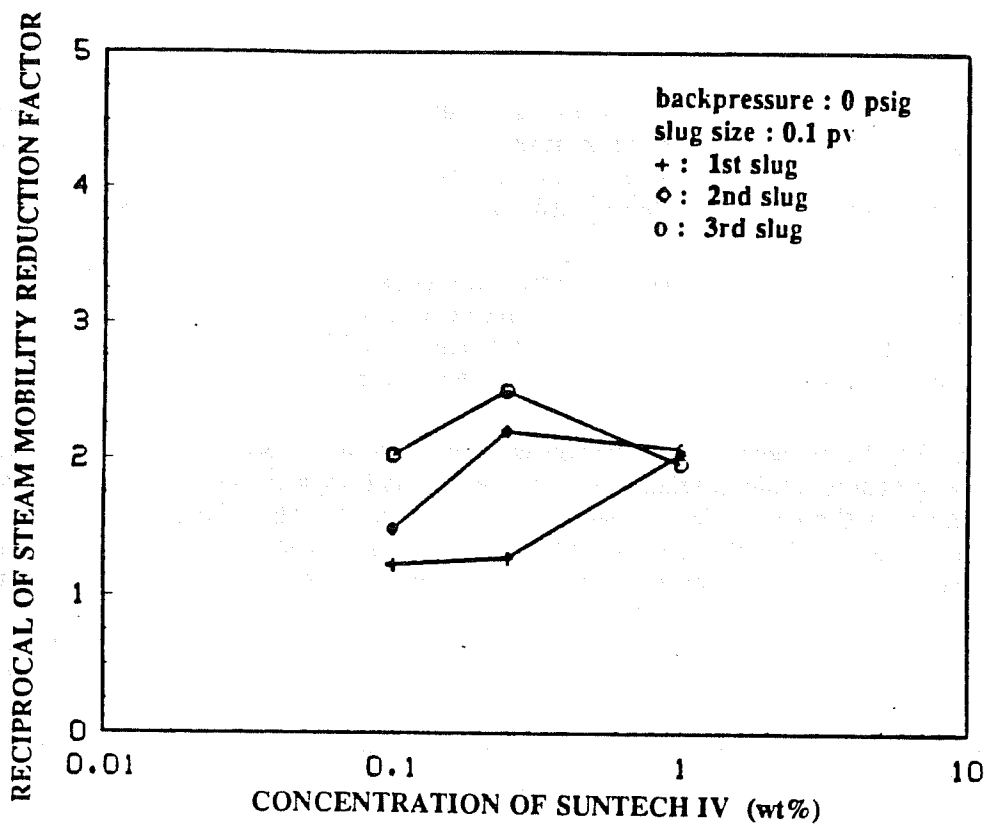


Fig. 8.27 Steam Mobility Reduction Factor vs Concentration of Suntech IV for Run Set II at 0.101 MPa.

8.3.2. Runs at 0.584 MPa (85 psia) at Outlet End

Four runs at Suntech IV concentrations of 0.0, 0.05, 0.22 and 1.12 wt% were performed at 0.584 MPa (85 psia). The sizes of surfactant slugs used in these runs were 0.1 pore volume. In these runs, only steam was injected during the cycles of steam injection.

Run #54 was a steam injection with three alternate water slugs. Figures 8.28, 8.29 and 8.30 show data of pressure gradient, relative steam mobility and relative steam permeability. The alternate water slugs had no effect on steam mobilities in any of the sections.

Run #28 was a steam injection with four alternate surfactant slugs at 0.05 wt%. Data on pressure gradient, relative steam mobility and apparent relative steam permeability are shown in Figs. 8.31, 8.32 and 8.33. There was essentially no reduction of steam mobility because the surfactant concentration was so low. The dimensionless produced surfactant concentration is shown in Fig. 8.34.

Run #47 was a steam injection with three alternate surfactant slugs at 0.22 wt%. Data on pressure gradient, relative steam mobility and apparent relative steam permeability are shown in Figs. 8.35, 8.36 and 8.37. There was only minor reduction of steam mobility because the surfactant concentration was low. The produced surfactant concentrations were not measured.

In Run #34, the surfactant concentration was increased to 1.12 wt%. Figures 8.38, 8.39 and 8.40 show data on pressure gradient, relative steam mobility and apparent relative steam permeability. The first surfactant slug showed a slight steam mobility reduction. The effect was significantly increased by the second slug. During the injection of the third surfactant slug, the pump was partially plugged and the actual amount of the injected surfactant solution was less than the designed value of 0.1 pore volume. The effect of this slug on steam mobility reduction was markedly reduced. A further steam mobility reduction was observed during the fourth slug injection when the actual slug size was 0.1 pore volume. Figure 8.41 shows the concentration profile of Suntech IV in the produced fluids.

Figure 8.42 graphs the reciprocal of steam mobility reduction factor (*i.e.* the increased pressure drop) for this set of runs as a function of the Suntech IV concentration. The steam mobility ratios were calculated using the average relative steam mobility. At a backpressure of 0.584 MPa, concentration had virtually no effect on the steam mobility for the first surfactant slug. For the second surfactant slug, the steam mobility decreased with the increase of surfactant concentration. The effect of number of surfactant slugs increases with the concentration.

8.3.3. Effect of Nitrogen on Mobility Reduction

It has been observed in this study and Doscher's (1982) that steam/foam was more effective in the inlet half of the sandpack than the outlet half in most cases. Two possible reasons for this phenomenon are the effects of steam quality and turbulent flow. The higher steam quality represents a higher foam quality and may result in lower steam mobility. When the steam condenses along the sandpack, the effect of turbulent flow is reduced. Both effects tend to increase steam mobility with distance. However, it has been observed that the lowest steam mobility occurred in the second section instead of the first section in some runs as shown in Figs. 8.3 and 8.7.

Dilgren *et al.* (1978), Doscher *et al.* (1982), Brigham *et al.* (1984) and Duerksen (1984) showed that injecting noncondensable gases with steam further reduced the steam mobility. One advantage of the addition of nitrogen in steam is that it may reduce steam mobility further downstream.

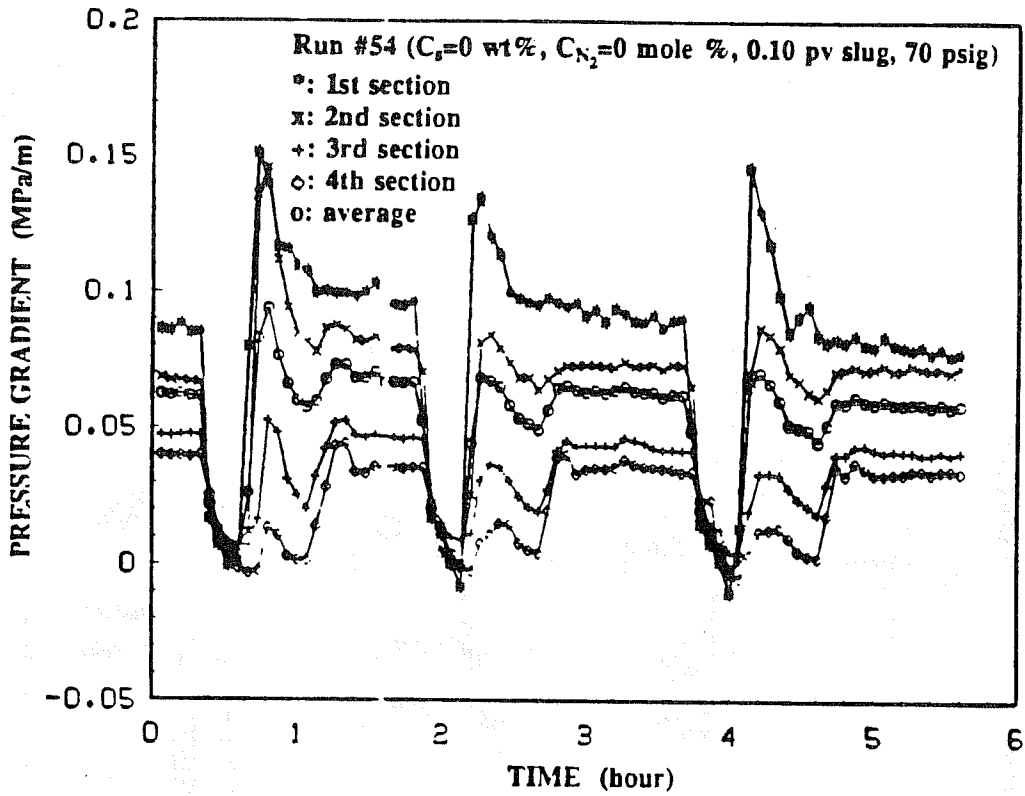


Fig. 8.28 Pressure Gradients vs Time for Run #54.

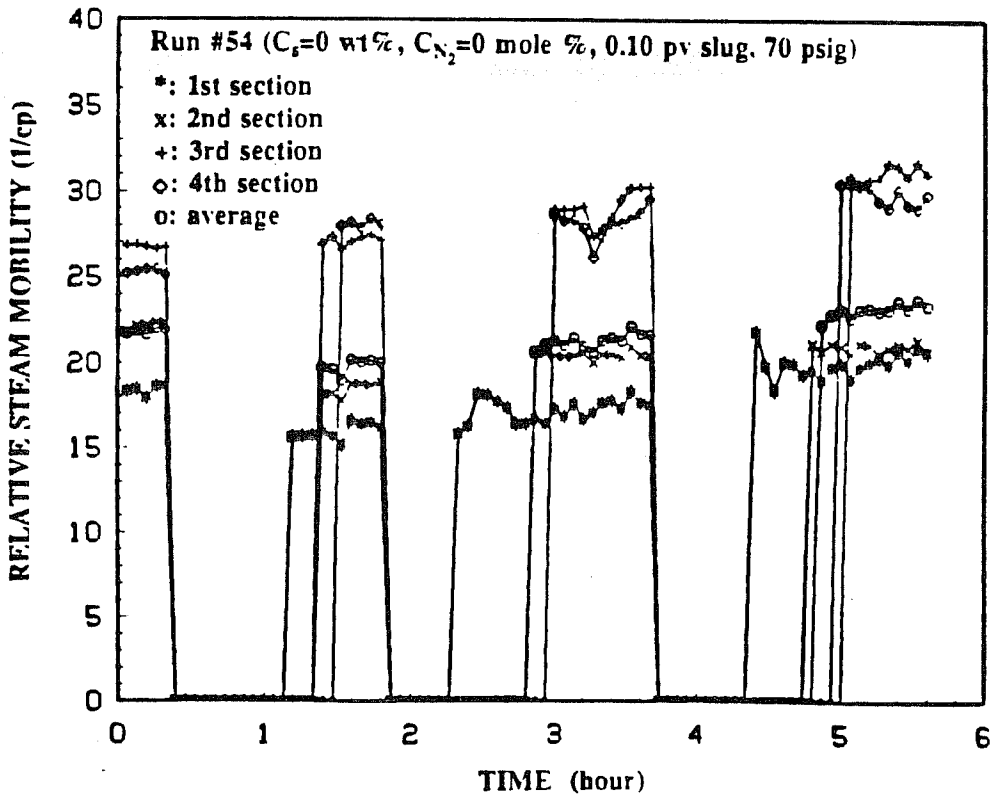


Fig. 8.29 Relative Steam Mobility vs Time for Run #54.

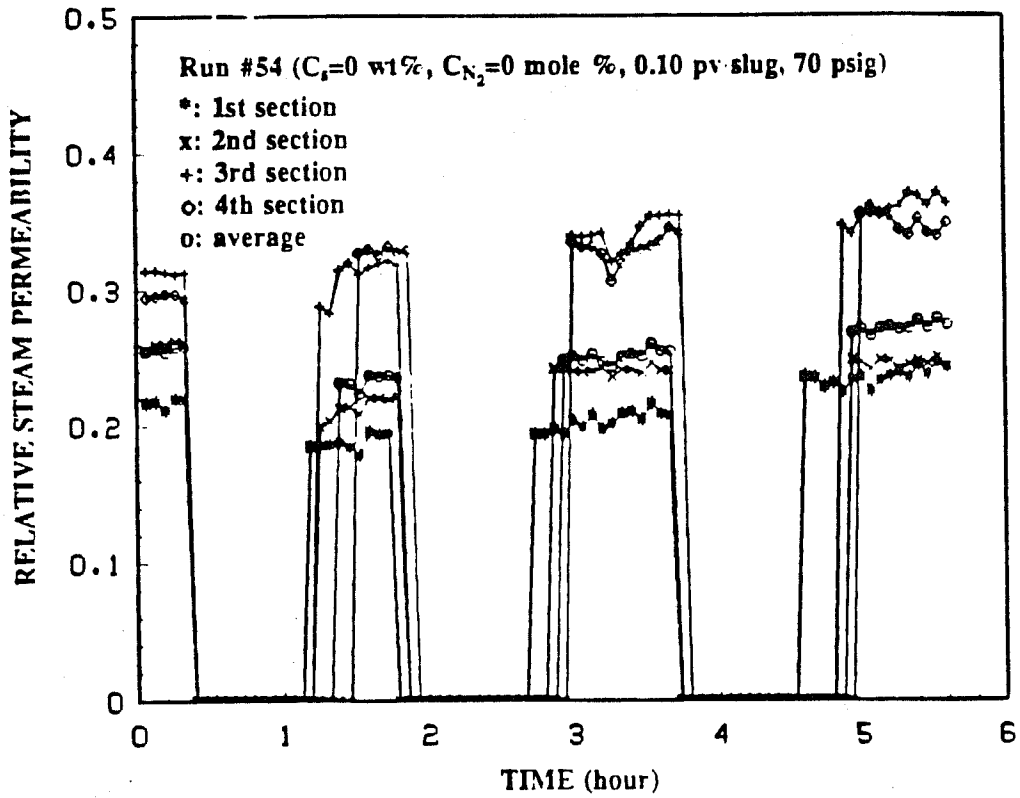


Fig. 8.30 Apparent Relative Steam Permeability vs Time for Run #54.

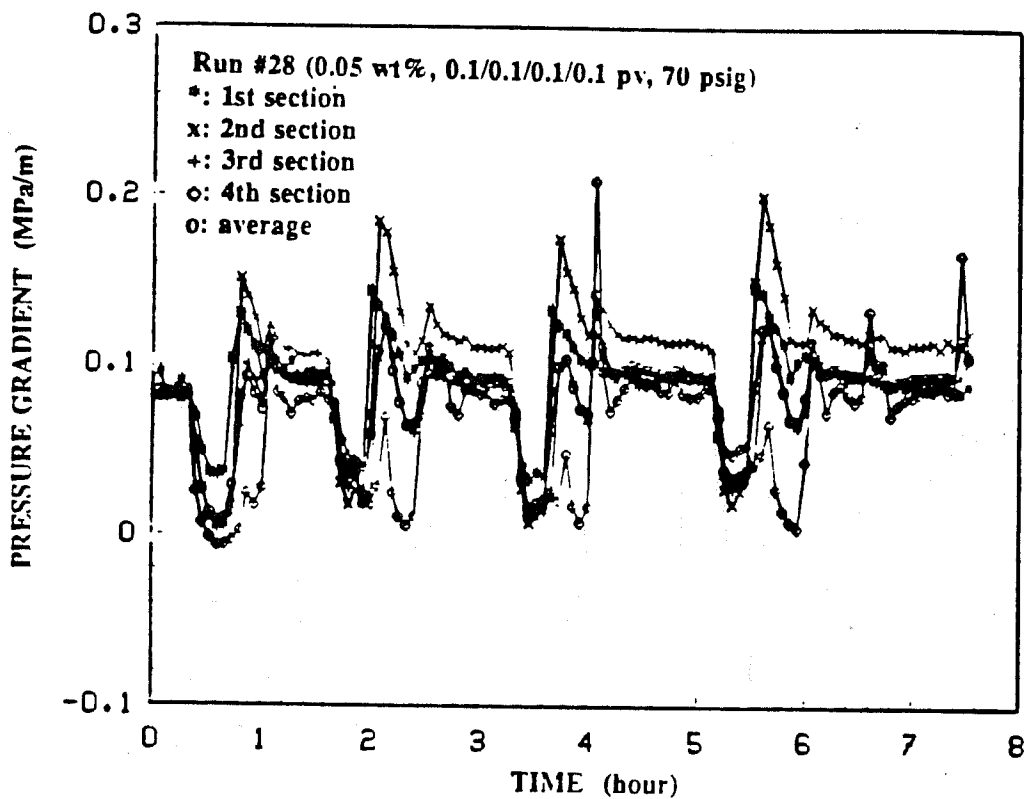


Fig. 8.31 Pressure Gradients vs Time for Run #28.

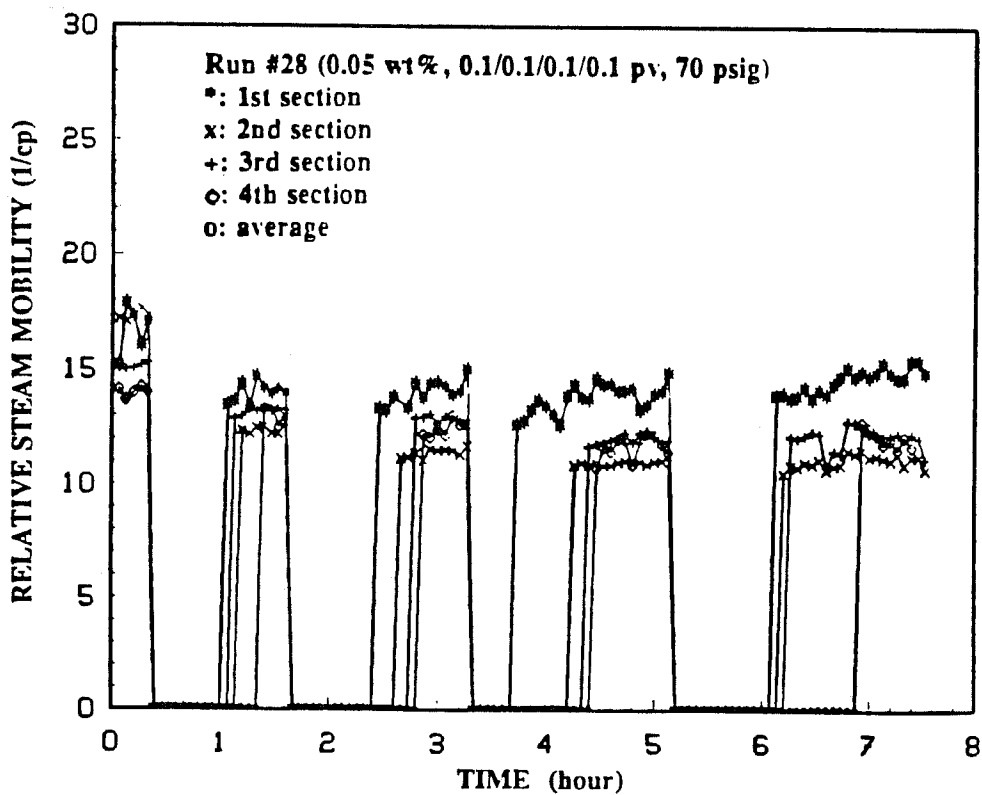


Fig. 8.32 Relative Steam Mobility vs Time for Run #28.

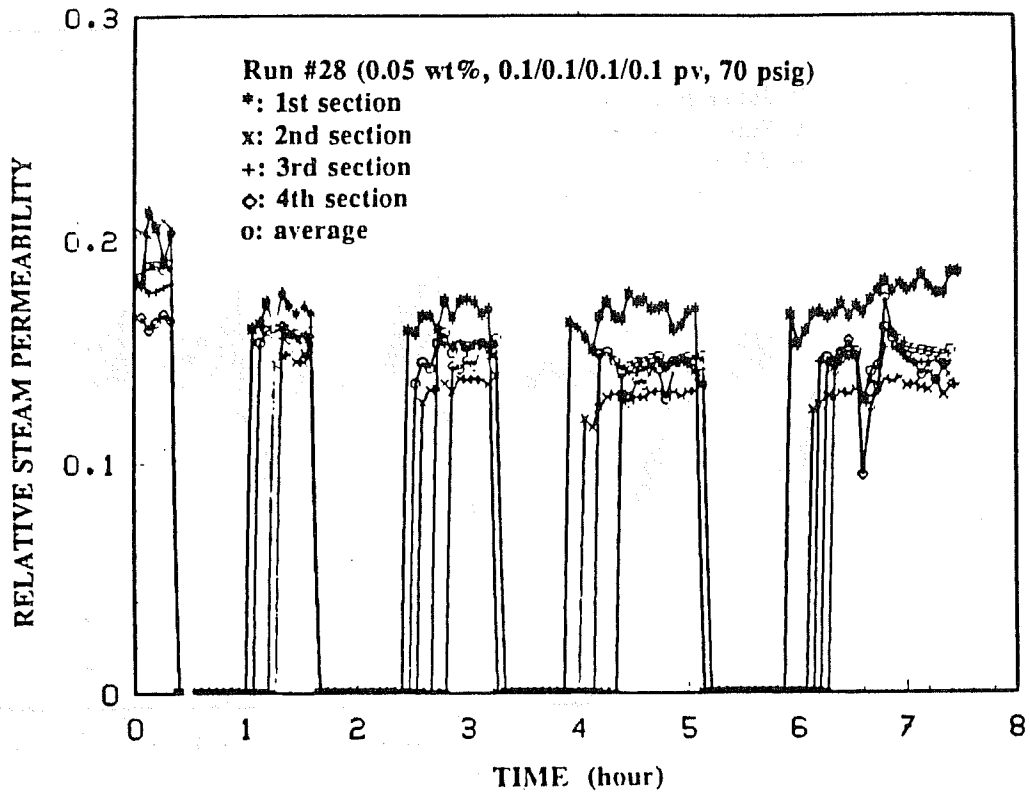


Fig. 8.33 Apparent Relative Steam Permeability vs Time for Run #28.

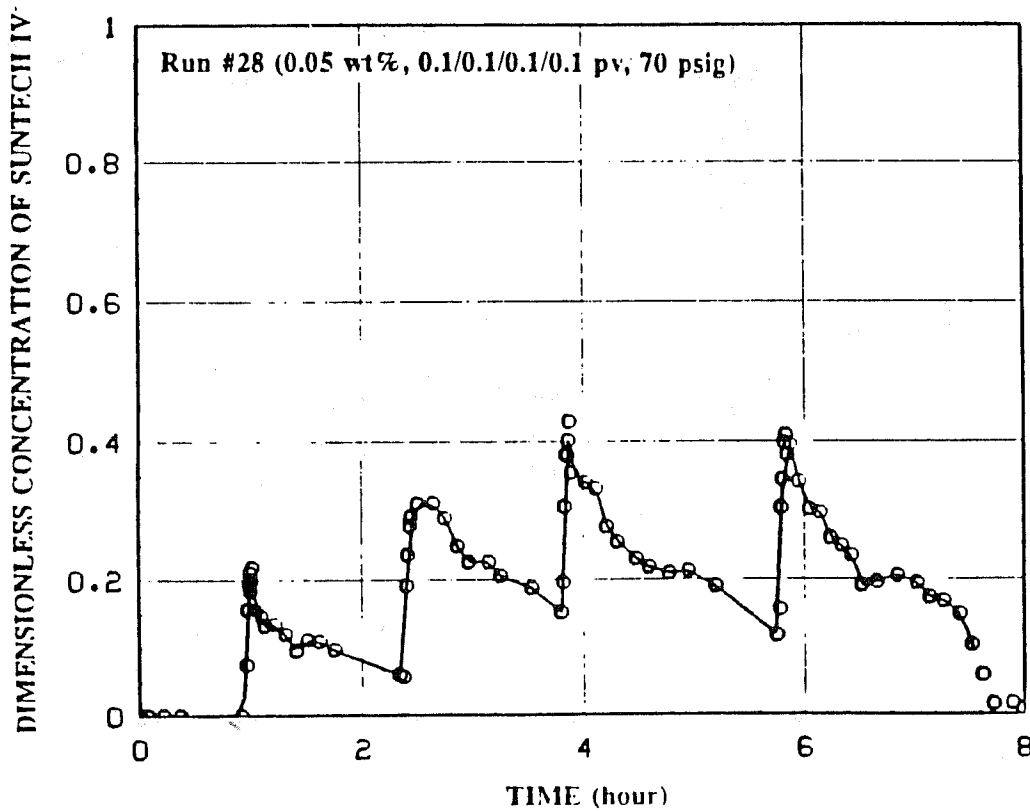


Fig. 8.34 Dimensionless Concentration of Suntech IV in Produced Fluid for Run #28.

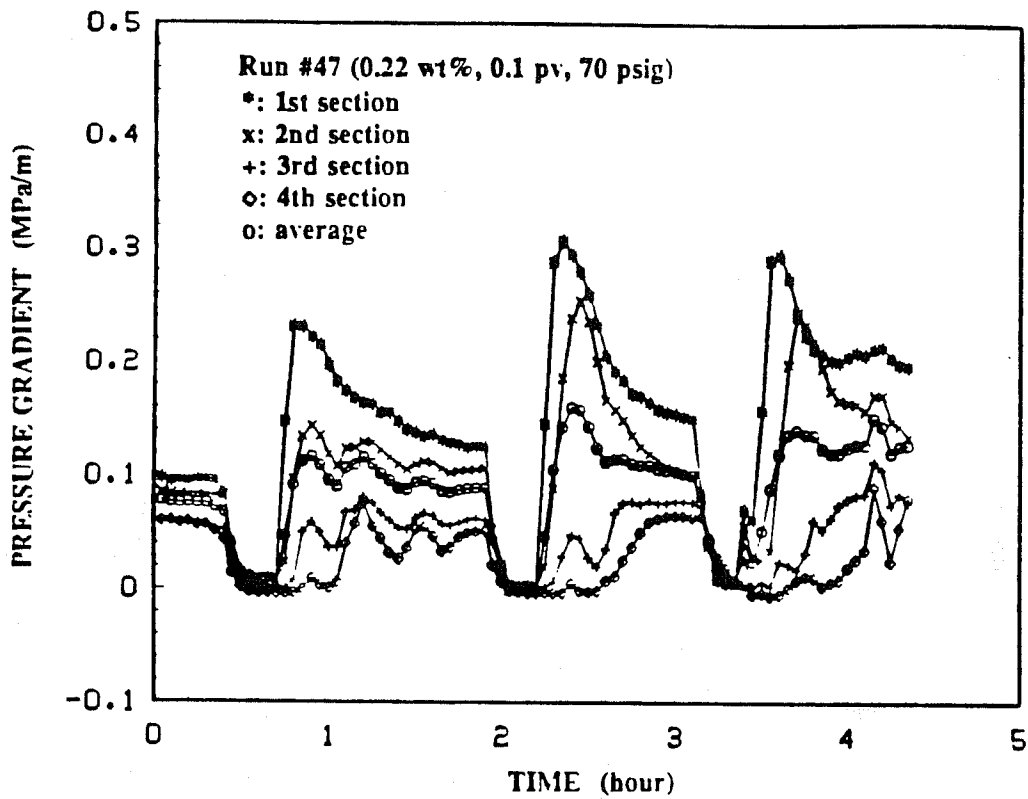


Fig. 8.35 Pressure Gradients vs Time for Run #47.

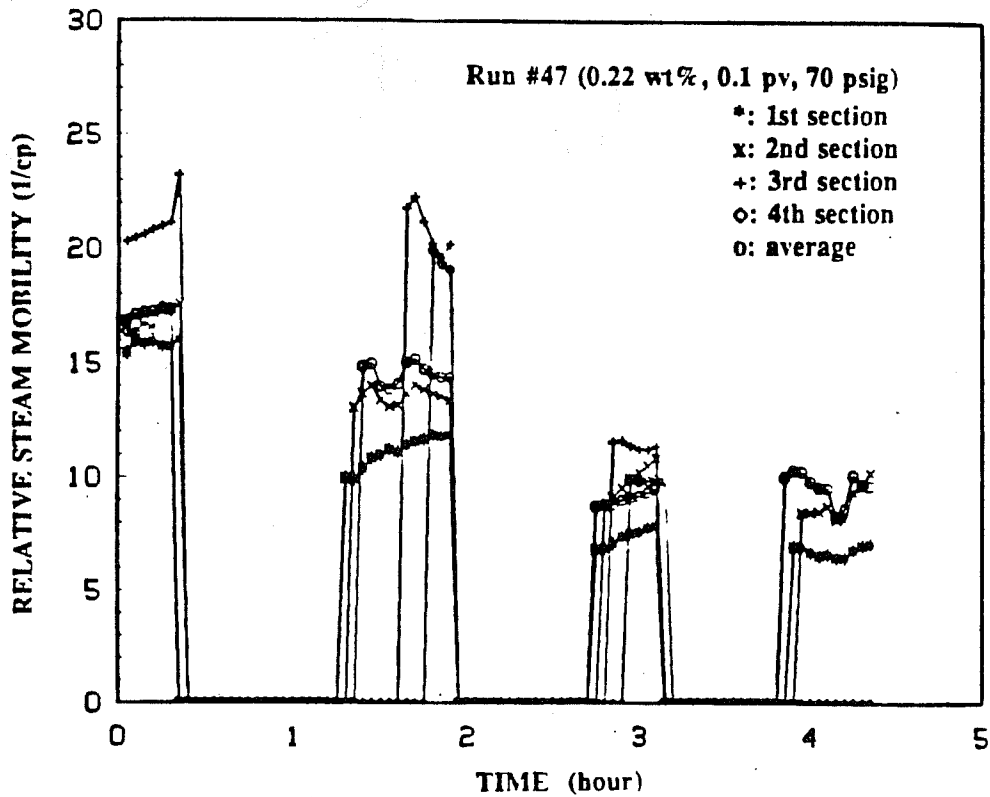


Fig. 8.36 Relative Steam Mobility vs Time for Run #47.

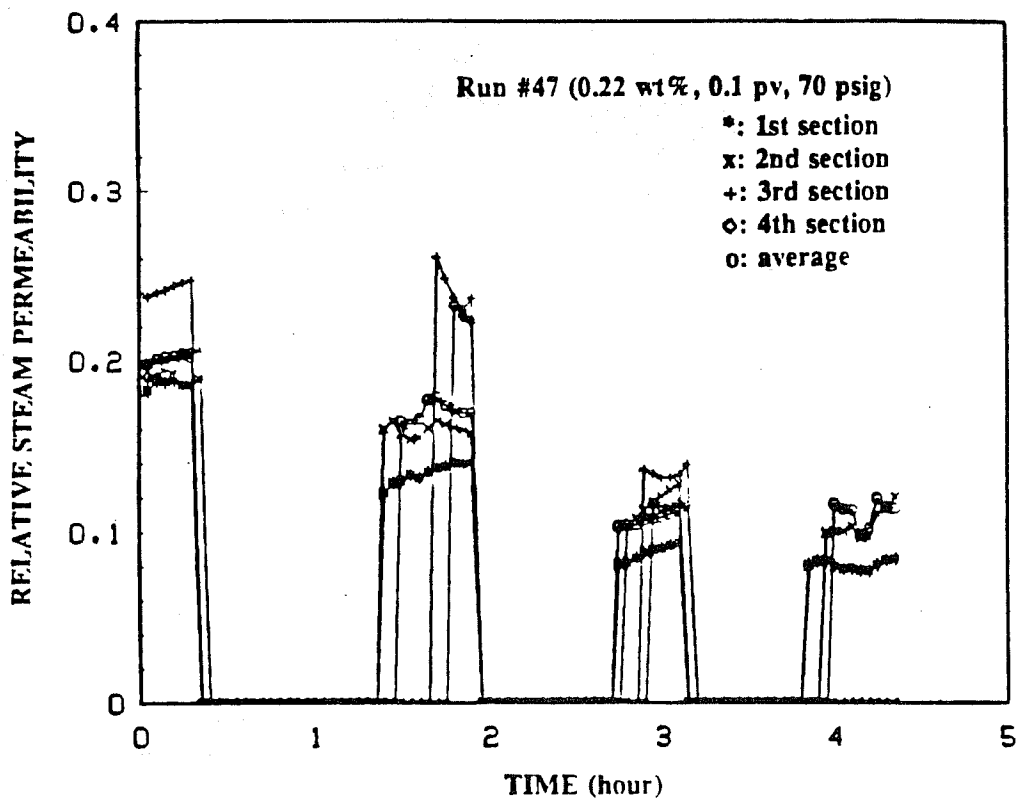


Fig. 8.37 Apparent Relative Steam Permeability vs Time for Run #47.

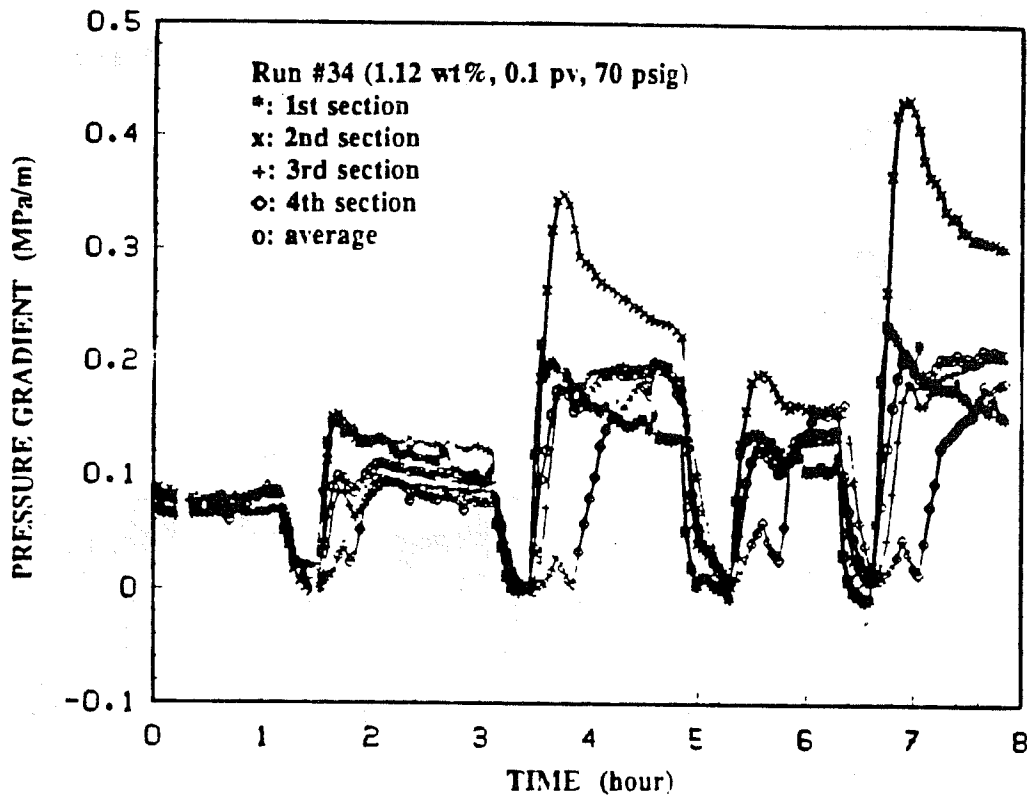


Fig. 8.38 Pressure Gradients vs Time for Run #34.

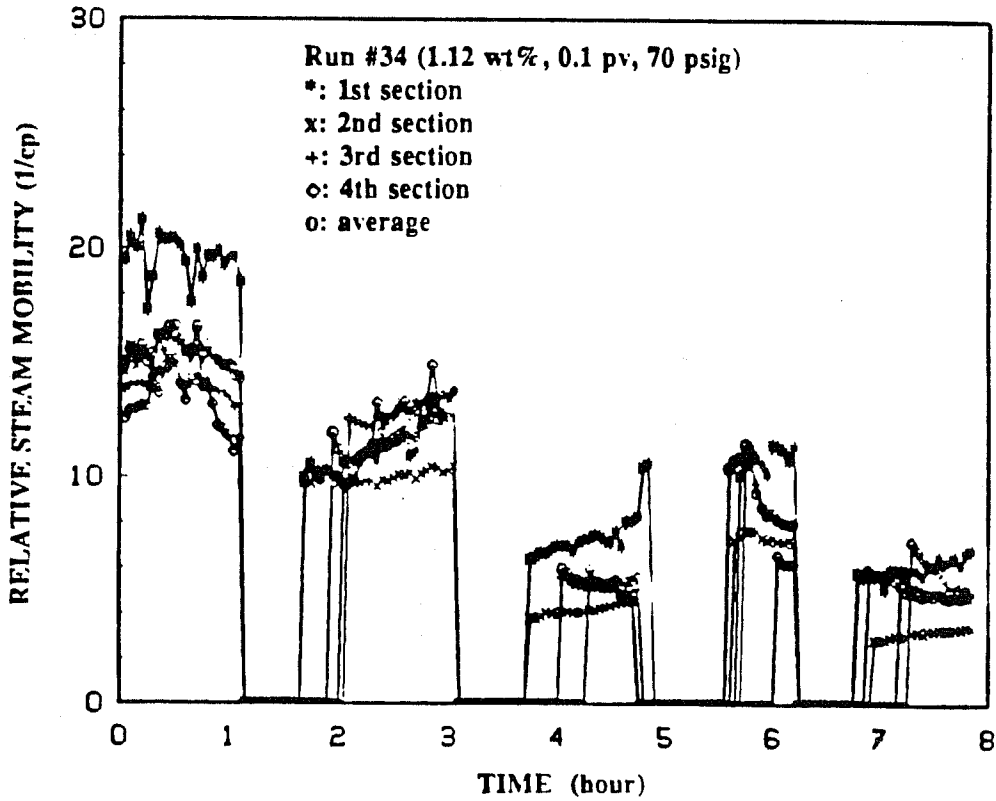


Fig. 8.39 Relative Steam Mobility vs Time for Run #34.

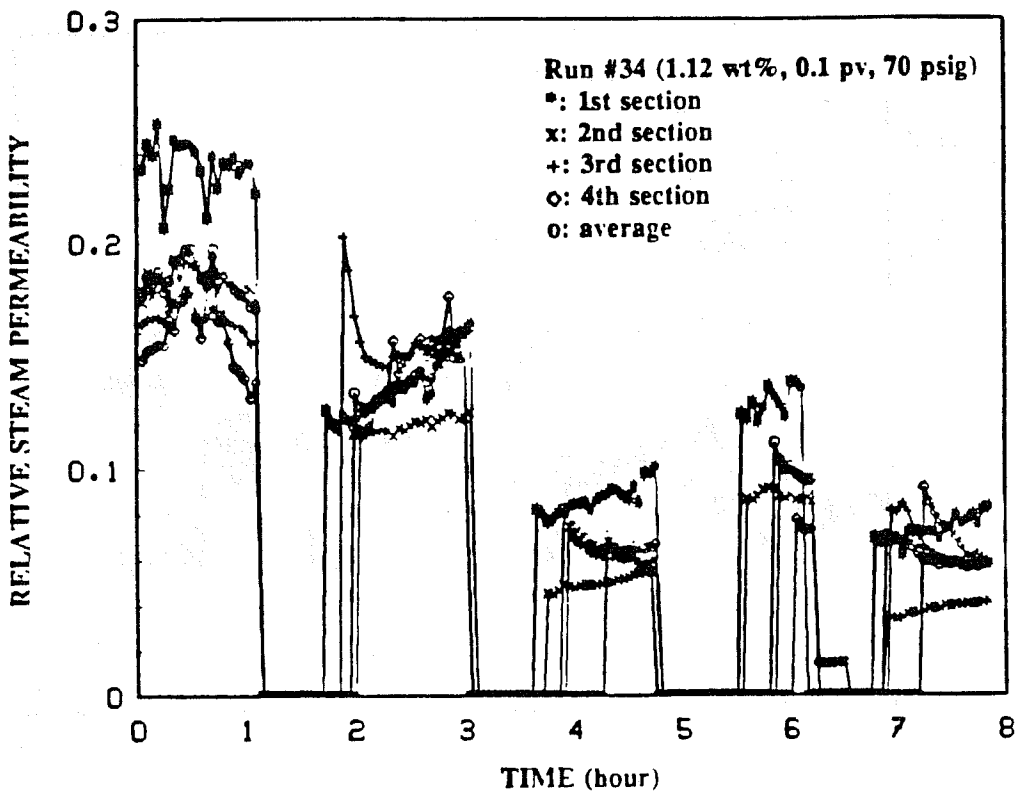


Fig. 8.40 Apparent Relative Steam Permeability vs Time for Run #34.

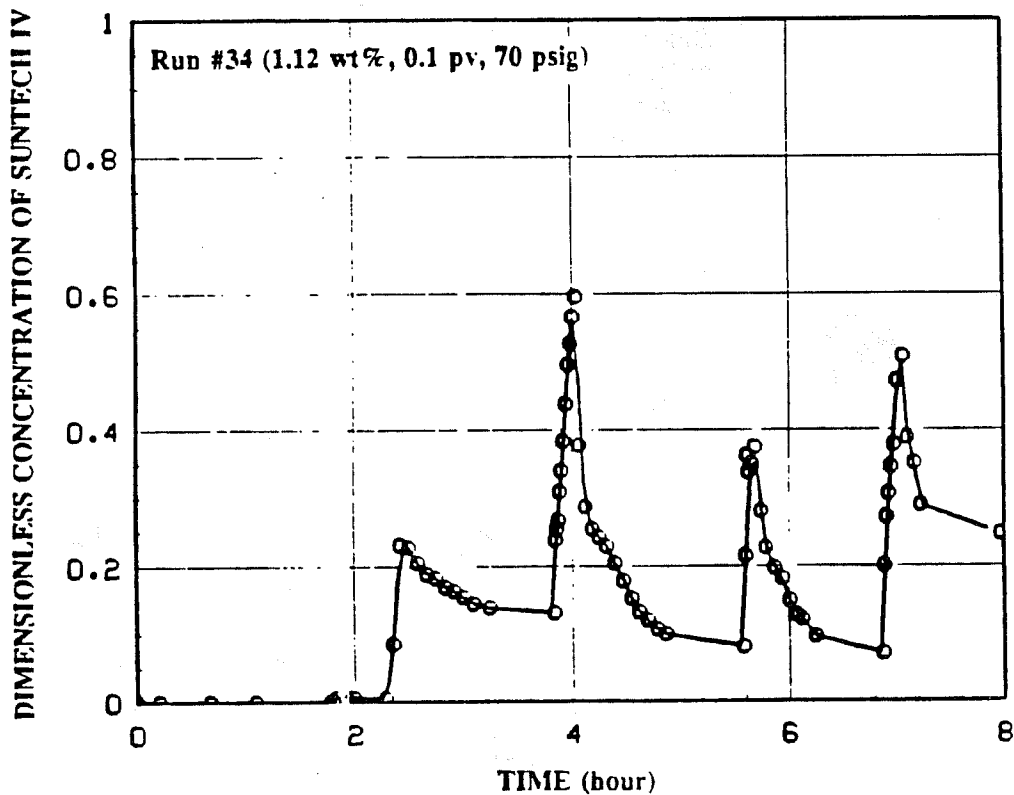


Fig. 8.41 Dimensionless Concentration of Suntech IV in Produced Fluid for Run #34.

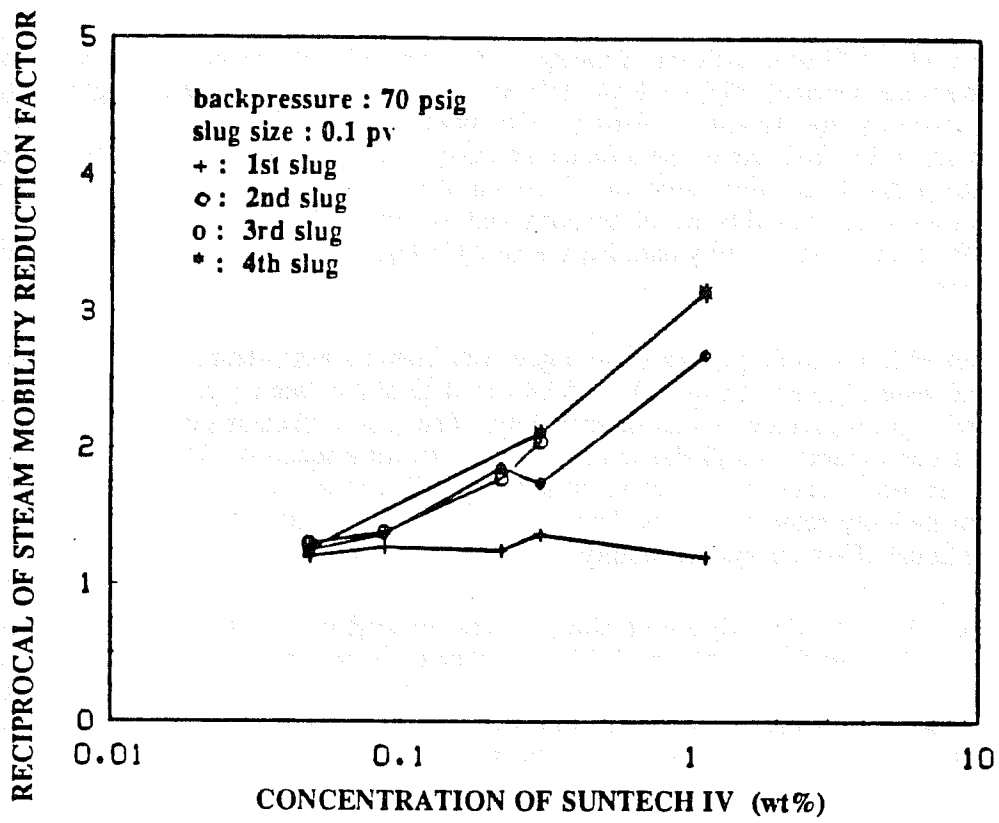


Fig. 8.42 Steam Mobility Reduction Factor vs Concentration of Suntech IV for Runs at 0.584 MPa.

A series of experiments were conducted to study the effect of nitrogen concentration on the steam mobility reduction. The backpressures of these experiments were about 0.584 MPa (85 psia) and the surfactant concentration was 0.22 wt%. The mole fraction of nitrogen in injected steam varied from 0 to 2%. All runs started with steam injection in the absence of both nitrogen and surfactant, and followed by injecting alternate slugs of surfactant solution and steam plus nitrogen. During the injection of surfactant slugs, neither steam nor nitrogen were injected.

In Run #55, pure water slugs instead of surfactant slugs were used. The nitrogen concentration in the steam was 1.1 mole percent. Figure 8.43 shows the pressure gradient data. The first water slug reduced the steam mobility slightly and no further reductions were seen for the second and third water slugs.

In Run #50, 0.75 mole percent of nitrogen was injected with steam. Three surfactant slugs of 0.1 pore volume were injected. Figures 8.44, 8.45 and 8.46 show data on pressure gradient, apparent relative steam mobility and apparent relative steam permeability. The first surfactant slug reduced the steam mobility in the first section by a factor of three, and had a moderate reduction in the second section and had a small mobility reduction in the third and fourth sections. The second surfactant slug further reduced steam mobility in all sections and the third slug showed no further effect on steam mobility. By comparing mobility data from Run #47 (Fig. 8.36), the effect of the addition of nitrogen was moderate.

In Run #51, 1.1 mole percent of nitrogen was injected with steam. Five surfactant slugs of 0.1 pore volume were injected. Figures 8.47, 8.48 and 8.49 show data on pressure gradient, relative steam mobility and apparent relative steam permeability. The first surfactant slug reduced the steam mobility in the first section markedly and showed little effect on other sections. The second and third surfactant slug further reduced steam mobilities in all sections. The fourth surfactant slug showed a slight additional steam mobility reduction in the first and second sections and the fifth surfactant slug had virtually no additional effect on steam mobility.

In Run #52, 2.1 mole percent of nitrogen was injected with steam. Four 0.1 pv surfactant slugs were injected. Figures 8.50, 8.51 and 8.52 show data on pressure gradient, relative steam mobility and relative steam permeability. The steam mobility in the first two sections was reduced for the first slug and further reduced for each of the following two slugs. The steam mobility in the first two sections in the fourth cycle was slightly higher than the steam mobility in the third cycle. In the last two sections, the mobility reduction was more modest, and did not vary much with subsequent surfactant slugs.

The results of this set of runs are summarized in Fig. 8.53 for the first section, Fig. 8.54 for the second section and Fig. 8.55 for the average of the entire sandpack. All three figures show that nitrogen had a little effect on steam mobility for the first surfactant slugs. However, the nitrogen effect increases with the nitrogen concentration in steam for the second and third slugs. In general, the nitrogen showed a moderate effect on steam mobility reductions. Comparing Fig. 8.53 with Fig. 8.54 reveals that the nitrogen effect was more pronounced in the first section than other sections. The advantage of using nitrogen with steam is to reduce the surfactant consumption and make the process more economical. From Figs. 8.42 and 8.55, it can be seen that injecting 0.22 wt% surfactant slugs alternating with steam plus 2.1 mole percent nitrogen slug could reduced the steam mobility to the same degree as injecting 1.0 wt% surfactant slugs alternating only with steam.

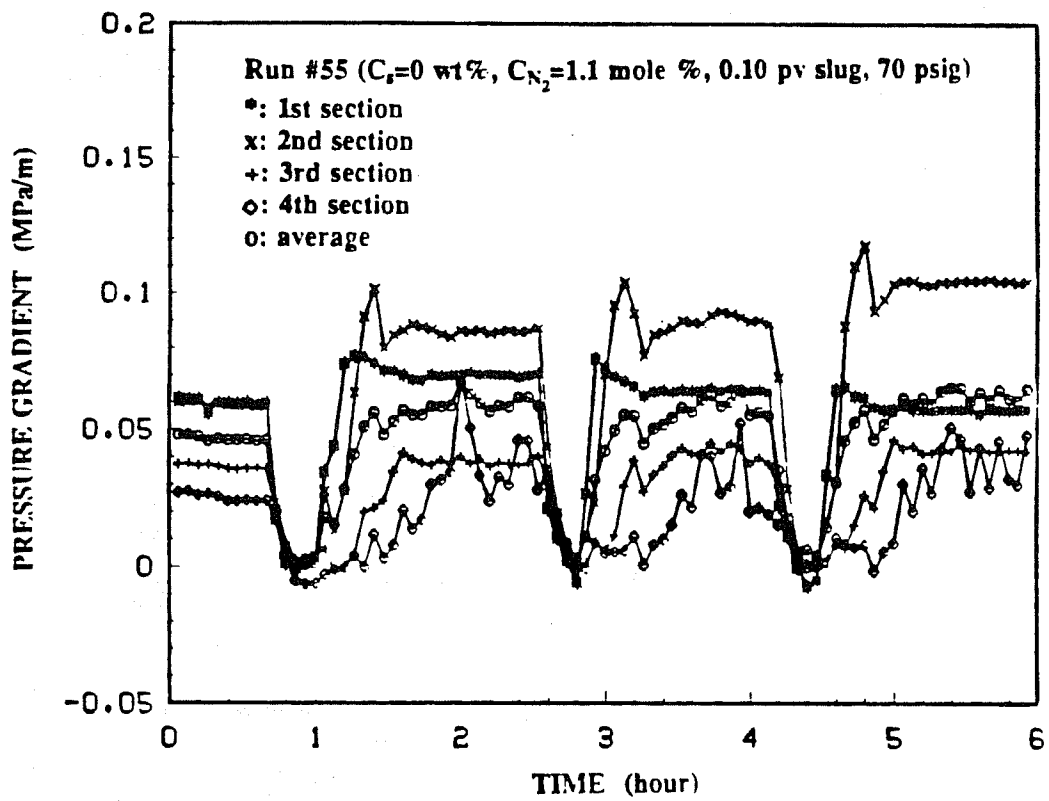


Fig. 8.43 Pressure Gradients vs Time for Run #55.

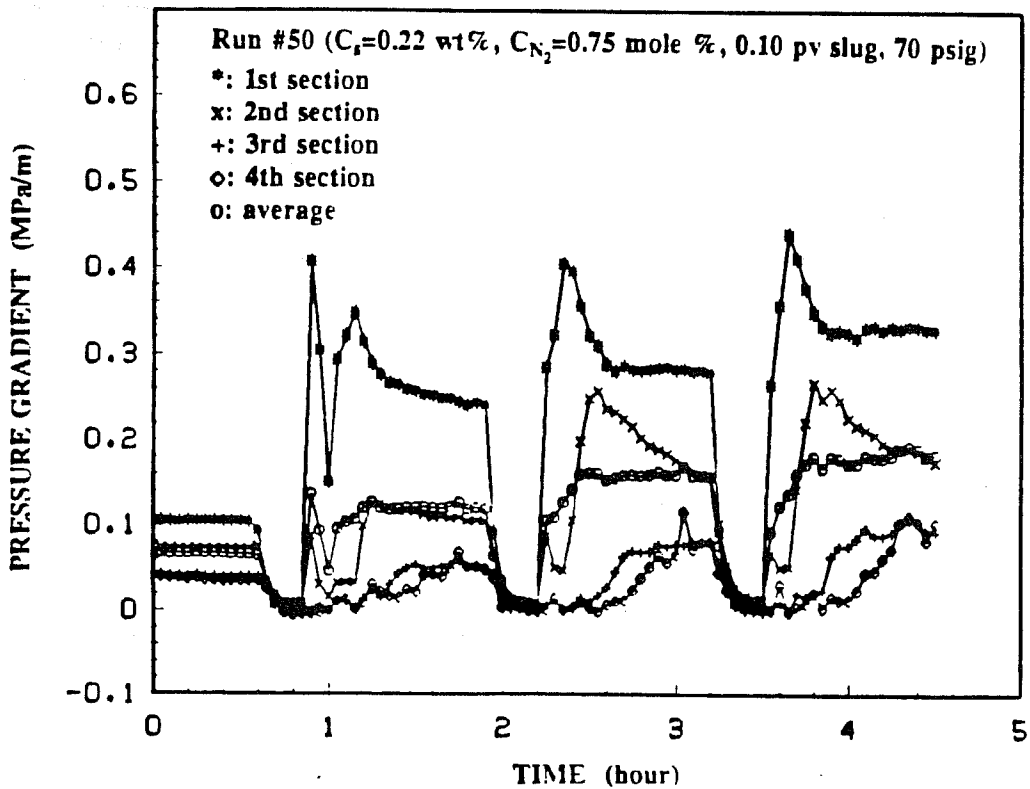


Fig. 8.44 Pressure Gradients vs Time for Run #50.

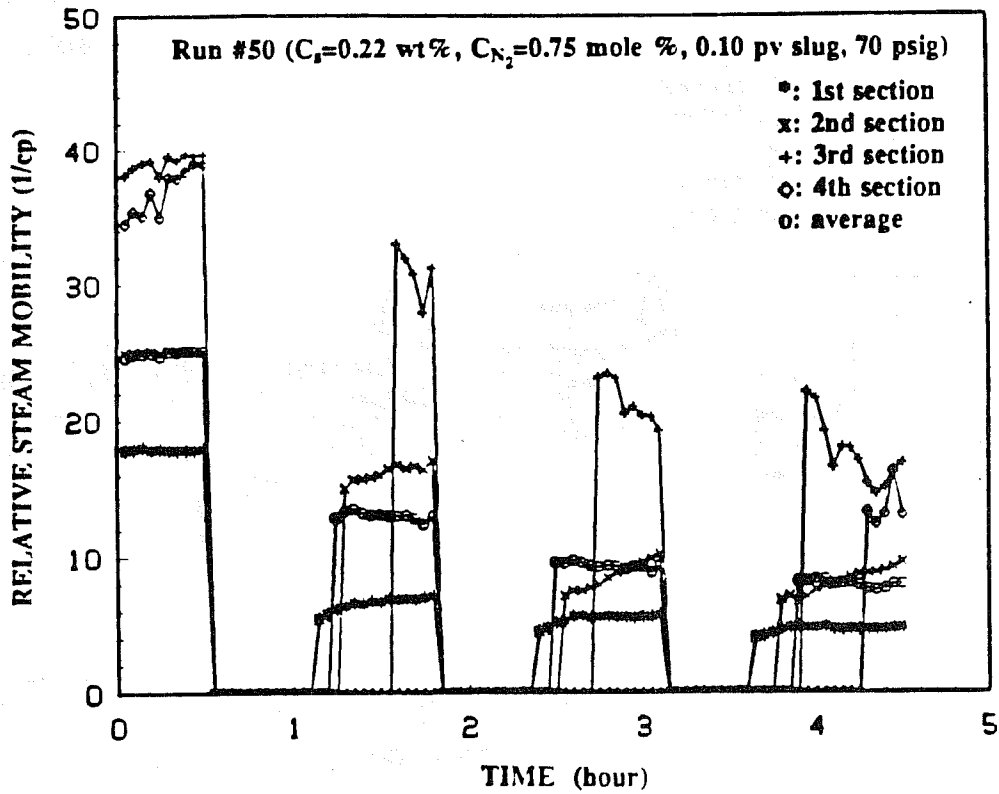


Fig. 8.45 Relative Steam Mobility vs Time for Run #50.

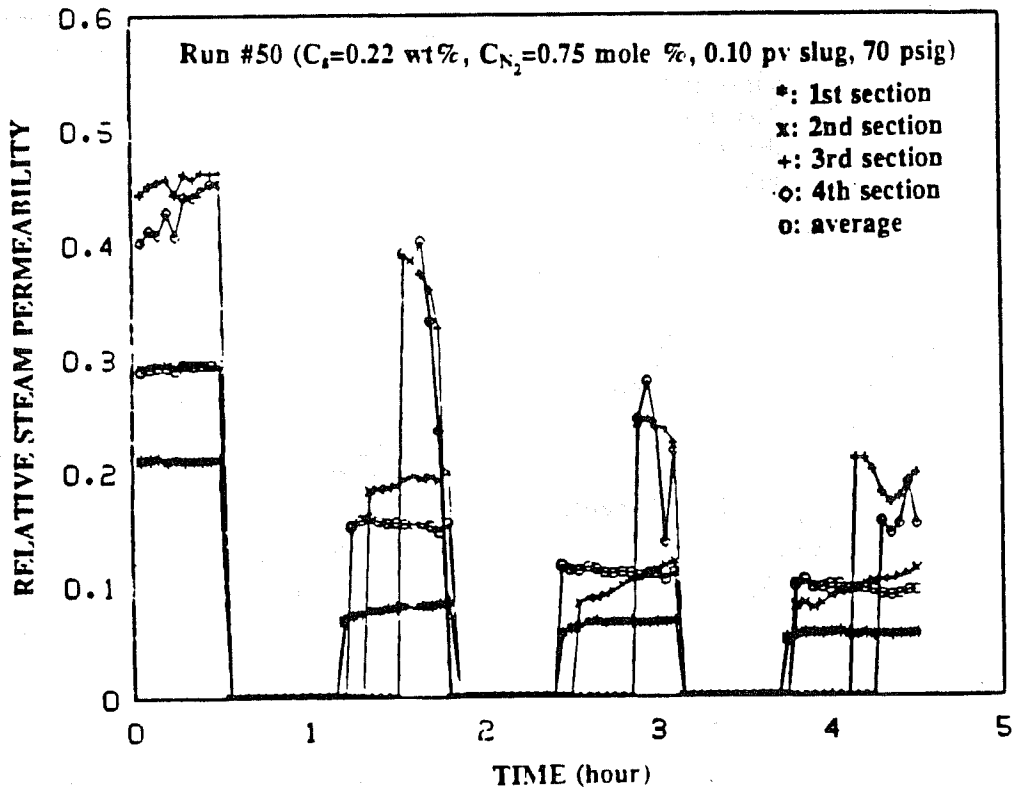


Fig. 8.46 Apparent Relative Steam Permeability vs Time for Run #50.

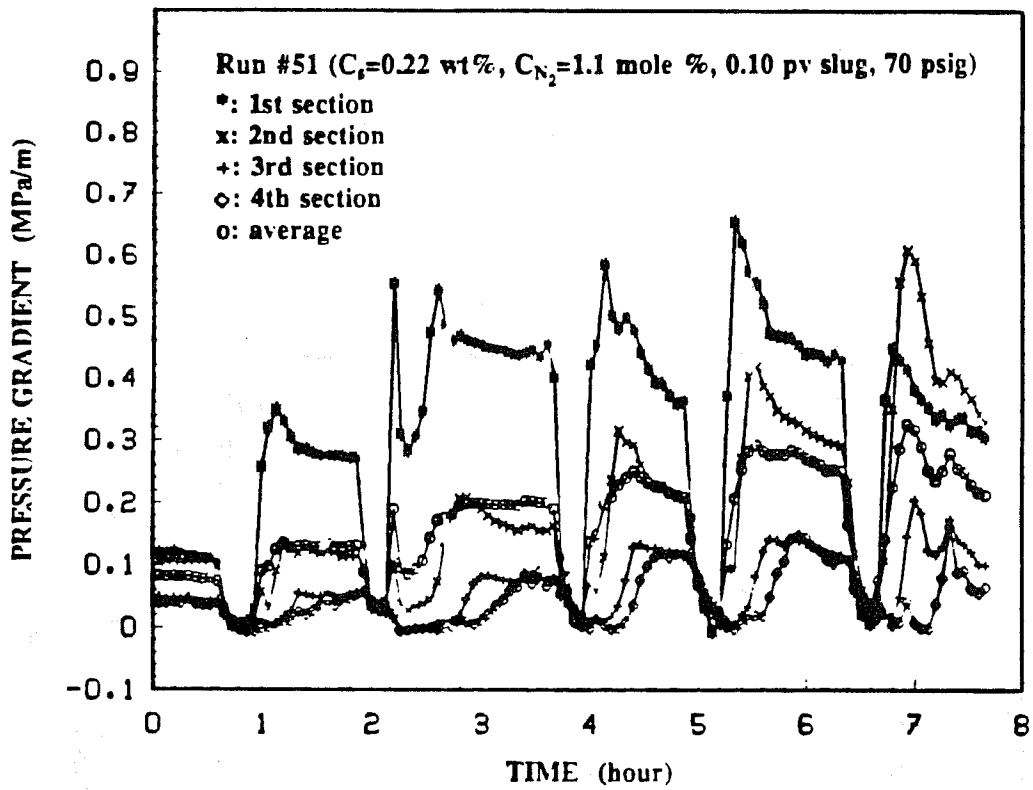


Fig. 8.47 Pressure Gradients vs Time for Run #51.

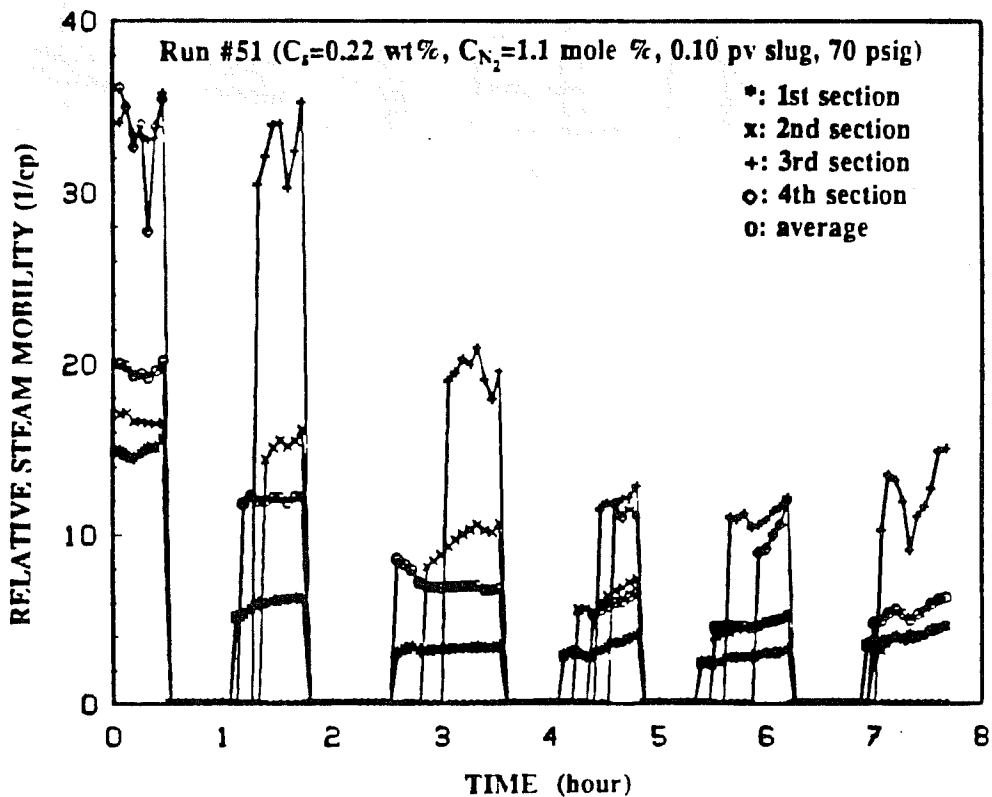


Fig. 8.48 Relative Steam Mobility vs Time for Run #51.

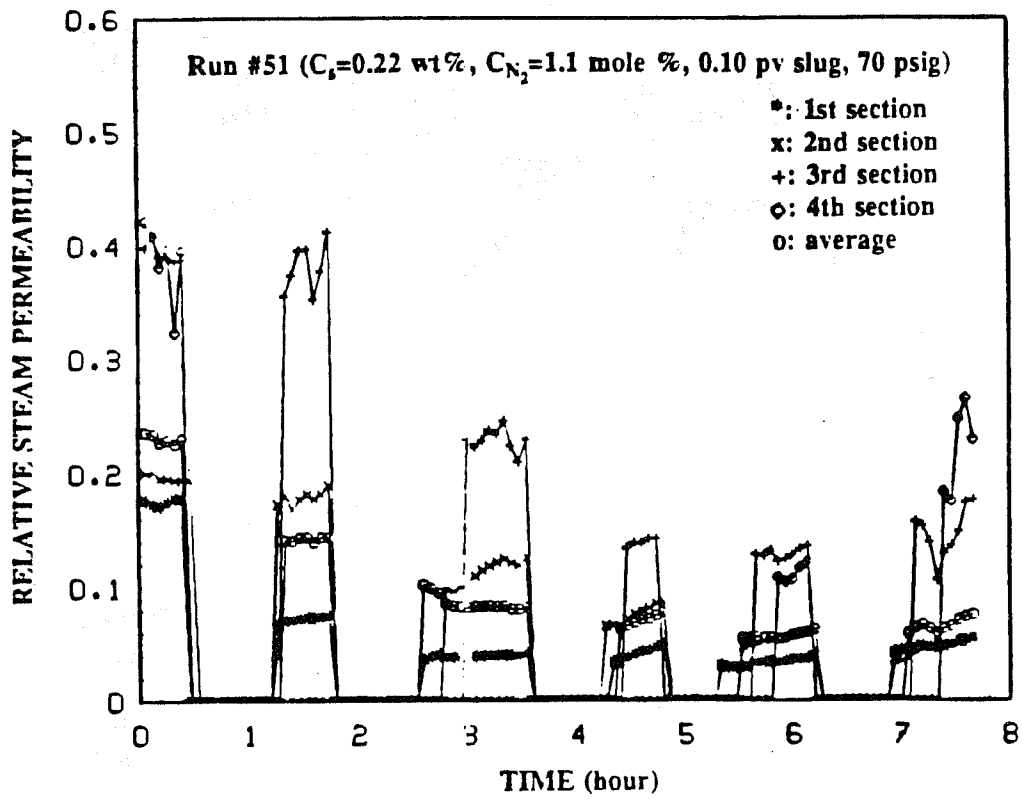


Fig. 8.49 Apparent Relative Steam Permeability vs Time for Run #51.

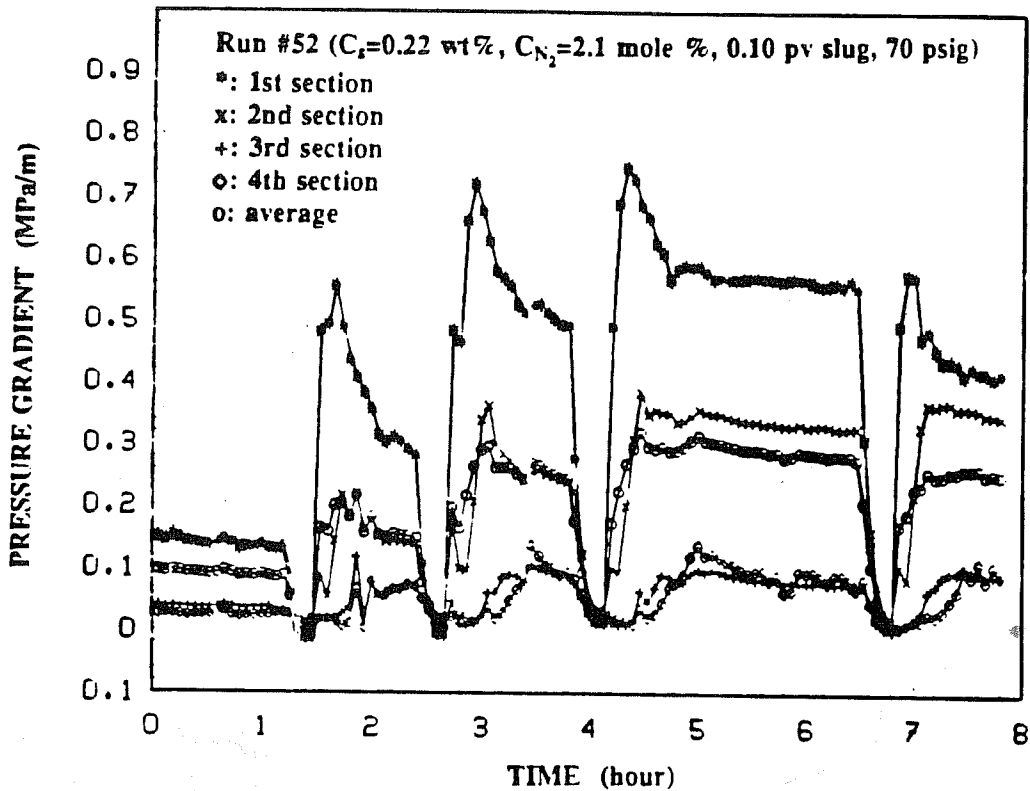


Fig. 8.50 Pressure Gradients vs Time for Run #52.

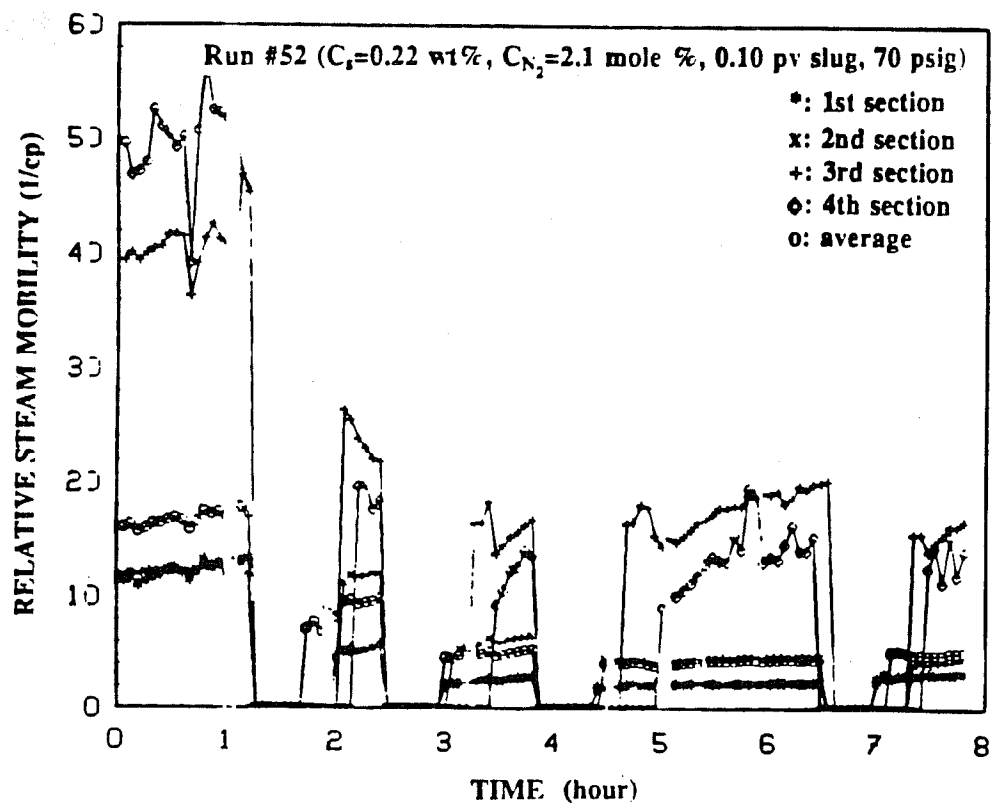


Fig. 8.51 Relative Steam Mobility vs Time for Run #52.

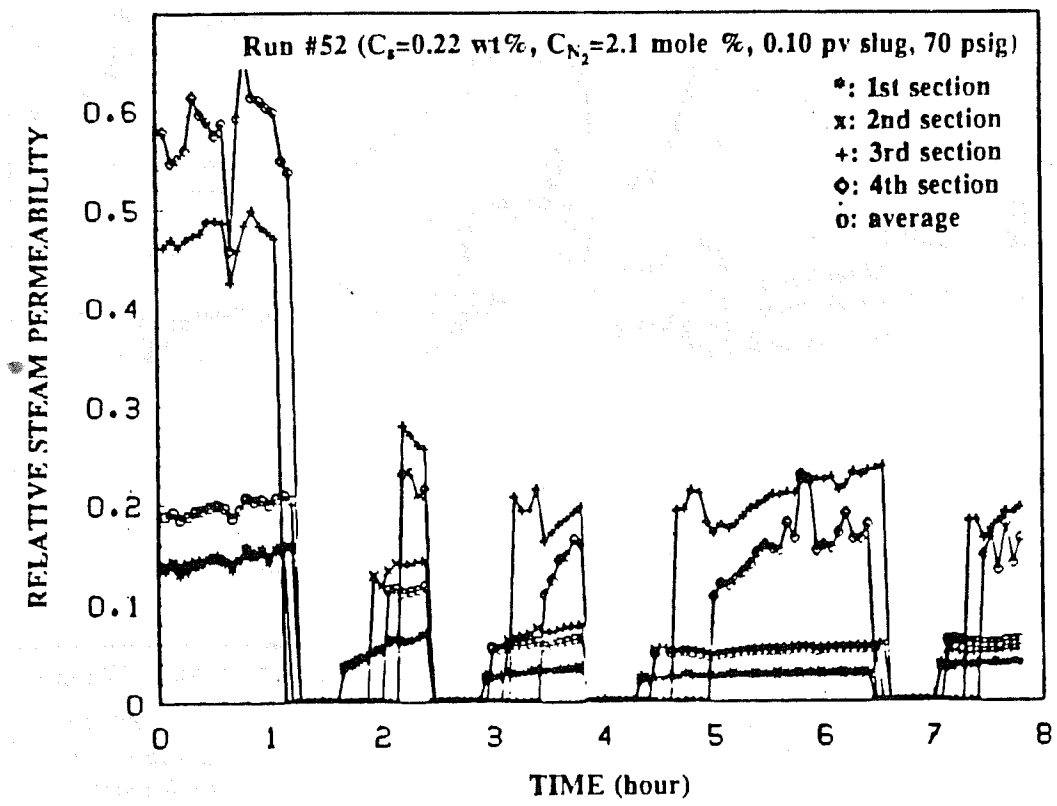


Fig. 8.52 Apparent Relative Steam Permeability vs Time for Run #52.

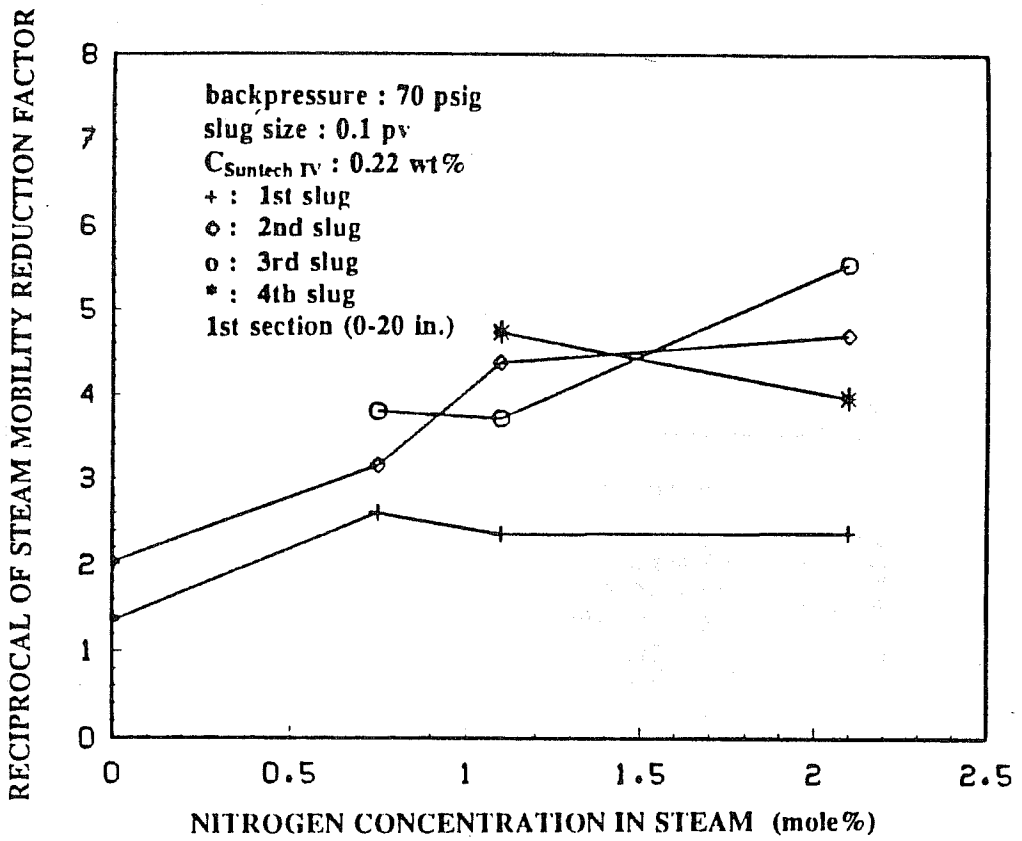


Fig. 8.53 Steam Mobility Reduction Factor for the First Section vs Nitrogen Concentration in Steam for Runs at 0.584 MPa.

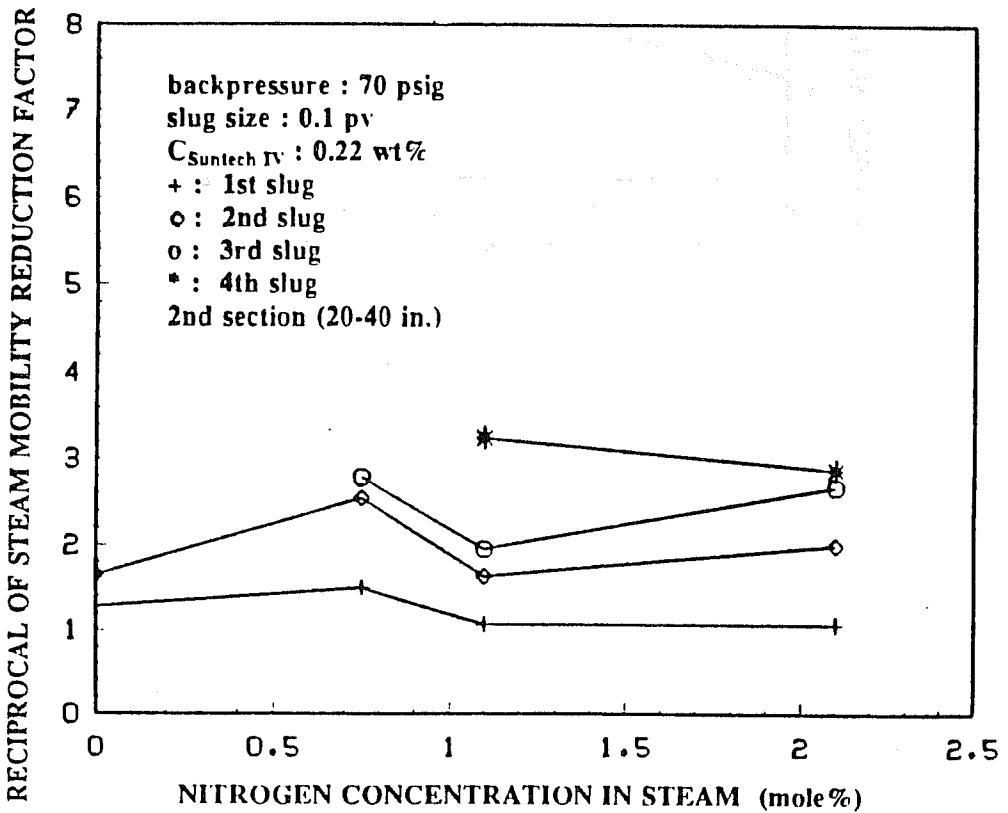


Fig. 8.54 Steam Mobility Reduction Factor for the Second Section vs Nitrogen Concentration in Steam for Runs at 0.584 MPa.

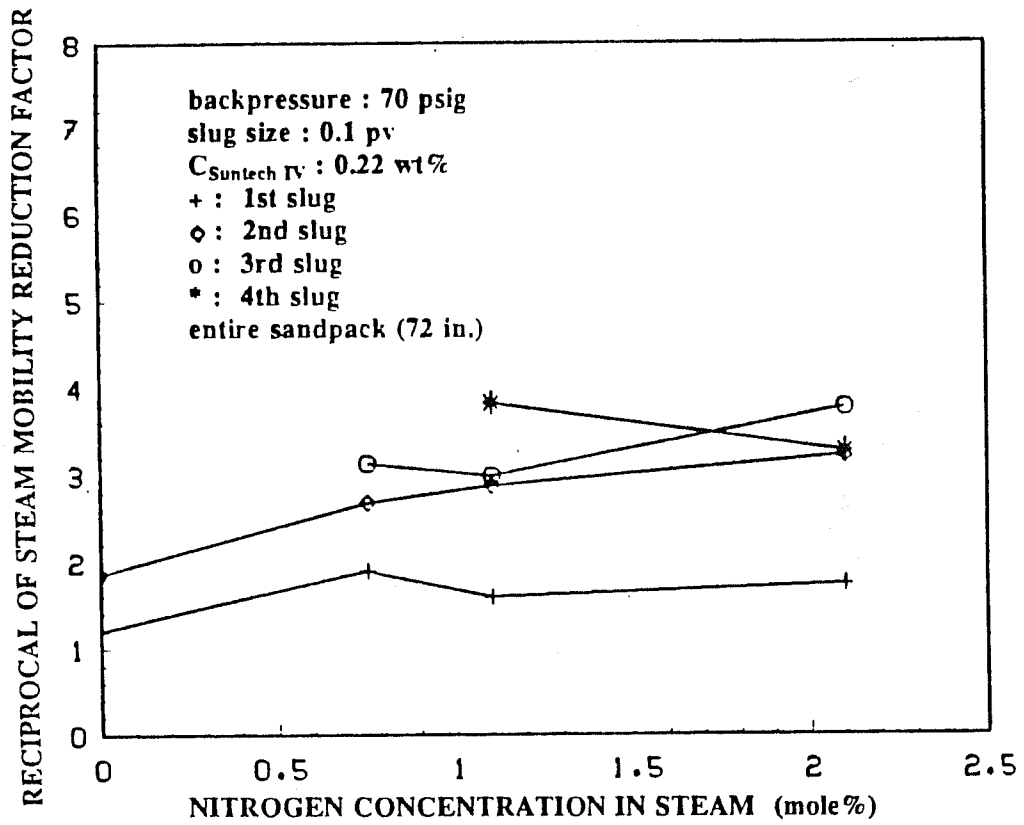


Fig. 8.55 Steam Mobility Reduction Factor for the Entire Sandpack vs Nitrogen Concentration in Steam for Buns at 0.584 MPa.

9. CONCLUSIONS

Three main topics in this study were the heat frontal movement in a cylindrical core, the theory of the development of the steam swept volume and the effect of surfactant (Suntech IV) and nitrogen on steam mobility reduction.

The Marx and Langenheim model was used to obtain an analytic solution for the heat frontal movement in a cylindrical core with a finite composite insulation layer. This solution showed that the heat front movement is dependent on the injection rate when the Biot modulus at either the inner or the outer boundary is less than 100. For steam displacement in the linear core used herein, the Biot modulus at the inner boundary was greater than 100. The Biot modulus at the outer boundary was about 15, thus the process was somewhat sensitive to rate. The solution for heat frontal movement in a system with only one layers of insulation could be used to approximate the heat frontal movement in a actual system with two layers, one of stainless steel and one of insulation, provided that the solution was adjusted by the ratio of the steady-state solutions for the two systems.

Steam displacement experiments were carried out in a cylindrical sandpack at pressures varying from 0.11 to 1.42 MPa (16 to 206 psia) with irreducible oil in place (from steam) and at initial oil saturations varying from 0.345 to 0.88. The analytical solution for heat frontal movement was used to match the experimental heat fronts from these experiments and from these matches obtained a functional relation between the apparent thermal conductivity and temperature for the insulation system of the bench model. By using this relation and the method of succession of steady states combined with the superposition on the analytical solution, the heat fronts were accurately calculated in experiments at different initial oil saturations where pressure and temperature varied both with time and distance. For displacements using Kaydol as the in-place oil, the initial oil saturation had little effect on irreducible oil saturation and the displacements appeared to be stable.

The development of the steam swept volume depends on two major parameters: the critical time and the fraction of the total heat which is latent heat. Mandl and Volek defined a dimensionless critical time as the time when the steam frontal velocity equals the sharp front temperature velocity of a hot-water displacement at the same injection rate and temperature as the steam displacement. From the heat transfer point of view, this critical time is the time when the rate of heat loss from the steam zone equals the rate of latent heat injection. The Mandl and Volek critical time was modified herein by using the fluid flow velocity rather than the temperature velocity. This resulted in the new critical time being smaller than the Mandl and Volek critical time by a factor of 1.2 to 5 depending on the heat capacity, porosity and saturations. Because the water saturation in the steam zone is less than one, the true critical time is believed to be even smaller than the critical time based on the fluid flow velocity of a hot-water displacement at 100% water saturation.

A new method was developed for approximating the steam swept volume after the critical time. This method is to change the time scale using the fraction latent heat to an empirical factor, f_{hv}^n , as a factor to adjust the time scale after the critical time. The power, n , which varies from a maximum at the critical time to a minimum at large times, was determined by the physical constraints of the steam injection process. This new method predicts lower values of steam swept volume than the methods now in general use. This is especially noticeable for f_{hv} less than 0.5 and t_D less than 2. A laboratory experiment at low steam injection rate confirmed the validity of this new critical time concept and use of the empirical power, f_{hv}^n .

Experimental data showed the steam mobility can be reduced by injecting alternate Suntech IV in water slugs and steam. The reduction was a function of backpressure, surfactant concentration, size and number of surfactant slugs, and nitrogen fraction in the injected steam. The data at atmospheric backpressure were not consistent nor conclusive. However, this pressure level is too low to be of value for practical field operations. At 0.584 MPa (85 psia), for clean Ottawa sand, surfactant

concentration of about 0.2 wt%, or higher than the critical micelle concentration (CMC), is preferred. The steam mobility reductions were moderate for sandpacks with permeability about $5 \mu m^2$ (about 5 Darcy). Two or more slugs of 0.1 pore volume or larger were required to achieve the maximum steam mobility reduction of three to four fold. The addition of nitrogen in the injected steam further reduced the steam mobility to about five fold and little effect was seen at nitrogen concentrations above about one mole percent. Thus, with the addition of nitrogen at surfactant concentration of 0.2 wt%, the mobility reduction was as large or greater than that found with 1.0 wt% surfactant without nitrogen.

NOMENCLATURE

a	= constant defined by Eq. 2.3
A	= cross-sectional area, m^2
A_D	= dimensionless area, m^2
A_s	= area of heat transfer surface, m^2
A_{sD}	= dimensionless area of heat transfer surface in steam zone
B_1	= Modified Biot number at the inner boundary
B_2	= Modified Biot number at the outer boundary
B_{i1}	= Biot number at the inner boundary
B_{i2}	= Biot number at the outer boundary
C, C_p	= specific heat at constant pressure, $J/kg \cdot ^\circ K$
D_p	= particle diameter, m
D_t	= tube diameter, m
E_h	= thermal efficiency, fraction
E_s	= thermal efficiency of the steam swept zone, fraction
f_{hv}	= fraction of latent heat to total heat injected
f_{ic}	= correction factor for t_{cMV}
G	= function for the Marx and Langenheim Equation
$G1$	= function for the steam swept volume
h_f	= heat transfer coefficient, $W/m^2 \cdot ^\circ K$
h_{f1}	= heat transfer coefficient at inner boundary, $W/m^2 \cdot ^\circ K$
h_{f2}	= heat transfer coefficient at outer boundary, $W/m^2 \cdot ^\circ K$
h_{fg}	= latent heat, J/kg
h_o	= oil enthalpy, J/kg
h_s	= steam enthalpy, J/kg
h_{sand}	= sand enthalpy, J/kg
h_S	= enthalpy of surrounding material, J/kg
h_t	= formation thickness, m
h_v	= enthalpy of superheated steam, J/kg
h_w	= water enthalpy, J/kg
\hat{h}^1_r	= volumetric heat of reservoir at initial temperature, J/m^3
\hat{h}^2_r	= volumetric heat of reservoir at steam temperature, J/m^3
H_{inj}	= heat injected, J
H_R	= heat stored in the reservoir, J
H_s	= heat stored in the steam swept zone, J
\dot{H}	= total heat injection rate, J/s
\dot{H}_D	= dimensionless total heat injection rate
\dot{H}_{fg}	= latent heat injection rate, J/s
\dot{H}_{fgD}	= dimensionless latent heat injection rate

\dot{H}_{lsD}	= dimensionless rate of heat loss
\dot{H}_{lx}	= rate of heat loss to position x , J/s
\dot{H}_{wD}	= dimensionless rate of heat flowing into the hot-water zone
\dot{H}_0	= initial heat injection rate, J/s
\dot{H}_{0D}	= dimensionless initial heat injection rate
\bar{H}_D	= dimensionless heat injection rate in Laplace space
I_0, I_1	= modified Bessel functions of the first kind
k	= thermal conductivity, W/m · °K
k_a	= absolute permeability, μm^2
k_l	= thermal conductivity of flowing liquid, W/m · °K
k_{rs}	= relative steam permeability
k_{rs1}	= relative steam permeability of pure steam
k_{rs2}	= relative steam permeability in the presence of surfactant
k_s	= steam permeability, μm^2
k_{ss}	= thermal conductivity of stainless steel, W/m · °K
k_1	= thermal conductivity of inner layer, W/m · °K
k_2	= thermal conductivity of second layer, W/m · °K
K_0, K_1	= modified Bessel functions of the second kind
$\left[\frac{k_r}{\mu} \right]_s$	= relative steam mobility, 1/cp
L	= length of the core, m
\dot{m}	= mass injection rate of steam, kg/s
n	= power index on f_{hv}
n_1	= power index on f_{hv} at t_{cD}
n_2	= power index on f_{hv} at large times
N_u	= Nusselt number
p	= pressure, MPa
p_s	= saturation pressure, MPa
p_1	= upstream pressure, MPa
p_2	= downstream pressure, MPa
P_r	= Prantl number
q_c	= rate of convective heat flow, J/s
r	= radial distance, m
r_D	= dimensionless radius
r_1	= radial distance at the inner boundary of insulation, m
r_2	= radial distance at the interface between insulations, m
r_3	= radial distance at the outer boundary of insulation, m
R_e	= Reynolds number
s	= Laplace variable
S_o	= oil saturation

S_s	= steam saturation
S_w	= water saturation
t	= elapsed time, s
t_A	= time when the heat front reaches a distance with area A, s
t_c	= critical time, s
t_{cD}	= dimensionless critical time
t_{cDMV}	= dimensionless critical time defined by Mandl and Volk
t_{cMV}	= critical time defined by Mandl and Volk, s
t_D	= dimensionless time
T	= temperature, °K
T_D	= dimensionless temperature, °K
T_i	= injection temperature, °K
T_r	= reservoir temperature, °K
T_s	= saturation temperature, °K
T_1	= temperature in inner insulation, °K
T_2	= temperature in the second insulation, °K
T_3	= temperature in the third insulation, °K
T_{1D}	= dimensionless temperature in inner insulation
T_{2D}	= dimensionless temperature in the second insulation
T_{3D}	= dimensionless temperature in the third insulation
T_∞	= ambient temperature, °K
\bar{T}_D	= dimensionless temperature in Laplace space
U	= overall heat transfer coefficient, W/m ² ·°K
v_s	= steam frontal velocity, m/s
V	= volume, m ³
V_D	= dimensionless volume
V_s	= steam swept volume, m ³
V_{sD}	= dimensionless steam swept volume
V_t	= total heated volume, m ³
x	= longitudinal distance, m
x_s	= stagnation point, m
X	= longitudinal distance, m
X_s	= steam frontal position, m
X_D	= dimensionless distance
\bar{X}_D	= dimensionless distance in Laplace space
α	= thermal diffusivity, m ² /s
α_D	= thermal diffusivity ratio
α_{ss}	= thermal diffusivity of stainless steel, m ² /s
α_S	= thermal diffusivity of surroundings, m ² /s
α_1	= thermal diffusivity of the inner insulation, m ² /s

α_2	= thermal diffusivity of the second insulation, m^2/s
β_1	= 0.000579246
β_2	= 0.004375274
γ_1	= 0.9588
γ_2	= 0.874035
γ_o	= oil gravity
λ_D	= conductivity ratio
σ	= volumetric heat capacity ratio
ρ	= density, kg/m^3
ρ_o	= oil density, kg/m^3
ρ_s	= steam density, kg/m^3
ρ_{sand}	= sand density, kg/m^3
ρ_S	= density of surrounding material,
ρ_w	= water density, kg/m^3
τ	= elapsed time, s
μ	= viscosity, $Pa \cdot s$
μ_l	= viscosity of flowing liquid, $Pa \cdot s$
μ_o	= oil viscosity, $Pa \cdot s$
μ_s	= steam viscosity, $Pa \cdot s$
μ_w	= water viscosity, $Pa \cdot s$
ν	= kinematic viscosity, mm^2/s
ν_o	= kinematic viscosity of oil, mm^2/s
ν_s	= kinematic viscosity of steam, mm^2/s
ν_w	= kinematic viscosity of water, mm^2/s
χ	= steam quality
ϕ	= porosity, fraction

Subscript

c	= critical
D	= dimensionless
fg	= latent
i	= time step
o	= oil
R	= reservoir
s	= steam, steam front
ss	= stainless steel
sw	= saturated water
S	= surroundings (or insulator)

- t** = total
- w** = water
- 1** = layer 1
- 2** = layer 2
- ∞** =ambient

REFERENCES

1. Afoeju, B.I.: "Conversion of Steam Injection to Waterflood, East Coalinga Field," *J. Pet. Tech.* (Nov. 1974), 1227-1232.
2. Ahmed, G.: "An Experimental Study of Recovery from a 2-D Layered Sandmodel," MS Thesis, Stanford University, Stanford, CA (1984).
3. Al-Khafaji, A.H., Castanier, L.M. and Brigham, W.E.: *Effect of Temperature on Degradation, Adsorption and Phase Partitioning of Surfactants used in Steam Injection for Oil Recovery*, SUPRI TR-38 (1983), Stanford, CA.
4. Ali, J., Burley, R. and Nutt, C.W.: *Foam Enhanced Oil Recovery From Sandpacks*, unpublished, 1984.
5. Akers, W.W., Deans, H.A. and Crosser, O.K.: "Condensing Heat Transfer within Horizontal Tubes," *Chem. Eng. Prog. Series* (1959), No. 29, vol. 55, 171-176.
6. Arihara, N.: "A Study of Non-Isothermal Single and Two-Phase Flow through Porous Media," PhD Dissertation, Stanford University, Stanford, CA (1975).
7. Atkinson, P.G.: "Mathematical Modelling of Single-Phase Fluid Flow through Porous Media," PhD Dissertation, Stanford University, Stanford (1976).
8. Ault, J.W., Johnson, W.M. and Kamilos, G.N.: "Conversion of Mature Steamfloods to Low-Quality Steam and/or Hot-Water Injection projects," paper SPE 13604, presented at the SPE 1985 California Regional Meeting, Bakersfield, CA., March 27-29, 1985.
9. Baker, P.E.: "Experimental Study of Heat Flow in Steam Flooding," *Soc. Pet. Eng. J.* (March 1969) 89-99.
10. Baker, P.E.: "Effect of Pressure and Rate on Steam Zone Development in Steamflooding," *Soc. Pet. Eng. J.* (Oct. 1973) 274-284.
11. Blevins, T.R. and Billingsley, R. H.: "The Ten-Pattern Steamflood, Kern River Field, California," *J. Pet. Tech.* (Dec. 1975) 1505-1514.
12. Blevins, T.R., Aseltine, R.J. and Kirk, R.S.: "Analysis of a Steam Drive Project, Inglewood Field, California," *J. Pet. Tech.* (Sept. 1969) 1141-1150.
13. Brigham, W.E., Marcou, J.A., Sanyal, S.K., Malito, O.P. and Castanier, L.M.: "A Field Experiment of Improved Steam Drive With In-Situ Foaming," paper SPE 12784, presented at the SPE 1984 California Regional Meeting, Long Beach, CA, April 11-13, 1984.
14. Bursell, C.G. and Pittman, G.M.: "Performance of Steam Displacement in Kern River Field," *J. Pet. Tech.* (August 1975) 997-1004.
15. Carslaw, H.S. and Jaeger, J.C.: *Conduction of Heat in Solids*, 2nd ed., Oxford, 1959.

16. Carter, R.D.: Appendix to "Optimum Fluid Characteristics for Fracture Extension," by G.C. Howard and G.R. Fast, *Drill. and Prod. Prac., API* (1957) 267.
17. Chiang, J.C., Sanyal, S.K., Castanier, L.M., Brigham, W.E. and Sufi, A.: "Foam as a Mobility Control Agent in Steam Injection Processes," paper SPE 8912, presented at the 50th California Regional Meeting, Pasadena, CA, April 9-11, 1980.
18. Clampitt, R.L.: "Selective Plugging of Formations with Foam," U.S. Patent No. 3,993,133 (1976).
19. Clampitt, R.L.: "Foamable Composition and Formation Treatment," U.S. Patent No. 4,300,634 (1981).
20. Closman, P.J. and Seba, R.D.: "Laboratory Test on Heavy Oil Recovery by Steam Injection," *Soc. Pet. Eng. J.* (June 1983) 417-426.
21. Coats, K.H., George, W.D., Chu, C. and Marcum, B.E.: "Three Dimensional Simulation of Steamflooding," *Soc. Pet. Eng. J.* (Dec. 1974) 573-592.
22. Colburn, A.P.: "Heat Transfer and Pressure Drop in Empty, Baffled, and Packed Tubes," *Ind. Eng. Chem.* 23, No. 8 (Aug. 1931) 910-913.
23. Crichlow, H.B.: "Heat Transfer in Hot Fluid Injection in Porous Media," PhD Dissertation, Stanford University, Stanford, CA (1972).
24. De Haan, H.J. and Schenk, L.: "Performance and Analysis of a Major Steam Drive Project in the Tia Juana Field, Western Venezuela," *J. Pet. Tech.* (Jan. 1969) 111-119.
25. Dilgren, R.E., Hirasaki, G.J., Hill, H.J. and Whitten, D.G.: "Steam Channel-Expanding Steam Foam Drive," U.S. Patent No. 4,086,964 (May 1978).
26. Dilgren, R.E., Deemer, A. R. and Owens, K. B.: "The Laboratory Development and Field Testing of Steam/Noncondensable Gas Foams for Mobility Control in Heavy Oil Recovery," paper SPE 10774, presented at the 1982 California Regional Meeting of the Society of Petroleum Engineers, San Francisco, March 24-26, 1982.
27. Doscher, T.M., Bowman, R.W. and Horcher, C.G.: "Field Demonstration of Steam Drive with Ancillary Material," *Proc.*, 1981 Annual Heavy Oil/EOR Contractor Reports, July 28-30, 1981.
28. Doscher, T.M. and Hammershaimb, E.C.: "Field Demonstration of Steam Drive with Ancillary Materials," *J. Pet. Tech.* (July 1982) 1535-1542.
29. Duerksen, J.H.: "Laboratory Study of Foaming Surfactants as Steam Diverting Additives," paper SPE 12785, presented at the SPE 1984 California Regional Meeting, Bakersfield, April 11-13, 1984.
30. El-Saleh, M.M. and Farouq Ali, S.M.: "A Theoretical and Experimental Study of Steam Drive," paper SPE 2234, presented at the 43rd Annual Fall Meeting of SPE/AIME, Houston, Sept. 2-Oct. 2, 1968.

31. Ersoy, D.: "Temperature Distribution and Heat Efficiency of Oil Recovery by Hot-Water Injection," PhD Dissertation, Stanford, CA (1969).
32. Eson, R.L. and O'Nesky, S.K.: "The Application of In-Situ Foams to Improve Recovery in Mature Steam Drives," paper SPE 11704, presented at 1983 California Regional Meeting, Ventura, March, 1983.
33. Flock, D.L. and Lee, J.: "An Experimental Investigation of Steam Displacement of a Medium Gravity Crude Oil," *The Oil sands of Canada and Venezuela 1977, CIM*, Montreal (1978).
34. Gambill, W.R.: "You Can Predict Heat Capacity," *Chemical Engineering*, (June 1957).
35. Gopalakrishnan, P., Bories, S.A. and Combarous, M.: "An Enhanced Oil Recovery Method: Injecting of Steam with Surfactant solutions," paper SPE 7109, 1978.
36. Greaser, G.R. and Shore, R.A.: "Steamflood Performance in the Kern River field," paper SPE 8834, presented at the First joint SPE/DOE Symposium on Enhanced Oil Recovery, Tulsa, April 20-23, 1980.
37. Hall, A.L. and Bowman, R.W.: "Operation and performance of the Slocum Thermal Recovery Project," *J. Pet. Tech.* (April 1973) 402-408.
38. Hirasaki, G.J. and Lawson, J.B.: "Mechanisms of Foam in Porous Media - Apparent Viscosity in Smooth Capillaries," *SPE Paper #12192*, presented at the 58th Annual Technical Conference and Exhibition, San Francisco, Oct. 5-8, 1983.
39. Hearn, C.L.: "Effect of Latent Heat Content of Injected Steam in Steam Drive," *J. Pet. Tech.* (April 1969) 374-375.
40. Hilsenrath, J. and Touloukian, Y.S.: "The Viscosity, Thermal Conductivity and Prandtl Number for Air, O₂, N₂, NO, H₂, CO, CO₂, H₂O, He and A," *Trans., ASME* (August 1954) 967-985.
41. Hong, K.C.: "Guidelines for Converting Steamflood to Waterflood," paper SPE 13605, presented at the SPE 1985 California Regional Meeting, Bakersfield, March 27-29, 1985.
42. Ikoku, C.U.: "The Transient Flow of Non-Newtonian Power-Law Fluids in Porous Media," PhD Dissertation, Stanford University, Stanford, March 1978.
43. Isaacs, E.E., Prowse, D. R. and Rankin, J. P.: "The Role of Surfactant Additives in the In-Situ Recovery of Bitumen from Oil Sands," *J. Can. Pet. Tech.* (May-June 1982) 33-41.
44. Jenkins, R. and Aronofsky, J.S.: "Analysis of Heat Transfer Processes in Porous Media-New Concepts in Reservoir Heating Engineering," *Prod. Monthly* (May 1954) 37.
45. Keenan, J.H. and Keyes, F.G.: *Thermodynamic Properties of Steam*, 1st ed., John Wiley and Sons, Inc., New York, 1967.
46. Kesler, M.G. and Lee, B.I.: "Improved Prediction of Enthalpy of Fractions," *Hydrocarbon Processing*, (March 1976) 153-158.

47. Lauwerier, H.A.: "The Transport of Heat in Oil Layer Caused by Injection of Hot Fluid," *Applied Science Research* (1955) A5, 145-150.
48. Lawson, J.B. and Reisberg, J.: "Alternate Slugs of Gas and Dilute Surfactant for Mobility Control During Chemical Flooding," paper SPE 8839, presented at the First joint SPE/DOE Symposium on Enhanced Oil Recovery, Oklahoma, April 20-23, 1980.
49. Leonard, J.: "Increased Rate of EOR Brightens Outlook," *Oil and Gas J.* (April 14, 1986) 71, 71-101.
50. Leva, M.: "Heat Transfer to Gases through Packed Tubes," *Ind. Eng. Chem.* 39, (July 1947) No. 3, 857-862.
51. Leva, M., Weintraub, M., Grummer, M. and Clark, E.L.: "Cooling of Gases through Packed Tubes," *Ind. Eng. Chem.* 40, (April 1948) No. 4, 747-752.
52. Mahmood, S.M.: "Two-Dimensional Homogenous Model," in SUPRI TR-42, 3.22-3.29, Stanford, CA, 1983.
53. Mahmood, S.M.: "The 2-D Displacement of Oil by Gas/Surfactant Under Foaming Condition," PhD Dissertation, Stanford University, Stanford, CA (1986).
54. Malmberg, E.W.: *Large-Scale Sample of Sulfonates for Laboratory Studies in Tertiary Recovery Preparation and Related Studied*, Final Report, SUNTECH Inc., Richardson, Texas, 1979.
55. Mandl, G. and Volek, C.W.: "Heat and Mass Transport in Steam Drive processes," *Soc. Pet. Eng. J.* (March 1969), 59-79.
56. Marsden, S.S., Elson, T.D. and Guppy, K.H.: "Literature Review of the Selective Blockage of Fluids in Thermal Recovery Projects," SUPRI TR-3 (Nov. 1977), Stanford Petroleum Research Institute, Stanford, CA.
57. Marsden, S.S. and Khan, S.A.: "The Flow of Foam Through Short Porous Media and Apparent Viscosity Measurements," *Soc. Pet. Eng. J.* (March 1966) 17-25.
58. Marx, J.W. and Langenheim, R.H.: "Reservoir Heating by Hot Fluid Injection," *Trans. AIME*, 216, (1959), 312-315.
59. Meldau, R.F., Shipley, R.G. and Coats, K.H.: "Cyclic Gas/Steam Stimulation of Heavy-Oil Wells," *J. Pet. Tech.* (Oct. 1981), 1990-1998.
60. Miller, C.A.: "Stability of Moving Surfaces in Fluid Systems Heat and Mass Transport; III. Stability of Displacement Fronts in Porous Media," *AIChE J.* (May 1975), 474-479.
61. Miller, M.A.: "Effect of Temperature on Oil-Water Relative Permeabilities of Unconsolidated and Consolidated Sands," PhD Dissertation, Stanford University, Stanford, CA (1983).
62. Myhill, N.A. and Stegemeier, G.L.: "Steam Drive Correlation and Prediction," *Soc. Pet. Eng. J.* (Feb. 1978), 173-182.

63. Needham, R.B.: "Method of Recovery Oil Using Steam," U.S. Patent No. 3,994,345, (Nov. 1976).
64. Oglesby, K.D., Blevins, T.R., Rogers, E.E. and Johnson, W.M.: "Status of the Ten Pattern Steamflood, Kern River Field, California," *J. Pet. Tech.* (Oct. 1982), 2251-2257.
65. Owete, O.S. and Brigham, W.E.: "Flow of Foam Through Porous Media," SUPRI TR-37 (Sept. 1982), Stanford, CA.
66. Ploeg, J.F. and Duerksen, J.H.: "Two Successful Steam/Foam Field Tests, Sections 15A and 26C, Midway-Sunset Field," paper SPE 13609, presented at the SPE 1985 California Regional Meeting, Bakersfield, CA., March 27-29, 1985.
67. Pollock, C.B. and Buxton, T.S.: "Performance of a Forward Steam Injection Project - Nugget Reservoir, Winkelman Dome Field, Wyoming," *J. Pet. Tech.* (Jan. 1969) 35-40.
68. Prats, M.: "The Efficiency of Thermal Recovery Processes," *J. Pet. Tech.* (March 1969) 323-332.
69. Prats, M.: *Thermal Recovery*, Monograph vol. 7, Society of Petroleum Engineers of AIME, Dallas, 1982.
70. Ramey, H.J. Jr.: "Discussion of Reservoir Heating by Hot Fluid Injection," *Trans., AIME 216*, (1959) 364-365.
71. Ramey, H.J. Jr.: "How to Calculate Heat Transmission by Hot Fluid Injection," *Pet. Eng.* (Nov. 1964) 110-120.
72. Rubinshtein, L.I.: "The Total Heat Losses in Injection of a Hot Liquid into a Stratum," *Neft'i Gas*, (1959), 2, No. 9, 41.
73. Rubinshtein, L.I.: "On the Temperature Distribution within the Reservoir During Hot Fluid Injection," *Trans. 121*, Kazan State University (1961), Book #5, Issue of Kazan State University.
74. Salter, S.J. and Mohanty, K.K.: "Mutiphase Flow in Porous Media: I. Macroscopic Observations and Modeling," paper SPE 11017, presented at the SPE 57th Annual Fall Meeting, New Orleans, Sept 26-29, 1982.
75. Satman, A, Brigham, W.E. and Ramey, H.J. Jr.: "An Investigation of Steam Plateau Phenomena," paper SPE 7965, presented at the SPE 1979 California Regional Meeting, Ventura, April 18-20, 1979.
76. Satman, A, Zolotukhin, A.B. and Soliman, M.Y.: "Application of the Time-Dependent Overall Heat Transfer Coefficient Concept to Heat Transfer Problems in Porous Media," paper SPE 8909, presented at the SPE 1980 California Regional Meeting, Los Angles, April 9-11, 1980.
77. Schwartz, A.M. and Perry, J.W.: *Surface Active Agents: Their Chemistry and Technology*, Interscience Publishers, Inc., New York, 1949, 328-338.

78. Schwartz, A.M., Perry, J.W. and Berch, J.: *Surface Active Agents and Detergents, Vol. II*, Interscience Publishers, Inc., New York, 1958, 452-464.
79. Soliman, M., Schuster, J.R. and Berenson, P.J.: "A General Heat Transfer Correlation for Annular Flow Condensation," *J. of Heat Transfer, Trans. ASME, Series C* (May 1968) 267-276.
80. Somerton, W.H.: "Some Thermal Characteristics of Porous Rocks," *Trans., AIME 213*, (1958) 375-378.
81. Stehfest, H.: "Algorithm 368, Numerical Inversion of Laplace Transforms," D-5, *Communication of ACM 13*, (Jan. 1970), No. 1, 49.
82. Shutler, N.D.: "Numerical Three-Phase Model of the Two-Dimensional Steamflooding Process," *Soc. Pet. Eng. J.* (Dec. 1970) 405-417.
83. Turner, W.C. and Malloy, J.F.: *Properties of Thermal Insulation*, McGraw Hill Book Co., New York, 1981.
84. Van Lookeren, J.: "Calculation Methods for Linear and Radial Steam Flow in Oil Reservoirs," *Soc. Pet. Eng. J.* (June 1983) 427-439.
85. Volek, C.W. and Pryor, J.A.: "Steam Distillation Drive - Brea Field, California," *J. Pet. Tech.* (August 1972) 899-906.
86. Weinstein, H.G., Wheeler, J.A. and Woods, E. G.: "Numerical Model for Thermal Processes," *Soc. Pet. Eng. J.* (Feb. 1977) 65-78.
87. Willman, B.T., Valleroy, V.V., Runberg, G.W., Cornelius, A.J., and Powers, L.W.: "Laboratory Studies of Oil Recovery by Steam Injection," *J. Pet. Tech.* (July 1961) 681-690.
88. Wright, W.A.: "An Improved Viscosity-Temperature Chart for Hydrocarbons," *J. of Material 4*, (March, 1969), JMLSA, No. 1.
89. Yortsos, Y.C. and Gavalas, G.R.: "Analytical Modeling of Oil Recovery by Steam Injection: Part II - Asymptotic and Approximate Solutions," *Soc. Pet. Eng. J.* (April 1982) 179-190.
90. Zolotukhin, A.B.: "Analytical Definition of Overall Heat Transfer Coefficient," paper SPE 7964, presented at the SPE 1979 California Regional Meeting, Ventura, April 18-20, 1979.

APPENDIX A

EVALUATION OF RATE OF HEAT LOSS FROM THE STEAM ZONE

This appendix includes a brief review of the Marx and Langenheim model and related terms currently used with it, as well as a description of the method of evaluating the rate of heat loss from the steam zone.

A.1 Marx and Langenheim Model

A review of the Marx and Langenheim model was given in Section 2.1. The model is based on a simple heat balance on the rate of heat injection, the rate of heat loss from the heated zone and the rate of heat stored in the reservoir. For a constant heat injection rate, it can be stated as:

$$\dot{H} = 2 \int_0^t \frac{k_S \Delta T}{\sqrt{\pi \alpha_S (t-\tau)}} \frac{dA}{d\tau} d\tau + (\rho C)_R \Delta T \frac{dV}{dt} \quad (A.1)$$

where

- \dot{H} = rate of heat injection,
- k_S = thermal conductivity of the adjacent formation,
- α_S = thermal diffusivity of the adjacent formation,
- ΔT = temperature difference, $T_s - T_r$,
- $(\rho C)_R$ = volumetric heat capacity of the heated zone,
- A = area of heat transfer surface,
- V = heated volume, Ah
- t and τ = elapsed time.

The rate of heat loss from the heated zone is represented by the convolution integral in which the rate of heat conduction into a semi-infinite slab is superposed upon the area of the heated surface. Employing the following dimensionless variables:

$$V_D = \frac{V}{h^3 H_D}, \quad A_D = \frac{A}{h^2 H_D},$$

$$H_D = \frac{\dot{H}}{4\sigma k_S h \Delta T}, \quad \sigma = \frac{(\rho C)_S}{(\rho C)_R},$$

$$t_D = \frac{4\sigma k_S t}{(\rho C)_R h^2},$$

the Marx and Langenheim equation in dimensionless form becomes:

$$1 = \int_0^{t_D} \frac{1}{\sqrt{\pi(t_D-\tau_D)}} \frac{dA_D}{d\tau_D} d\tau_D + \frac{dV_D}{dt_D} \quad (A.2)$$

For cases of constant thickness (h), the terms V_D and A_D are the same. The function, V_D , is often called the G function in the literature (Prats 1982) and the solution for G is given as:

$$G(t_D) = 2\sqrt{\frac{t_D}{\pi}} - 1 + e^{t_D} \operatorname{erfc}(\sqrt{t_D}) . \quad (\text{A.3})$$

The rate of heat stored in the reservoir (or the rate of the growth of heated volume) in dimensionless form is obtained by differentiating Eq. A.3:

$$\frac{dG}{dt_D} = e^{t_D} \operatorname{erfc}(\sqrt{t_D}) . \quad (\text{A.4})$$

Then, the dimensionless rate of heat loss (\dot{H}_{ID}) becomes:

$$\dot{H}_{ID} = 1 - e^{t_D} \operatorname{erfc}(\sqrt{t_D}) , \quad (\text{A.5})$$

where \dot{H}_{ID} is defined as \dot{H}_I/\dot{H}_0 . The fraction of the injected heat remaining in the reservoir (the reservoir heat efficiency, E_h) is:

$$E_h = \frac{H_R}{H_{inj}} = \frac{G}{t_D} . \quad (\text{A.6})$$

The dimensionless critical time (t_{cDMV}) defined by Mandl and Volek (1969) is given by:

$$e^{t_{cDMV}} \operatorname{erfc}(\sqrt{t_{cDMV}}) = \left[1 + \frac{h_{fg}}{C_w \Delta T} f_{st} \right]^{-1} , \quad (\text{A.7})$$

where

- h_{fg} = latent heat of steam,
- C_w = average heat capacity of hot water,
- f_{st} = steam quality.

The right-hand side of Eq. A.7 equals $(1 - f_{hv})$, where f_{hv} is the fraction of total heat which is latent heat. With this equality, Eq. A.7 can be rewritten as:

$$1 - e^{t_{cDMV}} \operatorname{erfc}(\sqrt{t_{cDMV}}) = f_{hv} . \quad (\text{A.8})$$

Equation A.8 denotes that at the Mandl and Volek dimensionless critical time the rate of heat loss from the heated zone equals the rate of latent heat injection.

A.2 Evaluation of Rate of Heat Loss From The Steam Zone

When the steam swept zone becomes smaller than the heated zone, the rate of heat loss from the steam zone is less than that from the heated zone. The rate of heat loss from the steam swept zone is given by:

$$\dot{H}_{lsD} = \int_0^{A_{sD}} \frac{1}{\sqrt{\pi(t_D - \tau_D)}} dA_D = \int_0^{t_{sD}} \frac{1}{\sqrt{\pi(t_D - \tau_D)}} \frac{dG}{d\tau_D} d\tau_D, \quad (\text{A.9})$$

where A_{sD} is the dimensionless heat transfer surface of the steam swept zone and t_{sD} is the time when the heat front arrived to the present steam frontal position. This time (t_{sD}) is less than the total time (t_D). The heat growth rate ($dG/d\tau_D$) is given by Eq. A.4. Equation A.9 can be evaluated numerically by the trapezoidal rule.

In the following, the method for calculating the rate of heat loss from the steam zone is presented using the method proposed in Section 7.2 for approximating the steam swept volume by shifting the time scale. In order to evaluate Eq. A.9 at time t_{sD} , a corresponding current time t_D can be obtained by solving the following equations. The t_D' for each t_{sD} is obtained by solving:

$$G(t_{sD}) = G(t_{cD}) + f_{hv} [G(t_D') - G(t_{cD}')]. \quad (\text{A.10})$$

The t_D is defined by:

$$t_D = f_{hv}^n t_D'. \quad (\text{A.11})$$

Although the n functions are given in Section 7.2, they are provided here again for convenience:

$$n = n_2 + (n_1 - n_2) e^{\beta \sqrt{t_D - t_{cD}}}, \quad (\text{A.12})$$

where

$$n_1 = 1.075 + 0.0109 f_{hv} + 0.956 f_{hv}^2,$$

$$n_2 = 0.286 + 1.227 f_{hv} + 0.223 f_{hv}^2.$$

Because n is a function of the dimensionless time (t_D), Eq. A.11 is solved by iteration.

In this method, the rate of heat loss from the steam zone is a function of the dimensionless time, f_{hv} and β . For each f_{hv} , the effect of β on the calculated rate of heat loss from the steam zone was studied. Figures A.1 to A.8 show the results of the effect of β on the calculated heat loss rate from the steam zone. In these figures, f_{hv} was varied from 0.1 to 0.8. The heat loss rates from the steam zone increased with the decrease in β and gradually converged at large times. When β was small, the calculated heat loss rate increased to peak values, and then decreased with time as Figs. A.1 to A.4 indicate. Therefore, for each f_{hv} , this rate increased continuously with time only when β exceeded a certain value; e.g. this value of β was 0.4 for $f_{hv} = 0.4$ (Fig. A.4).

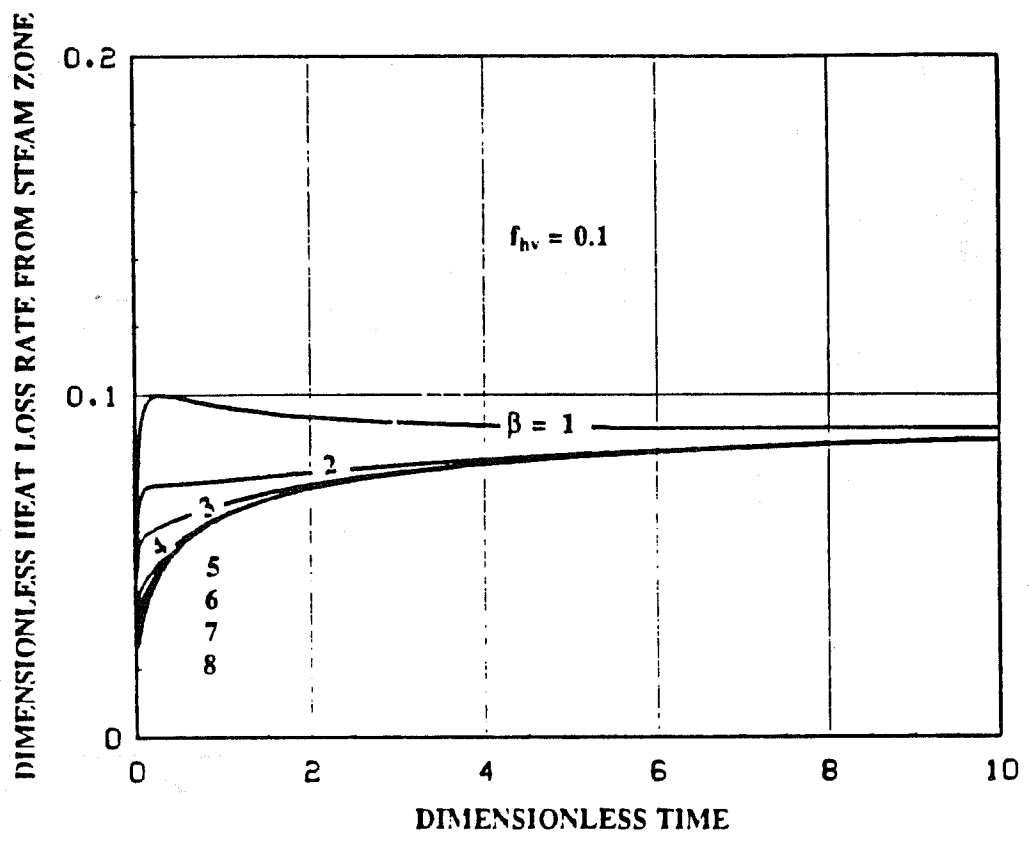


Fig. A.1 Effect of β on Rate of Heat Loss from Steam Zone for $f_{hv} = 0.1$.

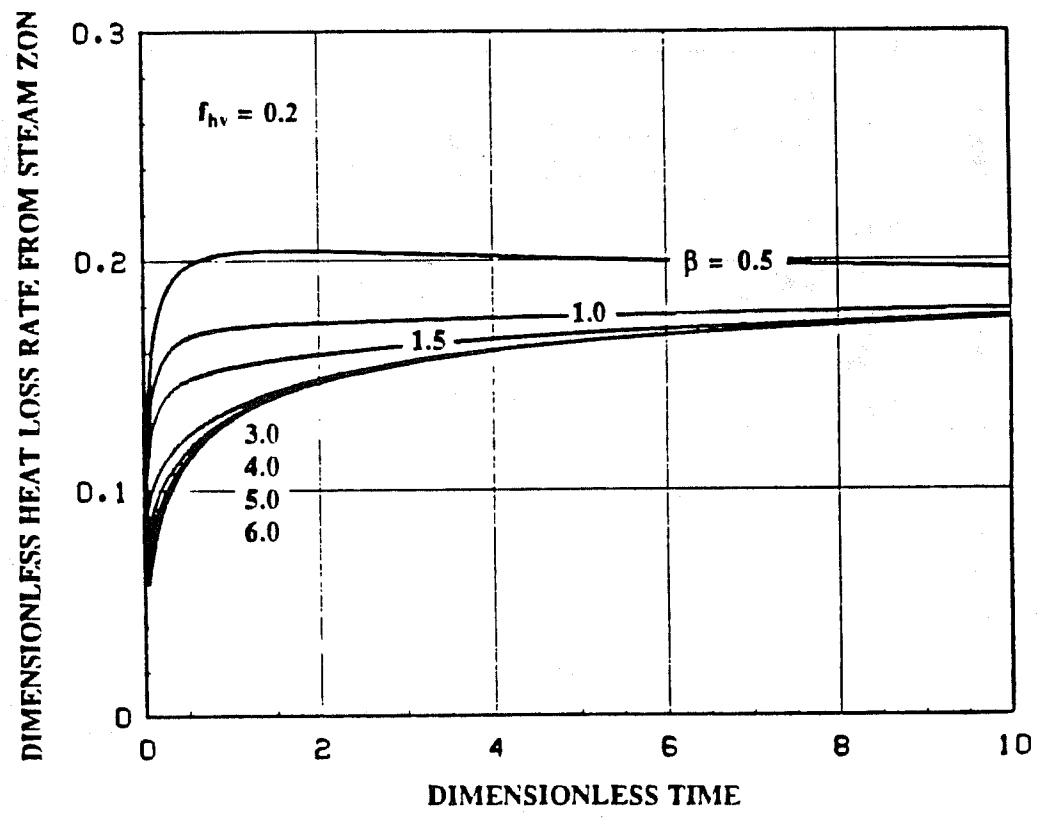


Fig. A.2 Effect of β on Rate of Heat Loss from Steam Zone for $f_{hv} = 0.2$.

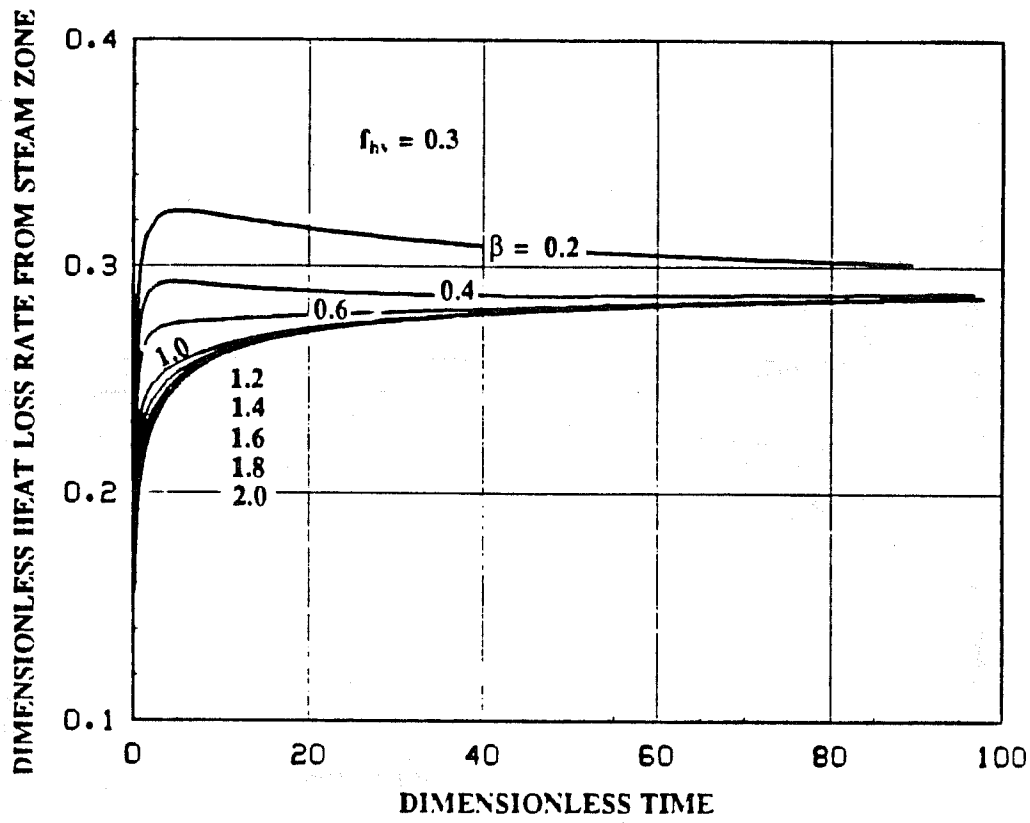


Fig. A.3 Effect of β on Rate of Heat Loss from Steam Zone for $f_{hv} = 0.3$.

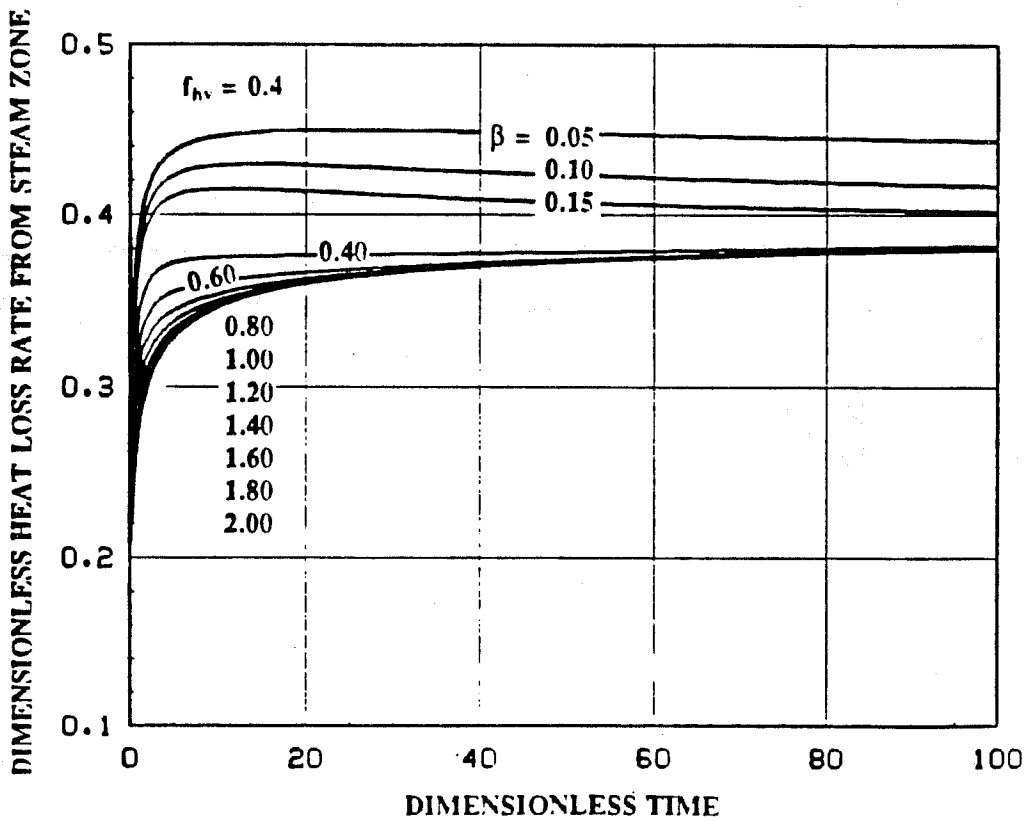


Fig. A.4 Effect of β on Rate of Heat Loss from Steam Zone for $f_{hv} = 0.4$.

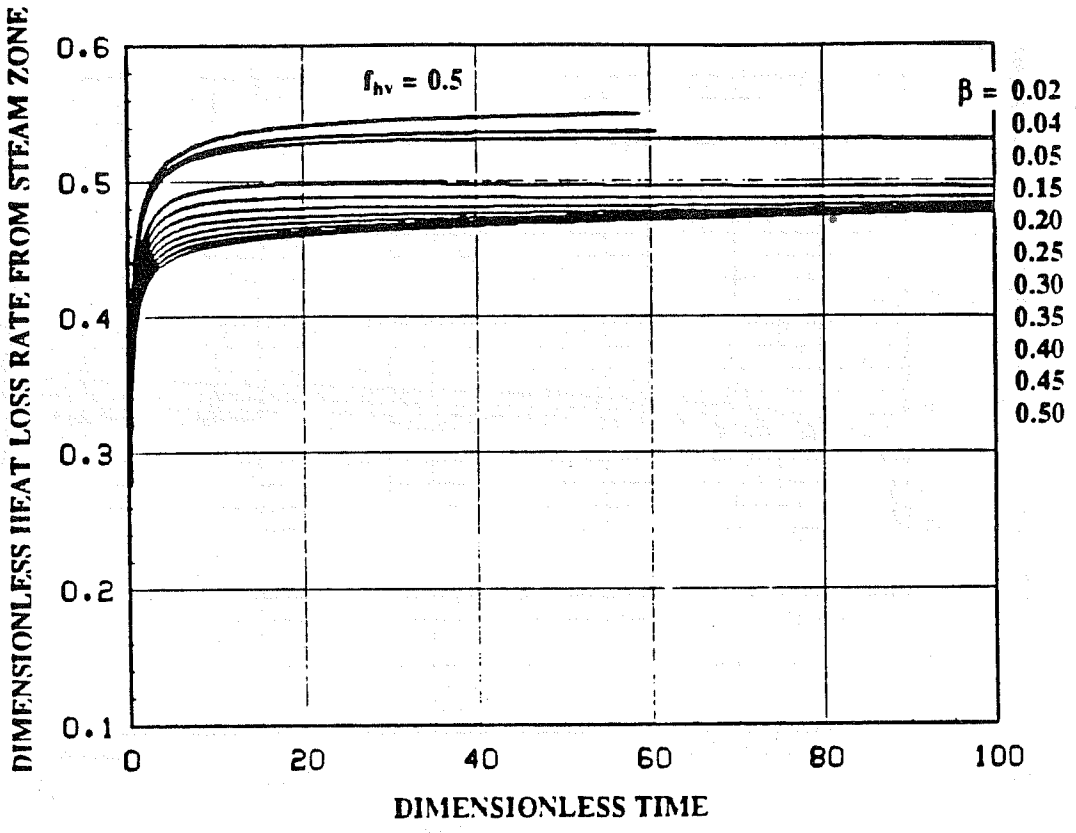


Fig. A.5 Effect of β on Rate of Heat Loss from Steam Zone for $f_{hv} = 0.5$.

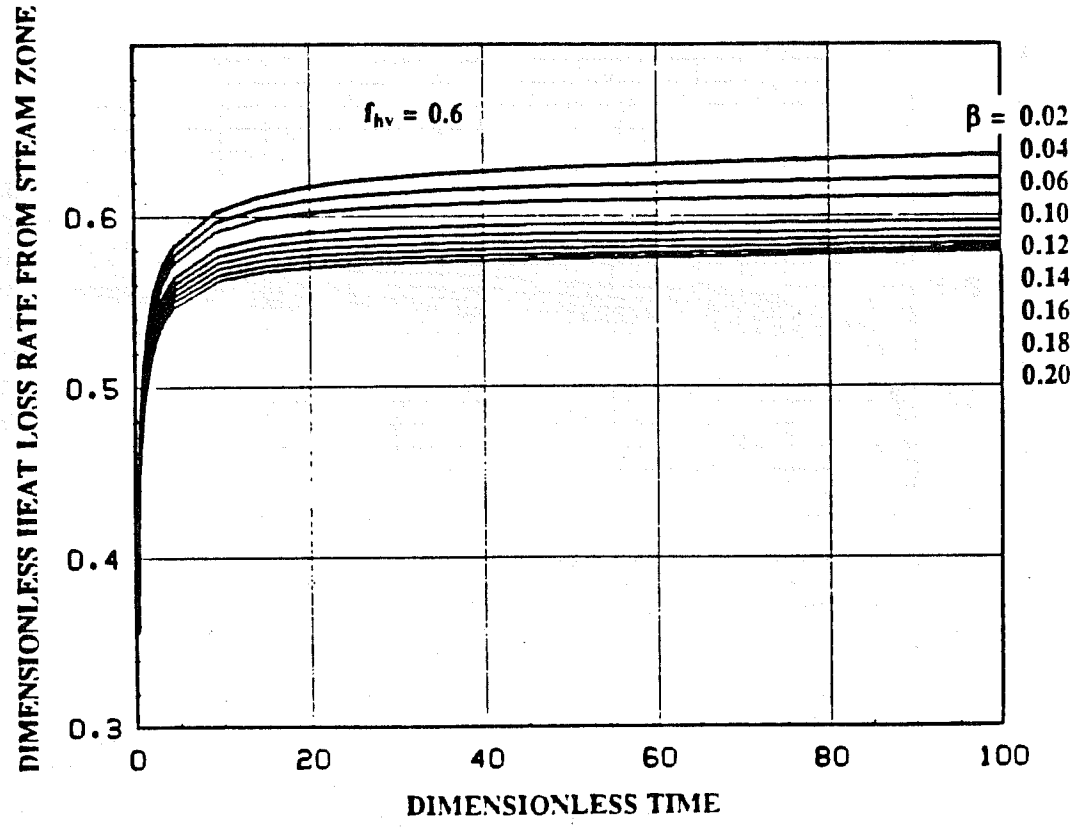


Fig. A.6 Effect of β on Rate of Heat Loss from Steam Zone for $f_{hv} = 0.6$.

DIMENSIONLESS HEAT LOSS RATE FROM STEAM ZONE.

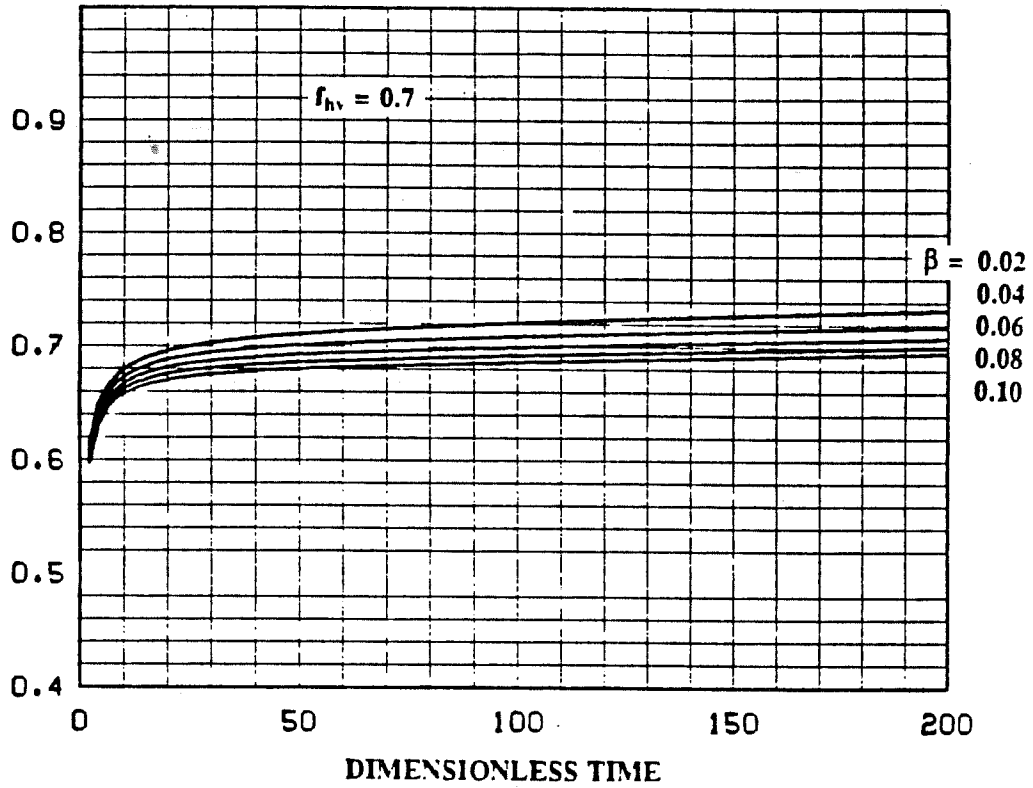


Fig. A.7 Effect of β on Rate of Heat Loss from Steam Zone for $f_{hv} = 0.7$.

DIMENSIONLESS HEAT LOSS RATE FROM STEAM ZONE.

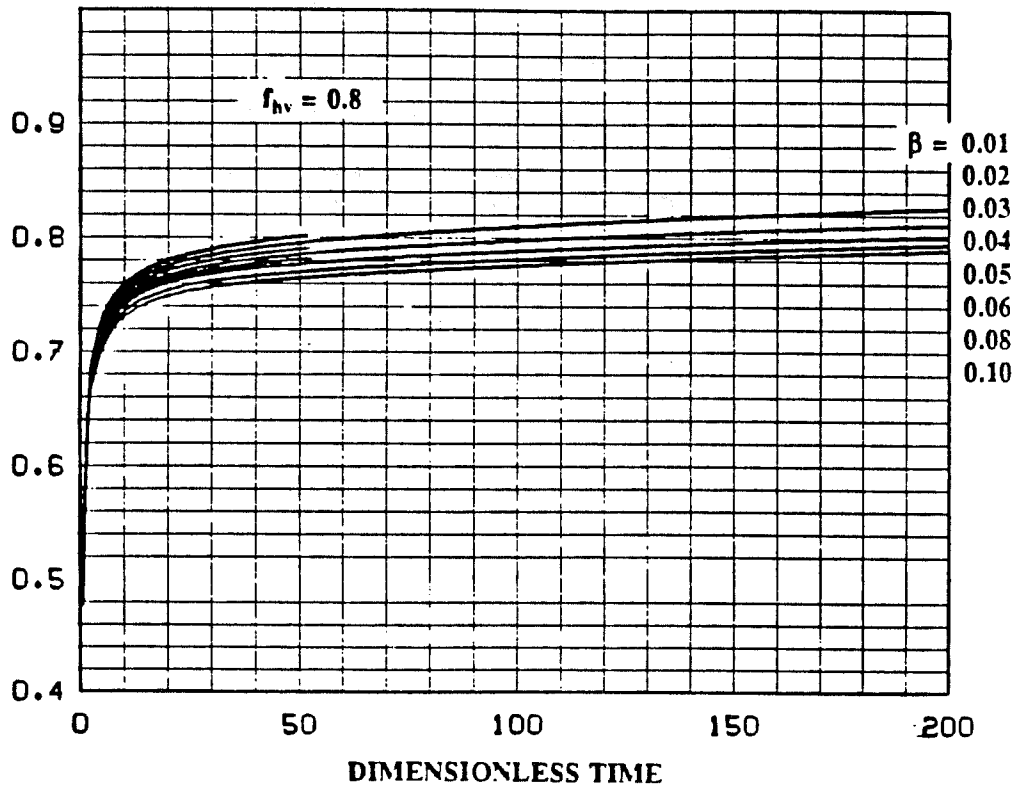


Fig. A.8 Effect of β on Rate of Heat Loss from Steam Zone for $f_{hv} = 0.8$.

The values of β shown in Fig. 7.4 and Table 7.1 were determined by the criteria that:

- (1) the heat loss rate from the steam zone must increase continuously with time after the dimensionless critical time, and
- (2) the heat loss rate from the steam zone is slightly smaller than the latent heat injection rate at the dimensionless time greater than 100.

As indicated in Figs. A.7 and A.8, it is not possible to use the second criterion to determine proper values for β for $f_{hv} \geq 0.7$ because the dimensionless time of 100 is too small for the second criterion and this method is not valid when t_D is greater than 100 (as discussed in Section 7.2.1. However, the calculated steam swept volume is not very sensitive to the value of β and the second criterion is satisfied by using the extrapolated value for β given by Eq. 7.16 and Fig. 7.4 for f_{hv} greater than 0.6.

For all values of f_{hv} , in short periods of time immediately after t_{cD} the calculated heat loss rates from the steam zone were lower than the heat loss rates from the heated zone at t_{cD} . Physically, this discrepancy means that the actual steam swept volumes are slightly greater than the calculated steam swept volumes during periods of time immediately after the critical time. This is the reason that the thermal efficiency curves shown in Fig. 7.7 are not smooth immediately after the critical times.

APPENDIX B

SOLUTION IN LAPLACE SPACE FOR HEAT CONDUCTION IN A COMPOSITE FINITE RADIAL SYSTEM

The solution in Laplace space is presented in this appendix for heat conduction in a composite finite radial system composed of the porous medium surrounded by two concentric insulators. This system is described by Eqs. 4.2 to 4.8 given in Section 4. With the dimensionless variables defined in Section 4.1, Eqs. 4.2 to 4.8 are rewritten in dimensionless forms as:

Governing differential equations

$$\frac{\partial^2 T_{1D}}{\partial r_D^2} + \frac{1}{r_D} \left[\frac{\partial T_{1D}}{\partial r_D} \right] = \frac{1}{\alpha_D} \left[\frac{\partial T_{1D}}{\partial t_D} \right], \quad (\text{B.1})$$

$$\frac{\partial^2 T_{2D}}{\partial r_D^2} + \frac{1}{r_D} \left[\frac{\partial T_{2D}}{\partial r_D} \right] = \frac{\partial T_{2D}}{\partial t_D}, \quad (\text{B.2})$$

Boundary conditions

at $r_D = 1$, the inner boundary of the insulation,

$$Bi_1(1 - T_{1D}) = -\frac{\partial T_{1D}}{\partial r_D}, \quad (\text{B.3})$$

at $r_D = r_{2D}$, the boundary between the two insulations,

$$T_{1D} = T_{2D}, \quad (\text{B.4})$$

$$-\lambda_D \left[\frac{\partial T_{1D}}{\partial r_D} \right] = -\frac{\partial T_{2D}}{\partial r_D}, \quad (\text{B.5})$$

and at $r_D = r_{3D}$, the outer boundary of the insulation,

$$-\frac{\partial T_{2D}}{\partial r_D} = Bi_2 T_{2D}, \quad (\text{B.6})$$

Initial Conditions

$$T_{1D}(r, 0) = T_{2D}(r, 0) = 0. \quad (\text{B.7})$$

By taking the Laplace transform of Eqs. B.1 to B.7, the following equations result:

$$\bar{T}'_{1D} + \frac{1}{r_D} \bar{T}_{1D} = \frac{s}{\alpha_D} \bar{T}_{1D}, \quad (\text{B.8})$$

$$\bar{T}'_{2D} + \frac{1}{r_D} \bar{T}_{2D} = s \bar{T}_{2D}, \quad (\text{B.9})$$

Boundary Conditions in Laplace Space

at $r_D = 1$, the inner boundary of the insulation,

$$Bi_1 \left(\frac{1}{s} - \bar{T}_{1D} \right) = -\bar{T}'_{1D}, \quad (\text{B.10})$$

at $r_D = r_{2D}$, the boundary between two insulations,

$$\bar{T}_{1D} = \bar{T}_{2D}, \quad (\text{B.11})$$

$$\lambda_D \bar{T}'_{1D} = \bar{T}'_{2D}, \quad (\text{B.12})$$

and at $r_D = r_{3D}$, the outer boundary of the insulation,

$$-\bar{T}'_{2D} = Bi_2 \bar{T}_{2D}. \quad (\text{B.13})$$

The solutions of Eqs. B.8 and B.9 are expressed in the form of modified Bessel functions of zero order of the first kind and the second kind as:

$$\bar{T}_{1D} = E_1 I_0 \left(r_D \sqrt{\frac{s}{\alpha_D}} \right) + F_1 K_0 \left(r_D \sqrt{\frac{s}{\alpha_D}} \right), \quad (\text{B.14})$$

and

$$\bar{T}_{2D} = E_2 I_0(r_D \sqrt{s}) + F_2 K_0(r_D \sqrt{s}). \quad (\text{B.15})$$

where E_1 , E_2 , F_1 and F_2 are constants evaluated from the boundary conditions. The derivatives are expressed in Eqs. B.16 and B.17 in forms of modified Bessel functions of the first order of the first kind and the second kind as:

$$\bar{T}'_{1D} = \sqrt{\frac{s}{\alpha_D}} \left[E_1 I_1 \left(r_D \sqrt{\frac{s}{\alpha_D}} \right) - F_1 K_1 \left(r_D \sqrt{\frac{s}{\alpha_D}} \right) \right] \quad (\text{B.16})$$

and

$$\bar{T}'_{2D} = \sqrt{s} \left[E_2 I_1(r_D \sqrt{s}) - F_2 K_1(r_D \sqrt{s}) \right]. \quad (\text{B.17})$$

Substituting Eqs. B.14 to B.17 into Eqs. B.10 to B.13, E_1 , F_1 , E_2 and F_2 are solved:

$$E_1 = \frac{f_3 \hat{q}_4 - f_4 \hat{q}_3}{\hat{p}_3 \hat{q}_4 - \hat{p}_4 \hat{q}_3}, \quad (\text{B.18})$$

$$F_1 = \frac{Bi_1 - s\hat{p}_1 A_1}{s\hat{q}_1}, \quad (\text{B.19})$$

$$E_2 = \frac{f_3 - A_1 \hat{p}_3}{\hat{q}_3}, \quad (\text{B.20})$$

and

$$F_2 = -\frac{A_2 \hat{p}_2}{\hat{q}_2}. \quad (\text{B.21})$$

where

$$\hat{p}_1 = Bi_1 I_0(u) - u I_1(u),$$

$$\hat{p}_2 = Bi_2 I_0(z) + v I_1(z),$$

$$\hat{p}_3 = I_0(w) - \frac{\hat{p}_1 K_0(w)}{\hat{q}_1},$$

$$\hat{p}_4 = \frac{\lambda_D}{\sqrt{\alpha_D}} \left[I_1(w) + \frac{\hat{p}_1 K_1(w)}{\hat{q}_1} \right],$$

$$\hat{q}_1 = Bi_1 K_0(u) + u K_1(u),$$

$$\hat{q}_2 = Bi_2 K_0(z) - v K_1(z),$$

$$\hat{q}_3 = -I_0(y) + \frac{\hat{p}_2 K_0(y)}{\hat{q}_2},$$

$$\hat{q}_4 = -I_1(y) - \frac{\hat{p}_2 K_1(y)}{\hat{q}_2},$$

$$f_3 = -\frac{Bi_1 K_0(w)}{\hat{q}_1},$$

$$f_4 = \frac{Bi_1 K_1(w)}{\hat{q}_1},$$

$$u = \sqrt{\frac{s}{\alpha_D}},$$

$$v = \sqrt{s},$$

$$w = r_{2D}u,$$

$$y = r_{2D}v,$$

and

$$z = r_{3D}v.$$

Equation B.16 at $r_D = 1$ can then be substituted into Eq. 4.9 to obtain the solution for the heat front in Laplace space. The long time approximation of Eq. 4.9 is given in Appendix C.

APPENDIX C

STEADY-STATE SOLUTION OF HEAT FRONT IN A THREE-LAYER MODEL

In this appendix, the steady-state solution for the heat front in a linear tubular model with three layers of insulation is derived. The system can be used to simulate heat conduction through a composite, finite, radial model comprising a stainless steel inner layer, an insulation layer and an aluminum outer layer. The steady-state temperature in each layer is obtained by solving the following set of equations.

Differential Equations

$$\frac{\partial}{\partial r_D} r_D \frac{\partial T_{1D}}{\partial r_D} = 0, \quad (C.1)$$

$$\frac{\partial}{\partial r_D} r_D \frac{\partial T_{2D}}{\partial r_D} = 0, \quad (C.2)$$

$$\frac{\partial}{\partial r_D} r_D \frac{\partial T_{3D}}{\partial r_D} = 0, \quad (C.3)$$

Boundary Conditions

at $r_D = 1$, the inner boundary,

$$-\frac{\partial T_{1D}}{\partial r_D} + Bi_1 T_D = Bi_1, \quad (C.4)$$

at $r_D=r_{2D}$, interface between layer 1 and layer 2,

$$T_{1D} = T_{2D}, \quad (C.5)$$

$$\lambda_{1D} T_{1D}' = T_{2D}', \quad (C.6)$$

at $r_D=r_{3D}$, the interface between layer 2 and layer 3,

$$T_{2D} = T_{3D}, \quad (C.7)$$

$$T_{2D}' = \lambda_{2D} T_{2D}', \quad (C.8)$$

and at $r_D = r_{4D}$, the outer boundary,

$$\frac{\partial T_{3D}}{\partial r_D} + Bi_2 T_D = 0. \quad (C.9)$$

The steady-state temperatures in each layer can be expressed as

$$T_{Di} = C_i \ln r_D + D_i \quad (C.10)$$

where i is from 1 to 3. The heat-conduction rate at the inner boundary is obtained by using the boundary conditions:

$$\begin{aligned} -\left[r_D \frac{\partial T_D}{\partial r_D} \right]_{r_D=1} &= -C_1 \\ &= \left[\lambda_{1D} \ln \frac{r_{3D}}{r_{2D}} - \ln r_{2D} + \frac{1}{Bi_1} + \frac{\lambda_{1D}}{\lambda_{2D} Bi_2 r_{4D}} + \frac{\lambda_{1D} \ln \frac{r_{4D}}{r_{3D}}}{\lambda_{2D}} \right]^{-1} \end{aligned} \quad (C.11)$$

By substituting Eq. C.11 into Eq. 4.9, the steady-state solution for the heat front in Laplace space can be obtained:

$$\bar{X}_D = \frac{-1}{2\sigma \lambda_{1D} C_1 s} \quad (C.12)$$

The solution for the heat front is:

$$\begin{aligned} 2\sigma X_D &= \frac{-1}{\lambda_{1D} C_1} \\ &= \ln r_{3D} - \ln r_{2D} + \frac{\ln r_{2D}}{\lambda_{1D}} + \frac{1}{B_1} + \frac{1}{B_2} - \frac{\ln r_{4D} - \ln r_{3D}}{\lambda_{2D}} \end{aligned} \quad (C.13)$$

where B_1 and B_2 are modified Biot numbers which are defined as follows by using the conductivity of the reference layer (layer 2):

$$B_1 = \frac{h_{f1} r_1}{k_2} = \lambda_{1D} Bi_1, \quad (C.14)$$

$$B_2 = \frac{h_{f4} r_4}{k_2} = \lambda_{2D} Bi_2 r_{4D}. \quad (C.15)$$

Eq. C.13, simplified to treat the two layer case, was used in Section 4.2 as Eq. 4.11 to analyze long time behaviors.

APPENDIX D

EQUATIONS FOR PROPERTIES OF MATERIAL

Some equations used in this study are obtained by least-squares fit on measured or reported data. Prats (1982) in his monograph has given a thorough coverage of rock and fluid properties of general interest in thermal recovery. The density and the viscosity of Kaydol were measured. Gambill's equation (1957) is used for estimating the heat capacity and the enthalpy of Kaydol. Equations for calculating densities and enthalpies of saturated water and steam are fitted on data from Keenan and Keyes' steam table (1967). The units of temperature and pressure for the following equations are °F and psia.

Oil (Kaydol)

density (gm/cc):

$$\rho_o = 0.89898e^{-3.79394 \times 10^{-4} T} \quad (D.1)$$

heat capacity (Btu·lb_m ·°F) (Gambill, 1957):

$$C_p = \frac{0.388 + 0.00045 T}{\sqrt{\gamma_o}}, \quad (D.2)$$

where γ_o is oil specific gravity.

viscosity (cp) (Wright, 1969):

$$\begin{aligned} \log \log(z) &= 10.47765 - 3.7134 \log(T + 459.7) \\ \mu_o &= \rho_o(z - 0.6) \end{aligned} \quad (D.4)$$

Water

density (gm/cc):

$$\rho_w = e^{(0.005625 + 1.77 \times 10^{-6} T - 1.12 \times 10^{-6} T^2) e^{(3.4 \times 10^{-6} p)}} \quad (D.5)$$

enthalpy (Btu/lb_m) at atmospheric pressure:

$$h_w = (1.01160 - 0.0002259T + 9.2 \times 10^{-7} T^2) (T - 32) \quad (D.6)$$

Saturated Water

density (gm/cc):

$$\rho_{ws} = 1.01012 - 1.19137 \times 10^{-4} T - 7.0988 \times 10^{-7} T^2 \quad (D.7)$$

viscosity (cp): (Miller, 1983)

$$\ln \ln(208.9 \mu_w) = 1.3926 + 0.3084 \ln T - 0.05714 (\ln T)^2 \quad (D.8)$$

enthalpy (Btu/lb_m):

$$h_w = 29.4581 + 0.7678(T - 32) + 0.0004616(T - 32)^2 \quad (D.9)$$

$$212^\circ\text{F} < T < 600^\circ\text{F}$$

Saturated Steam

density (gm/cc):

$$\rho_s = 0.00004528 p_{st}^{0.953645} \quad (D.10)$$

viscosity (cp) (Bonilla, 1951):

$$\mu_s = (0.20056T + 81.9352) \times 10^{-4} \quad (D.11)$$

kinematic viscosity (cm²/s):

$$\left[\frac{\mu}{\rho} \right]_s = (0.004466 p_{st}^{0.8704})^{-1} \quad (D.12)$$

latent heat (Btu/lb_m):

$$h_{fg} = 1028.2375 - 0.03627T - 0.001174T^2 \quad (D.13)$$

Superheated Steam

enthalpy (Btu/lb_m):

$$\begin{aligned} h_s = & (1011.00031 + 0.82587T - 0.00087T^2) \\ & + (0.65492 - 0.001848T + 1.77 \times 10^{-6}T^2)(p_s - p) \\ & + (-0.0011885 + 4.13 \times 10^{-6}T - 3.757 \times 10^{-9}T^2)(p_s - p)^2 \end{aligned} \quad (D.14)$$

Ottawa Sand

enthalpy (Btu/lb_m):

$$\begin{aligned} h_{sand} = & 0.1795(T-32) + 7.6869 \times 10^{-5} (T-32)^2 \\ & - 1.4379 \times 10^{-8} (T-32)^3 \end{aligned} \quad (D.15)$$

